BioMed Research International

Neurovascular Disorders: Novel Perspectives on Pathogenesis, Diagnosis, and Treatment

Guest Editors: David Hasan, Nohra Chalouhi, Aaron S. Dumont, Robert M. Starke, and Pascal Jabbour

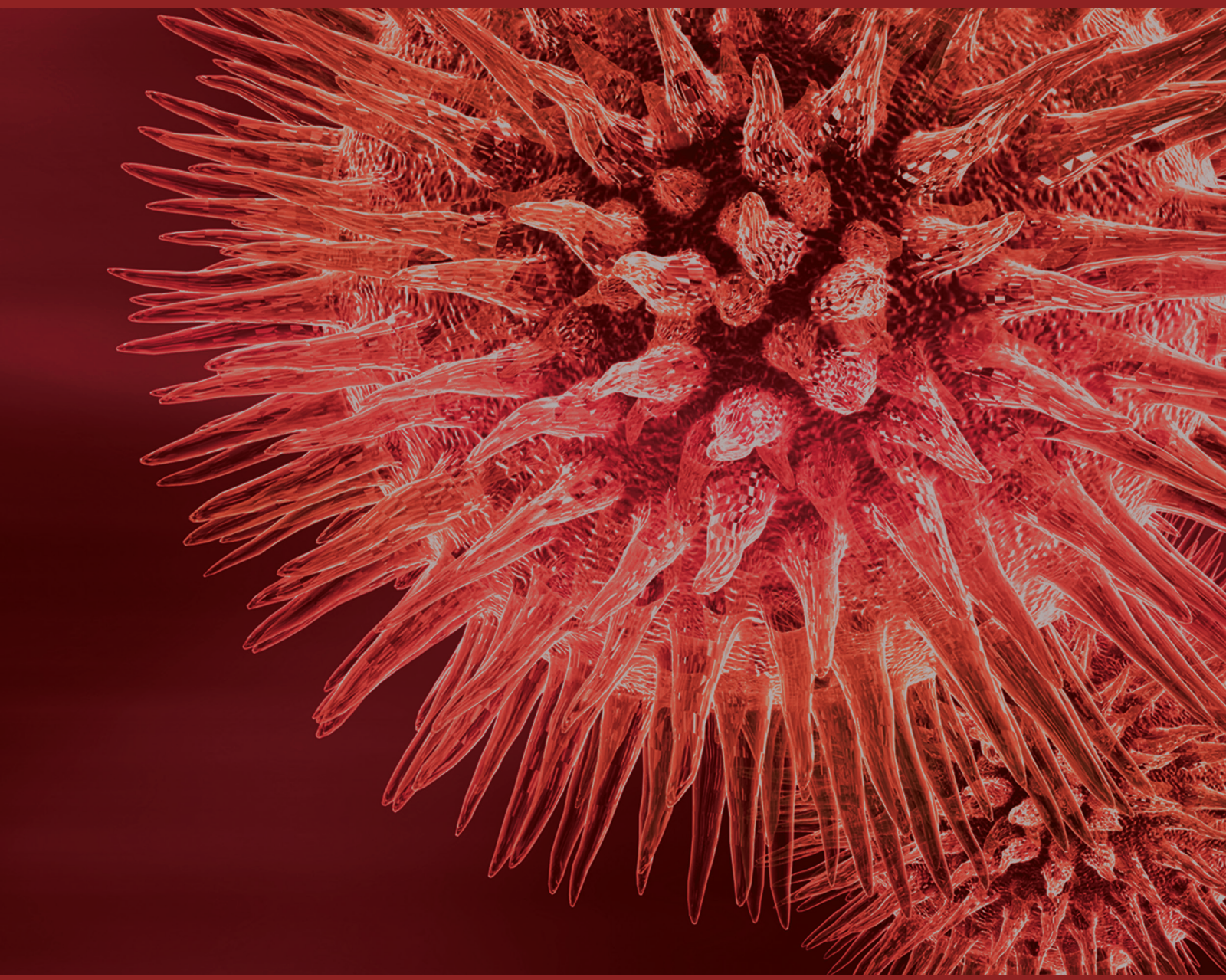

Neurovascular Disorders: Novel Perspectives on Pathogenesis, Diagnosis, and Treatment

BioMed Research International

Neurovascular Disorders: Novel Perspectives on Pathogenesis, Diagnosis, and Treatment

Guest Editors: David Hasan, Nohra Chalouhi,
Aaron S. Dumont, Robert M. Starke, and Pascal Jabbour

Contents

Hindawi Publishing Corporation
BioMed Research International
Volume 2016, Article ID 9291327, 1 page
http://dx.doi.org/10.1155/2016/9291327

Editorial

Neurovascular Disorders: Novel Perspectives on Pathogenesis, Diagnosis, and Treatment

David Hasan,[1] Nohra Chalouhi,[2] Aaron S. Dumont,[3] Robert M. Starke,[4] and Pascal Jabbour[2]

[1] *University of Iowa, Iowa City, IA, USA*
[2] *Thomas Jefferson University, Philadelphia, PA, USA*
[3] *Tulane University, New Orleans, LA, USA*
[4] *University of Virginia, Charlottesville, VA, USA*

Correspondence should be addressed to David Hasan; david-hasan@uiowa.edu

Received 21 December 2015; Accepted 21 December 2015

Neurovascular disorders include subarachnoid hemorrhage, intracranial aneurysms, arteriovenous malformations, cavernous malformations, carotid disease, acute ischemic stroke, intracerebral hemorrhage, and moyamoya disease. Recently, there has been a greater understanding of both the genetic links and the basic mechanisms behind the pathophysiology of neurovascular diseases. Additionally, there have been significant advances in diagnosis, medical treatment, and microsurgical/endovascular therapies.

This special issue on neurovascular disorders sheds light on several important aspects of common neurovascular disorders including acute ischemic stroke, arteriovenous malformations (AVMs), and subarachnoid hemorrhage.

Among several nicely conducted studies published in this issue, Y. Zhang et al. provide us with a study demonstrating that somatosensory and brainstem auditory evoked potentials assessed between 4 and 7 days after severe stroke onset may predict unfavorable outcome. S. Hillman et al. study temporal changes in the quality of acute stroke care in five national audits in Europe and report a general trend towards a better quality of stroke care over time signaling that monitoring of stroke care performance contributes to the improvement of quality of care. In a nicely designed experiment, N. Iwata et al. report that repeated administration of etanercept may prevent exacerbation of cerebral ischemic injury in diabetic rats. W. Li et al. demonstrate that *SAMHD1* gene mutations are associated with cerebral large-artery atherosclerosis. In a pilot study, C.-P. Chung et al. report that the level of circulating endothelial progenitor cell is associated with cerebral vasoreactivity. With regard to AVMs, M. Xu et al. provide us with a timely review of animal models for studying cerebral AVMs. Finally, A. Benet et al. elegantly demonstrate the feasibility of implanting a 3D-printed brain aneurysm model in human cadavers for use in neurosurgical research, case planning, and operative training.

Improvements in diagnosis, imaging, and therapies will lead to improved outcomes for neurovascular disorders. It is crucial to study the safety and efficacy of new therapies and compare them to the existing modalities to identify the best options for our patients. Within this compilation of studies, we hope to elucidate areas of uncertainty, recent developments, and clinical necessity.

David Hasan
Nohra Chalouhi
Aaron S. Dumont
Robert M. Starke
Pascal Jabbour

Hindawi Publishing Corporation
BioMed Research International
Volume 2015, Article ID 196148, 6 pages
http://dx.doi.org/10.1155/2015/196148

Research Article

Somatosensory and Brainstem Auditory Evoked Potentials Assessed between 4 and 7 Days after Severe Stroke Onset Predict Unfavorable Outcome

Yan Zhang,[1] Ying Ying Su,[1] Shu Ying Xiao,[2] and Yi Fei Liu[1]

[1]*Department of Neurology, Xuanwu Hospital, Capital Medical University, Beijing 100053, China*
[2]*Department of Neurology, Luhe Hospital, Capital Medical University, Beijing 100053, China*

Correspondence should be addressed to Yan Zhang; zhangylq@sina.com

Received 8 August 2015; Revised 12 November 2015; Accepted 19 November 2015

Academic Editor: Erwin van Wegen

Our objective was to explore the best predictive timing of short-latency somatosensory evoked potentials (SLSEP) and brainstem auditory evoked potentials (BAEP) for unfavorable outcomes in patients with early stage severe stroke. One hundred fifty-six patients with acute severe supratentorial stroke were monitored according to SLSEP, BAEP, and the Glasgow Coma Scale (GCS) at 1–3 days and 4–7 days after the onset of stroke. All patients were followed up for outcomes at 6 months after onset using the modified Rankin Scale (mRS), with a score of 5-6 considered unfavorable. The predictive values of SLSEP, BAEP, and the GCS at 1–3 days were compared with 4–7 days after onset. Our results show that, according to the analysis of prognostic authenticity, the predictive values of SLSEP and BAEP at 4–7 days after stroke onset improved when compared with the values at 1–3 days for unfavorable outcomes. Most of the patients with change of worsening evoked potentials from 1–3 days to 4–7 days after onset had unfavorable outcomes. In conclusion, SLSEP and BAEP assessed at 4–7 days after onset predicted unfavorable outcomes for acute severe stroke patients. The worsening values of SLSEP and BAEP between 1–3 days and 4–7 days also present a prognostic value.

1. Introduction

Evoked potentials (EPs) have been widely utilized to predict the outcome of patients with acute severe strokes. Although previous studies have reviewed various timings, that is, within 7 days, 10 to 15 days, 30 days, 10 weeks, and 3 months after stroke onset [1–6], precise timing at early stage remains unclear. Physicians often prefer earlier predictions on prognosis in order to improve treatment strategies. Previous studies have found that short-latency somatosensory evoked potentials (SLSEP) N20 and brainstem auditory evoked potentials (BAEP) wave V within 7 days after stroke were highly consistent with the outcomes of patients [1, 2, 5, 6]. However, 7 days is a relatively long period. Additionally, patients' conditions may change due to brain edemas during the 7-day period after stroke, especially in severe stroke patients. If optimal evaluations can be determined within the 7-day period that accurately predicts outcomes, properly informed and earlier medical treatments can be planned, enabling the optimal use of resources. It is well known that brain edemas take place 3-4 days after stroke, increased intracranial pressure peaks at 4–7 days, and patients often worsen at 4–7 days [7]. We hypothesized that the SLSEP and BAEP could be used to predict more accurate outcomes at 4–7 days than at 1–3 days after the onset of a severe stroke. Accordingly, we conducted a prospective blinded study to test our hypothesis.

2. Materials and Methods

2.1. Patients. Patients with acute severe supratentorial stroke admitted to the neurointensive care unit (NICU) of Xuanwu Hospital of Capital Medical University between January 2008 and December 2013 were enrolled in the study. The inclusion criteria were the following: (1) age from 18 to 85 years; (2) 1 to 3 days after the onset of the acute severe supratentorial stroke; (3) Glasgow Coma Scale (GCS) [8] ≤12; and (4) severe cerebral infarction or intracranial hemorrhage confirmed by

computed tomography and/or magnetic resonance imaging, that is, cerebral infarction volume ≥66% of the middle cerebral artery (MCA) territory [9] and hematoma amount ≥25 mL [10]. The exclusion criteria were the following: (1) presence of severe skin edemas of the upper extremities, cervical or head area; (2) history of severe hearing problems; (3) history of previous stroke; (4) lesions in posterior circulation territory; (5) undergoing intravenous thrombolysis or mechanical thrombectomy therapy; or (6) death within 3 days after the onset. The following parameters were recorded: (1) demographics (age and gender) and (2) stroke presentation, including the baseline National Institutes of Health Stroke Scale (NIHSS) (1–3 days after stroke onset) and the etiology of the brain lesion (infarction or hemorrhage).

2.2. Clinical Assessments and Evoked Potentials Monitoring. With the permission of the local ethics committee and the consent of the patients' families, we performed the clinical assessments of GCS and monitored the EPs, including SLSEP and BAEP. The GCS and EPs were examined by two experienced neurologists, respectively, at 1–3 days and 4–7 days after stroke onset. The physician assessing the GCS was blinded to the EPs results. The physician performing the EPs was blinded to the clinical assessments. The EPs were recorded as described previously by Zhang et al. [11] on the electromyography/evoked potential machine (Nicolet Select, Nicolet, Madison, WI, USA) with Ag/AgCl-sintered electrodes.

2.3. Clinical Assessments and EPs Parameters. The GCS includes tests of eye opening (1–4 points), speech response (1–5 points), and motor response (1–6 points). The maximum total score is 15 points. A GCS score of 6–12 was defined as a favorable prognostic predictor, and a score of 3–5 was defined as an unfavorable prognostic predictor [12, 13]. The classification of the EPs was defined according to the responses of N20 of SLSEP and V of BAEP: Grade 1, bilaterally normal responses; Grade 2, unilaterally normal responses and pathological responses in the other lateral; Grade 3, bilaterally pathological responses; Grade 4, unilaterally normal responses and absence of responses in the other lateral; Grade 5, unilaterally pathological response and absence of responses in the other lateral; and Grade 6, bilateral absence of responses. Normal EPs limits were defined at 3 SD from the mean value using the normal data bank of our NICU. The unfavorable prognostic predictors of the EPs included any abnormality of responses, that is, Grade 2 to Grade 6, and bilateral absence of responses, that is, Grade 6.

2.4. Outcome Evaluation. We assessed outcomes at 6 months because stroke patients may improve following rehabilitation training administered within 6 months after stroke onset. Patients were followed up at 6 months by two physicians who were blinded to the clinical assessments and the EPs results. The modified Rankin Scale (mRS) [14] was utilized to measure outcomes. A score of 0–4 was considered a favorable outcome, whereas a score of 5-6 was graded as an unfavorable one [15]. The optimal outcome achieved within 6 months after stroke was used for analysis.

2.5. Statistical Analysis. SPSS version 17.0 was used to analyze the data. The prognosis differences in baseline characteristics and different parameters were assessed with the Mann-Whitney test for continuous variables and Fisher's exact tests for the categorical variables. The authenticity predictions included sensitivity, specificity, positive predictive value (PPV), and negative predictive value (NPV) of the predictors, including GCS 3–5, parameters (N20 was abnormal and bilateral N20 was absent) of SLSEP, and parameters (wave V was abnormal and bilateral wave V was absent) of BAEP for unfavorable outcome. Exact 95% confidence intervals (CIs) were estimated using the binomial distribution. Positive likelihood ratios (LR+) with 95% CIs were also analyzed. If any of the cells of the 2×2 table contained no observations, we added a value of 0.5 to each cell to calculate LR+ [16].

3. Results

3.1. Baseline Data. A total of 156 patients were enrolled of which 94 were men and 62 were women aged between 23 and 85 years (64 ± 14, on average). A total of 123 patients suffered from supratentorial infarction, and 33 patients suffered from cerebral hemispheric hemorrhage. Sixty-seven patients had favorable outcomes, while 89 patients had unfavorable outcomes (Table 1). A total of 111 patients survived.

3.2. Prognostic Authenticity Analysis of Possible Predictors for Unfavorable Outcomes at 1–3 Days after Stroke Onset (the First Time). SLSEP (any abnormality of N20 and bilateral absence of N20) and BAEP (bilateral absence of V) were statistically significant in different outcomes based on Fisher's exact test analysis ($P < 0.05$) at 1–3 days after stroke onset (Table 2). The prognostic authenticity analysis showed that the sensitivity of any abnormality of N20 (96.6%, 95% CI: 89.8%–99.1%) was the best among the clinical assessment of the GCS and EPs. The specificity of bilateral absence of N20 and of bilateral absence of V was the best (100%, 95% CI: 93.2%–100%). The PPV of bilateral absence of N20 (100%, 95% CI: 51.7%–100%) and of bilateral absence of V (100%, 95% CI: 65.5%–100%) was also the best. The NPV of any abnormality of N20 was relatively high (80.0%, 95% CI: 51.4%–94.7%) (Table 3).

3.3. Prognostic Authenticity Analysis of Possible Predictors for Unfavorable Outcomes at 4–7 Days after Stroke Onset (the Second Time). The GCS, SLSEP, and BAEP were all statistically significant in different outcomes based on Fisher's exact test analysis ($P < 0.05$) at 4–7 days after stroke onset (Table 2). The prognostic authenticity analysis showed that the sensitivity of any abnormality of N20 (100%, 95% CI: 94.8%–100%) was the best among the clinical assessment of GCS and EPs. The specificity of bilateral absence of N20 and of bilateral absence of V was the best (100%, 95% CI: 93.2%–100%). The PPV of bilateral absence of N20 (100%, 95% CI: 89.8%–100%) and of bilateral absence of V (100%, 95% CI: 87.4%–100%) was also the best. The NPV of any abnormality of N20 was the best (100%, 95% CI: 78.1%–100%). Furthermore, the bilateral absence of N20 showed the highest LR+ of 65.22 (95% CI: 4.09–1040.76), which was superior to other

Table 1: Baseline characteristics and the brain lesions of patients with different outcomes at 6 months after stroke.

	Unfavorable outcome (mRS 5-6)	Favorable outcome (mRS 1–4)	*P* value
Age, median (IQR)	70 (62–76)	60 (47–69)	<0.001
Gender			
Male, *n* (%)	52 (55.3)	42 (44.7)	0.623
Female, *n* (%)	37 (59.7)	25 (40.3)	
NIHSS baseline, median (IQR)	28 (24–32)	27 (22–34)	0.414
Hemisphere stroke			
Left, *n* (%)	47 (55.3)	38 (44.7)	0.745
Right, *n* (%)	42 (59.2)	29 (40.8)	
Etiology of the brain lesion			
Infarction, *n* (%)	73 (59.3)	50 (40.7)	0.323
Hemorrhage, *n* (%)	16 (48.5)	17 (51.5)	
Total, *n* (%)	89 (57.1)	67 (42.9)	

NIHSS, National Institutes of Health Stroke Scale; IQR, interquartile range.

Table 2: Prognostic predictors at 1–3 d and 4–7 d after stroke onset with different outcomes at 6 months after stroke.

Prognostic predictors	Unfavorable outcome (mRS 5-6) 1–3 d /4–7 d *n* (%)	Favorable outcome (mRS 1–4) 1–3 d/4–7 d *n* (%)	*P* value 1–3 d/4–7 d
GCS			
3–5	20 (66.7)/56 (81.2)	10 (33.3)/13 (18.8)	0.306/<0.001
6–12	69 (54.8)/33 (37.9)	57 (45.2)/54 (62.1)	
SLSEP			
Abnormality of N20	86 (61.0)/89 (64.5)	55 (39.0)/49 (35.5)	0.004/<0.001
Normality of N20	3 (20.0)/0 (0)	12 (80.0)/18 (100)	
SLSEP			
Bilateral absence of N20	6 (100)/43 (100)	0 (0)/0 (0)	0.037/<0.001
Appearance of N20	83 (55.3)/46 (40.7)	67 (44.7)/67 (59.3)	
BAEP			
Abnormality of V	67 (61.5)/81 (68.1)	42 (38.5)/38 (31.9)	0.113/<0.001
Normality of V	22 (46.8)/8 (21.6)	25 (53.2)/29 (78.4)	
BAEP			
Bilateral absence of V	10 (100)/34 (100)	0 (0)/0 (0)	0.005/<0.001
Appearance of	79 (54.1)/55 (45.1)	67 (45.9)/67 (54.9)	
Total	89 (57.1)	67 (42.9)	

GCS, Glasgow Coma Scale; SLSEP, short-latency somatosensory evoked potential; BAEP, brainstem auditory evoked potential.

predictors (Table 3). When compared with 1–3 days after onset, the prognostic authenticity of the GCS, SLSEP, and BAEP improved at 4–7 days.

3.4. Analysis of Dynamic Changes of EPs from 1–3 Days to 4–7 Days after Stroke Onset. From 1–3 days to 4–7 days after stroke onset, decreases were noticed with the GCS (from 6–12 to 3–5) in 103 patients; deteriorations were noticed with SLSEP N20 (upgrade, for example, from Grade 2 to Grade 5) in 74 patients with BAEP wave V (upgrade) in 62 patients. These worsening changes were all significant in the different outcomes ($P < 0.05$). Sixty-six of 74 patients (89.2%) with worsening SLSEP and 60 of 62 patients (96.8%) with worsening BAEP ultimately had unfavorable outcomes (Table 4).

4. Discussion

We found that SLSEP and BAEP can predict unfavorable outcomes of stroke patients more accurately when assessed at

Table 3: Prognostic authenticity of possible predictors for unfavorable outcomes at 1–3 d and 4–7 d after stroke onset.

Prognostic predictors	Sensitivity % (95% CI) 1–3 d/4–7 d	Specificity % (95% CI) 1–3 d/4–7 d	Positive predictive value % (95% CI) 1–3 d/4–7 d	Negative predictive value % (95% CI) 1–3 d /4–7 d	Positive likelihood ratios % (95% CI) 1–3 d/4–7 d
GCS					
3–5	22.5 (14.6–32.8)/ 62.9 (52.0–72.7)	85.1 (73.8–92.2)/ 80.6 (68.8–88.9)	66.7 (47.1–82.1)/ 81.2 (69.6–89.2)	45.2 (36.4–54.3)/ 62.1 (51.0–72.1)	1.51 (0.76–3.00)/ 3.24 (1.94–5.42)
SLSEP					
Abnormality of N20	96.6 (89.8–99.1)/ 100 (94.8–100)	17.9 (90.0–29.6)/ 26.9 (17.1–39.3)	61.0 (52.4–69.0)/ 64.5 (55.8–72.3)	80.0 (51.4–94.7)/ 100 (78.1–100)	1.18 (1.05–1.33)/ 1.37 (1.18–1.58)
Bilateral absence of N20	6.7 (2.8–14.6)/ 48.3 (37.7–59.1)	100 (93.2–100)/ 100 (93.2–100)	100 (51.7–100)/ 100 (89.8–100)	44.7 (36.6–53.0)/ 59.3 (49.6–68.3)	9.10 (0.52–160.13)/ 65.22 (4.09–1040.76)
BAEP					
Abnormality of V	75.3 (64.8–83.5)/ 91.0 (82.6–95.8)	37.3 (26.1–50.0)/ 43.3 (31.4–55.9)	61.5 (51.6–70.5)/ 68.1 (58.8–76.1)	53.2 (38.2–67.6)/ 78.4 (61.3–89.3)	1.20 (0.96–1.50)/ 1.60 (1.29–2.00)
Bilateral absence of V	11.2 (5.8–20.1)/ 38.2 (28.3–49.2)	100 (93.2–100)/ 100 (93.2–100)	100 (65.5–100)/ 100 (87.4–100)	45.9 (37.7–54.3)/ 54.9 (45.7–63.9)	15.17 (0.91–255.14)/ 51.57 (3.22–826.44)

GCS, Glasgow Coma Scale; SLSEP, short-latency somatosensory evoked potential; BAEP, brainstem auditory evoked potential.

Table 4: Analysis of dynamic changes of EPs from 1–3 days to 4–7 d after stroke onset.

Prognostic predictors	Unfavorable outcome (mRS 5-6) *n* (%)	Favorable outcome (mRS 1–4) *n* (%)	*P* value	Sensitivity % (95% CI)	Specificity % (95% CI)	Positive predictive value % (95% CI)	Negative predictive value % (95% CI)	Positive likelihood ratios % (95% CI)
GCS								
Worse (from 6–12 to 3–5)	65 (63.1)	38 (36.9)	0.041	73.0 (62.4–81.6)	26.9 (16.0–41.3)	63.1 (53.0–72.2)	36.8 (22.3–54.0)	1.00 (0.81–1.23)
SLSEP								
Worse (upgrade)	66 (89.2)	8 (10.8)	<0.001	74.2 (63.6–82.6)	88.1 (77.3–94.3)	89.2 (79.3–94.9)	72.0 (60.8–81.0)	6.21 (3.20–12.04)
BAEP								
Worse (upgrade)	60 (96.8)	2 (3.2)	<0.001	67.4 (56.6–76.8)	97.0 (88.7–99.5)	96.8 (87.8–99.4)	69.1 (58.7–78.0)	22.58 (5.72–89.12)

GCS, Glasgow Coma Scale; SLSEP, short-latency somatosensory evoked potential; BAEP, brainstem auditory evoked potential; 95% CI, 95% confidence intervals.

4–7 days after stroke onset than at 1–3 days. Brain edemas take place 3-4 days after stroke, and increased intracranial pressure peaks at 4–7 days [7]. Patients often worsen during this time period. The predictive timing of acute stroke assessments at 4–7 days after onset is believed to more accurately reflect brain function than assessments at 1–3 days. We also found that SLSEP and BAEP have better predictive accuracy for brain function than GCS.

The absence of N20 indicates an extensive injury of the cerebral cortex and therefore a poor outcome. From our data, the specificity and PPV of bilateral absence of N20 were both 100% within 7 days after stroke onset, which was best among predictors and as good as that of bilateral absence of V of BAEP. SLSEP N20 is generated from a large section of the cortex-subcortex area. After a large number of neurons and/or axes are damaged, N20 will be completely absent. In prior studies, the bilateral loss of SLSEP component N20 in severe brain damage often implied a fatal prognosis in all adult patients (specificity = 93.3% and sensitivity = 59.3%). Only a young child with predominant brainstem hemorrhagic contusion regained consciousness with mild-to-moderate resultant neurological deficits (Glasgow Outcome Scale 3-4) during long-term follow-up of 4 years [17, 18]. We observed that although bilateral N20 emerged in some cases, any N20 abnormality also indicated the possibility of poor outcomes. The sensitivity and NPV of either lateral abnormality of N20 were 100% for unfavorable prognosis.

The bilateral absence of wave V was also a reliable predictor of poor outcomes, especially for bilateral abnormalities. In the present study, the specificity and PPV of the bilateral absence of V were both 100% within 7 days after stroke onset, which was also best among predictors. This is consistent with Liu's findings about patients with putaminal hemorrhage [19]. The BAEP wave V is a robust indicator of brainstem function.

If any primary or secondary supratentorial disease deteriorates and impairs the function of brainstem, the V of BAEP originating from the inferior colliculus will first change [6]. Therefore, BAEP wave V is the most reliable predictor for unfavorable outcome of supratentorial stroke.

The worsening of the SLSEP and BAEP between 1–3 days and 4–7 days also provided a prognostic value. Our dynamic assessments found that the GCS, SLSEP, and BAEP worsened in some patients within 7 days after stroke. For more than one-third of 156 patients, the SLSEP and BAEP worsened, and most of these affected patients (89.2–96.8%) had poor outcomes. This indicated that worsening SLSEP and BAEP might be a reliable predictor of the degree of irreversible deterioration. Additionally, the reliability increased with serial recordings. In conclusion, patients with uncertain prognoses 1–3 days after stroke should be further evaluated, especially for the SLSEP and BAEP, to discover the brain function changes for proper and timely clinical decisions [20].

5. Conclusions

From this study, 4–7 days after stroke onset was a better timing for predicting outcome, and the SLSEP N20 and BAEP wave V were the most reliable predictors for patients with severe supratentorial strokes. Predictors at 1–3 days after stroke can provide reference values; the worsening of the SLSEP and BAEP between 1–3 days and 4–7 days could provide a strong prognostic value. This study was limited by the small sample size and the use of patients from a single center and could be further expanded by conducting a prospective multicenter study.

Conflict of Interests

The authors declare that they have no conflict of interests related to this work.

Acknowledgment

This study is supported by National Natural Science Foundation of China (81441037).

References

[1] L. Burghaus, W.-C. Liu, C. Dohmen, B. Bosche, and W. F. Haupt, "Evoked potentials in acute ischemic stroke within the first 24 h: possible predictor of a malignant course," *Neurocritical Care*, vol. 9, no. 1, pp. 13–16, 2008.

[2] W. F. Haupt, G. Pawlik, and A. Thiel, "Initial and serial evoked potentials in cerebrovascular critical care patients," *Journal of Clinical Neurophysiology*, vol. 23, no. 5, pp. 389–394, 2006.

[3] Y. Péréon, P. Aubertin, and P. Guihéneuc, "Prognostic significance of electrophysiological investigations in stroke patients: somatosensory and motor evoked potentials and sympathetic skin response," *Neurophysiologie Clinique*, vol. 25, no. 3, pp. 146–157, 1995.

[4] P. Tzvetanov and R. T. Rousseff, "Predictive value of median-SSEP in early phase of stroke: a comparison in supratentorial infarction and hemorrhage," *Clinical Neurology and Neurosurgery*, vol. 107, no. 6, pp. 475–481, 2005.

[5] Y. Y. Su, S. Y. Xiao, W. F. Haupt et al., "Parameters and grading of evoked potentials: prediction of unfavorable outcome in patients with severe stroke," *Journal of Clinical Neurophysiology*, vol. 27, no. 1, pp. 25–29, 2010.

[6] L. Burghaus, W.-C. Liu, C. Dohmen, W. F. Haupt, G. R. Fink, and C. Eggers, "Prognostic value of electroencephalography and evoked potentials in the early course of malignant middle cerebral artery infarction," *Neurological Sciences*, vol. 34, no. 5, pp. 671–678, 2013.

[7] E. F. M. Wijdicks, K. N. Sheth, B. S. Carter et al., "Recommendations for the management of cerebral and cerebellar infarction with swelling: a statement for healthcare professionals from the American Heart Association/American Stroke Association," *Stroke*, vol. 45, no. 4, pp. 1222–1238, 2014.

[8] G. Teasdale and B. Jennett, "Assessment of coma and impaired consciousness. A practical scale," *The Lancet*, vol. 304, no. 7872, pp. 81–84, 1974.

[9] J. Hofmeijer, A. Algra, L. J. Kappelle, and H. B. van der Worp, "Predictors of life-threatening brain edema in middle cerebral artery infarction," *Cerebrovascular Diseases*, vol. 25, no. 1-2, pp. 176–184, 2008.

[10] S. A. Mayer, C. E. Thomas, and B. E. Diamond, "Asymmetry of intracranial hemodynamics as an indicator of mass effect in acute intracerebral hemorrhage. A transcranial Doppler study," *Stroke*, vol. 27, no. 10, pp. 1788–1792, 1996.

[11] Y. Zhang, Y. Y. Su, W. F. Haupt et al., "Application of electrophysiologic techniques in poor outcome prediction among patients with severe focal and diffuse ischemic brain injury," *Journal of Clinical Neurophysiology*, vol. 28, no. 5, pp. 497–503, 2011.

[12] D. Agrawal, "Endovascular treatment for poorest-grade subarachnoid hemorrhage in the acute stage: has the outcome been improved?" *Neurosurgery*, vol. 52, no. 2, pp. 481–482, 2003.

[13] J. Inamasu, Y. Nakamura, R. Saito et al., "Endovascular treatment for poorest-grade subarachnoid hemorrhage in the acute stage: has the outcome been improved?" *Neurosurgery*, vol. 50, no. 6, pp. 1199–1206, 2002.

[14] G. Sulter, C. Steen, and J. De Keyser, "Use of the Barthel index and modified Rankin scale in acute stroke trials," *Stroke*, vol. 30, no. 8, pp. 1538–1541, 1999.

[15] J. M. Ferro, I. Crassard, J. M. Coutinho et al., "Decompressive surgery in cerebrovenous thrombosis: a multicenter registry and a systematic review of individual patient data," *Stroke*, vol. 42, no. 10, pp. 2825–2831, 2011.

[16] E. G. J. Zandbergen, A. Hijdra, J. H. T. M. Koelman et al., "Prediction of poor outcome within the first 3 days of post-anoxic coma," *Neurology*, vol. 66, no. 1, pp. 62–68, 2006.

[17] B. Fierro, V. La Bua, M. Oliveri, O. Daniele, and F. Brighina, "Prognostic value of somatosensory evoked potentials in stroke," *Electromyography and Clinical Neurophysiology*, vol. 39, no. 3, pp. 155–160, 1999.

[18] B. Pohlmann-Eden, K. Dingethal, H.-J. Bender, and W. Koelfen, "How reliable is the predictive value of SEP (somatosensory evoked potentials) patterns in severe brain damage with special regard to the bilateral loss of cortical responses?" *Intensive Care Medicine*, vol. 23, no. 3, pp. 301–308, 1997.

[19] C.-W. Liu, N.-S. Chu, and S.-J. Ryu, "CT, somatosensory and brainstem auditory evoked potentials in the early prediction of functional outcome in putaminal hemorrhage," *Acta Neurologica Scandinavica*, vol. 84, no. 1, pp. 28–32, 1991.

[20] W. F. Haupt and G. Pawlik, "Contribution of initial median-nerve somatosensory evoked potentials and brainstem auditory evoked potentials to prediction of clinical outcome in cerebrovascular critical care patients: a statistical evaluation," *Journal of Clinical Neurophysiology*, vol. 15, no. 2, pp. 154–158, 1998.

Hindawi Publishing Corporation
BioMed Research International
Volume 2015, Article ID 432497, 8 pages
http://dx.doi.org/10.1155/2015/432497

Research Article

Temporal Changes in the Quality of Acute Stroke Care in Five National Audits across Europe

Steffi Hillmann,[1] Silke Wiedmann,[1,2] Alec Fraser,[3] Juan Baeza,[4] Anthony Rudd,[5] Bo Norrving,[6] Kjell Asplund,[7] Maciej Niewada,[8] Martin Dennis,[9] Peter Hermanek,[10] Charles D. A. Wolfe,[5,11] and Peter U. Heuschmann[1,2,12]

[1] *Institute of Clinical Epidemiology and Biometry, University of Würzburg, 97080 Würzburg, Germany*
[2] *Comprehensive Heart Failure Center, University Hospital of Würzburg, 97080 Würzburg, Germany*
[3] *Faculty of Public Health and Policy, London School of Hygiene and Tropical Medicine, London WC1E 7HT, UK*
[4] *Department of Management, School of Social Science and Public Policy, King's College London, London SE1 3QD, UK*
[5] *Division of Health and Social Care Research, King's College London, London SE1 1UL, UK*
[6] *Department of Clinical Sciences, Neurology, Lund University, 221 00 Lund, Sweden*
[7] *Department of Public Health and Clinical Medicine, Umeå University, Umeå 901 85, Sweden*
[8] *Department of Experimental and Clinical Pharmacology, Medical University Warsaw, 02-091 Warsaw, Poland*
[9] *Department of Clinical Neurosciences, Western General Hospital, Edinburgh EH4 2XU, UK*
[10] *Bavarian Permanent Working Party for Quality Assurance, 80331 Munich, Germany*
[11] *National Institute for Health Research Biomedical Research, Centre Guy's & St Thomas' NHS Foundation Trust and King's College London, London SE1 9RT, UK*
[12] *Clinical Trial Center Würzburg, University Hospital Würzburg, 97080 Würzburg, Germany*

Correspondence should be addressed to Steffi Hillmann; steffi.hillmann@uni-wuerzburg.de

Received 21 August 2015; Accepted 22 November 2015

Academic Editor: Gelin Xu

Background. Data on potential variations in delivery of appropriate stroke care over time are scarce. We investigated temporal changes in the quality of acute hospital stroke care across five national audits in Europe over a period of six years. *Methods.* Data were derived from national stroke audits in Germany, Poland, Scotland, Sweden, and England/Wales/Northern Ireland participating within the European Implementation Score (EIS) collaboration. Temporal changes in predefined quality indicators with comparable information between the audits were investigated. Multivariable logistic regression analyses were performed to estimate adherence to quality indicators over time. *Results.* Between 2004 and 2009, individual data from 542,112 patients treated in 538 centers participating continuously over the study period were included. In most audits, the proportions of patients who were treated on a SU, were screened for dysphagia, and received thrombolytic treatment increased over time and ranged from 2-fold to almost 4-fold increase in patients receiving thrombolytic therapy in 2009 compared to 2004. *Conclusions.* A general trend towards a better quality of stroke care defined by standardized quality indicators was observed over time. The association between introducing a specific measure and higher adherence over time might indicate that monitoring of stroke care performance contributes to improving quality of care.

1. Introduction

In several countries, mainly from Europe and Northern America, stroke audits were implemented to provide information on the quality of acute hospital care for the local population [1–9]. In most of these audits, regular benchmarking activities were implemented by comparing measures of quality of care between the participating centers on a national or regional level [10].

Assessing potential trends in quality of stroke care over time within existing audits might be useful for identifying factors influencing changes in delivery of appropriate care on the population level. For example, specific strategies suspected to drive improvement in clinical practice and service development [11] could be linked with variations in quality of care observed within a given region. However, most previously published audit data did not provide distinct information of trends in quality of care over time [12–16]. There are only a few publications addressing temporal trends in quality of care [8, 9]. In addition, variations in methodology, data documentation, and variable definition of exiting audits in Europe currently hamper direct comparability of data from different national or regional audits [10]. Therefore, little data on time trends regarding delivery of appropriate stroke care in different countries or regions is available.

We investigated variations in quality of acute stroke care across five national audits in Europe using comparable variable definitions and assessed time trends in delivery of appropriate care over a period up to 6 years.

2. Methods

2.1. Data Collection. Data were derived from stroke audits participating within the European Implementation Score (EIS) project. The EIS Project is a European Union funded project (number 223153) aiming at developing a European methodology to assess the implementation of research evidence into practice. The selection and the characteristics of national or regional stroke audits participating in the EIS project have been described previously [8]. For the present analyses, audits providing datasets on more than two years of documentation during the study period 2004–2009 were included. Therefore, the Catalan Stroke Audit was excluded from the present analysis and the following stroke audits were included: the German Stroke Register Study Group [ADSR], Germany, the Hospital Stroke Registry of National Program for Prevention and Treatment of Cardiovascular Diseases [POLKARD], Poland, the Scottish Stroke Care Audit [SSCA], Scotland, the National Stroke Register in Sweden [Riks-Stroke], Sweden, and the National Sentinel Audit of Stroke [NSSA], England/Wales/Northern Ireland. An overview on the characteristic of the participating audits was published previously [17]. The study was limited to end at 2009 due to the end of the EIS project.

2.2. Data Definition. The following variables were documented in a comparable way over time across at least four of the five audits: demographics: age; sex; dependency pre-stroke (dependent, independent); stroke subtype (ischemic stroke [IS], intracerebral haemorrhage [ICH], and undefined [UND]); admission: time interval between onset and admission ($\leq$3 h, $\geq$3 h/missing); day of admission (weekend; weekday); comorbidities/risk factors: atrial fibrillation [AF] (No/Yes); process of care: brain imaging (No/Yes); intravenous treatment with tissue-plasminogen-activator [rt-PA] (No/Yes); Stroke Unit [SU] treatment (No/Yes); testing for swallowing disorders (NO/YES or unassessable if documented); antiplatelet therapy during hospital stay (No/Yes); anticoagulant therapy during hospital stay or recommended at discharge (No/Yes); length of hospital stay (days); level of consciousness an admission or worst level during first week (awake/disturbed). The definitions of the variables involved in the present analysis were stable over the whole time period in the participating audits. A standardized codebook was developed in cooperation with audit representatives before the data were pooled. The recoding of the variables was subsequently verified by audit representatives. Results were also checked by comparing outputs of this analysis with publications (e.g., papers or reports) of the participating audits.

2.3. Quality Indicators [QI]. Based on these variables the following quality indicators were calculated with inclusion and exclusion criteria proposed by a European consensus group: *screening for dysphagia* (numerator: number of stroke patients screened for swallowing disorders or patients that are unassessable; denominator: all patients with IS, ICH, or UND); *thrombolytic therapy* (numerator: number of stroke patients treated with rt-PA; denominator: all patients with IS aged 18–80 years); *treatment on a SU* (numerator: number of stroke patients treated on a SU; denominator all patients with IS, ICH, or UND); *antiplatelet therapy* (numerator: number of patients receiving antiplatelet therapy during hospital stay or at discharge; denominator: all patients with IS alive at discharge and without anticoagulant treatment); and *anticoagulant therapy* (numerator: number of patients treated with anticoagulants at discharge or recommended at discharge [Poland without recommendation at discharge]; denominator: all patients with IS and AF alive at discharge).

2.4. Statistical Analysis. For estimating the probability of adhering to a specific quality indicator over time within a respective audit, multivariable logistic regression analyses were performed. Analyses were adjusted for age (age group), sex, stroke subtype (if applicable), day of admission (weekend versus weekday), AF, and level of consciousness on admission (ADSR, POLKARD, Riks-Stroke) or within the first week (NSSA). For the adjusted point estimates, corresponding 95% confidence interval was calculated. The reference category was the year in which information for the respective quality indicator was available for the first time. To address a potential selection bias by nonmandatory participation in some of the audits, main analyses are based on centers participating continuously over the whole study period. As sensitivity analyses, performed calculations were repeated with inclusion of all centers during the assessed time period. The category "unassessable" for screening for dysphagia was not documented in all audits. Therefore, as sensitivity analysis for audits not documenting the category "unassessable" all analyses were repeated restricting patients with no disturbed level of consciousness.

For taking into account clustering of patients in centers with possibly different time trends in quality of care, mixed effects modelling with random effects was applied. Therefore a hierarchical logistic regression model with a random intercept for centers was calculated with the SAS procedure PROC GLIMMIX. The variance component of the

Table 1: Characteristics of participating audits, 2004–2009*.

	ADSR	POLKARD	SSCA	Riks-Stroke	NSSA
Number of centers#	193	45	18	74	208
	No. of patients per center per year, median (IQR)				
2004	143 (75–372)	205 (160–264)	0	256 (169–435)	40 (37–40)
2005	164 (80–360)	141 (76–188)	369 (225–514)	277 (183–426)	0
2006	0	0	269 (187–501)	270 (170–418)	66 (48–79)
2007	217 (85–456)	280 (168–342)†	339 (188–514)	261 (165–423)	0
2008	253 (79–535)	51 (33–69)†	382 (210–578)	269 (165–399)	59 (50–60)
2009	346 (86–616)	0	297 (191–601)	268 (177–427)	0

*Center participating continuously over the whole study period only; patients with missing center allocation or with missing/default year of admission were not considered; #number of centers referring to participating center, trusts, or departments; IQR: interquartile range; †no complete calendar years of documentation.

random intercept represents the between-centers variance. For calculating the proportion of the total variance explained by the level 2 variable the concept of the variance partition coefficient (VPC) was used. The latent variables method introduced by Snijders and Bosker [18] was used to calculate the VPC. Statistical analyses were performed using the SAS 9.2 Software Package.

2.5. Standard Protocol Approvals, Registrations, and Patient Consents. The study was approved by the ethics committee of the Charité-Universitätsmedizin Berlin (EA4/097/10) and is registered by ethics committee of the Medical Faculty of the University of Würzburg (215/11).

3. Results

Between 2004 and 2009, 930,978 patients (range between audits: 31,723 to 660,070) from 1,170 centers (trusts, hospitals, health boards, or departments; range between audits: 18 to 712) were registered within the participating audits. The presented results were restricted on centers participating continuously over the whole study period. The percentage of centers with continuous documentation ranged from 22% to 100% between audits. Centers not participating continuously had smaller numbers of patients (data not shown). Overall, 542,112 patients (range between audits: 31,155 to 303,023) were documented within the 538 centers (range between audits: 18 to 208) participating continuously over the whole study period (Table 1). The baseline characteristic of these patients is shown in Table 2.

3.1. Variations in Quality of Care over Time. The main results of univariate and multivariable analyses are presented in Table 3. A constant increase in the probability of screening for swallowing disorders was observed within the ADSR, Riks-Stroke, and NSSA with substantially lower absolute numbers within the ADSR. There was no clear time trend in the SSCA from 2005 to 2008 for screening for swallowing disorders until an increase in 2009. Restricting analyses to patients without disturbances of consciousness did not change results substantially (data not shown). Rates of thrombolysis increased in ischemic stroke patients aged 18–80 years in Riks-Stroke and the ADSR over time with a higher absolute proportion of patients receiving thrombolytic therapy within the ADSR. No clear time trend in the rate of thrombolysis was seen for POLKARD. Probability of receiving Stroke Unit treatment increased continuously in SSCA, Riks-Stroke, and NSSA with highest relative increase in the NSSA. No clear temporal patterns in antiplatelet therapy were observed in most audits except for the ADSR where rates of antiplatelet therapy were constantly increasing since 2007. Anticoagulant therapy in patients with atrial fibrillation increased in the ADSR and Riks-Stroke, both with an increase starting from 2007 onwards. No clear temporal changes in proportions of patients receiving anticoagulation were observed for POLKARD, the SSCA, and NSSA. No substantial differences were observed in the participating audits regarding variations in the investigated quality indicators over time when all centers were included in the analyses (data not shown).

To account for between-centers variations, variance partition coefficients (VPCs) are reported in Table 3. Between-centers variations differ between the audits as well as between quality indicators. For example, between-centers variation is very low for antiplatelet and anticoagulant therapy but substantially higher for treatment on a SU for some audits.

4. Discussion

For the first time, individual data from five prospective national stroke audits in Europe were pooled and analyzed over a 3- to 6-year time period between 2004 and 2009 when the EIS project was over. In most of the audits, a general trend towards a better quality of stroke care defined by standardized quality indicators was documented over the study period, mainly for swallowing testing, thrombolytic therapy, and Stroke Unit treatment. However, there were also some performance measures, such as antiplatelet therapy or anticoagulation in IS patients with AF, where no substantial variations in quality of care over time were observed in most of the audits. In some audits, a steeper increase from a specific year onwards in the defined performance measures was detected that might exceed a general constant trend toward a better provision of quality of stroke care.

Only a few studies investigated up to now time trends in delivery of quality of care within established audits. Similar to our findings for Riks-Stroke and the ADSR, Ferrari et al.

Table 2: Patient and clinical characteristics, 2004–2009, centers participating continuously over the whole study period*.

	ADSR (n = 303,023)	POLKARD (n = 31,564)	SSCA (n = 34,962)	Riks-Stroke (n = 141,389)	NSSA (n = 31,174)
Age, median (IQR)	75 (66–82)	73 (62–80)	75 (66–83)	78 (69–84)	78 (69–85)
Female sex, %	49.4	50.9	51.3	49.3	52.5
Dependency prestroke, %					
Independent	77.4	85.0	84.9	85.0	77.4
Dependent	22.5	15.0	15.1	15.0	22.6
Stroke subtype, %					
Ischemic stroke	85.1	86.6	82.7	84.1	74.3
Intracerebral haemorrhage	9.0	10.5	10.6	11.8	11.7
Unknown/undefined	5.9	2.9	6.7	4.1	14.0
Interval onset-admission, %					
<3 hours	29.3	19.3	#	25.2	19.7
>3 hours/missing	70.7	80.7	#	74.8	80.3
Day of admission, %					
Weekday	75.7	75.8	75.1	74.9	74.1
Weekend	24.3	24.2	24.9	25.1	25.9
Atrial fibrillation, %					
Yes	25.0	22.4	22.7	28.3	20.0
No	75.0	77.6	77.3	71.7	80.0
Level of consciousness, %†					
Awake	83.7	72.9	#	81.5	62.9
Disturbed (drowsy to coma)	16.3	27.1	#	18.5	37.1

*Analyses were restricted to patients with IS, ICH, or UND and without missing values in the respective variables; IQR: interquartile range; #variable not documented or not documented in a comparable way; †level of consciousness on admission or during first day except the NSSA, here worst level of consciousness during first week.

found a consistent increase of thrombolysis rates from 4.9% in 2003 to 18.3% in 2011 within the Austrian stroke registry [7]. The Registry of the Canadian Stroke Network (RCSN) reported slightly higher thrombolysis rates compared to our findings (14.0%, 2003–2005 [15], and 15.7%, 2003–2008) [19]. Saposnik et al. reported a similar prescription rate of antiplatelets at discharge (92.7%) within the RCSN compared to our study [15]. The only difference to our analysis is that the RCSN included oral anticoagulants in their definition for antiplatelets. Similar anticoagulation rates were found within the Danish Stroke Registry (2003–2011) where 41.5% had been prescribed anticoagulants and 35.7% were registered as having a contraindication [16]. The proportion of patients being tested for swallowing disorders also substantially varied in previous studies. Some studies such as the PCNASR and the RCSN found lower screening rates for swallowing disorders (45.5%, 2001–2004; 56.7%, 2005–2007; and 56.0%, 2003–2005, resp.) compared to our data, except the ADSR [12, 15]. The PCNASR excluded patients who were on "nothing per oral." Higher rates of assessment of swallowing disorders than in our study were reported from the population-based South London Stroke Register (SLSR), where 90.4% of the patients got a screening for swallowing disorders in 2004–2006 and 87.9% between 2007 and 2009 [20]. The SLSR observed also slightly higher SU admission rates between 2004 and 2006 of 76.4% and between 2007 and 2009 of 78.4% compared to the data from the NSSA [20].

There might be a number of potential reasons causing temporal changes of quality of acute stroke care within the different countries such as introduction of a new health care policy or new guidelines. For example, testing for swallowing disorders was implemented as quality indicator within the ADSR the first time in 2006 [21] and its documentation within Riks-Stroke in Sweden started in 2007 [22]. A similar increase of performance could be observed in both stroke audits after start of the documentation, but the ADSR started on a substantially lower level. This increase might reflect a better performance of the individual hospitals due to drawing attention to this measure. However, the increase might also be caused by a better documentation of hospitals within the audits, which might be perceived as improvement of quality of care in itself. However, also other methods of implementation, for example, better finance for stroke services and restructuring of stroke services, might have been reasons for improvement of quality of care [11]. The UK National Stroke Strategy 2007 recommended screening for dysphagia within 24 hours [23]. A consistent increase for screening for dysphagia has been reported within the NSSA already since 2006. The largest increase for thrombolysis was documented in the Swedish audit from 2006 onwards. Accordant to this finding, the Swedish acute care guidelines from 2005 recommended thrombolysis as an important part of the treatment of stroke patients [24]. The National Stroke Strategy in the UK recommended in 2007 the timely access

Table 3: Variations and changes in quality of care over time, 2004–2009, center participating continuously over the whole study period*.

	2004		2005		2006		2007		2008		2009		VPC‡‡
	%	OR (95% CI)	%	OR (95% CI)	%	OR (95% CI)	%	OR (95% CI)	%	OR (95% CI)	%	OR (95% CI)	
Swallowing test done†													
ADSR	#	#	#	#	#	#	52.9	1.00	63.7	1.65 (1.60–1.70)	70.3	2.44 (2.37–2.52)	0.3847
POLKARD	#	#	#	#	#	#	#	#	#	#	#	#	#
SSCA	#	#	74.9	1.00	78.4	1.10 (0.99–1.21)	73.3	1.02 (0.93–1.12)	72.4	0.88 (0.80–0.96)	83.8	1.94 (1.75–2.15)	0.2697
Riks-Stroke	#	#	#	#	#	#	84.1	1.00	89.1	1.65 (1.55–1.76)	92.7	2.68 (2.50–2.86)	0.0851
NSSA	75.4	1.00	#	#	77.2	1.08 (1.01–1.16)	#	#	81.2	1.45 (1.34–1.56)	#	#	0.1263
Thrombolysis‡													
ADSR	6.0	1.0	7.1	1.20 (1.11–1.30)	#	#	8.6	1.57 (1.45–1.69)	9.5	1.70 (1.58–1.82)	11.2	2.04 (1.90–2.19)	0.2794
POLKARD	0.9	1.0	0.6	0.70 (0.43–1.14)	#	#	1.5	1.85 (1.33–2.57)††	1.2	1.83 (1.05–3.17)††	#	#	0.3866
SSCA	#	#	#	#	#	#	#	#	#	#	#	#	#
Riks-Stroke	2.2	1.0	3.4	1.54 (1.31–1.82)	3.6	1.66 (1.41–1.96)	5.6	2.60 (2.24–3.03)	7.0	3.27 (2.82–3.79)	7.9	3.74 (3.24–4.32)	0.0824
NSSA	#	#	#	#	#	#	#	#	#	#	#	#	#
Treatment Stroke Unit§													
ADSR	#	#	#	#	#	#	#	#	#	#	#	#	#
POLKARD	86.7	1.0	91.3	1.99 (1.75–2.27)	#	#	90.0	1.71 (1.54–1.89)††	91.2	1.90 (1.59–2.27)††	#	#	0.5592
SSCA	#	#	66.2	1.0	72.7	1.25 (1.15–1.36)	76.0	1.49 (1.36–1.62)	74.6	1.36 (1.25–1.48)	78.1	1.71 (1.57–1.87)	0.3382
Riks-Stroke	77.4	1.0	78.0	1.07 (1.02–1.12)	81.1	1.30 (1.24–1.37)	82.1	1.38 (1.31–1.45)	84.0	1.58 (1.50–1.66)	86.8	2.04 (1.94–2.15)	0.2299
NSSA	45.6	1.0	#	#	61.4	2.46 (2.30–2.64)	#	#	72.8	4.07 (3.78–4.37)	#	#	0.3745
Antiplatelet therapy‖													
ADSR	91.4	1.0	91.4	0.98 (0.92–1.05)	#	#	95.5	1.92 (1.77–2.08)	96.4	2.35 (2.17–2.55)	97.0	2.73 (2.52–2.96)	0.0964
POLKARD	93.4	1.0	93.7	1.10 (0.93–1.30)	#	#	94.1	1.18 (1.03–1.36)††	88.8	0.68 (0.56–0.82)††	#	#	0.1520
SSCA	#	#	85.3	1.0	87.8	1.24 (1.08–1.42)	88.8	1.38 (1.21–1.58)	90.7	1.72 (1.49–1.98)	88.1	1.30 (1.14–1.48)	0.0239
Riks-Stroke	91.7	1.0	91.3	0.95 (0.87–1.03)	91.4	0.96 (0.88–1.04)	92.1	1.06 (0.97–1.15)	91.6	0.99 (0.91–1.08)	91.5	0.97 (0.90–1.06)	0.0239
NSSA	97.7	1.0	#	#	96.4	0.67 (0.51– 0.86)	#	#	97.6	1.04 (0.80– 1.36)	#	#	0.21790
Anticoagulant therapy**													
ADSR	37.7	1.0	36.6	0.99 (0.92–1.07)	#	#	49.6	1.82 (1.69–1.96)	52.2	2.06 (1.91–2.21)	55.3	2.30 (2.15–2.47)	0.1014
POLKARD	26.0	1.0	26.4	0.99 (0.82–1.21)	#	#	25.0	0.94 (0.80–1.11)††	20.5	0.76 (0.58–1.01)††	#	#	0.1436
SSCA	#	#	39.5	1.0	38.6	0.89 (0.69–1.15)	41.0	1.10 (0.83–1.44)	37.8	0.93 (0.70–1.24)	30.7	0.88 (0.66–1.18)	0.1297
Riks-Stroke	32.5	1.0	31.6	0.96 (0.87–1.05)	31.0	0.95 (0.87–1.05)	33.0	1.09 (0.99–1.20)	36.1	1.24 (1.13–1.36)	37.2	1.37 (1.25–1.51)	0.0556
NSSA	37.6	1.0	#	#	32.9	0.86 (0.70–1.05)	#	#	34.3	0.94 (0.77–1.15)	#	#	0.0456

*Analyses were restricted to patients without missing values; % refers to patients adhering to the specific quality indicator; OR: odds ratio; CI: confidence interval; OR and 95% CI were derived from a logistic regression model adjusted for age, sex, stroke subtype (if applicable), day of admission, AF, and level of consciousness; #not documented or not documented in a comparable way or no documentation in the respective year; †all patients with IS, ICH, or UND and patients with swallowing test done and unassessable status; ‡In IS only, age between 18 and 80 years; §all patients with IS, ICH, or UND; ‖anytime during stay or at discharge in patients with IS alive at discharge and without anticoagulant therapy; **anytime during stay or at discharge or recommended at discharge in patients with IS and AF alive at discharge; ††POLKARD no complete calendar year of documentation; ‡‡variance partition coefficient, to account for between-centers variation within the audits.

for 75% of stroke patients to an acute Stroke Unit [23]. This figure was already nearly achieved in 2008 based on the audit data (72.8%). Consistently high levels of antiplatelet therapy were observed within the NSSA. The proportion of about 97% of patients treated with antiplatelets at discharge in the NSSA might represent a ceiling effect with the highest possible treatment proportion. The 2004 National Clinical Guideline for Stroke already recommended the prescription of antiplatelet agents for all patients with ischemic stroke or TIA who are not on anticoagulation [25]. The substantial increase in uptake of antiplatelet therapy in ischemic stroke patients in the ADSR between 2005 and 2007 may be explained by the revised guideline on the topic of diagnostic and therapy in neurology in 2005 that recommended also antiplatelets in the early stage after stroke [26]. The between-centers variation was mostly low, except for Stroke Unit treatment. Differences might be partly explained by voluntary participation in some of the audits (ADSR, POLKARD).

The study has limitations. Within the study, data from existing audits across Europe were analyzed. In contrast to other initiatives [27], there was no agreement on a common set of variables or a common method of data collection before the study took place. In addition, data were collected using different approaches (e.g., documentation of consecutively admitted patients by staff members versus chart review for defined sample of patients). Therefore, we cannot exclude that variations in data collection methods might have introduced some information bias in our analyses. There was no complete or no comparable information over time for some of the investigated quality indicators across all audits. In some of the audits (e.g., ADSR or POLKARD), there were no formal checks established for estimating completeness of case ascertainment neither within a center nor of centers included within a country as the participation of hospitals within the audit initiatives was voluntary. Therefore, we cannot exclude that some of the findings were caused by selection biases rather than real changes in quality of care provided, for example, by variations in case mix or patient selection across participating centers and countries. To maintain data accuracy, all of the audits used data validation tools such as plausibility checks. Additionally, source data verification was conducted by some of the audits. No outcome data such as death or disability at 90 days could be calculated due to the limited availability within the audits. It remains unclear if the increasing number of patients per center observed in some of the audits might be caused by a more complete documentation within the center or by increasing admission rates within the participating centers. However, restricting analysis to centers with complete information over the whole time period yielded similar estimates compared to including all centers in the analyses. We had only very limited information regarding the characteristics of the participating centers within the audits. Therefore, we were not able to investigate the potential influence of the center characteristics on time trends of appropriate care delivery. Unfortunately, we did not have comparable information on stroke severity based on standardized instrumental scales across audits because the audits used different scales for assessing stroke severity (e.g., NIHSS, Glasgow coma scale, and level of consciousness). We therefore used level of consciousness as proxy for adjusting for stroke severity. Furthermore, data were derived between 2004 and 2009 and the situation may have changed since then.

5. Conclusions

Heterogeneous patterns were identified in the five participating European audits regarding trends in quality of care over time. A general trend towards a better quality of stroke care provided over the study period was observed in most audits. The introduction of a specific performance measure within an audit activity might contribute to improved quality of acute stroke care provided over time.

Disclosure

Results were presented as oral presentation at the European Stroke Conference 2014 in Nice.

Conflict of Interests

Steffi Hillmann, Alec Fraser, Juan Baeza, Anthony Rudd, Kjell Asplund, Martin Dennis, Peter Hermanek, and Charles D. A. Wolfe declare that there is no conflict of interests regarding the publication of this paper; Silke Wiedmann receives research support from the German Ministry of Research and Education; Bo Norrving received money from Astra Zeneca (DSMB), Bayer (lecture and advisory board fee), and Daiichi Sankyo (lecture and advisory board fee) and research support from the European Union for this project (European Implementation Score Collaboration [EIS]; no. 223153); Maciej Niewada received research support from the National program for Prevention and Treatment of Cardiovascular Diseases POLKARD and Ministry of Science and Higher Education; Peter U. Heuschmann reports receiving grants from the European Union (within EIS) during study conduct and from the German Ministry of Research and Education, Charité, Berlin Chamber of Physicians, German Parkinson Society, University Hospital Würzburg, Robert-Koch-Institute, Charité-Universitätsmedizin Berlin (within MonDAFIS; MonDAFIS is supported by an unrestricted research grant to the Charité from Bayer), University Göttingen (within FIND-AFrandomized; FIND-AFrandomized is supported by an unrestricted research grant to the University Göttingen from Boehringer-Ingelheim), and University Hospital Heidelberg (within RASUNOA-prime; RASUNOA-prime is supported by an unrestricted research grant to the University Hospital Heidelberg from Bayer, BMS, Boehringer-Ingelheim), outside submitted work.

Authors' Contribution

Steffi Hillmann contributed to analysis and interpretation of the data and drafting the paper; Silke Wiedmann contributed to conceptualization of the study, analysis and interpretation of the data, and revising the paper; Alec Fraser

contributed to conceptualization of the study, analysis and interpretation of the data, and revising the paper; Juan Baeza contributed to conceptualization of the study and revising the paper; Anthony Rudd contributed to conceptualization of the study and revising the paper; Bo Norrving contributed to conceptualization of the study and revising the paper; Kjell Asplund, Maciej Niewada, Martin Dennis, and Peter Hermanek revised the paper; Charles D. A. Wolfe contributed to conceptualization of the study, analysis and interpretation of the data, and revising the paper; Peter U. Heuschmann contributed to conceptualization of the study, analysis and interpretation of the data, and drafting the paper.

Acknowledgments

The following audits participated in the EIS collaboration: ADSR (Bjoern Misselwitz, Ralf Hohnhold, Ingo Bruder, Klaus Berger, Barbara Hoffmann, Christine Matthis, Alfred Janssen, and Christoph Burmeister); POLKARD Hospital Stroke Registry (Anna Członkowska, Danuta Ryglewicz, Iwona Sarzyńska-Długosz, and Marta Skowrońska); SSCA (David Murphy, Hazel Dodds, Mary-Joan McLeod, Peter Langhorne, and Mark Barber); Catalan Stroke Audit (Sònia Abilleira and Miquel Gallofré); Riks-Stroke (Fredrik Jonsson); NSSA (Alex Hoffmann); Quality Register of Flemish Hospital Network of the KU Leuven, Flanders (Vincent Thijs). The study was funded by the European Union within the seventh Framework program (European Implementation Score Collaboration [EIS]; no. 223153).

References

[1] K. Asplund, K. Hulter Åsberg, P. Appelros et al., "The Riks-Stroke story: building a sustainable national register for quality assessment of stroke care," *International Journal of Stroke*, vol. 6, no. 2, pp. 99–108, 2011.

[2] P. U. Heuschmann and K. Berger, "International experience in stroke registries: German Stroke Registers study group," *American Journal of Preventive Medicine*, vol. 31, no. 6, supplement 2, pp. S238–S239, 2006.

[3] M. Niewada, M. Skowrońska, D. Ryglewicz, B. Kamiński, and A. Członkowska, "Acute ischemic stroke care and outcome in centers participating in the Polish National Stroke Prevention and Treatment Registry," *Stroke*, vol. 37, no. 7, pp. 1837–1843, 2006.

[4] S. Abilleira, A. Ribera, G. Permanyer-Miralda, R. Tresserras, and M. Gallofré, "Noncompliance with certain quality indicators is associated with risk-adjusted mortality after stroke," *Stroke*, vol. 43, no. 4, pp. 1094–1100, 2012.

[5] G. Cloud, A. Hoffman, and A. Rudd, "National sentinel stroke audit 1998–2011," *Journal of Clinical Medicine*, vol. 13, no. 5, pp. 444–448, 2013.

[6] M. J. Reeves, J. P. Broderick, M. Frankel et al., "The Paul Coverdell National Acute Stroke Registry: initial results from four prototypes," *American Journal of Preventive Medicine*, vol. 31, no. 6, pp. S202–S209, 2006.

[7] J. Ferrari, L. Seyfang, and W. Lang, "Can online benchmarking increase rates of thrombolysis? Data from the Austrian stroke unit registry," *Journal of Neurology*, vol. 260, no. 9, pp. 2271–2278, 2013.

[8] L. H. Schwamm, S. F. Ali, M. J. Reeves et al., "Temporal trends in patient characteristics and treatment with intravenous thrombolysis among acute ischemic stroke patients at get with the Guidelines—stroke hospitals," *Circulation: Cardiovascular Quality and Outcomes*, vol. 6, no. 5, pp. 543–549, 2013.

[9] M. K. Kapral, J. Fang, F. L. Silver et al., "Effect of a provincial system of stroke care delivery on stroke care and outcomes," *Canadian Medical Association Journal*, vol. 185, no. 10, pp. E483–E491, 2013.

[10] S. Wiedmann, B. Norrving, T. Nowe et al., "Variations in quality indicators of acute stroke care in 6 European countries: the European Implementation Score (EIS) Collaboration," *Stroke*, vol. 43, no. 2, pp. 458–463, 2012.

[11] A. Boaz, J. Baeza, and A. Fraser, "Effective implementation of research into practice: an overview of systematic reviews of the health literature," *BMC Research Notes*, vol. 4, article 212, 2011.

[12] M. G. George, X. Tong, H. McGruder et al., "Paul coverdell national acute stroke registry surveillance—four states, 2005–2007," *Morbidity and Mortality Weekly Report Surveillance Summary*, vol. 58, no. 7, pp. 1–23, 2009.

[13] K. Huang, N. Khan, A. Kwan, J. Fang, L. Yun, and M. K. Kapral, "Socioeconomic status and care after stroke: results from the Registry of the Canadian Stroke Network," *Stroke*, vol. 44, no. 2, pp. 477–482, 2013.

[14] D. Nikneshan, R. Raptis, J. Pongmoragot et al., "Predicting clinical outcomes and response to thrombolysis in acute stroke patients with diabetes," *Diabetes Care*, vol. 36, pp. 2041–2047, 2013.

[15] G. Saposnik, S. E. Black, A. Hakim, J. Fang, J. V. Tu, and M. K. Kapral, "Age disparities in stroke quality of care and delivery of health services," *Stroke*, vol. 40, no. 10, pp. 3328–3335, 2009.

[16] S. F. Jespersen, L. M. Christensen, A. Christensen, and H. Christensen, "Use of oral anticoagulation therapy in atrial fibrillation after stroke: results from a nationwide registry," *Thrombosis*, vol. 2013, Article ID 601450, 7 pages, 2013.

[17] S. Wiedmann, S. Hillmann, S. Abilleira et al., "Variations in acute hospital stroke care and factors influencing adherence to quality indicators in 6 European audits," *Stroke*, vol. 46, no. 2, pp. 579–581, 2015.

[18] T. A. D. Snijders and R. J. Bosker, *Introduction to Multilevel Analysis*, Sage, London, UK, 1999.

[19] E. R. McGrath, M. K. Kapral, J. Fang et al., "Association of atrial fibrillation with mortality and disability after ischemic stroke," *Neurology*, vol. 81, no. 9, pp. 825–832, 2013.

[20] J. Addo, A. Bhalla, S. Crichton, A. G. Rudd, C. McKevitt, and C. D. A. Wolfe, "Provision of acute stroke care and associated factors in a multiethnic population: prospective study with the South London Stroke Register," *British Medical Journal*, vol. 342, Article ID d744, 2011.

[21] P. U. Heuschmann, M. K. Biegler, O. Busse et al., "Development and implementation of evidence-based indicators for measuring quality of acute stroke care: the Quality Indicator Board of the German Stroke Registers Study Group (ADSR)," *Stroke*, vol. 37, no. 10, pp. 2573–2578, 2006.

[22] Riks-Stroke: The Swedish Stroke Register, Variables, March 2015, http://www.riksstroke.org/wp-content/uploads/2014/09/Acute-form-2004.pdf, http://www.riksstroke.org/wp-content/uploads/2014/09/Acute-form-2007.pdf.

[23] Department of Health, National Stroke Strategy, London, UK, 2007, http://clahrc-gm.nihr.ac.uk/cms/wp-content/uploads/DoH-National-Stroke-Strategy-2007.pdf.

[24] Socialstyrelsen, *National Guidelines for Stroke Care. Support for Priority Setting*, The National Board of Health and Welfare, 2005, http://www.socialstyrelsen.se/Lists/Artikelkatalog/Attachments/8934/2007-102-10_200710210.pdf.

[25] Intercollegiate Stroke Working Party, *National Clinical Guidelines for Stroke*, Royal College of Physicians, London, UK, 2nd edition, 2004, http://catalogue.iugm.qc.ca/GEIDEFile/stroke_guidelines_2ed.PDF?Archive=196040291422&File=stroke_guidelines_2ed_PDF.

[26] Deutsche Gesellschaft für Neurologie, *Leitlinien für Diagnostik und Therapie in der Neurologie. Vaskuläre Erkrankungen. Ischämischer Schlaganfall: Akuttherapie, 3*, Überarbeitete Auflage, Deutsche Gesellschaft für Neurologie, Stuttgart, Germany, 2005, http://www.agbrn.de/media/file/pdf/leitlinie_schlaganfall.pdf.

[27] S. C. Chung, R. Gedeborg, O. Nicholas et al., "Acute myocardial infarction: a comparison of short-term survival in national outcome registries in Sweden and the UK," *The Lancet*, vol. 383, pp. 1305–1312, 2014.

Hindawi Publishing Corporation
BioMed Research International
Volume 2015, Article ID 189292, 10 pages
http://dx.doi.org/10.1155/2015/189292

Research Article

Effects of Etanercept against Transient Cerebral Ischemia in Diabetic Rats

Naohiro Iwata,[1] Hiroko Takayama,[1] Meiyan Xuan,[2] Shinya Kamiuchi,[1] Hirokazu Matsuzaki,[3] Mari Okazaki,[3] and Yasuhide Hibino[1]

[1]*Laboratory of Immunobiochemistry, Department of Clinical Dietetics & Human Nutrition, Faculty of Pharmaceutical Sciences, Josai University, Saitama 350-0295, Japan*
[2]*Laboratory of Organic and Medicinal Chemistry, School of Pharmaceutical Sciences, Faculty of Pharmaceutical Sciences, Josai University, Saitama 350-0295, Japan*
[3]*Laboratory of Pharmacology, School of Pharmaceutical Sciences, Faculty of Pharmaceutical Sciences, Josai University, Saitama 350-0295, Japan*

Correspondence should be addressed to Yasuhide Hibino; seitaib@josai.ac.jp

Received 17 August 2015; Accepted 28 October 2015

Academic Editor: Gelin Xu

Diabetes mellitus is known to exacerbate acute cerebral ischemic injury. Previous studies have demonstrated that infarction volumes caused by transient cerebral ischemia were greater in diabetic rats than in nondiabetic rats. Tumor necrosis factor-α (TNF-α) is a proinflammatory protein produced in the brain in response to cerebral ischemia that promotes apoptosis. Etanercept (ETN), a recombinant TNF receptor (p75)-Fc fusion protein, competitively inhibits TNF-α. Therefore, we evaluated the neuroprotective effects of chronic or acute treatment with ETN on cerebral injury caused by middle cerebral artery occlusion/reperfusion (MCAO/Re) in rats with streptozotocin-induced diabetes. Furthermore, we evaluated the effects of ETN against the apoptosis and myeloperoxidase activity. Single administration of ETN before MCAO significantly suppressed exacerbation of cerebral damage in nondiabetic rats, as assessed by infarct volume. In contrast, the diabetic state markedly aggravated MCAO/Re-induced cerebral damage despite ETN treatment within 24 h before MCAO. However, the damage was improved by repeated administration of ETN at 900 μg/kg/daily in rats in an induced diabetic state. These results suggested that repeated administration of ETN can prevent exacerbation of cerebral ischemic injury in the diabetic state and is mainly attributed to anti-inflammatory effects.

1. Introduction

Diabetes mellitus (DM) is a metabolic disorder associated with chronic hyperglycemia, which is known to enhance systemic oxidative stress, predisposing patients to diabetic complications. World Health Organization data show that approximately 386 million people worldwide are currently suffering from diabetes, which is a major risk factor for atherosclerotic diseases, such as acute brain ischemia [1, 2]. Moreover, diabetic patients have a higher risk of stroke than nondiabetic patients and are more likely to have a poor prognosis and increased mortality after stroke [3, 4]. Previous studies have demonstrated that diabetes increased oxidative stress and inflammation in the brain [5] and aggravated cerebral ischemic injury in animal models [6–8]. Brain injury induced by focal ischemia is characterized by significant and rapid upregulation of cytokines, such as tumor necrosis factor-α (TNF-α). It is well known that inflammation has an essential role in the pathogenesis of transient cerebral ischemic injury [9].

TNF-α is a proinflammatory cytokine produced not only by macrophages but also by a broad variety of other cell types, such as endothelial cells, adipose tissue, fibroblasts, and neuronal tissue. Furthermore, TNF-α has been implicated in the pathogenesis of several central nervous system disorders, including cerebral ischemia, Parkinson's disease, and brain injury [10], as central mediators of tissue injury and inflammation. Extracellular TNF-α interacts with two cognate receptors, such as low-affinity p55 (TNFR1) and high-affinity p75 (TNFR2). Moreover, the activation of TNFR1

predominantly results in initiation of caspases involved in apoptosis [11, 12]. Thus, intracellular signaling suppression by TNF-α inhibition may be expected to be neuroprotective.

Etanercept (ETN) is a completely human fusion TNF-soluble receptor that inhibits the effect of the proinflammatory cytokine TNF-α, which has an important role in synovitis and joint damage in rheumatoid arthritis (RA) [13]. ETN acts as a decoy receptor by binding to TNF-α and TNF-β. ETN has been approved for treatment of RA in Japan since 2005 to reduce the biological activity of TNF by inhibiting the interaction between TNF receptors and TNF, and a marked effect on RA has been observed. In contrast, patients with ischemic stroke or diabetes have been recognized to show higher plasma concentrations of TNF-α, which is caused by elevated inflammation. Moreover, it has been reported that TNF-α concentration is increased in the cerebrospinal fluid in the ischemia. In the previous report, the traumatic brain injury- (TBI-) induced overproduction of IL-1β, TNF-α, and IL-6 in serum was significantly reduced by anti-TNF-α blockers. In contrast, etanercept therapy significantly increased the serum levels of IL-10 during TBI in rats. Furthermore, inhibition of gliosis has been observed in the brain [14]. In addition, NMDA receptor antagonist (MK801) and dexmedetomidine treatment has been reported to inhibit the production of TNF-α and improve cerebral infarction in the MCAO model [15, 16]. In recent years, inflammatory markers have been attracting attention as potential diagnostic markers [17, 18]. Therefore, the inflammatory reactions occurring in ischemic brain damage have increased interest in the development of therapies.

The objective of this study was to determine whether ETN-induced inhibition of TNF-α biological activity could improve brain damage caused by cerebral ischemia in streptozotocin- (STZ-) induced diabetic rats.

2. Materials and Methods

2.1. Animals and Reagents. Male Sprague-Dawley rats (4 weeks old, weight 120–140 g) were purchased from Japan SLC (Shizuoka, Japan) and housed under standard conditions in a temperature-controlled environment (23°C ± 0.5°C) with a cycle of 12 h of light and 12 h of darkness. The animals were allowed free access to rodent chow (CE-2; CLEA Japan, Tokyo, Japan) and water. Type 1 diabetes was induced in the rats by a single intraperitoneal injection of STZ (Sigma-Aldrich, St. Louis, MO, USA) (50 mg/kg of body weight) dissolved in 0.1 mM sodium citrate, pH 4.5 (diabetic; DM group), and the normal control rats (nondiabetic; non-DM group) were injected with the buffer only [6, 19]. Seven days after the injection of STZ, a blood sample was collected by tail vein paracentesis, and then plasma glucose was measured using a glucose analyzer (Ascensia; Bayer Yakuhin, Osaka, Japan). Diabetes was defined as a blood glucose level >300 mg/dL. Following this, the DM and non-DM groups were divided into two groups each, and the rats were housed for additional 6 weeks until stroke was induced by middle cerebral artery occlusion/reperfusion (MCAO/Re). Animal care and surgical procedures were performed in accordance with the guidelines approved by the National Institutes of Health (USA) and the Josai University Animal Research Committee. ETN was purchased from Pfizer Japan Inc. (Tokyo, Japan). The rats subjected to MCAO were divided into six treatment groups: Treatment 1, where non-DM rats were treated with ETN (300, 450, and 900 μg/kg, i.p.) within 24 h before MCAO, Treatment 2, where non-DM rats were treated with ETN (300, 450, and 900 μg/kg, i.v.) immediately after MCAO, Treatment 3, where non-DM rats were treated with ETN (300, 450, and 900 μg/kg, i.v.) immediately after MCAO/Re, Treatment 4, where DM rats were treated with ETN (450 and 900 μg/kg, i.v.) within 24 h before MCAO, Treatment 5, where DM rats were treated with ETN (450 and 900 μg/kg, i.v.) immediately after MCAO, and Treatment 6, where ETN (450 or 900 μg/kg, twice/week, i.p.) was repeatedly administered after the onset of diabetes for 5 weeks.

2.2. Middle Cerebral Artery Occlusion/Reperfusion. The experimental MCAO/Re rat model was prepared as described previously [6, 19]. The rats were anesthetized with 4% halothane and maintained with 1.5% halothane and 30% oxygen under spontaneous respiration. After a midline incision on the neck, the right common carotid artery was exfoliated under an operating microscope. All of the branches of the external carotid artery were ligated and isolated. The tip of the 4-0 surgical nylon monofilament rounded by flame heating was inserted through the internal carotid artery. When mild resistance was felt, the insertion was stopped. After occlusion for 2 h, the filament was withdrawn to enable reperfusion. The distance from bifurcation of the common carotid artery to the tip of the suture was approximately 20 mm in all of the rats. Cerebral blood flow was measured by laser Doppler flowmetry (ATBF-LC1; Unique Medical, Tokyo, Japan), and approximately 50% reduction of the baseline flow rate associated with MCAO was established in the non-DM and DM rats. The rats were allowed to recover from anesthesia at room temperature. The rectal temperature was maintained at 37°C using a heat lamp and a heating pad during the operation. All of the rats were killed after 24 h of reperfusion. A sham (control) operation involved the same manipulations but without insertion of the monofilament.

2.3. Plasma TNF-α Concentration. Enzyme-linked immunosorbent assay (ELISA) kits (Shibayagi, Gunma, Japan) were used according to the manufacturer's instructions to determine the secretion of TNF-α in plasma.

2.4. Infarction Assessment. After 24 h of reperfusion, the rats were subjected to general anesthesia using halothane and then decapitated. The brain was immediately removed and placed in ice-cold saline. Each brain was then placed in a brain matrix, and coronal sections were cut into 2 mm slices. The brain slices were immediately immersed in 2% 2,3,5-triphenyl tetrazolium chloride (TTC) (Wako Pure Chemicals Industries, Osaka, Japan) at 37°C for 15 min and then in 4% formaldehyde [19, 20]. Following this, infarction areas were identified by an image analysis system (Scion Image 1.62; Scion Corporation, Frederick, MD, USA) and were combined

to obtain the infarction volumes per brain according to the following formula: corrected infarction volume (%) = [left hemisphere volume − (right hemisphere volume − the infarction volume)] × 100/left hemisphere volume.

2.5. Neurological Evaluation. Postischemic neurological deficits were evaluated after 24 h of reperfusion on a five-point scale as follows: grade 0, no deficit; grade 1, failure to fully extend the right forepaw; grade 2, spontaneous circling or walking to a contralateral side; grade 3, walking only when stimulated; grade 4, not responding to stimulation and a depressed level of consciousness; and grade 5, death [19, 20]. Before MCAO, the neurological score was zero in all rats. The rats that did not exhibit neurological deficits after MCAO/Re were excluded from the study. Scoring was performed blindly on individual animals and averaged in groups.

2.6. Terminal Deoxyribonucleotidyl Transferase-Mediated Biotin-16-dUTP Nick End-Labeling Staining. Apoptosis in the brain tissues was measured by the Apoptosis In Situ Detection Kit Wako (Wako Pure Chemicals Industries), which is based on the terminal deoxyribonucleotidyl transferase-mediated biotin-16-dUTP nick end-labeling (TUNEL) procedure and involves addition of fluorescein-deoxyuridine triphosphate to 3′-terminals of apoptotically fragmented DNA with terminal deoxynucleotidyl transferase followed by immunochemical detection using anti-fluorescein antibody conjugated with horseradish peroxidase and 3-3′-diaminobenzidine tetrachloride as a substrate. Coronal brain sections (8 μm thick) were used for the assay. The slides were lightly counterstained with hematoxylin and observed under a microscope (BX51W1; Olympus, Tokyo, Japan). Quantification of TUNEL-positive cells was achieved by cell counting in areas of the penumbral cortex affected by ischemia. Three randomly chosen visual fields were counted in each region by an investigator without knowledge of the experimental conditions. The percentage of apoptotic cells was calculated by the apoptosis index, that is, dividing the number of positive-stained nuclei by the total number of nuclei [8].

2.7. Immunohistochemistry. Immunohistochemical staining was performed as described previously [21, 22]. The brain was fixed with 4% phosphate-buffered paraformaldehyde. Coronal brain sections (8 μm thick) were incubated with 3% hydrogen peroxide for 40 min at room temperature to inhibit endogenous peroxidase and then incubated with blocking buffer (4% Block Ace; Dainippon Sumitomo Pharma, Osaka, Japan) for 2 h. Following this, the slices were incubated with polyclonal rabbit anti-TNF-α antibody (1 : 200; Hycult Biotech, PB Uden, Netherlands) and monoclonal mouse anti-myeloperoxidase (MPO) antibody (1 : 100, Hycult Biotech) in 10 mmol/L phosphate-buffered saline (PBS) overnight at 4°C. After washing with PBS, the slices were incubated with either Cy3-conjugated donkey anti-rabbit IgG antibody (1 : 200; Millipore, Billerica, MA, USA) or FITC-conjugated goat anti-mouse IgG antibody (1 : 100; Zymed Laboratories, San Francisco, CA, USA) at room temperature for 2 h.

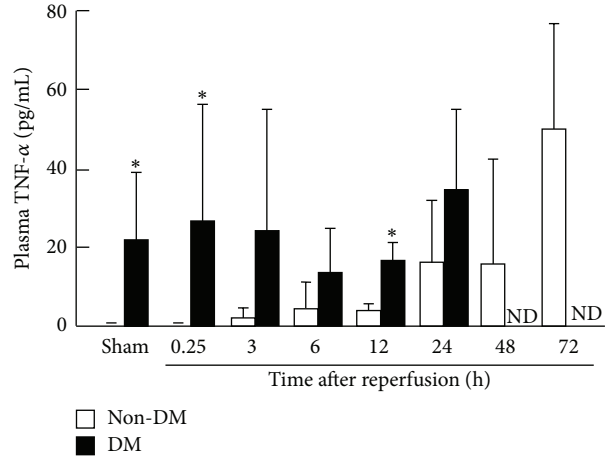

Figure 1: TNF-α concentrations in plasma after cerebral ischemia. The quantity of TNF-α in plasma after ischemia was determined by enzyme-linked immunosorbent assay. The open column is the non-DM group, and the closed column is the DM group. Data are means ± SDs (n = 4-5 per time point). $^*P < 0.05$ versus corresponding values for non-DM. DM, diabetes mellitus; ND, not determined; TNF, tumor necrosis factor.

Finally, the sections were incubated with the nuclear stain TO-PRO-3 (1 : 10,000; Invitrogen, Carlsbad, CA, USA) in PBS for 10 min at room temperature with gentle agitation, washed, and mounted using a 70% glycerol mounting medium. Immunofluorescence was visualized by a laser scanning confocal microscope (FluoView FV1000; Olympus). Fluorescence intensity was measured by imaging software (FV10-ASW 1.7; Olympus). Analyses of immunohistochemistry were performed by an investigator blinded to the treatment protocol. Three sections per rat and three to four rats per group were used for the analyses.

2.8. Statistical Analysis. The data are presented as mean ± SD. Two-way ANOVA and the subsequent post hoc Tukey's multiple comparison test were used for statistical analysis. Neurological deficit scores were analyzed by performing Kruskal-Wallis test followed by Mann-Whitney U test. In all cases, a P value of < 0.05 was assumed to denote statistical significance.

3. Results

3.1. Blood Glucose and Body Weight. Body weight and blood glucose data from the experimental rats were obtained throughout the study period (Table 1). The DM group had significantly decreased body weights and increased blood glucose levels relative to those of the non-DM control group. There were no significant differences in these parameters between the ETN-treated groups and their controls (data not shown).

3.2. Temporal Change in Plasma TNF-α Levels after Transient MCAO with Reperfusion. The plasma levels of TNF-α in the non-DM and DM groups were measured by ELISA (Figure 1). The concentration of TNF-α was gradually increased after

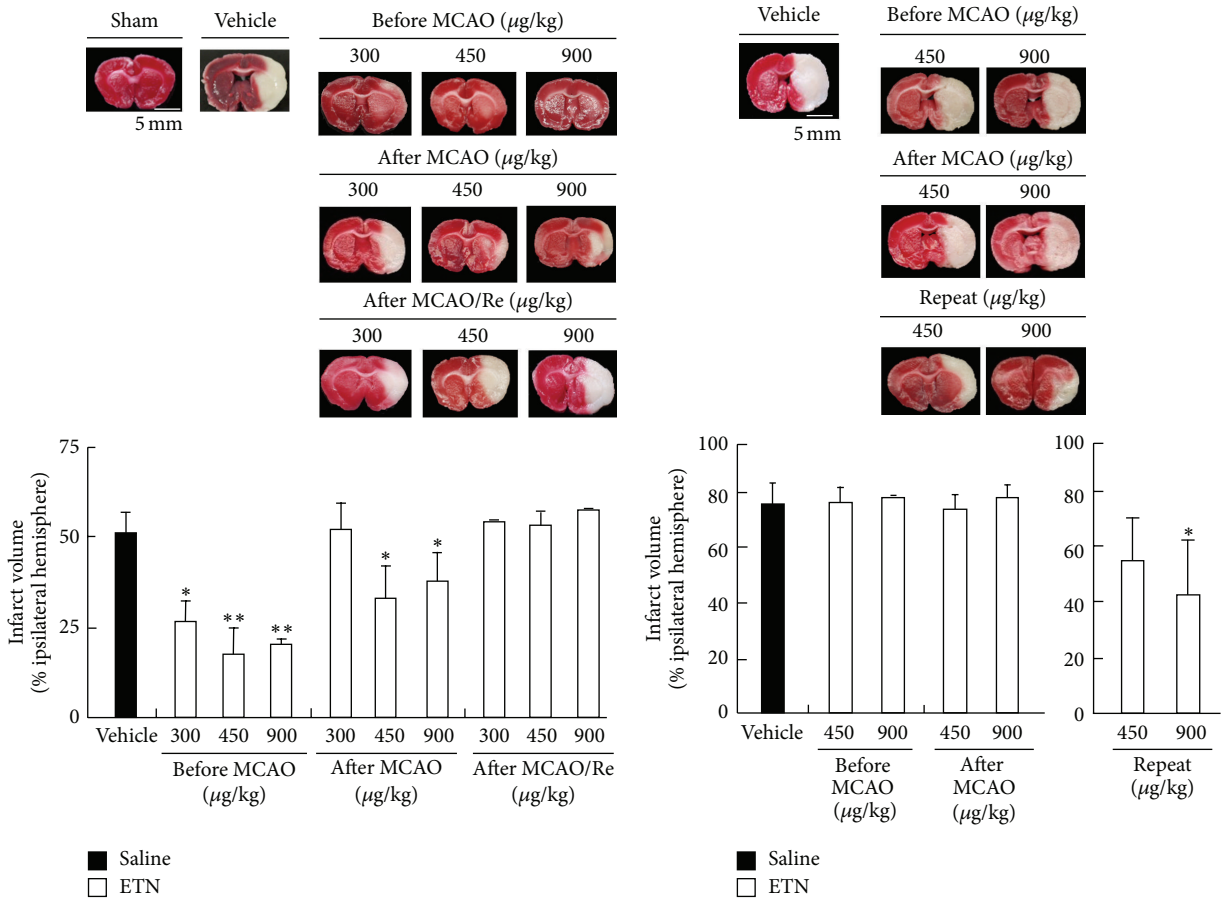

Figure 2: Effects of ETN on infarction induced by cerebral ischemia in non-DM and DM rat brains. (a) Representative coronal brain sections of the non-DM rats and the ETN group stained by TTC for various ETN administration conditions after reperfusion. (b) Representative coronal brain sections of the DM rats and the ETN group stained by TTC under various ETN administration conditions after reperfusion. The closed and open columns are the vehicle and ETN groups, respectively. Scale bar = 5 mm. Data are the means ± SDs (n = 3–6 per time point). $^{*,**}P < 0.05$ and 0.01 for statistical significance compared with the vehicle group. DM, diabetes mellitus; ETN, etanercept; TTC, 2,3,5-triphenyl tetrazolium chloride.

Table 1: Body weight and blood glucose levels in the non-DM and DM groups of rats.

Group	Body weight (g)	Blood glucose (mg/dL)
Non-DM	364 ± 27	123 ± 11
DM	261 ± 29**	423 ± 47**

The data are the means ± SD.
**$P < 0.01$ versus the non-DM group (n = 60).
DM, diabetes mellitus (n = 60).

reperfusion in the non-DM rats. In contrast, the amount of TNF-α was significantly increased (about 40-fold) in the sham-operated DM rats relative to that in the sham-operated non-DM rats. Furthermore, in the DM rats, TNF-α remained constant after reperfusion. No difference in the concentration of TNF-α in the DM rats was observed between sham-operation rats and after-reperfusion rats.

3.3. Infarction Volume after Transient MCAO with Reperfusion. Figure 2 shows representative coronal brain sections of the non-DM and DM rats stained by TTC after various ETN treatments and after or before cerebral ischemia. In the sham-operated rats, there was no apparent damage in any brain region. The infarction area in the non-DM after MCAO with 24 h reperfusion (vehicle-treated) rats was extended to the corpus striatum and cortex, whereas it was significantly decreased by ETN treatment (all groups within 24 h before MCAO or at 450 μg/kg ETN immediately after MCAO). In contrast, ETN administration to rats immediately after MCAO/Re did not improve brain damage (Figure 2(a)). Because the improvement effect was not observed for administration immediately after MCAO/Re in the non-DM group, this condition was not examined in the DM group. Instead, because increased expression of TNF-α was already observed in the sham DM group, a new group was prepared which received repeated ETN doses immediately after the onset of diabetes. Brain injury induced by MCAO/Re was remarkably exacerbated by DM state. In contrast, reduction of infarction was not observed in the single-dose group within 24 h before MCAO/Re or immediately after MCAO in the DM rats.

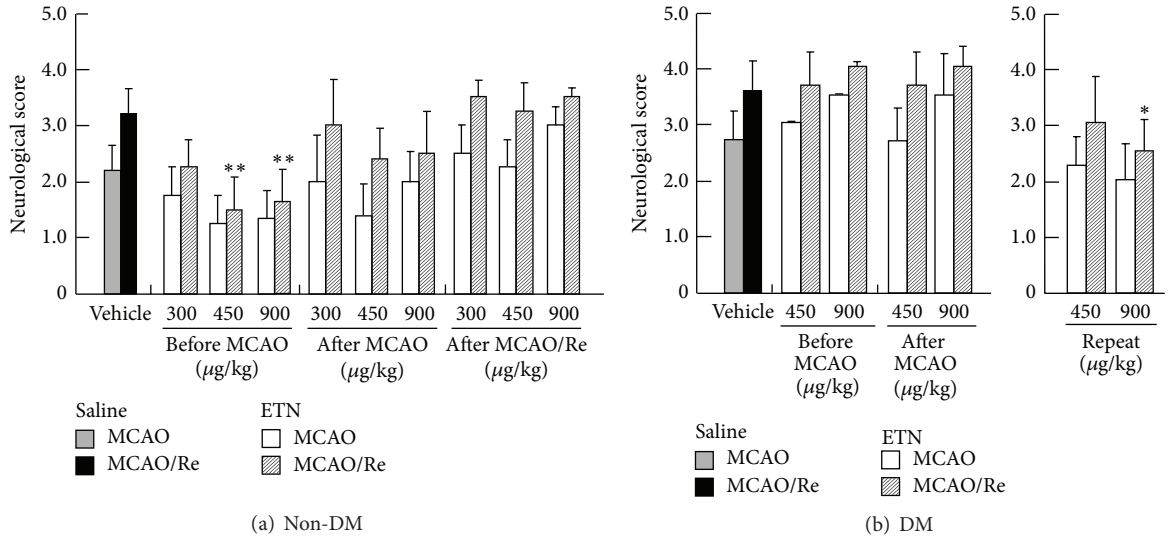

Figure 3: Effects of ETN on neurological deficits induced by cerebral ischemia in non-DM and DM rats. Assessment of neuronal damage after ischemia in non-DM (a) and DM (b) rats was determined by neurological score. Postischemic neurological deficits were evaluated at 2 h of MCAO and various ETN administration conditions after reperfusion. The shaded column is the MCAO-vehicle group; the closed column is the MCAO/Re-vehicle group; the open column is the MCAO-ETN group; the hatched column is the MCAO/Re-ETN group. Data are the means ± SDs (n = 3–6). $^{*,**}P < 0.05$ and 0.01 versus corresponding values for the MCAO/Re-vehicle group. DM, diabetes mellitus; ETN, etanercept; MCAO/Re, middle cerebral artery occlusion/reperfusion.

However, repeated administration of 450 μg/kg ETN led to a decreasing trend of infarction. In addition, significant improvement was clearly shown by the 900 μg/kg dose (Figure 2(b)). The timing of administration of saline had no effect (data not shown).

3.4. Neurological Deficits after Transient MCAO with Reperfusion. MCAO for 2 h in rats resulted in moderate neurological deficits, and the neurological evaluation value was increased (Figure 3). However, the ETN-pretreated (within 24 h before MCAO) non-DM rats showed significant alleviation in the neurological deficits relative to that in the vehicle-treated non-DM rats. In contrast, in the DM rats subjected to transient MCAO, severe neurological dysfunction was observed relative to that in the non-DM rats. In addition, ETN effect was not observed in the preischemic (within 24 h before MCAO) and immediately after MCAO-treatment rats. However, ETN-repeated treatment showed a significant improvement effect on neurological dysfunction caused by MCAO with reperfusion in diabetic rats. These results were consistent with those of the cerebral infarction volume.

3.5. Apoptosis Evaluation after MCAO with Reperfusion. Representative histological images of TUNEL staining in the non-DM vehicle, ETN-pretreated non-DM, DM vehicle, and ETN-pretreated DM groups subjected to MCAO and 24 h reperfusion are shown in Figure 4. Similar to the results of TTC staining, the number of TUNEL-positive cells was remarkably increased by MCAO/Re in the DM vehicle group relative to that in the non-DM vehicle group. Pretreatment of ETN (300, 450, and 900 μg/kg) significantly inhibited apoptosis activation induced by MCAO/Re in the non-DM groups. In contrast, ischemia treatment after administration of ETN (450 and 900 μg/kg) did not inhibit apoptosis in the DM rats. However, the DM rats were remarkably suppressed by repeated administration of ETN (450 and 900 μg/kg).

3.6. Inflammatory Activity after Transient MCAO with Reperfusion. To assess the effects of ETN treatment on expression of inflammatory factors, we performed immunohistochemical staining for TNF-α and MPO activities (Figure 5). The effect of expression of TNF-α in the brain cortex penumbra on infarction was evaluated by TTC staining in the non-DM and ischemia-treatment groups. Expression of TNF-α was reduced in a dose-dependent manner in the previous ETN treatment group. Furthermore, non-DM rats that were injected with ETN immediately after MCAO showed improvements at both concentrations of ETN (450 and 900 μg/kg). In contrast, the sham-operated DM rats had an increased number of TNF-α-positive cells. Expression of TNF-α was remarkably suppressed by repeated administration of ETN (450 and 900 μg/kg) in the DM rats. To examine the effect of ETN on the leukocytic infiltration, we investigated the expression of MPO (Figure 6). The MPO activity was decreased in a dose-dependent manner of ETN by the administration within 24 h before MCAO in the non-DM group. On the other hand, the MPO activity in the cortex that was increased during ischemia was enhanced in the DM group relative to that in the non-DM group. However, this activity was significantly suppressed by repeated administration of ETN from immediately after the onset of diabetes.

4. Discussion

Presence of diabetes is a risk factor for exacerbation of acute cerebral ischemic injury after cerebral infarction. In

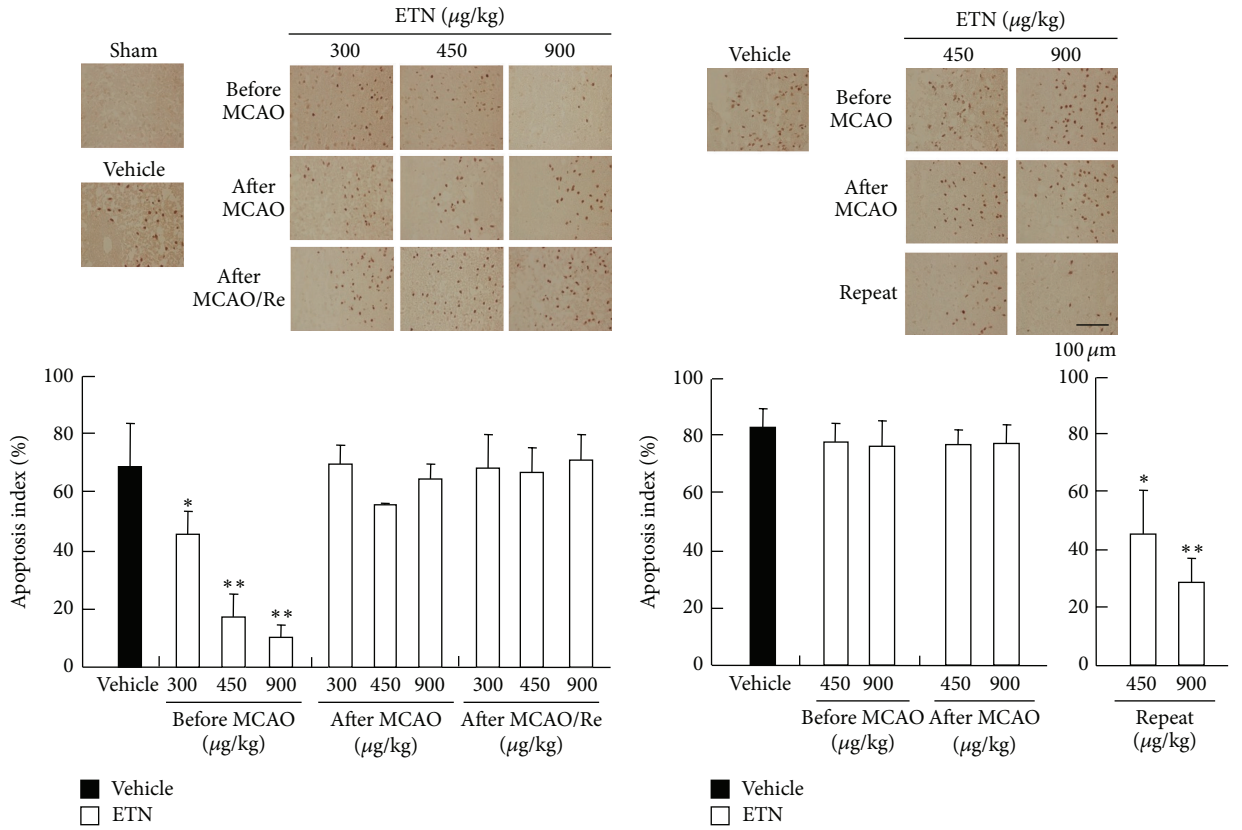

Figure 4: Effects of ETN on neuronal apoptosis induced by cerebral ischemia in rat brains. Representative photomicrograph and apoptosis index showing terminal deoxyribonucleotidyl transferase-mediated biotin-16-dUTP nick end-labeling-positive cells in the penumbra cortex in the non-DM group (a) and DM group (b) treated with ETN before and after ischemia. The closed column is the vehicle group, and the open column is the ETN group. Scale bar = 100 μm. Data are the means ± SDs (n = 3–7). $^{*,**}P < 0.05$ and 0.01 for statistical significance compared with the vehicle group. DM, diabetes mellitus; ETN, etanercept.

previous studies, we demonstrated that STZ-induced diabetic state markedly aggravated MCAO/Re-induced neurological deficits, infarction, and apoptosis in the rat brain [21]. Furthermore, we showed that levels of superoxide generation and proinflammatory cytokines (TNF-α and IL-1β) were upregulated in the DM cortex and were remarkably enhanced during reperfusion after ischemia [21, 22]. Therefore, we have assumed that the inflammatory response aggravates ischemic brain damage. The results of microarray analysis by IL-1β treatment of primary cultured astrocytes have been reported to give a change in the expression of 1,400 genes such as cytokines, chemokines, and matrix metalloproteinases (MMP) [16, 23]. In addition, TNF-α and IL-1β activate the NF-κB pathway, producing inflammatory materials such as IL-6. On the other hand, TNF-α and IL-1β are also known to promote release and production of neuroprotective factors. Therefore, the balance of the released inflammatory cytokines and anti-inflammatory cytokines will affect the subsequent cell failure [23, 24].

Blocking TNF-α has been proven to reduce brain damage and is considered to provide neuroprotective effects [25]. However, it is not clear if brain damage caused by cerebral infarctions exacerbated by diabetes is reduced by blocking TNF-α. We determined whether ETN-induced inhibition of TNF-α, which is upstream in the inflammatory response pathway, could provide protective effects against brain damage.

TNF-α is a proinflammatory cytokine that is synthesized in the brain within 1 h of an acute experimental ischemic stroke [26]. Intracerebroventricular injection of TNF-α exacerbates the extent of infarctions in experimental stroke [27]. Recent studies have reported that ETN suppressed brain injuries, such as cerebral contusions and subarachnoid hemorrhages [14, 28, 29]. Therefore, anti-TNF-α blockers such as ETN are expected to suppress aggravation of brain injury in diabetes. Measurements of blood TNF-α levels in rats with diabetes and ischemia showed that TNF-α increased with elapsed time after ischemia in the non-DM group. In contrast, TNF-α plasma concentrations in the DM group were about 40 times higher than those in the non-DM group. Thus, the diabetes pathology of chronic inflammatory reaction may have been enhanced in the whole body. Furthermore, because the plasma concentration of TNF-α was increased after cerebral ischemia, we assessed the cerebroprotective effect of ETN. In addition, to elucidate the effectiveness of administration of the drug, we examined the dose and

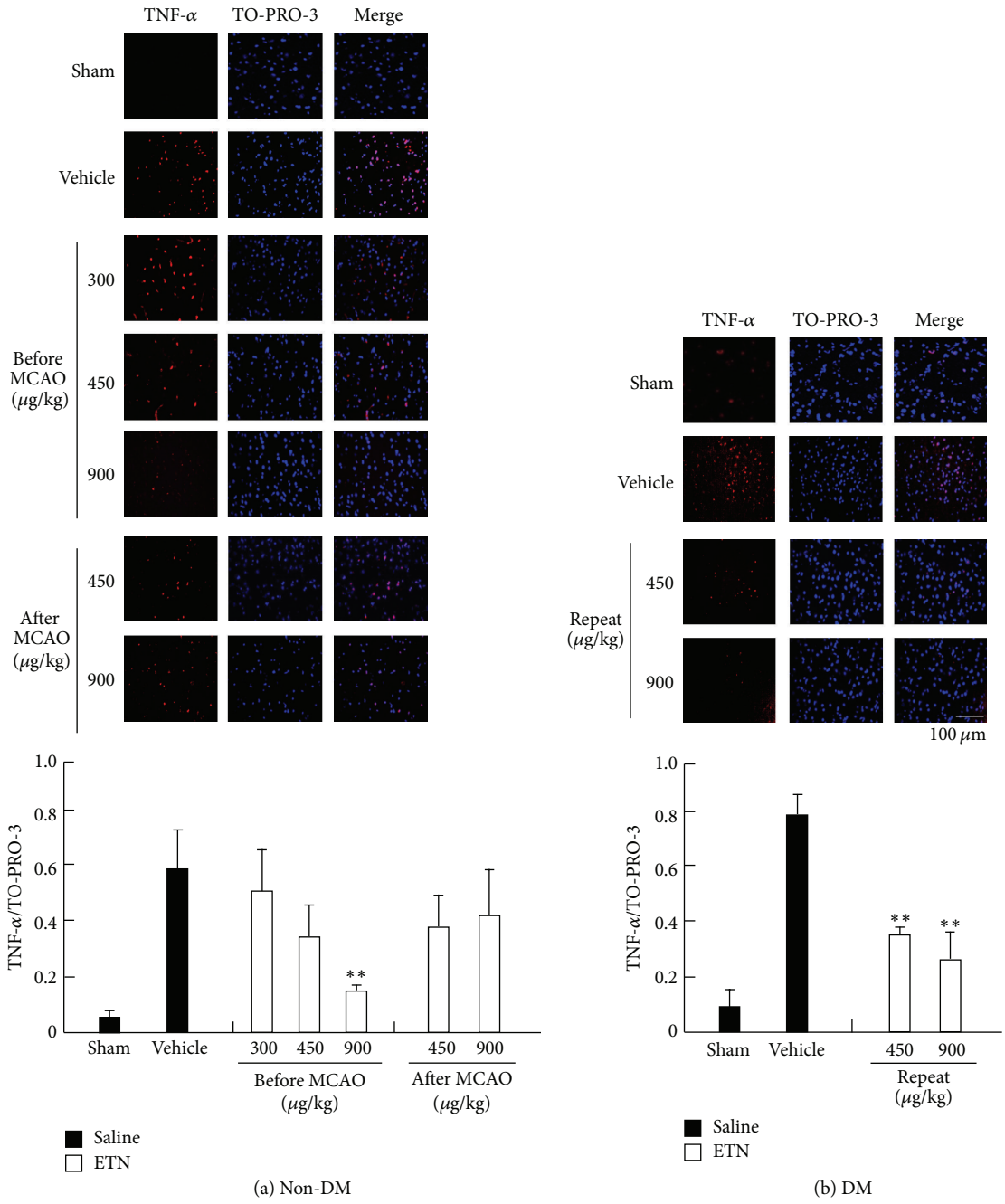

FIGURE 5: Immunohistochemical study of TNF-α in the cortex. Detection of TNF-α in the sham-operated non-DM (a) and DM (b) rat cortical neurons was determined by immunostaining and confocal imaging. The closed column is the sham or vehicle group, and the open column is the ETN group. Scale bar = 100 μm. $^{**}P < 0.01$ for statistical significance compared with the vehicle group. DM, diabetes mellitus; TNF, tumor necrosis factor.

timing of administration. We also examined the effectiveness of administration before and after treatment of cerebral ischemia. When ETN was intravenously administered after reperfusion in the non-DM rats, a cerebroprotective effect was not observed at any dose. However, improvement was observed at doses >450 μg/kg after ischemia. In addition, the non-DM group showed significantly decreased infarction size in all groups which were injected with ETN within 24 h before ischemia. In contrast, the DM group did not show any reduction of infarction size under all conditions. Therefore, we tried repeated administration of ETN for the purpose of inhibiting TNF-α in DM rats. A cerebroprotective effect was observed after repeated administration of ETN (900 μg/kg) immediately after diabetes onset. As shown in Figure 1, the amount of TNF-α in the sham-operation DM group was significantly increased relative to that in the non-DM group. Therefore, the cerebroprotective effect may depend on an effective ETN dose level. Activation of

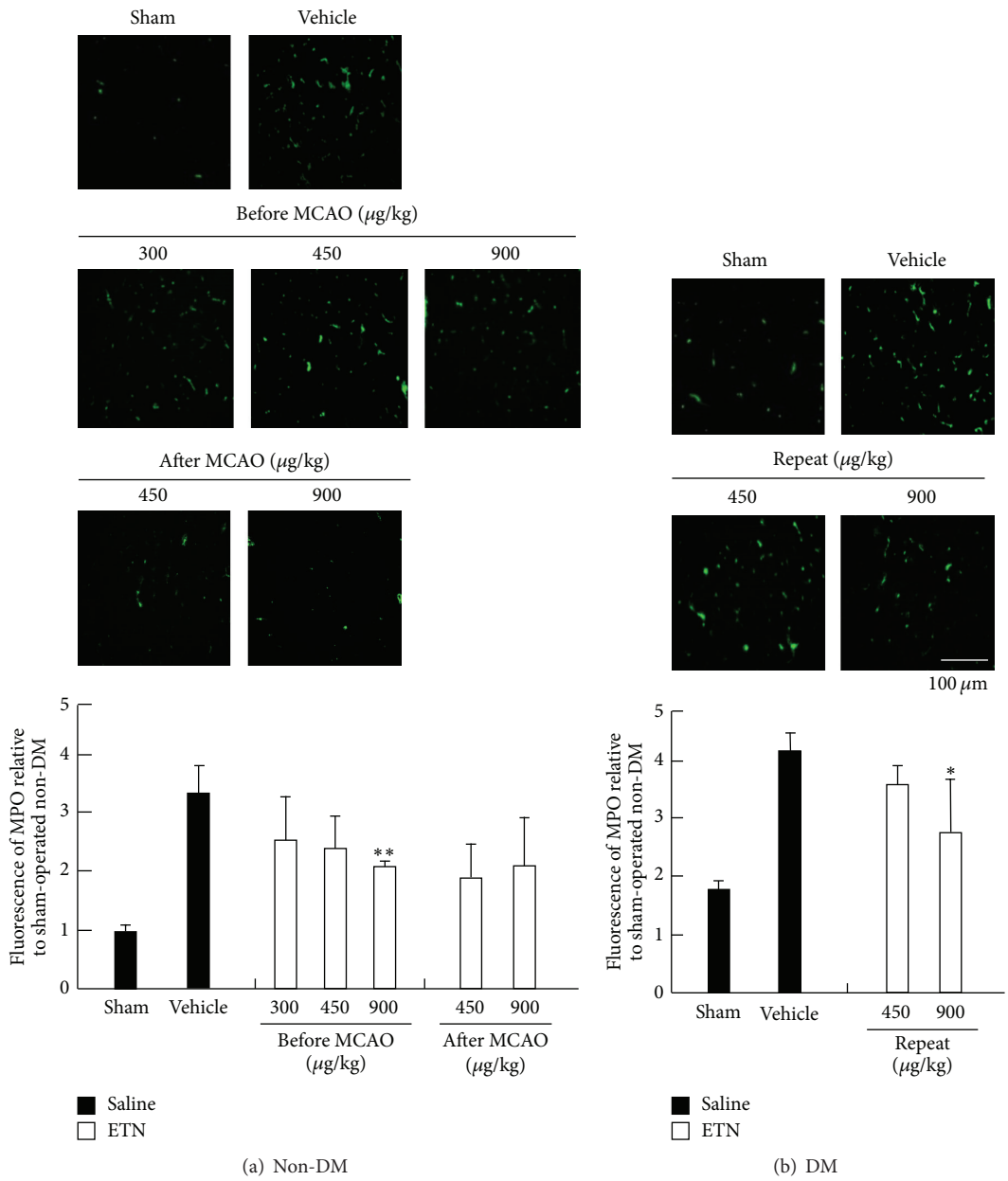

Figure 6: Immunohistochemical study of MPO activity in the cortex. Detection of MPO activity in the sham-operated non-DM (a) and DM (b) rat cortical neurons was determined by immunostaining and confocal imaging. The closed column is the sham or vehicle group, and the open column is the ETN group. Scale bar = 100 μm. $^{*,**}P < 0.05$ and 0.01 for statistical significance compared with the vehicle group. DM, diabetes mellitus; MPO, myeloperoxidase.

TNF-α signaling has been reported to induce apoptosis [30–33]. Moreover, TNF-α was shown to promote expression of MMP-9 and ICAM-1, induce infiltration of cells, and induce destruction of the blood-brain barrier (BBB) [34–36]. Furthermore, we confirmed that expression of TNF-α infiltration in leukocytes and apoptosis was observed after ischemia. However, ETN administration significantly inhibited inflammation and apoptosis. Expression of TNF receptors, such as TNFR1, was found to be elevated in the brain cortex in the DM and non-DM groups after ischemia (data not shown here). Therefore, diabetes, which may promote intracellular signaling by interaction with TNF receptors, may have enhanced inflammatory response.

For a drug to act in the brain, it is necessary to consider the permeability of the BBB. We do not have any data for the transition rate of ETN into the brain at present. Macromolecules in the blood are known to migrate to the brain from the results of permeation experiments after ischemia, as shown by Evans blue staining [22, 37, 38]. Consequently, ETN might have passed through to brain by the BBB failure after ischemia. The reason that there was no effect of the drug in the DM rats, compared with non-DM rats, may

be because of inflammation and nerve damage caused by ischemia. Recent evidence suggests that high-mobility group box 1 (HMGB1) prompted induction of proinflammatory mediators, including TNF-α, IL-1β, and cyclooxygenase-2 (COX-2), and contributed to postischemic brain damage [39–41]. In a previous study, we demonstrated that HMGB1 was released from necrotic cells in the early stage of ischemia in DM rats compared with non-DM rats [42]. Moreover, a COX inhibitor significantly attenuated TNF-α-induced BBB breakdown and free radical formation, which indicated that MMP-mediated BBB disruption during neuroinflammation can be significantly reduced by administration of COX inhibitors [43, 44]. It has been reported that the various cytokines causing ischemic brain disorders participate in complicated ways [9, 45]. Furthermore, TNF-α, which is involved in inflammation and cell injury, may affect the efficacy of a drug through two different activities that protect cells through TNFR2 [11, 12, 46]. To elucidate the details of ischemic injury in DM rats, further analysis is necessary in the future.

These results suggested that repeated administration of ETN relieves exacerbation of cerebral ischemic injury in diabetic rats primarily by its anti-inflammatory effects.

5. Conclusions

Our study results showed that inhibition of TNF-α by repeated ETN administration resulted in significant reduction of inflammation and neuronal cell death after experimentally induced cerebral ischemic brain injury in DM rats.

Conflict of Interests

The authors declare that there is no conflict of interests regarding the publication of this paper.

Acknowledgments

This study was supported by JSPS KAKENHI Grant nos. 23790750 and 15K21330. The authors would like to thank Enago (http://www.enago.jp/) for the English language review.

References

[1] J. W. Stephens, M. P. Khanolkar, and S. C. Bain, "The biological relevance and measurement of plasma markers of oxidative stress in diabetes and cardiovascular disease," *Atherosclerosis*, vol. 202, no. 2, pp. 321–329, 2009.

[2] J. W. Baynes, "Role of oxidative stress in development of complications in diabetes," *Diabetes*, vol. 40, no. 4, pp. 405–412, 1991.

[3] A. Vinik and M. J. Flemmer, "Diabetes and macrovascular disease," *Journal of Diabetes and its Complications*, vol. 16, no. 3, pp. 235–245, 2002.

[4] J. Biller and B. B. Love, "Diabetes and stroke," *The Medical Clinics of North America*, vol. 77, no. 1, pp. 95–110, 1993.

[5] T. Ahn, C.-H. Yun, and D.-B. Oh, "Tissue-specific effect of ascorbic acid supplementation on the expression of cytochrome P450 2E1 and oxidative stress in streptozotocin-induced diabetic rats," *Toxicology Letters*, vol. 166, no. 1, pp. 27–36, 2006.

[6] N. Iwata, M. Okazaki, C. Kasahara et al., "Protective effects of a water-soluble extract from culture medium of *Ganoderma lucidum* mycelia against neuronal damage after cerebral ischemia/reperfusion in diabetic rats," *Journal of Japan Society of Nutrition and Food Science*, vol. 61, no. 3, pp. 119–127, 2008.

[7] N. N. Rizk, J. Rafols, and J. C. Dunbar, "Cerebral ischemia induced apoptosis and necrosis in normal and diabetic rats," *Brain Research*, vol. 1053, no. 1-2, pp. 1–9, 2005.

[8] Z.-G. Li, M. Britton, A. A. F. Sima, and J. C. Dunbar, "Diabetes enhances apoptosis induced by cerebral ischemia," *Life Sciences*, vol. 76, no. 3, pp. 249–262, 2004.

[9] D. Amantea, G. Nappi, G. Bernardi, G. Bagetta, and M. T. Corasaniti, "Post-ischemic brain damage: pathophysiology and role of inflammatory mediators," *The FEBS Journal*, vol. 276, no. 1, pp. 13–26, 2009.

[10] U. Scherbel, R. Raghupathi, M. Nakamura et al., "Differential acute and chronic responses of tumor necrosis factor-deficient mice to experimental brain injury," *Proceedings of the National Academy of Sciences of the United States of America*, vol. 96, no. 15, pp. 8721–8726, 1999.

[11] O. Watters and J. J. O'Connor, "A role for tumor necrosis factor-α in ischemia and ischemic preconditioning," *Journal of Neuroinflammation*, vol. 8, article 87, 2011.

[12] K. M. Park and W. J. Bowers, "Tumor necrosis factor-alpha mediated signaling in neuronal homeostasis and dysfunction," *Cellular Signalling*, vol. 22, no. 7, pp. 977–983, 2010.

[13] T. Takeuchi, N. Miyasaka, S. Kawai et al., "Pharmacokinetics, efficacy and safety profiles of etanercept monotherapy in Japanese patients with rheumatoid arthritis: review of seven clinical trials," *Modern Rheumatology*, vol. 25, no. 2, pp. 173–186, 2015.

[14] C.-C. Chio, J.-W. Lin, M.-W. Chang et al., "Therapeutic evaluation of etanercept in a model of traumatic brain injury," *Journal of Neurochemistry*, vol. 115, no. 4, pp. 921–929, 2010.

[15] K. Sriram and J. P. O'Callaghan, "Divergent roles for tumor necrosis factor-α in the brain," *Journal of Neuroimmune Pharmacology*, vol. 2, no. 2, pp. 140–153, 2007.

[16] K. Tanabe and H. Iida, "The role of astrocytes in neuroprotection," *Anesthesia 21 Century*, vol. 15, no. 1–45, pp. 139–146, 2013.

[17] N. Sapojnikova, T. Kartvelishvili, N. Asatiani et al., "Correlation between MMP-9 and extracellular cytokine HMGB1 in prediction of human ischemic stroke outcome," *Biochimica et Biophysica Acta: Molecular Basis of Disease*, vol. 1842, no. 9, pp. 1379–1384, 2014.

[18] S. Oozawa, S. Sanoa, and M. Nishibori, "Usefulness of high mobility group box 1 protein as a plasma biomarker in patient with peripheral artery disease," *Acta Medica Okayama*, vol. 68, no. 3, pp. 157–162, 2014.

[19] N. Iwata, M. Okazaki, M. Xuan, S. Kamiuchi, H. Matsuzaki, and Y. Hibino, "Orally administrated ascorbic acid suppresses neuronal damage and modifies expression of SVCT2 and GLUT1 in the brain of diabetic rats with cerebral ischemia-reperfusion," *Nutrients*, vol. 6, no. 4, pp. 1554–1577, 2014.

[20] I. Kusaka, G. Kusaka, C. Zhou et al., "Role of AT_1 receptors and NAD(P)H oxidase in diabetes-aggravated ischemic brain injury," *American Journal of Physiology: Heart and Circulatory Physiology*, vol. 286, no. 6, pp. H2442–H2451, 2004.

[21] N. Iwata, M. Okazaki, R. Nakano et al., "Diabetes-mediated exacerbation of neuronal damage and inflammation after

cerebral ischemia in rat: protective effects of water-soluble extract from culture medium of *Ganoderma lucidum* mycelia," in *Advances in the Preclinical Study of Ischemic Stroke*, M. Balestrino, Ed., chapter 11, pp. 215–240, InTech, Rijeka, Croatia, 2012.

[22] L. Wang, Z. Li, X. Zhang et al., "Protective effect of shikonin in experimental ischemic stroke: Attenuated TLR4, p-p38MAPK, NF-κB, TNF-α and MMP-9 expression, up-regulated claudin-5 expression, ameliorated BBB permeability," *Neurochemical Research*, vol. 39, no. 1, pp. 97–106, 2014.

[23] S. M. Allan, P. J. Tyrrell, and N. J. Rothwell, "Interleukin-1 and neuronal injury," *Nature Reviews Immunology*, vol. 5, no. 8, pp. 629–640, 2005.

[24] Y. Zhao and D. A. Rempe, "Targeting astrocytes for stroke therapy," *Neurotherapeutics*, vol. 7, no. 4, pp. 439–451, 2010.

[25] C. A. Arango-Dávila, A. Vera, A. C. Londoño et al., "Soluble or soluble/membrane TNF-α inhibitors protect the brain from focal ischemic injury in rats," *International Journal of Neuroscience*, vol. 125, no. 12, pp. 936–940, 2015.

[26] T. Liu, R. K. Clark, P. C. McDonnell et al., "Tumor necrosis factor-alpha expression in ischemic neurons," *Stroke*, vol. 25, no. 7, pp. 1481–1488, 1994.

[27] F. C. Barone, B. Arvin, R. F. White et al., "Tumor necrosis factor-α. A mediator of focal ischemic brain injury," *Stroke*, vol. 28, no. 6, pp. 1233–1244, 1997.

[28] B.-F. Zhang, J.-N. Song, X.-D. Ma et al., "Etanercept alleviates early brain injury following experimental subarachnoid hemorrhage and the possible role of tumor necrosis factor-α and c-Jun n-terminal kinase pathway," *Neurochemical Research*, vol. 40, no. 3, pp. 591–599, 2015.

[29] A. Tuttolomondo, R. Pecoraro, and A. Pinto, "Studies of selective TNF inhibitors in the treatment of brain injury from stroke and trauma: a review of the evidence to date," *Drug Design, Development and Therapy*, vol. 8, pp. 2221–2238, 2014.

[30] L. W. Wang, Y. C. Chang, S. J. Chen et al., "TNFR1-JNK signaling is the shared pathway of neuroinflammation and neurovascular damage after LPS-sensitized hypoxic-ischemic injury in the immature brain," *Journal of Neuroinflammation*, vol. 11, article 215, 2014.

[31] L. Longhi, C. Perego, F. Ortolano et al., "Tumor necrosis factor in traumatic brain injury: effects of genetic deletion of p55 or p75 receptor," *Journal of Cerebral Blood Flow and Metabolism*, vol. 33, no. 8, pp. 1182–1189, 2013.

[32] M. Shuh, H. Bohorquez, G. E. Loss Jr., and A. J. Cohen, "Tumor necrosis factor-α: life and death of hepatocytes during liver ischemia/reperfusion injury," *Ochsner Journal*, vol. 13, no. 1, pp. 119–130, 2013.

[33] J. J. O'Connor, "Targeting tumour necrosis factor-α in hypoxia and synaptic signalling," *Irish Journal of Medical Science*, vol. 182, no. 2, pp. 157–162, 2013.

[34] H. Wei, S. Wang, L. Zhen et al., "Resveratrol attenuates the blood-brain barrier dysfunction by regulation of the MMP-9/TIMP-1 balance after cerebral ischemia reperfusion in rats," *Journal of Molecular Neuroscience*, vol. 55, no. 4, pp. 872–879, 2015.

[35] F. Takata, S. Dohgu, J. Matsumoto et al., "Brain pericytes among cells constituting the blood-brain barrier are highly sensitive to tumor necrosis factor-α, releasing matrix metalloproteinase-9 and migrating in vitro," *Journal of Neuroinflammation*, vol. 8, no. 106, 12 pages, 2011.

[36] G.-Y. Yang, C. Gong, Z. Qin, W. Ye, Y. Mao, and A. L. Bertz, "Inhibition of TNFα attenuates infarct volume and ICAM-1 expression in ischemic mouse brain," *NeuroReport*, vol. 9, no. 9, pp. 2131–2134, 1998.

[37] L. Wu, K. Zhang, G. Hu, H. Yang, C. Xie, and X. Wu, "Inflammatory response and neuronal necrosis in rats with cerebral ischemia," *Neural Regeneration Research*, vol. 9, no. 19, pp. 1753–1762, 2014.

[38] G. W. Kim, Y. Gasche, S. Grzeschik, J.-C. Copin, C. M. Maier, and P. H. Chan, "Neurodegeneration in striatum induced by the mitochondrial toxin 3-nitropropionic acid: role of matrix metalloproteinase-9 in early blood-brain barrier disruption?" *Journal of Neuroscience*, vol. 23, no. 25, pp. 8733–8742, 2003.

[39] Q.-W. Yang, J.-Z. Wang, J.-C. Li et al., "High-mobility group protein box-1 and its relevance to cerebral ischemia," *Journal of Cerebral Blood Flow and Metabolism*, vol. 30, no. 2, pp. 243–254, 2010.

[40] J. Qiu, M. Nishimura, Y. Wang et al., "Early release of HMGB-1 from neurons after the onset of brain ischemia," *Journal of Cerebral Blood Flow and Metabolism*, vol. 28, no. 5, pp. 927–938, 2008.

[41] M. Pizzi, I. Sarnico, A. Lanzillotta, L. Battistin, and P. Spano, "Post-ischemic brain damage: NF-κB dimer heterogeneity as a molecular determinant of neuron vulnerability," *The FEBS Journal*, vol. 276, no. 1, pp. 27–35, 2009.

[42] N. Iwata, M. Okazaki, S. Kamiuchi et al., "Early release of HMGB1 may aggravate neuronal damage after transient focal ischemia in diabetic rat brain," *International Journal of Diabetes and Clinical Research*, vol. 2, no. 1, 2015.

[43] E. Candelario-Jalil, Y. Yang, and G. A. Rosenberg, "Diverse roles of matrix metalloproteinases and tissue inhibitors of metalloproteinases in neuroinflammation and cerebral ischemia," *Neuroscience*, vol. 158, no. 3, pp. 983–994, 2009.

[44] E. Candelario-Jalil, S. Taheri, Y. Yang et al., "Cyclooxygenase inhibition limits blood-brain barrier disruption following intracerebral injection of tumor necrosis factor-α in the rat," *The Journal of Pharmacology and Experimental Therapeutics*, vol. 323, no. 2, pp. 488–498, 2007.

[45] S. Suzuki, K. Tanaka, and N. Suzuki, "Ambivalent aspects of interleukin-6 in cerebral ischemia: inflammatory versus neurotrophic aspects," *Journal of Cerebral Blood Flow and Metabolism*, vol. 29, no. 3, pp. 464–479, 2009.

[46] J. M. Hallenbeck, "The many faces of tumor necrosis factor in stroke," *Nature Medicine*, vol. 8, no. 12, pp. 1363–1368, 2002.

Hindawi Publishing Corporation
BioMed Research International
Volume 2015, Article ID 175719, 10 pages
http://dx.doi.org/10.1155/2015/175719

Research Article

The Effect of Body Weight Support Treadmill Training on Gait Recovery, Proximal Lower Limb Motor Pattern, and Balance in Patients with Subacute Stroke

Yu-Rong Mao,[1] Wai Leung Lo,[1] Qiang Lin,[1] Le Li,[1] Xiang Xiao,[1] Preeti Raghavan,[2] and Dong-Feng Huang[1]

[1]*Department of Rehabilitation Medicine, Guangdong Provincial Research Center for Rehabilitation Medicine and Translational Technology, The First Affiliated Hospital, Sun Yat-sen University, Guangzhou 510080, China*
[2]*Motor Recovery Research Laboratory, Department of Rehabilitation Medicine, RUSK Rehabilitation, New York, NY 10016, USA*

Correspondence should be addressed to Preeti Raghavan; preeti.raghavan@nyumc.org and Dong-Feng Huang; huangdf@mail.sysu.edu.cn

Received 23 July 2015; Accepted 21 October 2015

Academic Editor: Vida Demarin

Objective. Gait performance is an indicator of mobility impairment after stroke. This study evaluated changes in balance, lower extremity motor function, and spatiotemporal gait parameters after receiving body weight supported treadmill training (BWSTT) and conventional overground walking training (CT) in patients with subacute stroke using 3D motion analysis. *Setting*. Inpatient department of rehabilitation medicine at a university-affiliated hospital. *Participants*. 24 subjects with unilateral hemiplegia in the subacute stage were randomized to the BWSTT ($n = 12$) and CT ($n = 12$) groups. Parameters were compared between the two groups. Data from twelve age matched healthy subjects were recorded as reference. *Interventions*. Patients received gait training with BWSTT or CT for an average of 30 minutes/day, 5 days/week, for 3 weeks. *Main Outcome Measures*. Balance was measured by the Brunel balance assessment. Lower extremity motor function was evaluated by the Fugl-Meyer assessment scale. Kinematic data were collected and analyzed using a gait capture system before and after the interventions. *Results*. Both groups improved on balance and lower extremity motor function measures ($P < 0.05$), with no significant difference between the two groups after intervention. However, kinematic data were significantly improved ($P < 0.05$) after BWSTT but not after CT. Maximum hip extension and flexion angles were significantly improved ($P < 0.05$) for the BWSTT group during the stance and swing phases compared to baseline. *Conclusion*. In subacute patients with stroke, BWSTT can lead to improved gait quality when compared with conventional gait training. Both methods can improve balance and motor function.

1. Introduction

The worldwide prevalence of stroke was estimated in 2010 to be 33 million. Stroke is the second-leading global cause of death behind heart disease [1]. The incidence and prevalence of stroke in China are highest in the world [2, 3]. According to a recent epidemiological study on the global burden of stroke, the incidence of stroke in China has increased from 226/100,000 person-years in 1990 to 240/100,000 person-years in 2010 [1]. Walking ability and ambulatory independence determine the level of disability and likelihood of institutionalization in patients with hemiplegia [4, 5]. The degree to which gait can be restored after stroke is related to both the initial impairment in walking ability and the severity of lower extremity paresis [6, 7]. Early intervention with physical therapy to restore walking after stroke was recommended to improve motor function and decrease disability [8, 9]. Previous kinematic data indicated better outcome for patients who started rehabilitation programme at early stage than those who started late [10].

Gait performance is an indicator of mobility impairment and disability after stroke [6]. It predicts mortality, morbidity, and risk of future stroke [5, 11, 12]. Gait speed is responsive to short-term rehabilitation [8]. An improvement in gait speed

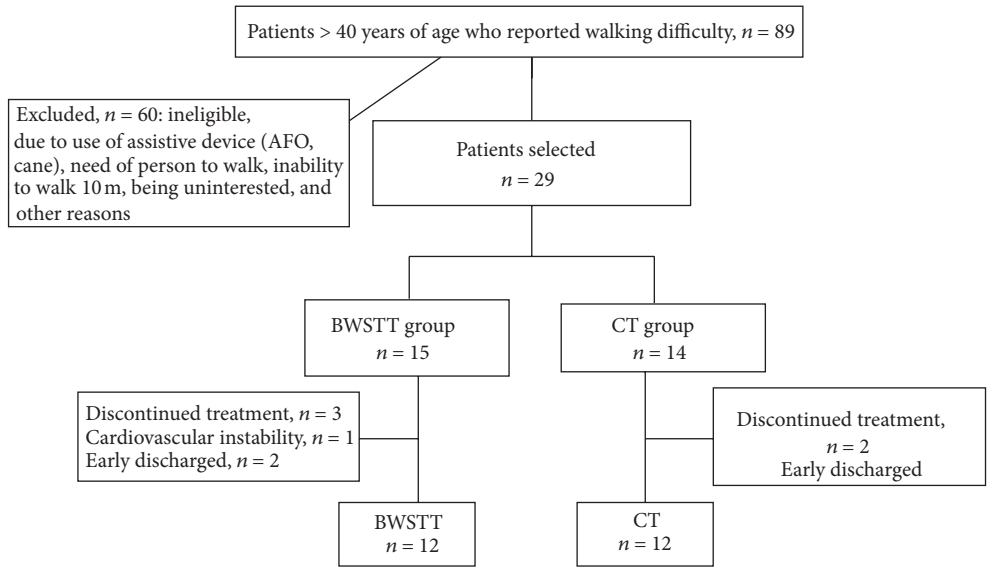

Figure 1: Flowchart for subjects selection process.

of 0.16 m/s can reduce the level of assistance in patients with subacute stroke and was recommended to be the minimum clinically significant difference [13]. The control of gait involves the planning and execution from multiple cortical areas, such as secondary and premotor cortex [14, 15]. Stroke patients often have gait impairment such as decreased gait speed and asymmetrical gait cycle [16] as a result of cortical reorganization [17, 18]. Repetitive mass motor task practice had been shown to facilitate neuroplasticity and brain reorganization in stroke patients, resulting in enhanced motor recovery after stroke [19–23]. Near-infrared spectroscopic imaging and functional magnetic resonance imaging have demonstrated treatment induced changes of brain activation pattern during walking and after gait training [18, 24, 25]. Abnormal gait pattern in stroke patients is characterized by altered kinematic and kinetic parameters of hip, knee, and ankle joint during a gait cycle. Published studies have shown that proximal lower limb control plays a key role in improving gait speed and walking performance after stroke [26, 27]. The greater hip sagittal range of motion could avert circumduction profiles [28].

Body weight supported treadmill training (BWSTT) is a task-oriented technique for gait restoration after stroke [29–31]. BWSTT has the advantage over conventional therapy as it offers higher intensity, more repetitive and task-oriented practice over the same period of time when compared to conventional therapy [32]. Several studies have showed that BWSTT was more effective in gait speed improvement than regular physiotherapy [29, 31–34]. It has been demonstrated that BWSTT induces changes in corticomotor excitability which lead to improved balance and gait performance with chronic stroke [18]. However, other studies have reported that BWSTT was not superior to conventional gait training [35, 36]. Recent studies have reported that BWSTT can increase walking endurance in the subacute stage after stroke, but no improvement was reported in balance and 10 m gait speed [37]. To date, there are very few studies that have used gait analysis to show how the improvements in gait parameters come about after BWSTT or conventional therapy. There is still a lack of basic understanding of gait training on human locomotion [38]. Since gait impairments are a result of deficient neuromuscular control, a better understanding of the impact of gait training on lower limb motor pattern is therefore essential. Improvement on individual biomechanical subtasks of walking such as leg swing or balance control is positively associated with walking performance [39]. The purpose of this study is to investigate the changes in spatiotemporal characteristics of gait after BWSTT intervention and conventional therapy (CT), using three-dimensional motion analysis of gait in patients with stroke at the subacute stage. Based on corticomotor excitability theory and the advantage of BWSTT over CT, it is hypothesized that BWSTT training is superior to CT training in improving kinetic and kinematic gait parameters from the period before to the one after training. In addition, we investigated the impact of BWSTT on balance and lower extremity impairment when compared to CT.

2. Methods

2.1. Subjects. Subjects with subacute stroke (18 to 76 days after stroke) were recruited for this study and were randomly assigned to the BWSTT and CT groups (Figure 1). The inclusion criteria for the hemiparetic subjects were (1) stroke confirmed by computed tomography or MRI; (2) unilateral hemiparesis for no more than 3 months resulting from first stroke; (3) residual gait impairment, defined by an abnormal 10 m walk time according to age (age < 60 = 10 seconds or longer or 1 m/s; age 60 to 69: 12.5 seconds or longer or 0.8 m/s; age ≥ 70: 16.6 seconds or longer, <0.6 m/s) [24]; and adequate mental and physical capacity to attempt the tasks as instructed (Mini Mental State Examination score ≥ 27,

average modified Ashworth scale score at hip, knee, and ankle ≤ 2).

Exclusion criteria were the presence of significant medical complications or unstable vital signs that precluded participation in the study. Twelve healthy adults matched for age, weight, leg length, and gender were also recruited to provide reference data for gait analysis. This study was approved by the Human Subjects Ethics Subcommittee of the First Affiliated Hospital, Sun Yat-sen University, China. Written consent was obtained from all participants prior to the experiment.

2.2. Training Protocol. All recruited stroke subjects received two hours of rehabilitation every weekday which was the standard of care in China. This included 60 minutes each of physical therapy and occupational therapy. The physical therapy sessions consisted of approximately 20–40 minutes of therapeutic exercises and 20–40 minutes of gait training. For gait training, subjects were randomly allocated to either BWSTT or conventional overground training for a period of 3 weeks. The therapeutic exercises component in all subjects remained the same and included range of motion and strengthening exercises, as well as facilitation techniques to recruit muscle activity on the paretic extremity. Occupational therapy session includes the use of functional stimulation and self-exercise program. All physical therapists involved in the study were trained on the protocol. Participants' daily compliance with the protocol was documented. In addition, the entire rehabilitation team was educated on the study protocol to ensure compliance when participants were not working with study-designated therapy staff.

The equipment for BWSTT consisted of a standard treadmill fitted with the weight supporting apparatus (Noramco Fitness and SpinoFlex, USA). The patient wore a modified mountain climber's harness with an adjustable belt around the pelvis and thigh and an adjustable belt above to support their body weight. A physiotherapist assisted with leg propulsion if the patient could not lift his/her paretic leg. At the beginning of training, some subjects needed two therapists to guide the movement of the pelvis forward and to flex and extend the hemiplegic leg during the swing and stance phases of gait. The initial body weight support was set at 30%~40%, the speed of the treadmill was set at 0.5 mph (miles per hour), and the duration of training was for 20 minutes. As treatment progressed, the body weight support was gradually decreased and the velocity was gradually increased. The two parameters were not changed simultaneously. By the third week the treadmill speed was increased to 2.5 mph and duration of training increased to 40 minutes. The training parameters were based on recommendation from previous literature [6]. Subjects were consulted throughout the training for fatigue level and tolerance of progression.

The CT group received individualized overground gait training by a physiotherapist for 30 minutes, five days a week, for three weeks. The training was based on the principles of neurodevelopmental therapy (Bobath method).

Heart rate and blood pressure were monitored in both groups before and after each session and during break using a digital sphygmomanometer.

2.3. Gait Analysis Protocol. Vicon Motion Analysis System (VICON MX13, VICON Peak, Oxford, UK) and two AMTI force plates (AMTI, OR6-7, Watertown, MA, USA) with sampling frequency of 1000 Hz recorded the joint angles and moments of the lower extremity in the sagittal plane simultaneously.

Six infrared 100 Hz cameras recorded the locations of 16 passive reflective markers taped to the skin overlying bony landmarks of the pelvis and both lower limbs, including the sacrum at the level of the posterior superior iliac spines, anterior superior iliac spines, lower lateral one-third and half-way points on the thighs, lateral epicondyle of knees, lower lateral one-third and half-way pints on the shank, lateral malleolus, the second metatarsal head, and the calcaneus at the same height as the second metatarsal head. The data were captured using Vicon Nexus (version 1.7.1) and Plugin Gait.

During gait analysis, all subjects were asked to walk back and forth at a self-selected walking speed on a 10-meter carpet. The subjects walked without canes, orthoses, or other assisted devices during the assessments. Five successful gait cycles (defined as one foot on one force plate) were selected for analysis at baseline and after 3 weeks of training. Marker trajectories were sampled at 100 Hz for the calculation of lower extremity joint angles and moments. Each walking trial was normalized to the total duration of the gait cycle (one foot strike to the next foot strike). Stance and swing phases of the gait cycle were presented as a percentage. The joint angles and moments were also normalized to the height and weight of each subject.

Lower limb impairment and balance were measured by Fugl-Meyer Lower Extremity Assessment (FMA-LE) [40] and the Brunel balance assessment [41, 42] scale. Measurements were recorded in stroke subjects at baseline and after 3 weeks of training by an examiner who was blinded to group assignment.

2.4. Data Processing. Spatiotemporal gait parameters, joint angles, and moment of the lower limb were processed using Polygon (version 3.5.1) and the mean data from 5 walking cycles were computed for each subject. The spatiotemporal parameters computed were cadence, stride time and length, step time and length, and walking speed. Kinematic and kinetic parameters of joint angles and moments at ankle, knee, and hip joints were recorded in the sagittal plane. Parameters were recorded at (1) maximum extension during the stance phase; (2) maximum flexion at the hip and knee joints during the swing phase; (3) plantarflexion during push-off; and (4) dorsiflexion during the swing phase of the gait cycle [43]. Spatiotemporal gait parameters of (1) cadence; (2) stride length; (3) stride time; (4) step length; (5) step time and gait speed; (6) peak angular flexion and extension; and (7) peak moments flexion and extension were recorded at the hip, knee, and angle joints in the sagittal plane.

2.5. Statistical Analysis. Data analyses were performed using SPSS version 15.0. Descriptive statistics were computed for demographic characteristics and for all parameters. Anthropometric data (age, body weight, postinjury date, and leg length) for the three groups were compared using one-way

Table 1: Summary of demographic data.

Demographics	Normal group X (SD)	BWSTT group X (SD)	CT group X (SD)	P
Sex, number (%) of women	10 (83%)	10 (83%)	9 (75%)	
Affected side, left, number (%)	—	6 (50%)	6 (50%)	
Cerebral infarction, number (%)	—	11 (91.7%)	10 (83.3%)	
Age (y)	58.83 (8.03)	59.55 (9.23)	60.82 (10.70)	0.906
Body weight (kg)	63.08 (11.31)	65.17 (10.26)	65.25 (11.42)	0.987
Leg length (mm)	828.33 (42.12)	826.7 (53.78)	817.10 (60.1)	0.680
Days of postinjury	—	49.25 (19.51)	47.67 (16.78)	0.860

Table 2: Lower extremity function and balance score for normal group, BWSTT group, and CT group.

	Normal group X (SD)	BWSTT group X (SD)	CT group X (SD)	Between-group difference
MMSE score (0–30)	30	28.41 (1.16)	28.33 (1.37)	0.874
FMA (pre)	34	22.42 (4.36)	22.08 (6.44)	0.868
FMA (post)	—	24.33 (4.58)*	25.17 (5.62)*	0.633
Brunel (pre)	12	10.33 (1.30)	10.42 (1.38)	0.884
Brunel (post)	—	10.83 (1.44)*	10.92 (1.68)*	0.870

*Differences between the period before and that after training were statistically significant.

ANOVA at baseline. Paired samples t-test was used to assess the differences between pre- and postintervention within each group. Between-group differences were assessed by independent samples t-test. Statistical significant level was set as $P < 0.05$ (2-tailed).

3. Results

Twenty-nine stroke subjects who met the inclusion criteria were recruited. Five subjects were dropped out from the study. One subject experienced changes in health status unrelated to the study and four subjects were prematurely discharged from the hospital due to medical insurance issues. Twenty-four stroke subjects who completed all experimental protocols were included in the final data analysis. The two stroke groups showed no statistical significant differences in age and other anthropomorphic parameters. They were matched with age, weight, leg length, and gender to a healthy control group. There is no statistical significant difference in FMA-LE and Brunel balance tests between the two stroke groups at baseline (Table 1).

3.1. Balance and Lower Extremity Function. After three weeks of training, both BWSTT and CT groups improved significantly on the FMA-LE and on the Brunel balance scale (Table 2). The between-group differences were not statistically significant.

3.2. Spatiotemporal Parameters. The BWSTT group improved significantly in all spatiotemporal gait parameters during a gait cycle after interventions, whereas the CT group did not (Table 3). Cadence and gait speed were significantly higher in the BWSTT group than CT group after training.

3.3. Kinematic and Kinetic Parameters during Gait. Averaged kinematic trajectories of the hip, knee, and ankle joints in healthy controls and subjects with stroke in the BWSTT and CT groups are shown in Figure 2. Subjects with stroke were able to flex their hip joints comparable to the healthy control group but could not extend the hip adequately before training (Figures 2(a) and 2(b)). BWSTT group showed significantly reduced hip flexion and increased peak hip extension after training (Table 4), whereas the CT group did not. There were no significant differences in the angle of knee flexion or extension and ankle dorsiflexion or plantarflexion or in the peak moments at the hip, knee, or ankle joints in either the BWSTT group or the CT group ($P > 0.05$) after interventions (Table 4).

4. Discussion

This study sought to investigate the effects of BWSTT and CT on lower extremity motor functions, balance, spatiotemporal gait parameters, and kinetic and kinematic parameters during a gait cycle in subjects with subacute stroke. After BWSTT or overground gait training for three weeks, both groups demonstrated improvement of lower extremity motor function and balance capacity. The BWSTT training group demonstrated significant improvement in kinematic parameters of lower limb joints and gait patterns which was not observed in the CT group.

4.1. Balance and Lower Extremity Motor Functions. Previous studies on functional recovery in animal models [44] and patients with stroke [45–47] have demonstrated that early treatment and training can facilitate improvement in motor functions and balance. In previous studies that compared

Table 3: Spatiotemporal parameters for normal, BWSTT, and CT group.

Spatiotemporal parameters	Normal group X (SD)	BWSTT group X (SD) Before training	X (SD) After training	P	CT group X (SD) Before training	X (SD) After training	P
Cadence (steps/min)	106.75 (8.68)	64.59 (18.31)	85.41 (12.53)	0.005	70.10 (18.92)	70.34 (15.45)	0.953
Stride length (metres)	1.07 (0.10)	0.58 (0.16)	0.69 (0.18)	0.005	0.56 (0.10)	0.56 (0.15)	0.963
Stride time (seconds)	1.13 (0.09)	2.02 (0.64)	1.44 (0.21)	0.018	1.88 (0.67)	1.85 (0.69)	0.915
Step length (metres)	0.55 (0.06)	0.30 (0.07)	0.37 (0.09)	0.005	0.30 (0.07)	0.30 (0.08)	0.808
Step time (seconds)	0.57 (0.05)	1.06 (0.30)	0.81 (0.13)	0.015	1.08 (0.53)	1.00 (0.40)	0.655
Gait speed (m/s)	0.96 (0.10)	0.33 (0.17)	0.50 (0.20)	0.000	0.33 (0.12)	0.33 (0.12)	0.997

Table 4: Angle and moment peak of lower limb joints at sagittal plane.

	Normal group X (SD)	BWSTT group X (SD)		P	CT group X (SD)		P
		Before training	After training		Before training	After training	
Kinematic parameters (°)							
Hip flexion	28.69 (9.51)	29.01 (13.61)	22.92 (10.76)	0.021	25.03 (6.45)	22.75 (6.94)	0.308
Knee flexion	58.82 (10.25)	36.50 (10.15)	37.96 (15.95)	0.787	43.10 (11.71)	41.62 (13.71)	0.329
Ankle dorsiflexion	10.03 (7.76)	16.51 (17.02)	9.79 (5.42)	0.301	13.56 (6.03)	14.67 (4.16)	0.524
Hip extension	−11.78 (8.51)	1.31 (11.84)	−8.67 (10.78)	0.020	1.45 (6.62)	−0.75 (7.54)	0.453
Knee extension	4.41 (5.08)	2.49 (8.54)	−0.39 (8.51)	0.235	9.82 (7.01)	7.22 (6.09)	0.239
Ankle plantarflexion	−18.73 (7.76)	−11.56 (4.41)	−10.88 (11.53)	0.878	−6.72 (7.15)	−4.25 (6.95)	0.189
Kinetic parameters (Nm/kg)							
Hip flexion	0.72 (0.32)	0.36 (0.29)	0.50 (0.30)	0.061	0.17 (0.11)	0.20 (0.15)	0.702
Knee flexion	0.52 (0.39)	0.77 (0.50)	0.62 (0.47)	0.649	0.60 (0.42)	0.86 (0.51)	0.164
Ankle dorsiflexion	1.23 (0.32)	0.68 (0.40)	0.83 (0.35)	0.339	0.37 (0.38)	0.72 (0.47)	0.080
Hip extension	0.68 (0.31)	0.50 (0.28)	0.57 (0.38)	0.636	0.42 (0.15)	0.46 (0.28)	0.682
Knee extension	0.35 (0.09)	0.40 (0.33)	0.47 (0.37)	0.302	0.16 (0.14)	0.19 (0.14)	0.753
Ankle plantarflexion	0.15 (0.11)	0.76 (0.47)	0.51 (0.38)	0.099	0.56 (0.46)	0.67 (0.45)	0.541

BWSTT with conventional overground gait training at early stage after stroke, similar gains were seen on the Fugl-Meyer and Berg balance scales in both groups [35, 48]. The results of this current study are consistent with published studies that early intervention can improve on balance and lower extremity motors functions in patients with subacute stroke. It is also consistent with Nilsson et al. [48] and Franceschini et al. [35] that BWSTT is at least as effective as CT to improve lower extremity functions and balance. The results indicate that two gait training strategies are similar in their clinical effects and could be used as routine therapeutic programs.

4.2. Kinematic Parameters. BWSTT is task-specific step training on treadmill with partial body weight support. Some research results showed that partial body supported on treadmill could result in better walking abilities than bearing their full weight of patients with stroke [31]. Other studies suggested that additional body weight support may reduce the stimulation to the affected side and may reduce the benefit in lower limb motor recovery [7]. Abnormal movement decreased after gait velocity improvement [49] and gait speed is a reliable outcome measure for short-term intervention in stroke patients. In this study, the subjects decreased body weight support from 40% at the beginning to zero by the end of the program. In addition, treadmill velocity was increased from 0.5 mph to 2.5 mph as early as possible, without causing abnormal changes in gait pattern to achieve optimal benefit of training [50, 51]. The results suggested that, after 3 weeks of BWSTT, improvement in temporal-spatial parameters (increased cadence, stride length and step length, and decreased stride time and step time) is achievable. Another research showed that a 12-week program of BWSTT coupled with overground walking practice led to increased floor walking speed with increased step lengths and cadence

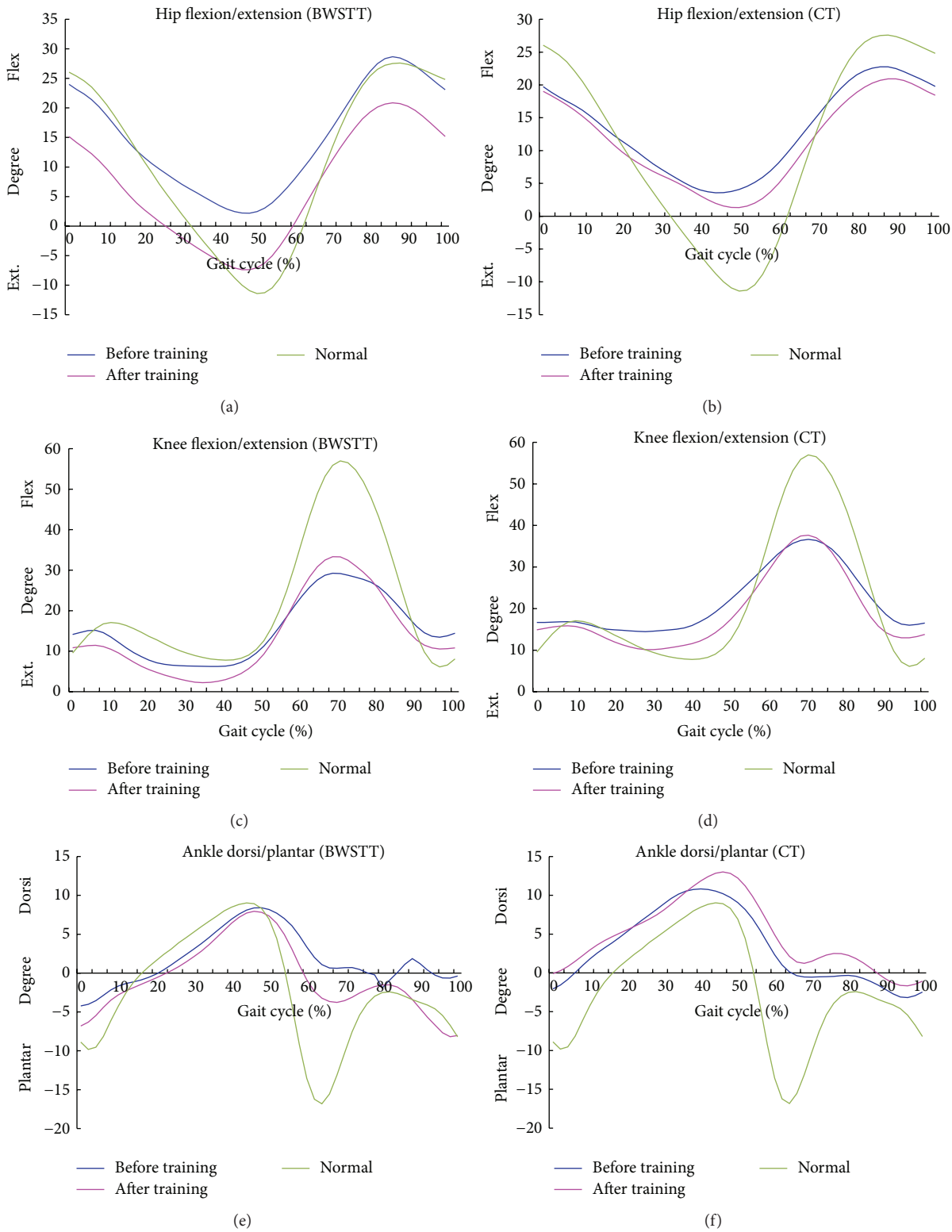

FIGURE 2: Average curves of lower limb kinematic at the sagittal plane for normal, BWSTT, and CT group. For the clearance of the comparison, the standard deviation was not shown in the figures.

in patients with chronic stroke [52]. Result from this study indicated that patients with subacute stroke could improve gait velocity after just 3 weeks of BWSTT when combined with strength training, muscle recruitment facilitation, and occupational therapy programme. Improvement in gait speed is a result of increased stride length, step length, and cadence [53]. Previous study also demonstrated that BWSTT can improve gait velocity, cadence, and stride length parameters in subjects with subacute and chronic stroke [53]. BWSTT programme is superior to conventional therapy because it permits greater number of steps performed within a fixed period of time when compared to CT, thus increasing the amount of task-specific practice [32]. Hesse and Werner [54] reported up to 1000 steps which could be performed in a 20-minute treadmill training session, compared with only 50 to 100 steps during a 20-minute session of conventional physiotherapy. In addition, the speed of the treadmill, the amount of body weight support, and the amount of assistance provided by the physiotherapist can all be adjusted in order to provide a sufficient training intensity for individual needs. This can encourage further cortical reorganization and promote gait recovery.

It has been demonstrated that BWSTT improves symmetry and gait efficiency by changing kinematic parameters in acute stroke patients [32]. Increased paretic step length is due to an increased hip extension angle in the paretic leg that allows the limb to swing farther backward [51]. Hip extension increase was associated with meaningful changes in walking speed [55]. The kinematic findings illustrated that the paretic hip peak extension had increased significantly in BWSTT group but not in CT group and the increasing hip extension at terminal swing can contribute to rectify the increasing hip flexion at toe off with hemiparetic gait. This may explain the improvement in walking speed, stride length, step length, and cadence observed in BWSTT group but not in CT group. This is in agreement with study by Mulroy et al. [55] which also reported improvement in hip flexion and extension motion in stroke patient who has high response to gait training. Mulroy et al. [55] also reported a tendency toward greater increase in ankle plantarflexion motion, which is also in agreement with this study (see Figure 2). Study by Jonsdottir et al. [26] also indicated that the capacity to increase work production at the ankle may be limited. Faster treadmill walking speed could increase hip extension angle significantly and knee flexion during swing phase; the positive improvement facilitated a more normal gait pattern after stroke [56]. The exact reason why hip joint motions are more responsive than knee and ankle to gait training is currently unclear. Increase in hip extension/flexion angle requires increased joint power generation during walking. A possible explanation is that the hip joint consists of large muscle group such as rectus femoris and psoas major which are responsible for flexion and extension motion. It is possible that large muscles group that are responsible for mass motor movement are more responsive to intervention than smaller muscles group. Another possible explanation for the observed significant difference at the hip but not at ankle and knee is that the change of range of movement at the hip joint is the greatest among the three joints during a gait cycle. Therefore the sample size has sufficient power to detect significant difference at hip joint but not the other joints.

4.3. Relationship between Kinematic Parameters and Gait Pattern. The control of proximal and distal lower limb plays a key compensatory role in the adaptation of gait pattern and velocity in stroke patients in early stage [26, 27]. Lower extremity gait kinematics and kinetics in the sagittal plane are commonly impaired after stroke. This study showed improvement of hip extension in the BWSTT group increasing (from flexion 2.19° to extension 7.38°) and flexion decreased (from 29.01° to 22.92°). The kinematic curves showed that the hip joint was extended instead of flexed during stance phase. Previous joint angle analysis studies indicated that hip joint motion is more affected than all other lower limbs' joint among stroke survivors in early stage [4]. Hip extension angle improved when patients walked at progressively faster treadmill speeds [55, 57] and the gait speed increase was strongly associated with hip extension and ankle plantarflexion [55, 57, 58]. The improved hip motion is translated from stance to swing phase and enables effective ground reaction force to be generated anteriorly [59, 60]. It is therefore biomechanically important to promote hip joint movement to aid the forward propulsion of the body for stroke patient during gait [51].

It was found that lower extremity motor function and balance improved in both groups after 3 weeks of training. However, gait analysis revealed that gait speed and cadence improved in the BWSTT group, but not in the CT group over this time period. Furthermore, maximal hip extension improved with BWSTT and approached that in healthy controls, but there was no obvious difference in the CT group. The extent of hip extension may be related to the observed improvement in gait speed in this group. These results suggest that treadmill training with body weight support provided at an early stage after stroke may be beneficial to improve walking speed after stroke and abnormal flexion of hip joint at stance phase, especially in hyperflexion at hip joint during walking.

4.4. Kinetic Parameters. It is not known whether BWSTT training can target kinetic functions specially. Both BWSTT and CT groups in this study demonstrate some improvement in kinetic parameters after interventions but differences did not reach statistical significance. These findings would suggest that moment peak may not be related to the gait trajectories or gait speed improvement. Treadmill training is task specific to facilitate the development of new motor development after the new state following a stroke. It is possible that there was no direct relationship between improvement in muscle strength and gait improvement. However, patients with drop-foot have to increase the ankle joint plantarflexion moment during walking [61]. This study observed a decrease in plantarflexion moment after three weeks of intervention for ankle joint with BWSTT group. On the contrary, the plantarflexion moment increased in overground walking training. Therefore, it may be beneficial to adjust the abnormal gait curve. It is uncertain whether the lack of significant difference is due to the small sample size which lacks the power to detect

small difference or the short three-week intervention period which was not sufficiently long to produce further changes.

5. Limitations

This study has several limitations. The sample size was small and was not power calculated to detect changes in gait parameter. This study only included stroke patients who were at the subacute stage. Results of this study may not be generalised to the larger stroke population. In addition, this study did not measure lower extremity muscle strength which limited the interpretation of the kinematic data. Thus, it is recommended that future research include muscle strength recording such as sEMG and isokinetic instruments, especially at hip flexor, knee extensor, and ankle plantarflexor, to understand the underlying mechanism.

6. Conclusion

BWSTT has similar clinical effects to improve balance and lower extremity function as conventional overground walking training for patients with subacute stroke. BWSTT can significantly improve spatiotemporal parameters with three weeks of training. Improvement in gait pattern is related to the improvement of hip joint motion during walking. It would be clinically beneficial to incorporate hip joint motion training to improve gait pattern, especially for those who are not suitable for treadmill training. Rehabilitation programme for subacute stroke patients should therefore incorporate kinematic training of proximal lower limb to facilitate gait recovery.

Clinical Messages

(i) BWSTT is superior to conventional overground therapy in improving spatiotemporal parameters.

(ii) Improvement in gait pattern is related to the improvement of kinematic pattern of proximal lower limb.

(iii) Kinematic training of proximal lower limb may facilitate gait recovery.

Conflict of Interests

No commercial party has a direct financial interest in the results of the research, supported this paper, or will confer a benefit upon the authors or upon any organization with which the authors are associated.

Acknowledgments

This work was supported by the National Science Foundation of China (nos. 30973165, 31100669, and 81372108), in part by Science and Technology Planning Project of Guangdong Province, China (no. 2013b090500099), and in part by 5010 Clinical Medical Research of Sun Yat-sen University (no. 2014001).

References

[1] V. L. Feigin, M. H. Forouzanfar, R. Krishnamurthi et al., "Global and regional burden of stroke during 1990–2010: findings from the Global Burden of Disease Study 2010," *The Lancet*, vol. 383, no. 9913, pp. 245–254, 2014.

[2] D. Zhao, J. Liu, W. Wang et al., "Epidemiological transition of stroke in China: twenty-oneyear observational study from the sino-MONICA-Beijing project," *Stroke*, vol. 39, no. 6, pp. 1668–1674, 2008.

[3] T. Truelsen and R. Bonita, "Epidemiological transition of stroke in China?" *Stroke*, vol. 39, no. 6, pp. 1653–1654, 2008.

[4] A. P. McGinn, R. C. Kaplan, J. Verghese et al., "Walking speed and risk of incident ischemic stroke among postmenopausal women," *Stroke*, vol. 39, no. 4, pp. 1233–1239, 2008.

[5] F. M. Collen, D. T. Wade, and C. M. Bradshaw, "Mobility after stroke: reliability of measures of impairment and disability," *International Disability Studies*, vol. 12, no. 1, pp. 6–9, 1990.

[6] R. W. Bohannon, A. W. Andrews, and S. S. Glenney, "Minimal clinically important difference for comfortable speed as a measure of gait performance in patients undergoing inpatient rehabilitation after stroke," *Journal of Physical Therapy Science*, vol. 25, no. 10, pp. 1223–1225, 2013.

[7] S. Hesse, "Treadmill training with partial body weight support after stroke: a review," *NeuroRehabilitation*, vol. 23, no. 1, pp. 55–65, 2008.

[8] S. A. Hesse, M. T. Jahnke, C. M. Bertelt, C. Schreiner, D. Lücke, and K.-H. Mauritz, "Gait outcome in ambulatory hemiparetic patients after a 4-week comprehensive rehabilitation program and prognostic factors," *Stroke*, vol. 25, no. 10, pp. 1999–2004, 1994.

[9] S. B. Perry, "Stroke rehabilitation: guidelines for exercise and training to optimize motor skill," *Journal of Neurologic Physical Therapy*, vol. 28, no. 2, p. 101, 2004.

[10] R. K. Nielsen, K. L. Samson, D. Simonsen, and W. Jensen, "Effect of early and late rehabilitation onset in a chronic rat model of ischemic stroke-assessment of motor cortex signaling and gait functionality over time," *IEEE Transactions on Neural Systems and Rehabilitation Engineering*, vol. 21, no. 6, pp. 1006–1015, 2013.

[11] X. Liu, S. Zhang, M. Liu et al., "Chinese guidelines for endovascular management of ischemic cerebrovascular diseases," *Interventional Neurology*, vol. 1, no. 3-4, pp. 171–184, 2013.

[12] B. Jiang, W.-Z. Wang, H. Chen et al., "Incidence and trends of stroke and its subtypes in China: results from three large cities," *Stroke*, vol. 37, no. 1, pp. 63–68, 2006.

[13] J. K. Tilson, K. J. Sullivan, S. Y. Cen et al., "Meaningful gait speed improvement during the first 60 days poststroke: minimal clinically important difference," *Physical Therapy*, vol. 90, no. 2, pp. 196–208, 2010.

[14] T. Drew and D. S. Marigold, "Taking the next step: cortical contributions to the control of locomotion," *Current Opinion in Neurobiology*, vol. 33, pp. 25–33, 2015.

[15] T. Huppert, B. Schmidt, N. Beluk, J. Furman, and P. Sparto, "Measurement of brain activation during an upright stepping reaction task using functional near-infrared spectroscopy," *Human Brain Mapping*, vol. 34, no. 11, pp. 2817–2828, 2013.

[16] S. J. Olney and C. Richards, "Hemiparetic gait following stroke. Part I: characteristics," *Gait & Posture*, vol. 4, no. 2, pp. 136–148, 1996.

[17] C. Calautti and J.-C. Baron, "Functional neuroimaging studies of motor recovery after stroke in adults: a review," *Stroke*, vol. 34, no. 6, pp. 1553–1566, 2003.

[18] C.-L. Yen, R.-Y. Wang, K.-K. Liao, C.-C. Huang, and Y.-R. Yang, "Gait training-induced change in corticomotor excitability in patients with chronic stroke," *Neurorehabilitation and Neural Repair*, vol. 22, no. 1, pp. 22–30, 2008.

[19] D. U. Jette, N. K. Latham, R. J. Smout, J. Gassaway, M. D. Slavin, and S. D. Horn, "Physical therapy interventions for patients with stroke in inpatient rehabilitation facilities," *Physical Therapy*, vol. 85, no. 3, pp. 238–248, 2005.

[20] H. Woldag and H. Hummelsheim, "Evidence-based physiotherapeutic concepts for improving arm and hand function in stroke patients: a review," *Journal of Neurology*, vol. 249, no. 5, pp. 518–528, 2002.

[21] L. Sawaki, C. W.-H. Wu, A. Kaelin-Lang, and L. G. Cohen, "Effects of somatosensory stimulation on use-dependent plasticity in chronic stroke," *Stroke*, vol. 37, no. 1, pp. 246–247, 2006.

[22] J. D. Schaechter, C. A. M. M. Van Oers, B. N. Groisser et al., "Increase in sensorimotor cortex response to somatosensory stimulation over subacute poststroke period correlates with motor recovery in hemiparetic patients," *Neurorehabilitation and Neural Repair*, vol. 26, no. 4, pp. 325–334, 2012.

[23] P. Celnik, F. Hummel, M. Harris-Love, R. Wolk, and L. G. Cohen, "Somatosensory stimulation enhances the effects of training functional hand tasks in patients with chronic stroke," *Archives of Physical Medicine and Rehabilitation*, vol. 88, no. 11, pp. 1369–1376, 2007.

[24] I. Miyai, H. Yagura, I. Oda et al., "Premotor cortex is involved in restoration of gait in stroke," *Annals of Neurology*, vol. 52, no. 2, pp. 188–194, 2002.

[25] A. R. Luft, L. Forrester, R. F. Macko et al., "Brain activation of lower extremity movement in chronically impaired stroke survivors," *NeuroImage*, vol. 26, no. 1, pp. 184–194, 2005.

[26] J. Jonsdottir, M. Recalcati, M. Rabuffetti, A. Casiraghi, S. Boccardi, and M. Ferrarin, "Functional resources to increase gait speed in people with stroke: strategies adopted compared to healthy controls," *Gait and Posture*, vol. 29, no. 3, pp. 355–359, 2009.

[27] C.-L. Chen, H.-C. Chen, S. F.-T. Tang, C.-Y. Wu, P.-T. Cheng, and W.-H. Hong, "Gait performance with compensatory adaptations in stroke patients with different degrees of motor recovery," *American Journal of Physical Medicine and Rehabilitation*, vol. 82, no. 12, pp. 925–935, 2003.

[28] C. M. Kim and J. J. Eng, "Magnitude and pattern of 3D kinematic and kinetic gait profiles in persons with stroke: relationship to walking speed," *Gait and Posture*, vol. 20, no. 2, pp. 140–146, 2004.

[29] S. Hesse, M. Konrad, and D. Uhlenbrock, "Treadmill walking with partial body weight support versus floor walking in hemiparetic subjects," *Archives of Physical Medicine and Rehabilitation*, vol. 80, no. 4, pp. 421–427, 1999.

[30] K. J. McCain, F. E. Pollo, B. S. Baum, S. C. Coleman, S. Baker, and P. S. Smith, "Locomotor treadmill training with partial body-weight support before overground gait in adults with acute stroke: a pilot study," *Archives of Physical Medicine and Rehabilitation*, vol. 89, no. 4, pp. 684–691, 2008.

[31] M. Visintin, H. Barbeau, N. Korner-Bitensky, and N. E. Mayo, "A new approach to retrain gait in stroke patients through body weight support and treadmill stimulation," *Stroke*, vol. 29, no. 6, pp. 1122–1128, 1998.

[32] J. Mehrholz, M. Pohl, and B. Elsner, "Treadmill training and body weight support for walking after stroke," *The Cochrane Database of Systematic Reviews*, vol. 1, Article ID CD002840, 2014.

[33] S. Mudge, L. Rochester, and A. Recordon, "The effect of treadmill training on gait, balance and trunk control in a hemiplegic subject: a single system design," *Disability and Rehabilitation*, vol. 25, no. 17, pp. 1000–1007, 2003.

[34] C. Werner, A. Bardeleben, K.-H. Mauritz, S. Kirker, and S. Hesse, "Treadmill training with partial body weight support and physiotherapy in stroke patients: a preliminary comparison," *European Journal of Neurology*, vol. 9, no. 6, pp. 639–644, 2002.

[35] M. Franceschini, S. Carda, M. Agosti, R. Antenucci, D. Malgrati, and C. Cisari, "Walking after stroke: what does treadmill training with body weight support add to overground gait training in patients early after stroke?: a single-blind, randomized, controlled trial," *Stroke*, vol. 40, no. 9, pp. 3079–3085, 2009.

[36] I. T. da Cunha Jr., P. A. Lim, H. Qureshy, H. Henson, T. Monga, and E. J. Protas, "Gait outcomes after acute stroke rehabilitation with supported treadmill ambulation training: a randomized controlled pilot study," *Archives of Physical Medicine and Rehabilitation*, vol. 83, no. 9, pp. 1258–1265, 2002.

[37] M. MacKay-Lyons, A. McDonald, J. Matheson, G. Eskes, and M.-A. Klus, "Dual effects of body-weight supported treadmill training on cardiovascular fitness and walking ability early after stroke: a randomized controlled trial," *Neurorehabilitation and Neural Repair*, vol. 27, no. 7, pp. 644–653, 2013.

[38] J. C. Moreno, F. Barroso, D. Farina et al., "Effects of robotic guidance on the coordination of locomotion," *Journal of NeuroEngineering and Rehabilitation*, vol. 10, article 79, 2013.

[39] R. L. Routson, D. J. Clark, M. G. Bowden, S. A. Kautz, and R. R. Neptune, "The influence of locomotor rehabilitation on module quality and post-stroke hemiparetic walking performance," *Gait and Posture*, vol. 38, no. 3, pp. 511–517, 2013.

[40] A. R. Fugl Meyer, L. Jaasko, and I. Leyman, "The post stroke hemiplegic patient. I. A method for evaluation of physical performance," *Scandinavian Journal of Rehabilitation Medicine*, vol. 7, no. 1, pp. 13–31, 1975.

[41] S. F. Tyson and L. H. DeSouza, "Development of the Brunel Balance Assessment: a new measure of balance disability post stroke," *Clinical Rehabilitation*, vol. 18, no. 7, pp. 801–810, 2004.

[42] S. F. Tyson, M. Hanley, J. Chillala, A. B. Selley, and R. C. Tallis, "The relationship between balance, disability, and recovery after stroke: predictive validity of the Brunel Balance Assessment," *Neurorehabilitation and Neural Repair*, vol. 21, no. 4, pp. 341–346, 2007.

[43] L. R. Sheffler, S. N. Bailey, R. D. Wilson, and J. Chae, "Spatiotemporal, kinematic, and kinetic effects of a peroneal nerve stimulator versus an ankle foot orthosis in hemiparetic gait," *Neurorehabilitation and Neural Repair*, vol. 27, no. 5, pp. 403–410, 2013.

[44] T. A. Jones, J. A. Kleim, and W. T. Greenough, "Synaptogenesis and dendritic growth in the cortex opposite unilateral sensorimotor cortex damage in adult rats: a quantitative electron microscopic examination," *Brain Research*, vol. 733, no. 1, pp. 142–148, 1996.

[45] J. M. W. W. Myint, G. F. C. Yuen, T. K. K. Yu et al., "A study of constraint-induced movement therapy in subacute stroke patients in Hong Kong," *Clinical Rehabilitation*, vol. 22, no. 2, pp. 112–124, 2008.

[46] M. Katz-Leurer, I. Sender, O. Keren, and Z. Dvir, "The influence of early cycling training on balance in stroke patients at

the subacute stage. Results of a preliminary trial," *Clinical Rehabilitation*, vol. 20, no. 5, pp. 398–405, 2006.

[47] C. L. Richards, F. Malouin, S. Wood-Dauphinee, J. I. Williams, J.-P. Bouchard, and D. Brunet, "Task-specific physical therapy for optimization of gait recovery in acute stroke patients," *Archives of Physical Medicine and Rehabilitation*, vol. 74, no. 6, pp. 612–620, 1993.

[48] L. Nilsson, J. Carlsson, A. Danielsson et al., "Walking training of patients with hemiparesis at an early stage after stroke: A comparison of walking training on a treadmill with body weight support and walking training on the ground," *Clinical Rehabilitation*, vol. 15, no. 5, pp. 515–527, 2001.

[49] I. A. Kramers De Quervain, S. R. Simon, S. Leurgans, W. S. Pease, and D. McAllister, "Gait pattern in the early recovery period after stroke," *The Journal of Bone and Joint Surgery—American Volume*, vol. 78, no. 10, pp. 1506–1514, 1996.

[50] M. K. Aaslund, J. L. Helbostad, and R. Moe-Nilssen, "Walking during body-weight-supported treadmill training and acute responses to varying walking speed and body-weight support in ambulatory patients post-stroke," *Physiotherapy Theory and Practice*, vol. 29, no. 4, pp. 278–289, 2013.

[51] C. M. Tyrell, M. A. Roos, K. S. Rudolph, and D. S. Reisman, "Influence of systematic increases in treadmill walking speed on gait kinematics after stroke," *Physical Therapy*, vol. 91, no. 3, pp. 392–403, 2011.

[52] P. Plummer, A. L. Behrman, P. W. Duncan et al., "Effects of stroke severity and training duration on locomotor recovery after stroke: a Pilot Study," *Neurorehabilitation and Neural Repair*, vol. 21, no. 2, pp. 137–151, 2007.

[53] L. Ada, C. M. Dean, J. M. Hall, J. Bampton, and S. Crompton, "A treadmill and overground walking program improves walking in persons residing in the community after stroke: a placebo-controlled, randomized trial," *Archives of Physical Medicine and Rehabilitation*, vol. 84, no. 10, pp. 1486–1491, 2003.

[54] S. Hesse and C. Werner, "Poststroke motor dysfunction and spasticity: novel pharmacological and physical treatment strategies," *CNS Drugs*, vol. 17, no. 15, pp. 1093–1107, 2003.

[55] S. J. Mulroy, T. Klassen, J. K. Gronley, V. J. Eberly, D. A. Brown, and K. J. Sullivan, "Gait parameters associated with responsiveness to treadmill training with body-weight support after stroke: an exploratory study," *Physical Therapy*, vol. 90, no. 2, pp. 209–223, 2010.

[56] M. Krawczyk, E. Szczerbik, and M. Syczewska, "The comparison of two physiotherapeutic approaches for gait improvement in sub-acute stroke patients," *Acta of Bioengineering and Biomechanics*, vol. 16, no. 1, pp. 11–18, 2014.

[57] S. Hesse, D. Uhlenbrock, and T. Sarkodie-Gyan, "Gait pattern of severely disabled hemiparetic subjects on a new controlled gait trainer as compared to assisted treadmill walking with partial body weight support," *Clinical Rehabilitation*, vol. 13, no. 5, pp. 401–410, 1999.

[58] A.-L. Hsu, P.-F. Tang, and M.-H. Jan, "Analysis of impairments influencing gait velocity and asymmetry of hemiplegic patients after mild to moderate stroke," *Archives of Physical Medicine and Rehabilitation*, vol. 84, no. 8, pp. 1185–1193, 2003.

[59] L. J. Turns, R. R. Neptune, and S. A. Kautz, "Relationships between muscle activity and anteroposterior ground reaction forces in hemiparetic walking," *Archives of Physical Medicine and Rehabilitation*, vol. 88, no. 9, pp. 1127–1135, 2007.

[60] M. G. Bowden, C. K. Balasubramanian, R. R. Neptune, and S. A. Kautz, "Anterior-posterior ground reaction forces as a measure of paretic leg contribution in hemiparetic walking," *Stroke*, vol. 37, no. 3, pp. 872–876, 2006.

[61] E. B. Simonsen, "Contributions to the understanding of gait control," *Danish Medical Journal*, vol. 61, no. 4, Article ID B4823, 2014.

Hindawi Publishing Corporation
BioMed Research International
Volume 2015, Article ID 178407, 13 pages
http://dx.doi.org/10.1155/2015/178407

Review Article

Animal Models in Studying Cerebral Arteriovenous Malformation

Ming Xu,[1] Hongzhi Xu,[2] and Zhiyong Qin[2]

[1]*Department of Anesthesiology, Huashan Hospital, Fudan University, Shanghai 200040, China*
[2]*Department of Neurosurgery, Huashan Hospital, Fudan University, Shanghai 200040, China*

Correspondence should be addressed to Hongzhi Xu; xuhongzhi95@sina.com

Received 6 August 2015; Revised 11 October 2015; Accepted 25 October 2015

Academic Editor: Aaron S. Dumont

Brain arteriovenous malformation (AVM) is an important cause of hemorrhagic stroke. The etiology is largely unknown and the therapeutics are controversial. A review of AVM-associated animal models may be helpful in order to understand the up-to-date knowledge and promote further research about the disease. We searched PubMed till December 31, 2014, with the term "arteriovenous malformation," limiting results to animals and English language. Publications that described creations of AVM animal models or investigated AVM-related mechanisms and treatments using these models were reviewed. More than 100 articles fulfilling our inclusion criteria were identified, and from them eight different types of the original models were summarized. The backgrounds and procedures of these models, their applications, and research findings were demonstrated. Animal models are useful in studying the pathogenesis of AVM formation, growth, and rupture, as well as in developing and testing new treatments. Creations of preferable models are expected.

1. Introduction

Brain arteriovenous malformations (AVMs) are vascular anomalies where arteries and veins are directly connected through a complex, tangled web of abnormal vessels instead of a normal capillary network. There is usually high flow through the feeding arteries, nidus, and draining veins. AVMs represent a high risk for hemorrhagic stroke, leading to significant neurological morbidity and mortality in relatively young adults [1]. How the pathological and hemodynamic features play a role in AVM rupture is unknown.

The management in the case of sudden bleeding is focused on restoration of vital function and prevention of recurrent hemorrhage, usually with some combination of surgical resection, embolization, and stereotactic radiotherapy. But all of these treatments pose a risk of serious complications, and the optimal treatment needs to be evaluated [2]. For nonruptured AVMs, whether the preventive treatments are beneficial is uncertain, because nonintervention may result in favorable long-term outcome [3].

As considered to be embryonic origin and postnatal development, AVMs are highly dynamic rather than static [4, 5]. Angiogenesis or vascular proliferation occurs in the AVM lesion. Understanding the exact molecular mechanisms of AVM formation and progression is critical for developing novel therapies such as the vascular targeting therapy and the gene therapy.

Animal models are warranted to meet the needs mentioned above. Up to now, several experimental animal models have been developed in studying the AVM-related hemodynamics, pathogenesis, and treatments. Hence, a review was made about the background, the procedure, and the application of these models, and their advantages and disadvantages were briefly analyzed.

The aim of the review was to encourage creating more advantageous AVM models and promote further studies of the disorder.

2. Methods

We searched PubMed till December 31, 2014, using the term "arteriovenous malformation," limiting results to animals and English language.

Table 1: The highlights of the original models for AVMs.

Type	Author [Reference]	Year	Animal	Characteristics	Applications
Carotid jugular fistula (CJF)	Spetzler et al. [6]	1978	cat	Different types of CJF to cause cerebral hypoperfusion and/or draining venous hypertension, fistula opening and closing simulating the presence and resection of the AVM lesion	To evaluate the hemodynamic and pathophysiological changes of AVM adjacent parenchyma, but not the AVM lesion itself. To explain the AVM symptoms and the postoperative complications
	Morgan et al. [7]	1989	rat		
	Bederson et al. [8]	1991	rat		
	Hai et al. [9]	2002	rat		
	Scott et al. [10]	1978	monkey		
Intracranial arteriovenous fistula	Numazawa et al. [11]	2005	dog	A venous graft shunting blood from a branch of the MCA to the SSS, the arterial territory as the blood stolen tissue surrounding AVMs	As above, more precisely in regional parenchyma, but not in the whole brain
Rete mirabile (RM) as the AVM nidus	Chaloupka et al. [12]	1994	pig	Inserting a needle to communicate the RM with the cavernous sinus	To Test and evaluate the embolization and radiosurgery therapy
	Massoud et al. [13]	1994	pig	Establishing a CJF to retrogradely drain the blood from the RM	
	Qian et al. [14]	1999	sheep		
Venous plexus as the AVM nidus	Yassari et al. [15]	2004	rat	Creating a CJF, arterialized venous vessels as an extracranial AVM lesion	To study molecular mechanism of AVM development and the effect of radiosurgery
AVM-like lesions derived from implants	Pietilä et al. [16]	2000	dog	A pedicled muscle graft implanted to the brain with an arteriovenous bypass	To emonstrate angiogenic mechanism of the AVM formation and development
Xenograft arteriovenous fistula	Lawton et al. [17]	2004	rat	Inserting an arterial graft from transgenic mice between the CCA and the EJV of nude rats	To evaluate the mechanism of radiotherapy and to develop novel therapies
AVM tissue -implanted cornea model	Konya et al. [18]	2005	rat	Transplanting human AVM tissues to the rat's cornea	To evaluate the angiogenic property and its mechanism of human AVM specimens
AVM lesions by gene manipulation	Details in Table 2				

AVM: arteriovenous malformation; MCA: middle cerebral artery; SSS: superior sagittal sinus; CCA: common carotid artery; EJV: external jugular vein.

Two investigators read the titles and abstracts of the publications to find out the possibly relevant ones that described creations of AVM animal models or investigated AVM-related mechanisms and treatments using these models. The articles describing the creation of the dural arteriovenous fistula models or AVM lesions in other organs were excluded. Full texts of the selected articles were obtained, and those fulfilling our inclusion criteria were identified and finally summarized.

The emphases of the review were on the background, the procedure, and the application of each particular model. The chosen animals, the advantage, and the disadvantage of each model were also briefly discussed.

3. Results

From the result of total 911 publications found according to the search term, we picked up more than 100 articles, by the inclusion criteria of either describing the creation of original or modified animal models or adopting these models to make experimental researches.

The animal models in the study of AVMs were diverse in accordance with research purpose, ranging from those based on the changes of the cerebrovascular circulation to those based on gene manipulation techniques. Eight different types of the original models were summarized and their highlights were shown in Tables 1 and 2.

3.1. The Carotid-Jugular Fistula. To explain a phenomenon that brain tissue surrounding the AVM lesion is subject to swelling and hemorrhage immediately following surgical excision of the lesion, Spetzler et al. firstly suggested that the chronic ischemic brain tissue near high flow AVMs might experience a loss of vascular autoregulatory capacity, the theory of normal perfusion pressure breakthrough (NPPB), by using carotid-jugular fistula (CJF) model in cats [6].

Table 2: The highlights of AVM models by gene manipulation.

Type	Author [Reference]	Year	Animal	Characteristics	Applications
AVM lesions by gene manipulation	Bourdeau et al. [19]	1999	mouse	Generating $Eng^{+/-}$ mutant mice: modest cerebrovascular abnormality	To investigate the pathogenic mechanisms of AVMs in genetic factors
	Satomi et al. [20]	2003			
	Oh et al. [21]	2000	mouse	Generating $Alk1^{+/-}$ mutant mice: minimal cerebrovascular abnormality	
	Srinivasan et al. [22]	2003			
	Xu et al. [23]	2004	mouse	Focal virus-mediated VEGF gene transferred in the brain of $Eng^{+/-}$ mice: cerebral microvascular dysplasia	To investigate the pathogenic mechanisms of AVMs in genetic and environmental factors
	Hao et al. [24, 25]	2008	mouse	Focal virus-mediated VEGF gene transferred in the brain of $Alk1^{+/-}$ mice: cerebral microvascular dysplasia, less severe compared to $Eng^{+/-}$ mice, promoted by increased cerebral perfusion	
	Sung et al. [26]	2009	mouse	Conditional knockout of $Alk1^{2LoxP/2LoxP}$ by globally expressed Cre in adult mice: AV fistula formations and spontaneous hemorrhage in other organs, not remarkable in the brain	To investigate the pathogenic and hemorrhagic mechanisms of AVMs
	Choi et al. [27]	2014	mouse	Conditional knockout of $Eng^{2LoxP/2LoxP}$ by globally expressed Cre in adult mice: no remarkable effects on brain vasculature, angiogenesis and cerebrovascular lesions mimicking human AVM nidus developed with focal virus-mediated VEGF gene transferred	
	Walker et al. [28]	2011	mouse	Focal virus-mediated Cre and VEGF gene transferred in $Alk1^{2LoxP/2LoxP}$ mice: AVM lesions resembling the human disease	To investigate the pathogenic mechanisms of AVMs and to test the potential treatments
	Choi et al. [29]	2012	mouse	Focal virus-mediated Cre and VEGF gene transferred in $Eng^{2LoxP/2LoxP}$ mice: AVM lesions resembling the human disease	
	Chen et al. [30]	2014	mouse	Conditional knockout of $Alk1^{2LoxP/2LoxP}$ specifically in endothelial cells in adult mice: AVM formation and spontaneous hemorrhage in other organs and brain areas with previously focal virus-mediated VEGF gene transferred	To evaluated the role of endothelia in the pathogenesis of AVMs
	Mahmoud et al. [31]	2010	mouse	Conditional knockout of $Eng^{2LoxP/2LoxP}$ specifically in endothelial cells in postnatal mice: endothelial proliferation and AVM formation in neonatal retina, local venomegaly in adult skin induced by angiogenic stimulation	
	Milton et al. [32]	2012	mouse	Mating $Alk1^{2LoxP/2LoxP}$ mice with SM22-Cre mutant mice: spontaneous AVMs in the brain and spinal cord, partial lesions undergoing spontaneous hemorrhage	To investigate the hemorrhagic mechanisms of AVMs and to test the potential treatments
	Choi et al. [27]	2014	mouse	Mating $Eng^{2LoxP/2LoxP}$ mice with SM22-Cre mutant mice: spontaneous AVMs in the brain and spinal cord, partial lesions undergoing spontaneous hemorrhage	
	Murphy et al. [33]	2008	mouse	Induced overexpression of constitutively active *Notch4* and *Notch1* in neonatal mice: hallmarks of AVMs in the brain and cerebral hemorrhage	To investigate the pathogenic mechanisms of AVMs in genetic factors
	Yao et al. [34]	2013	mouse	Generating $Mgp^{-/-}$ mutant mice: vascular enlargement and AV shunting	
	Nielsen et al. [35]	2014	mouse	Deleting *Rbpj* gene in neonatal mice: AV shunting and tortuous vessels	

AVM: arteriovenous malformation; VEGF: vascular endothelial growth factor.

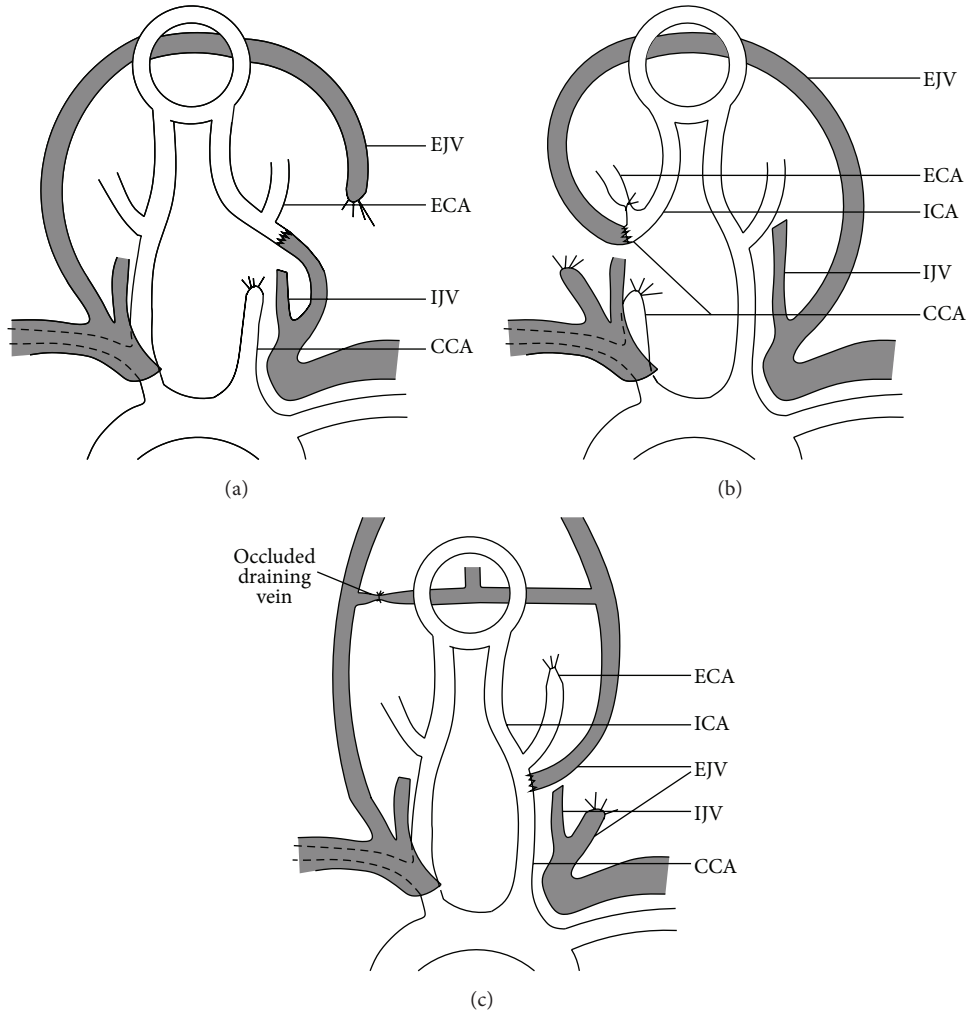

Figure 1: Animal models with carotid-jugular fistulae. (a) Spetzler's model, (b) Morgan's model, and (c) Hai's model. CCA: common carotid artery; ICA: internal carotid artery; ECA: external carotid artery; EJV: external jugular vein; IJV: internal jugular vein.

This model was created by means of an anastomosis between the rostral end of the common carotid artery (CCA) and the caudal end of the external jugular vein (EJV) together with the ligation of the remaining vessel stumps, so that noninfarction cerebral hypoperfusion was achieved by draining the blood from the circle of Willis retrogradely through the anastomosis (Figure 1(a)). After 6 weeks, only the animals with marked dilatation of the fistula vessels exhibited diminished cerebrovascular autoregulation with both open and closed fistulae, indicating the detrimental effect of high flow through AVMs on surrounding tissues. The other investigators reevaluated this cat model but found that the cerebrovascular hemodynamic changes were actually minimal and transient by the CJF formation and systematic blood pressure interference, and CO_2 reactivity in the closed fistula was preserved. This model was probably not enough to clarify the mechanisms of the NPPB phenomenon [36–38].

Therefore, a modified CJF model in rats was introduced by Morgan and colleagues. They made an end-to-end anastomosis of both rostral ends of the CCA and the EJV (the internal jugular vein in rats is hypoplastic, and the cerebral venous blood drains mainly to the EJV) on the right side and ligated the caudal ends of both vessels and the ipsilateral external carotid artery (ECA), creating a functional arteriovenous fistula between the circle of Willis and the right lateral sinus (Figure 1(b)). After a period of 8 to 12 weeks, the presence of CJF significantly reduced the cerebral blood flow (CBF) on the fistula side compared to the baseline. Fistula closure significantly elevated CBF, causing the blood-brain barrier (BBB) breakdown under induced hypertension, but not under a normal pressure [7, 39, 40]. Further studies verified that the histopathological change of the cerebral capillaries was the structural basic of the NPPB phenomenon [41]. Interestingly, the CO_2 reactivity of cerebral vessels remained intact throughout the experiment. The research group recommended the avoidance of intraoperative hyperventilation and postoperative hypertension for the removal of AVM lesions. By using this model, a research group tested the hypothesis that intracerebral, extracellular norepinephrine could be the key factor influencing CBF

levels [42], and another group evaluated the effect of ionizing radiation on the blood-stolen parenchyma and concluded that the radiotherapy-related damage in the normal or the hypoperfused brain tissues was similar [43].

Besides, "occlusive hyperemia" was also suggested to be related to the brain edema and hemorrhage following the large AVM resection. High blood flow and mass effect of AVM lesions might cause obstruction of the venous outflow and stagnation of arterial inflow in their adjacent parenchyma, with subsequent worsening of the existing hypoperfusion and ischemia in these tissues. Bederson et al. evaluated this presumption in a rat CJF model by a proximal CCA to distal EJV anastomosis with contralateral EJV occlusion [8]. The fistula significantly increased torcular pressure and decreased systematic pressure, and the venous occlusion for one week caused venous infarction, subarachnoid hemorrhage, and severe brain edema. Based on this, Hai et al. developed a more moderate model of chronic cerebral hypoperfusion combined with draining vein hypertension, by an end-to-side anastomosis between the EJV and the CCA on the right side with ligations of bilateral ECAs and the left vein draining the transvers sinus (Figure 1(c)). After 90 days, occlusion of CJF led to the NPPB phenomenon, which was further demonstrated to share similar pathological mechanisms with acute ischemia reperfusion injury such as infiltration of inflammatory cells and activation of oxygen free radicals [9, 44]. Hemodilution with high-concentration human serum albumin has a certain pretreatment effect on this brain injury [45]. Kojima et al. created very similar rat CJF models with not only the drop in perfusion pressure but also the impaired draining venous outflow [46].

Rats were mostly chosen as the model animal probably because they are economic and accessible in spite of their anatomical differences related to humans. CJF models were also tried in monkeys; however, they were hard to handle, expensive to create, and also with intricate ethical concerns [10].

3.2. The Intracranial Arteriovenous Fistula. Carotid-jugular fistulae resulted in the hemodynamic changes in whole brain or predominantly the hemisphere in the fistula side, but not in the regional parenchyma. A dog model with local cerebral hypoperfusion was tried using an intracranial arteriovenous fistula [11]. The dog was chosen not only because its brain was large enough for operation, but also because the physiology and hemodynamic situation were comparable between the dog and human brains. After craniotomy, a fistula was created by a femoral venous graft with end-to-side anastomosis both to the cortical branch of the middle cerebral artery (MCA) and to the superior sagittal sinus (SSS). Shunt opening markedly decreased regional CBF (rCBF) in the MCA territory, but not in other areas. Shunt reocclusion caused rCBF to rebound and return to the preopening value within 15 minutes. Regional CO_2 reactivity decreased significantly at shunt opening. The regional hemodynamic changes in this animal model simulated a real condition of brain tissues surrounding human AVMs. However, this was an acute model and the procedure was a bit complicated.

Both extracranial and intracranial arteriovenous fistula models lacked a real AVM nidus, these models were focusing on the hemodynamic and pathophysiological changes of AVM adjacent parenchyma, but not the AVM lesion itself.

3.3. The Rete Mirabile as the AVM Nidus. The carotid rete mirabile (RM) of the swine is a special vascular structure with a tangle of microarteries and arterioles situated at the termination of each ascending pharyngeal artery (APA) as it perforates the cranial base. The two sides of the RM, which are connected with each other across the midline, are also supplied by other small collateral arteries and effuse to form internal carotid arteries ipsilaterally (Figure 2(a)). At the end of 1980s, several authors began to report that the swine RM could be used as the AVM nidus to evaluate different materials for embolization and the single-dose radiation effects, due to their morphological similarities [47–50]. The occlusive effect of the treatments could be evaluated by superselective angiography and histopathological observation. An important distinction between the RM structure and a real AVM nidus is the hemodynamic difference; the former is arterioarterial system, but the latter is an arteriovenous system with a higher pressure gradient between feeding and draining vessels.

To address this shortfall, Chaloupka et al. produced a high flow arteriovenous shunt in the swine RM by inserting a needle through the orbit to create communications between the rete and the surrounding cavernous sinus [12]. Superselective angiography into the APA showed rapid sequential filling of the rete, cavernous sinus, and basilar sinus. However, this model had limitations of obvious eye complications, spontaneous occlusion of the arteriovenous shunt, and being only for short-term investigations.

Massoud et al. developed a distinguished swine AVM model with induced high blood flow across both retia, by surgical formation of a side-to-side arteriovenous fistula between the CCA and the EJV with the ligation of the CCA proximal to the fistula on the right side [13]. The angiography showed a clear demonstration of the feeding arteries (mainly the left APA), the nidus (bilateral retia), and the draining vein (the right APA down to the fistula), very similar to human AVMs (Figure 2(b)). An average blood pressure of the left APA dropped from 77 mmHg to 67 mmHg after model formation, and the right APA pressure dropped further to 46 mmHg. By additional occlusion of the rete branches on the right side, the research group also successfully preserved the same model for follow-up study up to 180 days [51]. In the chronic model, striking transmural changes of nidus vessels were observed, representative of realistic histopathologic features in human AVMs. Both the acute and the chronic models were widely adopted in the study of AVMs [52–58], especially in the aspects of hemodynamic changes, embolization therapy, and radiosurgery.

Based on Massoud's model, modified swine AVM models were introduced. They posed a higher pressure gradient closer to values found in human AVMs, thereby reducing the rate of spontaneous thrombosis in the rete [59, 60].

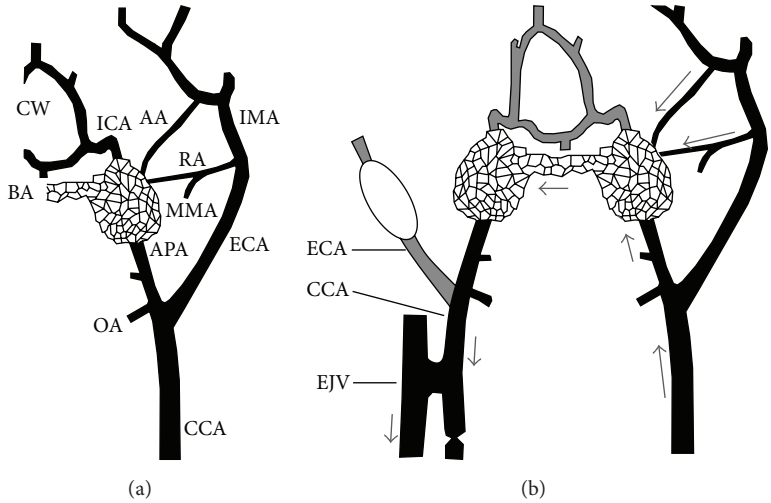

Figure 2: Anatomic basis and features of the swine AVM model. (a) Schematic representation of the normal left carotid arterial anatomy of the swine. The carotid rete mirabile is situated at the termination of the APA. ICA: internal carotid artery; ECA: external carotid artery; CCA: common carotid artery; IMA: internal maxillary artery; MMA: middle meningeal artery supplying the ramus anastomoticus; RA: ramus anastomoticus; AA: arteria anastomotica; APA: ascending pharyngeal artery; OA: occipital artery; BA: basilar artery; CW: circle of Willis; EJV: external jugular vein. (b) Schematic representation of the AVM model after creation of a right carotid-jugular fistula. Arrows indicate direction of flow, that is, from the left CCA to both retia mirabilia via the three feeding arteries (the left APA, RA, and AA), and retrograde down the right APA toward the right carotid-jugular fistula. Note balloon occlusion of the right ECA.

Besides, in the pig, the natural structure of carotid RM is also seen in the other artiodactyl animals such as the sheep, goat, ox, and cat, but not in the dog, rabbit, and rat. Whether the swine RM models can be duplicated in the other animals was unknown, except for a feasibility study in the sheep [14]. The vascular structure and blood supply of the RM in the sheep (the ascending pharyngeal artery is atrophy) slightly differ from those in the pig. A sheep AVM model was successfully created by a side-to-side surgical anastomosis between the CCA and the EJV with ligations of the vein above and the artery below the anastomosis (Figure 3). An angiographic appearance was demonstrated to simulate human AVMs in all the animal models. Creating the sheep model was rather simple and cost-effective, but it was not routinely adopted in AVM study.

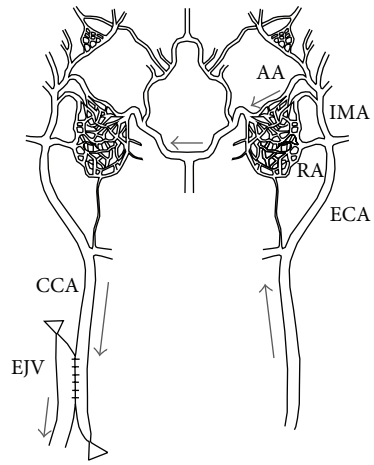

Figure 3: Anatomic basis and features of the sheep AVM model. Arrows indicate direction of flow, that is, from the left side of the carotid artery through both retia mirabilia, retrograde to the right carotid artery and jugular vein following surgical creation of an anastomosis. CCA: common carotid artery; ECA: external carotid artery; IMA: internal maxillary artery; RA: ramus anastomoticus; AA: arteria anastomotica; EJV: external jugular vein.

3.4. The Extracranial Venous Plexus as the AVM Nidus. In 2004, Yassari et al. described a rat model with the sham AVM nidus simply by ligating the left EJV at the confluence of the subclavian vein and making an end-to-side anastomosis of the EJV to the CCA [15]. These rats were observed up to 90 days. Angiographic and hemodynamic examinations showed that a high blood flow was diverted across fistula into the EJV (as the feeding artery), through a network of venous branches (as the nidus), then reconnected, and drained to the sigmoid sinus (as the draining vein), presenting a similar feature as in human AVMs (Figure 4). The high flow occurred immediately and kept stable after fistula formation, while the mean pressure in the fistula significantly dropped on day 7 and tended to stabilize by day 21.

Further analysis in this model demonstrated that the nidus vessels underwent morphological changes from normal veins to those similar to immature vessels in human AVMs, including heterogeneously thickened walls, splitting of the elastic lamina, and thickened endothelial layers [61]. Another study found out that the endothelial molecular changes in the nidus occurred, such as increased expression of vascular endothelial growth factor (VEGF), also similar to those observed in human AVMs [62]. These findings supported the theory that vascular changes in AVMs are

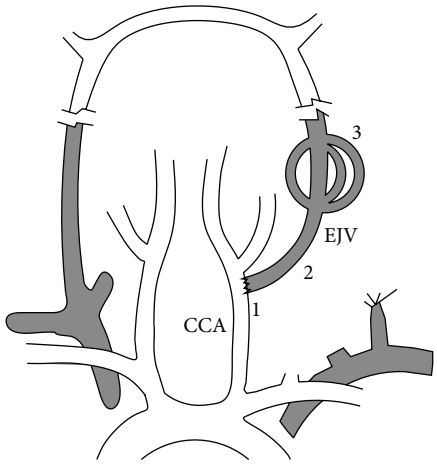

Figure 4: The arteriovenous fistula of the rat arteriovenous malformation model. 1: fistula; 2: arterialized jugular vein; 3: nidus; CCA: common carotid artery; EJV: external jugular vein.

secondary to increased flow rather than a primary phenotypic abnormality.

The activation of vascular cells in the nidus made it a unique model for studying the occlusive effect of radiosurgery on AVM vessels, because little was known about the molecular mechanisms of radiation mediated vascular obliteration. One study using the model showed that the expression of endothelial adhesion molecules in the nidus cells changed after radiosurgery [63]. Other studies tried to seek strategies to enhance AVM obliteration and reported an improved obliteration rate by induced thrombosis in the nidus with radiosurgery and coadministration of low-dose lipopolysaccharide and soluble tissue factor [64].

3.5. The AVM-Like Lesion Derived from Implants. Both the AVM lesions with simulated niduses using the RM and the venous plexus did not actually locate in the cerebral parenchyma. Pietilä et al. developed a novel model with an induced AVM lesion in the dog brain [16]. A vascular bypass was created between the MCA and the SSS by interposing a superficial temporal artery (STA) segment. A muscle graft supplied by a branch of the interposed vessel segment was implanted in the blood-stolen brain area due to the arteriovenous shunt. Postoperative angiography after 6 months demonstrated the feeding artery (the STA segment near the MCA) and the dilated draining vein (the STA segment near the SSS). Between them, AVM-like lesions with newly developed vessels were seen surrounding the muscle implant. The histopathological examination after 8 months demonstrated pronounced gliosis and endothelium/capillaries proliferation in this area. All proliferating vessels had delicate walls and small lumens and lacked differentiation into arterial and venous vessels. These suggested that AVM lesions in the adult brain could develop in the course of time, primarily as a result of angiogenesis, on the condition of cerebral ischemia and/or venous hypertension. The idea of using a pedicle muscle graft as a stimulus for inducing the intracerebral AVM-like lesion was derived from observational and therapeutic studies of Moyamoya disease.

There were some highlight features of this model resembling the appearance of AVMs in human, including thickening and fibrosis of the draining venous wall, new formation of vessels, and vascular proliferation, surrounding brain tissues with signs of ischemia and hemorrhage. Although an exquisite surgical technology was required for producing the animal model, it might help discovering the pathological mechanisms involved in AVM development.

3.6. The Xenograft Arteriovenous Fistula. Currently, radiosurgery was a kind of less invasive treatment for AVMs. It took a therapeutic effect by obliterating the AVM nidus, with a low obliterating rate and a latency period up to 2 years. Further understanding of the mechanism of radiosurgery might be helpful to develop advanced pharmacological therapies to improve the occlusive effects based on conventional radiosurgery.

For this purpose, the xenograft arteriovenous fistula model was created, as a segment of main arteries from transgenic mice was interposed between the caudal end of the CCA and the rostral end of the EJV in immune-deficient nude rats [17]. The implanted arterial graft was not a real AVM nidus but shared the AVM hemodynamic features with low resistance and high flow. Mice were chosen as the resource of donor arteries because diverse transgenic mice were available. The small size of mice made homotransplantations difficult, so rats were chosen as the receptor.

In this model, the arteriovenous fistula with radiation pretreatment reproduced distinct radiation arteriopathy as observed in resected human AVM specimens pretreated with radiosurgery. If radiation pretreatment would result in a specific molecular change in the fistula graft, or if the fistula graft from different transgenic mice would have a different response to radiation, this model probably yielded clues to the vascular targeting therapy and the gene therapy. One study had detected that some robust but modified radiation responses occurred in Endoglin and eNOS knockout transgenic arteriovenous fistulae [65].

The model was technically feasible and the overall angiographic patency rate was about 50%. However, there was a time limitation of 4 months for allowing transplanted tissues to retain their phenotypes due to the rejection reaction.

3.7. The Rat Cornea with Human AVM Tissues. The surgically resected human AVM lesions were valuable specimens for the histopathological study. When the specimens were transplanted into the corneal micropocket of the rats, they kept alive and growing. The angiogenic activity of the implanted tissues could be repeatedly measured according to a standard of neovascularization assessed by microvessel counts and VEGF expression [18].

Based on the model, the implanted AVM tissues showed the highest angiogenesis compared to other cerebrovascular disorders, cavernous malformation, and venous angioma, indicating that the AVM niduses were more likely to be active and progressive. The implanted AVM tissues previously

treated with embolization exhibited the highest angiogenic activity, followed by untreated and gamma knife treated AVM tissues; this might explain why AVM recurrence after intravascular embolization was more common. Moreover, this rat cornea model containing human AVM tissues could be used for evaluating molecular mechanisms of the neovascularization process over time [66].

3.8. The AVM Lesions by Gene Manipulation. Hereditary hemorrhagic telangiectasia (HHT) is an autosomal dominant vascular disorder characterized by recurrent nosebleeds, mucocutaneous telangiectases, and AVM formations in the brain and other visceral organs [67]. Heterozygous mutations in two genes, endoglin (*Eng*) and Activin receptor-like kinase 1 (*Alk1*), respectively, cause HHT type 1 and type 2. It is logical that animal models containing spontaneous or induced AVM lesions could be generated by regulating the genes.

Knockdown of *Alk1* by its splice-site blocking morpholino caused a spectrum of morphologic and functional defects as AVM lesions in zebrafish embryos [68]. The transgenic mice lacking both alleles of either *Eng* or *Alk1* genes died in embryonic period due to defects in vessel and heart developments [19, 21, 69]. Both $Eng^{+/-}$ and $Alk1^{+/-}$ haploinsufficient mice could be successfully generated. These mice develop vascular lesions in various organs, but spontaneous lesions in the brain were modest in $Eng^{+/-}$ mice and minimal in $Alk1^{+/-}$ mice [20, 22]. A research group headed by Su et al. induced cerebral microvascular dysplasia by transferring virus-mediated VEGF gene to the brain of $Eng^{+/-}$ or $Alk1^{+/-}$ adult mice [23–25]. The AVM-like capillary dysplasia was more pronounced in $Eng^{+/-}$ mice than in $Alk1^{+/-}$ mice. Interestingly, increased cerebral perfusion by intraventricular infusion of hydralazine or nicardipine after VEGF delivery promoted capillary dysplasia in $Alk1^{+/-}$ mice. These studies demonstrated that VEGF delivery into the brain of wide type mice led to increased microvessel counts but not microvascular dysplasia, and saline injection did not cause significant microvascular changes even in the haploinsufficient mice, approving that the development and progression of AVM lesions in adult brains were possible, when hereditary variation was combined with endogenous or exogenous growth factor delivery. Although sharing the somewhat alike phenotype, the induced local microvascular dysplasias were not enough to stand for direct models of the disease. However, they might be useful in identifying the possible factors which took a role in the pathogenesis of AVMs.

The conditional knockout technique with Cre/LoxP recombination system made it possible to delete target genes at the planned time or in the expected cells, because the Cre enzyme expression could be precisely controlled. Conditional deletion of both *Alk1* alleles in adult mice by tamoxifen-inducible Cre resulted in AV fistula formations and spontaneous hemorrhage mostly in the lung, gastrointestinal track, and uterus, but not remarkably in the brain, although de novo vascular malformation lesions developed upon induction of skin wounding in these mice [26]. The similar phenomenon could be observed in conditional *Eng* deletion mice, in which vessel abnormalities mimicking human AVM nidus were induced in the brain with the presence of angiogenic stimulation such as mechanical injury or VEGF delivery [27]. Meanwhile, Su's research group successfully produced AVM lesions in the adult mouse brain resembling the human disease, by injecting vectors expressing both Cre and VEGF into the basal ganglia of $Alk1^{2\text{LoxP}/2\text{LoxP}}$ and $Eng^{2\text{LoxP}/2\text{LoxP}}$ mice [28, 29]. The results showed that cerebrovascular lesions were more severe in $Alk1^{2\text{LoxP}/2\text{LoxP}}$ mice due to more effective gene deletion. In fact, regional deletion of *Eng* caused more severe cerebrovascular malformation per copy than *Alk1* with VEGF stimulation. These models were promising for evaluating the pathogenic mechanisms of AVMs and for discovering potential medical therapies to slow AVM growth and stabilize the rupture-prone abnormal vasculature.

Antenatal deletion of both *Alk1* alleles in restricted endothelial cells (ECs) caused severe and fatal visceral arteriovenous malformations [70]. Conditional deletion of *Alk1* specifically in ECs in adult mice resulted in AVM formations in the intestine, lung, and around ear-tag wounds, as well as in the brain area previously injected with vectors expressing EVGF [30]. Model mice died in 6–13 days due to bleeding and anemia. This phenotype was the same as that of mice with global *Alk1* deletion [26], indicating the pivotal role of ECs in pathogenesis of AVMs. In contrast, deletion of *Alk1* in pericytes alone was not sufficient to initiate AVM development in adult mice. Similarly, endothelial specific deletion of *Eng* led to endothelial proliferation and AVM formations in neonatal retina and local venomegaly in the adult skin induced by mechanical and VEGF stimulation [31]. Owing to the lack of brain-dominant lesions, Milton et al. successfully generated mouse models with spontaneous AVMs in the brain and/or spinal cord by deleting *Alk1* in the embryo by SM22-Cre, which was expressed in smooth muscle cells, ECs, and some other cell types in different organs [32]. Most of the mice showed a paralysis or lethality phenotype due to internal hemorrhage during the first 10 to 15 weeks of life. However, the mice that survived this period showed reduced lethality rates even though they carried multiple AVMs. Choi et al. created a similar model with the spontaneous onset AVMs in $Eng^{2\text{LoxP}/2\text{LoxP}}$; with SM22-Cre expressed mice, in which AVMs were found in the central nervous system and intestine, more than half of the mice died from internal hemorrhage before 6 weeks of age [27]. These distinctive models possibly allowed us to study pathophysiology of AVM rupture.

Other genes involved in angiogenesis would also be manipulated to create AVM models. Taking essential roles in vascular development and remolding, Notch signaling pathway was upregulated in human AVMs and might be an important molecular regulator of AVM pathogenesis [71]. Both Notch loss-of-function and gain-of-function mutations impair vascular development, resulting in arteriovenous shunting in zebrafish and mouse embryos, indicating that proper spatial and temporal patterns of Notch activity were critical for angiogenesis [33, 72, 73]. Postnatal overexpression of constitutively active *Notch4* in the endothelium by the tetracycline-regulatory system elicited cerebral arteriovenous shunting in mice, and gene repression reversed the AVM

progression [33]. Further analysis of this model showed that AVMs arose from enlargement of preexisting microvessels in size of capillaries, without smooth muscle cell coverage but with high blood flow, implying cellular and hemodynamic mechanisms underlying AVM pathogenesis [74]. Similarly, endothelial expression of constitutively active *Notch1* led to AVM formations in the neonatal mouse brain, and activation of Notch1 in adult mouse caused AVM formations in other organs, but not in the brain [73, 74].

The lack of matrix Gla protein (Mgp) also caused AVMs in mice. Cerebral enlarged vessels and direct connections between arteries and veins were detected in the $Mgp^{-/-}$ mice, but not in $Mgp^{+/-}$ mice at 4 weeks of age. Mgp is a bone morphogenetic protein (BMP) inhibitor. Increased BMP activity due to the deficiency of Mgp induced expression of Alk1 and subsequently enhanced expression of Notch ligands Jagged 1 and Jagged 2, which abnormally increased Notch activity. As expected, reduced Jagged expression in the $Mgp^{-/-}$ mice by crossing them with Jagged deficient mice normalized endothelial differentiation and prevented AVM formations [34]. Moreover, deletion of endothelial *Rbpj*, a mediator of Notch signaling, in postnatal day one resulted in features of AVMs in the mouse brain, including abnormal AV shunting and tortuous vessels. Deletion of the *Rbpj* gene in adult mice did not cause brain AVMs [35].

Cerebrovascular abnormalities, AVM formations, and hemorrhage occurred spontaneously in some cases where relevant genes were directly or conditionally deleted at the antenatal or postnatal stages, although in most cases, the model mice either displayed minimal vascular lesions or obvious vascular lesions out of the brain. The spontaneous cerebral AVM lesions partially simulated the natural clinical course of the disease, but the lesions lacked uniformity and reproducibility in size and location. Focal angiogenic stimulation based on gene deficiency helped to create adult onset models of induced AVM lesions in the brain. These models containing comparable AVM lesions might be more suitable for mechanism and therapeutic studies. In spite of posing disadvantages such as complicated procedures, high expanding, and being time consuming, the models by gene manipulation were unique for investigating the AVM pathogenesis and testing new therapies.

4. Discussion and Conclusions

As shown in Tables 1 and 2, animal models in studying AVMs were diverse. In the early period, investigators produced hypoperfusion and/or venous hypertension in the whole or regional brain by extra- or intracranial arteriovenous fistulae, to evaluate the hemodynamic and pathophysiological changes of AVM adjacent parenchyma in the presence of an AVM lesion or after its resection, so as to explain the symptoms and to protect against postoperative complications. The discovery of the special vascular structures as the AVM nidus in animals (the RM in artiodactyls and the venous plexus in rats) made it possible to practice the occlusive treatments (endovascular embolization and radiotherapy) and to analyze therapeutic effects. Lately, the manipulation of angiogenesis-related genes helped to create mutant mice with real AVM lesions in the brain. With the improvement of its stability, this promising model was worthwhile for studying the mechanisms about the origination, progression, and rupture of AVMs. Other ingeniously designed models, including induced AVM-like lesions in the dog brain and implanted transgenic arteriovenous fistula from mice to rats, possessed their own values to investigate pathogenesis and novel treatments. The rat cornea model was to evaluated angiogenic mechanisms especially of human AVM specimens.

An ideal AVM model, which completely shared the same anatomic, physiologic, biological, and clinical features as human AVM disease, was lacking. Even the transgenic mice model carried out with spontaneous but systematic vascular malformation lesions could not fully represent the sporadic cases mostly seen in clinic. In spite of limitations, these various models provided assistance to answer particular questions in the study of AVMs.

The origin of AVM is still a mystery. It was generally believed that the vascular disorder was initiated during embryonic development. However, evidences from animal models demonstrated that postnatal formations of AVMs were possible, due to the two causal factors of angiogenic stimulation and gene deficiency. With genome-wide association study, investigators attempted to identify mutant genes associated with AVM susceptibility in sporadic AVM patients. The possible involved genes included Alk1, Eng, interleukin-6 (IL-6), and interleukin-1β (IL-1β) with single nucleotide polymorphisms (SNPs), but the limited results were inconsistent [75, 76].

The mechanisms that underlie AVM growth and progression remain poorly understood. Abnormally high blood flow and shear forces in nidal vessels activated molecular pathways in smooth muscle cells and ECs. Hypoperfusion and hypoxia in the nidal and surrounding tissues stimulated angiogenesis and inflammatory reactions. Both of them lead to vascular proliferation and remodeling [77]. These hypothetic mechanisms were demonstrated in Yassari's and Pietila's animal models and were also supported from the analysis of resected human AVM specimens, where the related factors like transforming growth factor (TGF), VEGF, matrix metalloproteinase-9 (MMP-9), BMP, cellular adhesion molecules, and so on were overexpressed [78].

Intracranial hemorrhage is the most severe and most common clinical presentation of AVM patients. Risk factors associated with AVM rupture include certain genetic mutations, intranidal aneurysms, exclusive or restricted venous drainage, deep or infratentorial location, and history of previous hemorrhage [79–81]. SNPs of IL-6, tumor necrosis factor-α (TNF-α), MMP-9, and other genes in AVM specimens appeared to influence clinical course of AVM rupture [82]. However, the exact molecular mechanisms of AVM rupture need to be scrutinized. Studies of human AVM lesions indicated that multiple mechanisms including inflammation, extracellular matrix remodeling, ECs abnormalities, and immature nidal vessels all likely contributed to hemorrhagic tendency [83]. Further researches are anticipated by using animal models with spontaneous hemorrhagic AVM lesions.

Among the conventional treatments, microsurgical resection is currently recommended for Spetzler-Martin Grades I and II AVMs. For high-grade AVMs, combined treatments are often used lacking a standard procedure. Given that the majority of high-grade lesions cannot be treated without relatively high morbidity and mortality, new biological therapies and gene therapies are under development aiming toward vascular remodeling. A study showed that losartan, an angiotensin II receptor antagonist, attenuated abnormal blood vessel morphology in the *Alk1* knockout zebrafish through modulating the BMP signaling pathway [84]. In the $Alk1^{2LoxP/2LoxP}$ mice model with focal AVMs by virus-mediated Cre and VEGF, the induced angiogenesis and vascular dysplasia were attenuated by administration of VEGF antagonist bevacizumab [85], which later successfully treated a female HHT patient [86]. Moreover, with the deeper understanding the therapeutic mechanisms of radiosurgery in Yassari's and Lawton's models, vascular targeting therapy might improve the obliterating rate and decrease the complications of radiosurgery.

We hope this review would provide the basic of currently available AVM models. The diverse techniques and methods displayed here might shed light on the creation of preferable AVM models in the future, overall promoting further studies of the disease.

Conflict of Interests

The authors declare that there is no conflict of interests regarding the publication of this paper.

Acknowledgments

The paper was supported by grants of the National Natural Science Foundation of China (no. 81000489) and Shanghai Municipal Science and Technology Commission Foundation (no. 13140903300).

References

[1] H. Kim, S. Sidney, C. E. McCulloch et al., "Racial/ethnic differences in longitudinal risk of intracranial hemorrhage in brain arteriovenous malformation patients," *Stroke*, vol. 38, no. 9, pp. 2430–2437, 2007.

[2] B. A. Gross and R. Du, "Diagnosis and treatment of vascular malformations of the brain," *Current Treatment Options in Neurology*, vol. 16, no. 1, article 279, 2014.

[3] J. P. Mohr, A. J. Moskowitz, C. Stapf et al., "The ARUBA trial: current status, future hopes," *Stroke*, vol. 41, no. 8, pp. e537–e540, 2010.

[4] H. Kim, L. Pawlikowska, Y. Chen, H. Su, G.-Y. Yang, and W. L. Young, "Brain arteriovenous malformation biology relevant to hemorrhage and implication for therapeutic development," *Stroke*, vol. 40, supplement 3, pp. S95–S97, 2009.

[5] M. Xu, H. Xu, Z. Qin, J. Zhang, X. Yang, and F. Xu, "Increased expression of angiogenic factors in cultured human brain arteriovenous malformation endothelial cells," *Cell Biochemistry and Biophysics*, vol. 70, no. 1, pp. 443–447, 2014.

[6] R. F. Spetzler, C. B. Wilson, P. Weinstein, M. Mehdorn, J. Townsend, and D. Telles, "Normal perfusion pressure breakthrough theory," *Clinical Neurosurgery*, vol. 25, pp. 651–672, 1978.

[7] M. K. Morgan, R. E. Anderson, and T. M. Sundt Jr., "A model of the pathophysiology of cerebral arteriovenous malformations by a carotid-jugular fistula in the rat," *Brain Research*, vol. 496, no. 1-2, pp. 241–250, 1989.

[8] J. B. Bederson, O. D. Wiestler, O. Brustle, P. Roth, R. Frick, and M. G. Yasargil, "Intracranial venous hypertension and the effects of venous outflow obstruction in a rat model of arteriovenous fistula," *Neurosurgery*, vol. 29, no. 3, pp. 341–350, 1991.

[9] J. Hai, M. Ding, Z. Guo, and B. Wang, "A new rat model of chronic cerebral hypoperfusion associated with arteriovenous malformations," *Journal of Neurosurgery*, vol. 97, no. 5, pp. 1198–1202, 2002.

[10] B. B. Scott, J. E. McGillicuddy, J. F. Seeger, G. W. Kindt, and S. L. Giannotta, "Vascular dynamics of an experimental cerebral arteriovenous shunt in the primate," *Surgical Neurology*, vol. 10, no. 1, pp. 34–38, 1978.

[11] S. Numazawa, T. Sasaki, S. Sato, Y. Watanabe, Z. Watanabe, and N. Kodama, "Experimental model of intracranial arteriovenous shunting in the acute stage," *Neurologia Medico-Chirurgica*, vol. 45, no. 6, pp. 288–292, 2005.

[12] J. C. Chaloupka, F. Vinuela, J. Robert, and G. R. Duckwiler, "An in vivo arteriovenous malformation model in swine: preliminary feasibility and natural history study," *American Journal of Neuroradiology*, vol. 15, no. 5, pp. 945–950, 1994.

[13] T. F. Massoud, C. Ji, F. Vinuela et al., "An experimental arteriovenous malformation model in swine: anatomic basis and construction technique," *American Journal of Neuroradiology*, vol. 15, no. 8, pp. 1537–1545, 1994.

[14] Z. Qian, S. Climent, M. Maynar et al., "A simplified arteriovenous malformation model in sheep: feasibility study," *American Journal of Neuroradiology*, vol. 20, no. 5, pp. 765–770, 1999.

[15] R. Yassari, T. Sayama, B. S. Jahromi et al., "Angiographic, hemodynamic and histological characterization of an arteriovenous fistula in rats," *Acta Neurochirurgica*, vol. 146, no. 5, pp. 495–504, 2004.

[16] T. A. Pietilä, J. M. Zabramski, A. Thèllier-Janko et al., "Animal model for cerebral arteriovenous malformation," *Acta Neurochirurgica*, vol. 142, no. 11, pp. 1231–1240, 2000.

[17] M. T. Lawton, C. L. Stewart, A. A. Wulfstat et al., "The transgenic arteriovenous fistula in the rat: an experimental model of gene therapy for brain arteriovenous malformations," *Neurosurgery*, vol. 54, no. 6, pp. 1463–1471, 2004.

[18] D. Konya, Ö. Yildirim, Ö. Kurtkaya et al., "Testing the angiogenic potential of cerebrovascular malformations by use of a rat cornea model: usefulness and novel assessment of changes over time," *Neurosurgery*, vol. 56, no. 6, pp. 1339–1345, 2005.

[19] A. Bourdeau, D. J. Dumont, and M. Letarte, "A murine model of hereditary hemorrhagic telangiectasia," *Journal of Clinical Investigation*, vol. 104, no. 10, pp. 1343–1351, 1999.

[20] J. Satomi, R. J. Mount, M. Toporsian et al., "Cerebral vascular abnormalities in a murine model of hereditary hemorrhagic telangiectasia," *Stroke*, vol. 34, no. 3, pp. 783–789, 2003.

[21] S. P. Oh, T. Seki, K. A. Goss et al., "Activin receptor-like kinase 1 modulates transforming growth factor-β1 signaling in the regulation of angiogenesis," *Proceedings of the National Academy of Sciences of the United States of America*, vol. 97, no. 6, pp. 2626–2631, 2000.

[22] S. Srinivasan, M. A. Hanes, T. Dickens et al., "A mouse model for hereditary hemorrhagic telangiectasia (HHT) type 2," *Human Molecular Genetics*, vol. 12, no. 5, pp. 473–482, 2003.

[23] B. Xu, Y. Q. Wu, M. Huey et al., "Vascular endothelial growth factor induces abnormal microvasculature in the endoglin heterozygous mouse brain," *Journal of Cerebral Blood Flow and Metabolism*, vol. 24, no. 2, pp. 237–244, 2004.

[24] Q. Hao, H. Su, D. A. Marchuk et al., "Increased tissue perfusion promotes capillary dysplasia in the ALK1-deficient mouse brain following VEGF stimulation," *The American Journal of Physiology—Heart and Circulatory Physiology*, vol. 295, no. 6, pp. H2250–H2256, 2008.

[25] Q. Hao, Y. Zhu, H. Su et al., "VEGF induces more severe cerebrovascular dysplasia in $Eng^{+/-}$ than in $Alk1^{+/-}$ mice," *Translational Stroke Research*, vol. 1, no. 3, pp. 197–201, 2010.

[26] O. P. Sung, M. Wankhede, J. L. Young et al., "Real-time imaging of de novo arteriovenous malformation in a mouse model of hereditary hemorrhagic telangiectasia," *Journal of Clinical Investigation*, vol. 119, no. 11, pp. 3487–3496, 2009.

[27] E.-J. Choi, W. Chen, K. Jun, H. M. Arthur, W. L. Young, and H. Su, "Novel brain arteriovenous malformation mouse models for type 1 hereditary hemorrhagic telangiectasia," *PLoS ONE*, vol. 9, no. 2, Article ID e88511, 2014.

[28] E. J. Walker, H. Su, F. Shen et al., "Arteriovenous malformation in the adult mouse brain resembling the human disease," *Annals of Neurology*, vol. 69, no. 6, pp. 954–962, 2011.

[29] E.-J. Choi, E. J. Walker, F. Shen et al., "Minimal homozygous endothelial deletion of eng with VEGF stimulation is sufficient to cause cerebrovascular dysplasia in the adult mouse," *Cerebrovascular Diseases*, vol. 33, no. 6, pp. 540–547, 2012.

[30] W. Chen, Z. Sun, Z. Han et al., "De novo cerebrovascular malformation in the adult mouse after endothelial Alk1 deletion and angiogenic stimulation," *Stroke*, vol. 45, no. 3, pp. 900–902, 2014.

[31] M. Mahmoud, K. R. Allinson, Z. Zhai et al., "Pathogenesis of arteriovenous malformations in the absence of endoglin," *Circulation Research*, vol. 106, no. 8, pp. 1425–1433, 2010.

[32] I. Milton, D. Ouyang, C. J. Allen et al., "Age-dependent lethality in novel transgenic mouse models of central nervous system arteriovenous malformations," *Stroke*, vol. 43, no. 5, pp. 1432–1435, 2012.

[33] P. A. Murphy, M. T. Y. Lam, X. Wu et al., "Endothelial Notch4 signaling induces hallmarks of brain arteriovenous malformations in mice," *Proceedings of the National Academy of Sciences of the United States of America*, vol. 105, no. 31, pp. 10901–10906, 2008.

[34] Y. Yao, J. Yao, M. Radparvar et al., "Reducing Jagged 1 and 2 levels prevents cerebral arteriovenous malformations in matrix Gla protein deficiency," *Proceedings of the National Academy of Sciences of the United States of America*, vol. 110, no. 47, pp. 19071–19076, 2013.

[35] C. M. Nielsen, H. Cuervo, V. W. Ding, Y. Kong, E. J. Huang, and R. A. Wang, "Deletion of Rbpj from postnatal endothelium leads to abnormal arteriovenous shunting in mice," *Development*, vol. 141, no. 19, pp. 3782–3792, 2014.

[36] T. Sakaki, S. Tsujimoto, M. Nishitani, Y. Ishida, and T. Morimoto, "Perfusion pressure breakthrough threshold of cerebral autoregulation in the chronically ischemic brain: an experimental study in cats," *Journal of Neurosurgery*, vol. 76, no. 3, pp. 478–485, 1992.

[37] Y. Miyasaka, K. Tokiwa, K. Irikura et al., "The effects of a carotid-jugular fistula on cerebral blood flow in the cat: an experimental study in the acute period," *Surgical Neurology*, vol. 41, no. 5, pp. 396–398, 1994.

[38] K. Tokiwa, Y. Miyasaka, K. Irikura, R. Tanaka, and M. Yamada, "The effects of a carotid-jugular fistula on cerebral blood flow in the cat: an experimental study in the chronic period," *Neurological Research*, vol. 17, no. 4, pp. 297–300, 1995.

[39] M. K. Morgan, R. E. Anderson, and T. M. Sundt Jr., "The effects of hyperventilation on cerebral blood flow in the rat with an open and closed carotid-jugular fistula," *Neurosurgery*, vol. 25, no. 4, pp. 606–612, 1989.

[40] K. Irikura, S. Morii, Y. Miyasaka, M. Yamada, K. Tokiwa, and K. Yada, "Impaired autoregulation in an experimental model of chronic cerebral hypoperfusion in rats," *Stroke*, vol. 27, no. 8, pp. 1399–1404, 1996.

[41] L. H. S. Sekhon, M. K. Morgan, and I. Spence, "Normal perfusion pressure breakthrough: the role of capillaries," *Journal of Neurosurgery*, vol. 86, no. 3, pp. 519–524, 1997.

[42] B. Meyer, M. Stoffel, C. Stuer et al., "Norepinephrine in the rat cortex before and after occlusion of chronic arteriovenous fistulae: a microdialysis study in an animal model of cerebral arteriovenous malformations," *Neurosurgery*, vol. 51, no. 3, pp. 771–780, 2002.

[43] M. Mut, K. Öge, F. Zorlu, Ü. Ündeğer, S. Erdem, and O. E. Özcan, "Effects of ionizing radiation on brain tissue surrounding arteriovenous malformations: an experimental study in a rat caroticojugular fistula model," *Neurosurgical Review*, vol. 27, no. 2, pp. 121–127, 2004.

[44] J. Hai, Q. Lin, S.-T. Li, and Q.-G. Pan, "Chronic cerebral hypoperfusion and reperfusion injury of restoration of normal perfusion pressure contributes to the neuropathological changes in rat brain," *Molecular Brain Research*, vol. 126, no. 2, pp. 137–145, 2004.

[45] J. Hai, Q. Lin, D.-F. Deng, Q.-G. Pan, and M.-X. Ding, "The pretreatment effect on brain injury during restoration of normal perfusion pressure with hemodilution in a new rat model of chronic cerebral hypoperfusion," *Neurological Research*, vol. 29, no. 6, pp. 583–587, 2007.

[46] T. Kojima, S. Miyachi, Y. Sahara et al., "The relationship between venous hypertension and expression of vascular endothelial growth factor: hemodynamic and immunohistochemical examinations in a rat venous hypertension model," *Surgical Neurology*, vol. 68, no. 3, pp. 277–284, 2007.

[47] D. H. Lee, C. H. Wriedt, J. C. E. Kaufmann, D. M. Pelz, A. J. Fox, and F. Vinuela, "Evaluation of three embolic agents in pig rete," *American Journal of Neuroradiology*, vol. 10, no. 4, pp. 773–776, 1989.

[48] M. F. Brothers, J. C. E. Kaufmann, A. J. Fox, and J. P. Deveikis, "n-Butyl 2-cyanoacrylate—substitute for IBCA in interventional neuroradiology: histopathologic and polymerization time studies," *American Journal of Neuroradiology*, vol. 10, no. 4, pp. 777–786, 1989.

[49] P. Lylyk, F. Vinuela, H. V. Vintes, J. Bentson, G. Duckwiler, and T. Lin, "Use of a new mixture for embolization of intracranial vascular malformations. Preliminary experimental experience," *Neuroradiology*, vol. 32, no. 4, pp. 304–310, 1990.

[50] A. A. F. De Salles, T. D. Solberg, P. Mischel et al., "Arteriovenous malformation animal model for radiosurgery: the rete mirabile," *American Journal of Neuroradiology*, vol. 17, no. 8, pp. 1451–1458, 1996.

[51] T. F. Massoud, H. V. Vinters, K. H. Chao, F. Vinuela, and R. Jahan, "Histopathologic characteristics of a chronic arteriovenous malformation in a swine model: preliminary study,"

American Journal of Neuroradiology, vol. 21, no. 7, pp. 1268–1276, 2000.

[52] Y. Murayama, T. F. Massoud, and F. Viñuela, "Hemodynamic changes in arterial feeders and draining veins during embolotherapy of arteriovenous malformations: an experimental study in a swine model," *Neurosurgery*, vol. 43, no. 1, pp. 96–106, 1998.

[53] Y. Murayama, F. Viñuela, A. Ulhoa et al., "Nonadhesive liquid embolic agent for cerebral arteriovenous malformations: preliminary histopathological studies in swine rete mirabile," *Neurosurgery*, vol. 43, no. 5, pp. 1164–1172, 1998.

[54] T. A. Becker, D. R. Kipke, M. C. Preul et al., "In vivo assessment of calcium alginate gel for endovascular embolization of a cerebral arteriovenous malformation model using the swine rete mirabile," *Neurosurgery*, vol. 51, no. 2, pp. 453–459, 2002.

[55] E. D. Akin, E. Perkins, and I. B. Ross, "Surgical handling characteristics of an ethylene vinyl alcohol copolymer compared with *N*-butyl cyanoacrylate used for embolization of vessels in an arteriovenous malformation resection model in swine," *Journal of Neurosurgery*, vol. 98, no. 2, pp. 366–370, 2003.

[56] T. A. Becker, M. C. Preul, W. D. Bichard, D. R. Kipke, and C. G. McDougall, "Calcium alginate gel as a biocompatible material for endovascular arteriovenous malformation embolization: six-month results in an animal model," *Neurosurgery*, vol. 56, no. 4, pp. 793–801, 2005.

[57] A. K. Wakhloo, B. B. Lieber, R. Siekmann, D. J. Eber, and M. J. Gounis, "Acute and chronic swine rete arteriovenous malformation models: hemodynamics and vascular remodeling," *American Journal of Neuroradiology*, vol. 26, no. 7, pp. 1702–1706, 2005.

[58] R. Jahan, T. D. Solberg, D. Lee et al., "An arteriovenous malformation model for stereotactic radiosurgery research," *Neurosurgery*, vol. 61, no. 1, pp. 152–159, 2007.

[59] R. Siekmann, A. K. Wakhloo, B. B. Lieber, M. J. Gounis, A. A. Divani, and L. N. Hopkins, "Modification of a previously described arteriovenous malformation model in the swine: endovascular and combined surgical/endovascular construction and hemodynamics," *American Journal of Neuroradiology*, vol. 21, no. 9, pp. 1722–1725, 2000.

[60] J. Klisch, F. Requejo, L. Yin, B. Eissner, and M. Schumacher, "The two-in-one model: a new variation of the arteriovenous malformation model in swine," *Neuroradiology*, vol. 43, no. 5, pp. 393–397, 2001.

[61] J. Tu, A. Karunanayaka, A. Windsor, and M. A. Stoodley, "Comparison of an animal model of arteriovenous malformation with human arteriovenous malformation," *Journal of Clinical Neuroscience*, vol. 17, no. 1, pp. 96–102, 2010.

[62] A. Karunanyaka, J. Tu, A. Watling, K. P. Storer, A. Windsor, and M. A. Stoodley, "Endothelial molecular changes in a rodent model of arteriovenous malformation: laboratory investigation," *Journal of Neurosurgery*, vol. 109, no. 6, pp. 1165–1172, 2008.

[63] K. P. Storer, J. Tu, M. A. Stoodley, and R. I. Smee, "Expression of endothelial adhesion molecules after radiosurgery in an animal model of arteriovenous malformation," *Neurosurgery*, vol. 67, no. 4, pp. 976–983, 2010.

[64] K. Storer, J. Tu, A. Karunanayaka et al., "Coadministration of low-dose lipopolysaccharide and soluble tissue factor induces thrombosis after radiosurgery in an animal arteriovenous malformation model," *Neurosurgery*, vol. 61, no. 3, pp. 604–611, 2007.

[65] M. T. Lawton, C. M. Arnold, Y. J. Kim et al., "Radiation arteriopathy in the transgenic arteriovenous fistula model," *Neurosurgery*, vol. 62, no. 5, pp. 1129–1138, 2008.

[66] A. Akakin, A. Ozkan, E. Akgun et al., "Endovascular treatment increases but gamma knife radiosurgery decreases angiogenic activity of arteriovenous malformations: an in vivo experimental study using a rat cornea model," *Neurosurgery*, vol. 66, no. 1, pp. 121–130, 2010.

[67] J. McDonald, P. Bayrak-Toydemir, and R. E. Pyeritz, "Hereditary hemorrhagic telangiectasia: an overview of diagnosis, management, and pathogenesis," *Genetics in Medicine*, vol. 13, no. 7, pp. 607–616, 2011.

[68] P. Corti, S. Young, C.-Y. Chen et al., "Interaction between alk1 and blood flow in the development of arteriovenous malformations," *Development*, vol. 138, no. 8, pp. 1573–1582, 2011.

[69] L. D. Urness, L. K. Sorensen, and D. Y. Li, "Arteriovenous malformations in mice lacking activin receptor-like kinase-1," *Nature Genetics*, vol. 26, no. 3, pp. 328–331, 2000.

[70] S. O. Park, J. L. Young, T. Seki et al., "ALK5- and TGFBR2-independent role of ALK1 in the pathogenesis of hereditary hemorrhagic telangiectasia type 2," *Blood*, vol. 111, no. 2, pp. 633–642, 2008.

[71] P. A. Murphy, G. Lu, S. Shiah, A. W. Bollen, and R. A. Wang, "Endothelial Notch signaling is upregulated in human brain arteriovenous malformations and a mouse model of the disease," *Laboratory Investigation*, vol. 89, no. 9, pp. 971–982, 2009.

[72] L. T. Krebs, J. R. Shutter, K. Tanigaki, T. Honjo, K. L. Stark, and T. Gridley, "Haploinsufficient lethality and formation of arteriovenous malformations in Notch pathway mutants," *Genes & Development*, vol. 18, no. 20, pp. 2469–2473, 2004.

[73] L. T. Krebs, C. Starling, A. V. Chervonsky, and T. Gridley, "Notch1 activation in mice causes arteriovenous malformations phenocopied by EphrinB2 and EphB4 mutants," *Genesis*, vol. 48, no. 3, pp. 146–150, 2010.

[74] P. A. Murphy, T. N. Kim, L. Huang et al., "Constitutively active Notch4 receptor elicits brain arteriovenous malformations through enlargement of capillary-like vessels," *Proceedings of the National Academy of Sciences of the United States of America*, vol. 111, no. 50, pp. 18007–18012, 2014.

[75] K. Boshuisen, M. Brundel, C. G. F. de Kovel et al., "Polymorphisms in ACVRL1 and endoglin genes are not associated with sporadic and HHT-related brain AVMs in Dutch patients," *Translational Stroke Research*, vol. 4, no. 3, pp. 375–378, 2013.

[76] L. Pawlikowska, J. Nelson, D. E. Guo et al., "The *ACVRL1* c.314—35A>G polymorphism is associated with organ vascular malformations in hereditary hemorrhagic telangiectasia patients with ENG mutations, but not in patients with *ACVRL1* mutations," *American Journal of Medical Genetics Part A*, vol. 167, no. 6, pp. 1262–1267, 2015.

[77] P. Moftakhar, J. S. Hauptman, D. Malkasian, and N. A. Martin, "Cerebral arteriovenous malformations. Part 2: physiology," *Neurosurgical Focus*, vol. 26, no. 5, article E11, 2009.

[78] P. Moftakhar, J. S. Hauptman, D. Malkasian, and N. A. Martin, "Cerebral arteriovenous malformations. Part 1: cellular and molecular biology," *Neurosurgical Focus*, vol. 26, no. 5, p. E10, 2009.

[79] S. Amin-Hanjani, "ARUBA results are not applicable to all patients with arteriovenous malformation," *Stroke*, vol. 45, no. 5, pp. 1539–1540, 2014.

[80] R. L. Novakovic, M. A. Lazzaro, A. C. Castonguay, and O. O. Zaidat, "The diagnosis and management of brain arteriovenous malformations," *Neurologic Clinics*, vol. 31, no. 3, pp. 749–763, 2013.

[81] P. P. Han, F. A. Ponce, and R. F. Spetzler, "Intention-to-treat analysis of Spetzler-Martin grades IV and V arteriovenous malformations: natural history and treatment paradigm," *Journal of Neurosurgery*, vol. 98, no. 1, pp. 3–7, 2003.

[82] H. Kim, D. A. Marchuk, L. Pawlikowska et al., "Genetic considerations relevant to intracranial hemorrhage and brain arteriovenous malformations," *Acta Neurochirurgica. Supplementum*, no. 105, pp. 199–206, 2008.

[83] L. Rangel-Castilla, J. J. Russin, E. Martinez-del-Campo, H. Soriano-Baron, R. F. Spetzler, and P. Nakaji, "Molecular and cellular biology of cerebral arteriovenous malformations: a review of current concepts and future trends in treatment," *Neurosurgical Focus*, vol. 37, no. 3, article E1, 2014.

[84] B. P. Walcott, "BMP signaling modulation attenuates cerebral arteriovenous malformation formation in a vertebrate model," *Journal of Cerebral Blood Flow and Metabolism*, vol. 34, no. 10, pp. 1688–1694, 2014.

[85] E. J. Walker, H. Su, F. Shen, V. Degos, K. Jun, and W. L. Young, "Bevacizumab attenuates VEGF-induced angiogenesis and vascular malformations in the adult mouse brain," *Stroke*, vol. 43, no. 7, pp. 1925–1930, 2012.

[86] J. Kochanowski, M. Sobieszczanska, S. Tubek, M. Żurek, and J. Pawełczak, "Successful therapy with bevacizumab in a case of hereditary hemorrhagic telangiectasia," *Human Vaccines & Immunotherapeutics*, vol. 11, no. 3, pp. 680–681, 2015.

Hindawi Publishing Corporation
BioMed Research International
Volume 2015, Article ID 257153, 6 pages
http://dx.doi.org/10.1155/2015/257153

Clinical Study

The Clinical Characteristics and Treatment of Cerebral Microarteriovenous Malformation Presenting with Intracerebral Hemorrhage: A Series of 13 Cases

Jing-Fang Hong,[1] Ying-Fang Song,[2] Hai-Bing Liu,[1] Zheng Liu,[1] and Shou-Sen Wang[1]

[1]*Department of Neurosurgery, Fuzhou General Hospital of Nanjing Military Command, Dongfang Hospital, Xiamen University, Fuzhou 350025, China*
[2]*Department of Pulmonary and Critical Care Medicine, Fuzhou General Hospital of Nanjing Military Command, Dongfang Hospital, Xiamen University, Fuzhou 350025, China*

Correspondence should be addressed to Shou-Sen Wang; wshsen@126.com

Received 21 August 2015; Accepted 28 September 2015

Academic Editor: Robert M. Starke

Object. The aim of this report was to explore the clinical presentation, radiological features, treatment methods, and outcome of micro-AVMs presenting with intracerebral hemorrhage. *Methods*. The clinical data, radiological features, treatment, and follow-up results for a consecutive series of 13 cases with micro-AVMs were retrospectively analyzed. *Results*. All 13 patients presented with intracerebral hemorrhage. Ten cases were confirmed by enhanced thin layer CT scanning and CTA, and the other 3 cases were confirmed by DSA. Treatment consisted of surgical removal in 10 cases, endovascular embolization in 1, and radiosurgery in 2. The modified GOS score was achieved in the third month after discharge: 10 cases were rated with 5 points (good recovery), 1 case was rated with 4 points (mild disability), and 2 cases were rated with 3 points (severe disability). During follow-up, No case of rebleeding was reported. *Conclusions*. Intracerebral hemorrhage is the main clinical manifestation of micro-AVMs. It is beneficial to find a tiny nidus of dense vessels located on hematoma wall on enhanced thin layer CT scanning for a clear diagnosis and to detect any abnormal feeding artery or venous drainage for an indirect diagnostic evidence. Resection is the main method of treatment for micro-AVMs.

1. Introduction

Arteriovenous malformation (AVM), composed of feeding artery, nidus, and venous drainage, is one of the most common vascular diseases of the cerebral hemorrhage. According to the clinical standard described by Yasargil, AVMs with a nidus smaller than or equal to 1 cm are called microarteriovenous malformations (micro-AVMs) [1]. In addition, the characteristics of small lesions and easy bleeding may pose a big challenge to the treatment and diagnosis of micro-AVMs. Meanwhile, there are only few reports and cases related to micro-AVMs to date, so the characteristics and treatment of the disease are still poorly understood. This study conducted a retrospective analysis from January 2008 to December 2013 and summarized the clinical data, radiological features, treatment, and outcome of these lesions in our department.

2. Patients and Methods

Thirteen cases of patients diagnosed as micro-AVMs were recruited in neurosurgery department of Fuzhou general hospital between January 2008 and December 2013. The patients were diagnosed as micro-AVMs with enhanced thin layer CT scanning, CT angiography (computed tomography angiography, CTA), cerebral digital subtraction angiography (DSA), or surgical exploration.

All patients underwent at least one enhanced thin layer CT scanning and CT angiography after being admitted to the hospital, and a following DSA examination would be conducted for the cases whose CTA finding was negative or questionable. Hematoma volume size was calculated according to formula $a \times b \times c/2$, where a, b, and c represent the maximal diameters of the hematoma in the 3 orthogonal planes.

Table 1: Overview of clinical features, diagnostic workup results, therapeutic methods, and outcome in the 13 patients with cerebral micro-AVMs.

Patient number/ age (y)/sex	Hematoma size (mL) & location	Enhanced thin layer CT scanning	CTA finding	DSA finding	Urgent surgery/treatment	Outcome (GOS)
1/11/M	20 Basal ganglia	Nidus	Micro-AVMs		No/surgery neuronavigation	5
2/31/F	10 Basal ganglia	Nidus	Abnormal feeding artery		No/radiotherapy	5
3/63/F	40 Parietal lobe	Nidus	Abnormal feeding artery		Yes/surgery	3
4/36/M	52 Temporoparietal lobe	Nidus	Micro-AVMs		Yes/surgery	5
5/18/M	27 Frontal lobe	Negative	Negative	Micro-AVMs	No/surgery	5
6/41/F	11 Frontal lobe	Nidus	Micro-AVMs		No/surgery neuronavigation	5
7/16/M	60 Temperoparietal lobe	Nidus	Micro-AVMs		Yes/surgery	5
8/15/M	16 Frontal lobe	Negative	Negative	Micro-AVMs	No/surgery	5
9/32/F	90 Temperoparietal lobe	Nidus	Micro-AVMs		Yes/surgery	4
10/24/M	10 Parietal lobe	Negative	Abnormal feeding artery	Abnormal feeding artery	No/radiotherapy	5
11/41/M	5 IVH	Nidus	Micro-AVMs	Micro-AVMs	No/endovascular embolization	5
12/61/M	48 Occipital lobe	Nidus	Micro-AVMs		Yes/surgery	5
13/35/M	50 Temperoparietal lobe	Nidus	Abnormal venous drainage	Micro-AVMs	Yes/surgery	3

The original data of thin CT scanning for angiography was transferred to data postprocessing workstation and to obtain new 3D-CTA image of VR and MIP.

The corresponding treatment protocol in our series should be chosen according to the characteristics and position of micro-AVMs, hematoma volume size, and the clinical status of the patients. (1) Surgical removal is the main method of treatment for the superficial lesion, under the condition that the volume of hematoma is more than 40 mL and the patients began to complain of consciousness disturbance. It is preferred to conduct urgent surgery after CTA. In principle, it is necessary to remove some or all of the hematomas, after the identification of vascular malformation; the first thing is to cut off the feeding artery and then to remove the nidus, ensured with protecting the venous drainage. (2) Endovascular embolization is suitable for the lesion site located in the deeper brain and is not suitable for surgery removal. What is more, there is an existing optional feeding artery in such case. (3) Radiation therapy is suitable for the patient with the lesion located in functional area, or the case whose tortuous feeding artery is difficult to trace during microcatheter navigation.

Follow-up evaluation was conducted by means of the outpatient visits and telephone interviews. Follow-up evaluation content includes clinical examinations, CTA in all patients, and DSA in two cases. The mean duration of follow-up was 35 months (range 15–75 months) and final outcome was classified according to GOS standard score.

3. Results

Among the cases, there were 9 males (69.2%) and 4 females (30.8%), and the age ranged between 11 and 63 years with an average age of 32.6 years (Table 1). In terms of medical history, there was only one case with hypertension, and no cases were reported with any family history of AVMs. All cases were manifested as acute onset of cerebral haemorrhage with clinical symptoms including 13 cases of sudden headache, 6 cases of consciousness disturbance, 7 cases of hemiparesis, and one case of epileptic seizure.

In evaluation of 13 cases with head CT scan, it was found that 12 patients had intracerebral hematoma, with 1 case of intraventricular hemorrhage. Among the cases, 4 hematomas were located in the temporoparietal lobe, 3 in the frontal lobe, 2 in the parietal lobe, 1 in the occipital lobe, 2 in the basal ganglia, and 1 in the left lateral ventricle. According to the formula, the hematoma was calculated to be 5~90 mL with an average value of 33 mL (Table 1). All 13 cases were examined with CTA, the enhanced thin layer CT scanning was applied to identify a tiny nidus of dense vessels located at hematoma

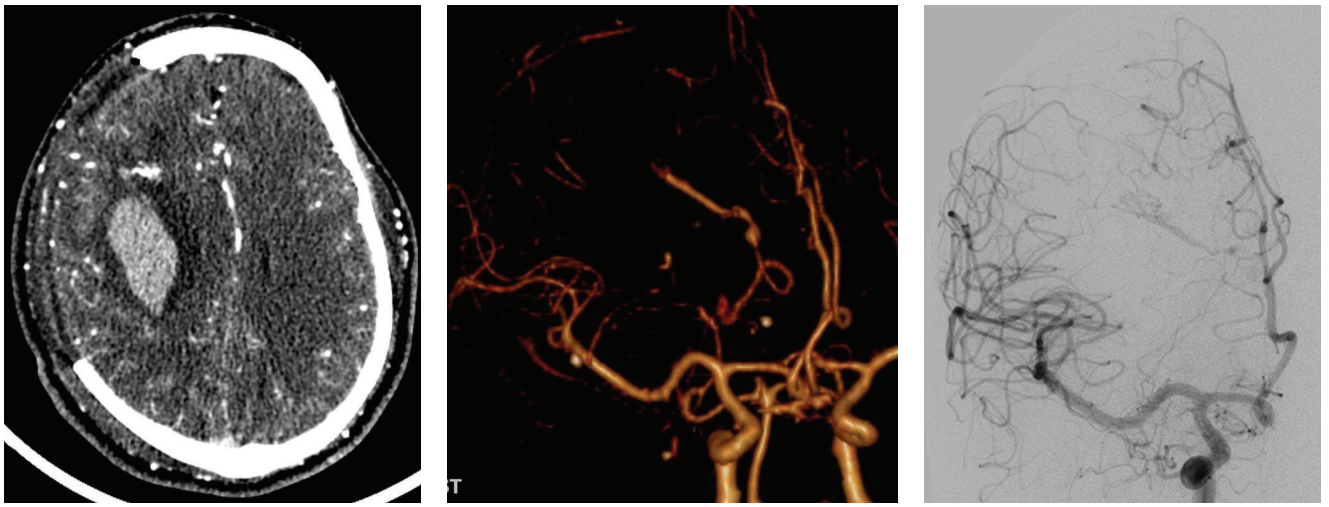

(a) (b) (c)

Figure 1: One case showed abnormal venous drainage in CTA. (a) Postoperative day 1 of decompressive craniectomy, enhanced thin layer CT scanning showing a tiny nidus of dense vessels in the front edge of hematoma. (b) VR reconstructed CTA images showing only abnormal venous drainage, no obvious nidus and feeding artery. (c) DSA confirmed micro-AVMs and feeding artery is a tiny branch of anterior cerebral arteries.

wall in 10 cases (Table 1). After the application of VR reconstruction in postprocessing workstation, a whole micro-AVM composed of feeding artery, nidus, and venous drainage was identified in 7 cases, with the nidus invisible, but abnormal feeding artery was identified in 2 cases and abnormal venous drainage was found in 1 case. Three cases were reported to be negative by CTA. Five cases were examined with DSA and 4 cases were identified to be micro-AVMs. Among these five cases, only abnormal venous drainage was observed in one case with CTA (Case 13, Figures 1(a)–1(c)), and the following DSA examination indicated that it was a micro-AVM whose feeding artery was a tiny branch of anterior cerebral arteries. In another case, only abnormal feeding artery without any nidus and venous drainage was found during initial CTA and DSA examination. After 8 months, this case has been confirmed to be micro-AVMs by later CTA and DSA, and meanwhile feeding artery, nidus, and venous drainage were clearly visible (Case 10, Figures 2(a)–2(e)).

All 13 cases underwent definitive treatment, including surgical resection in 10 cases, endovascular embolization in 1 case, and X-knife radiotherapy in 2 cases. In the case of surgical operation, all cases were identified to be micro-AVMs during operation. The hematoma volume of 6 cases is found to be more than 40 mL, and upon complaints of symptoms like consciousness disturbance, an urgent brain hematoma removal and micro-AVMs resection were preferred. As a result, 4 cases were chosen for selective operation when a clear diagnosis has been established, including 2 cases under MRI neuronavigation in surgeries for micro-AVMs to localize the nidus and plan the craniotomy. One case of endovascular embolization to treat micro-AVMs located in arterial blood supply of the ventricle and additional two cases of radiation therapy were performed. In patients subjected to radiotherapy, 1 case was for eloquent area, which was treated with conservative treatment for the first 8 months, and afterwards, this case has been confirmed to be micro-AVMs by DSA, for which X-knife treatment was applied. Another case was reported in basal ganglia which is treated with X knife treatment for function protection purposes after the hematoma was absorbed. All cases were survived, except for 1 case which appeared with transient declined myodynamia, and the remaining 12 cases were recovered without any new complications after treatment. According to Glasgow outcome score, achieved in the third month after discharge, 10 cases (76.9%) were rated with 5 points (good recovery), 1 case (7.7%) was rated with 4 points (mild disability), and 2 cases (15.4%) were rated with 3 points (severe disability). During follow-up period, no case of rebleeding or development of new symptoms was reported.

4. Discussion

In 1987, Yasargil [1] first defined arteriovenous malformation whose nidus is smaller than or equal to 1 cm as micro-AVMs. Micro-AVMs are visible on angiography but in some cases only abnormal arterial blood supply or abnormal venous drainage can be found. The lesion should be identified from cryptic AVMs which can only be confirmed by postoperative histological examination [1] and are undetectable on angiography and at surgery. The current literatures about micro-AVMs are rare, so the true incidence of this disease is difficult to ascertain. Some previous studies [2–4] found that 8–10% of arteriovenous malformation has been confirmed to be micro-AVMs. Our studies accounted for about 8.2% of all AVM cases in our department during this period and were consistent with the previous reported data. Micro-AVMs may represent a possible source of major cerebral hemorrhage in young and middle-aged adults. In our study, the average

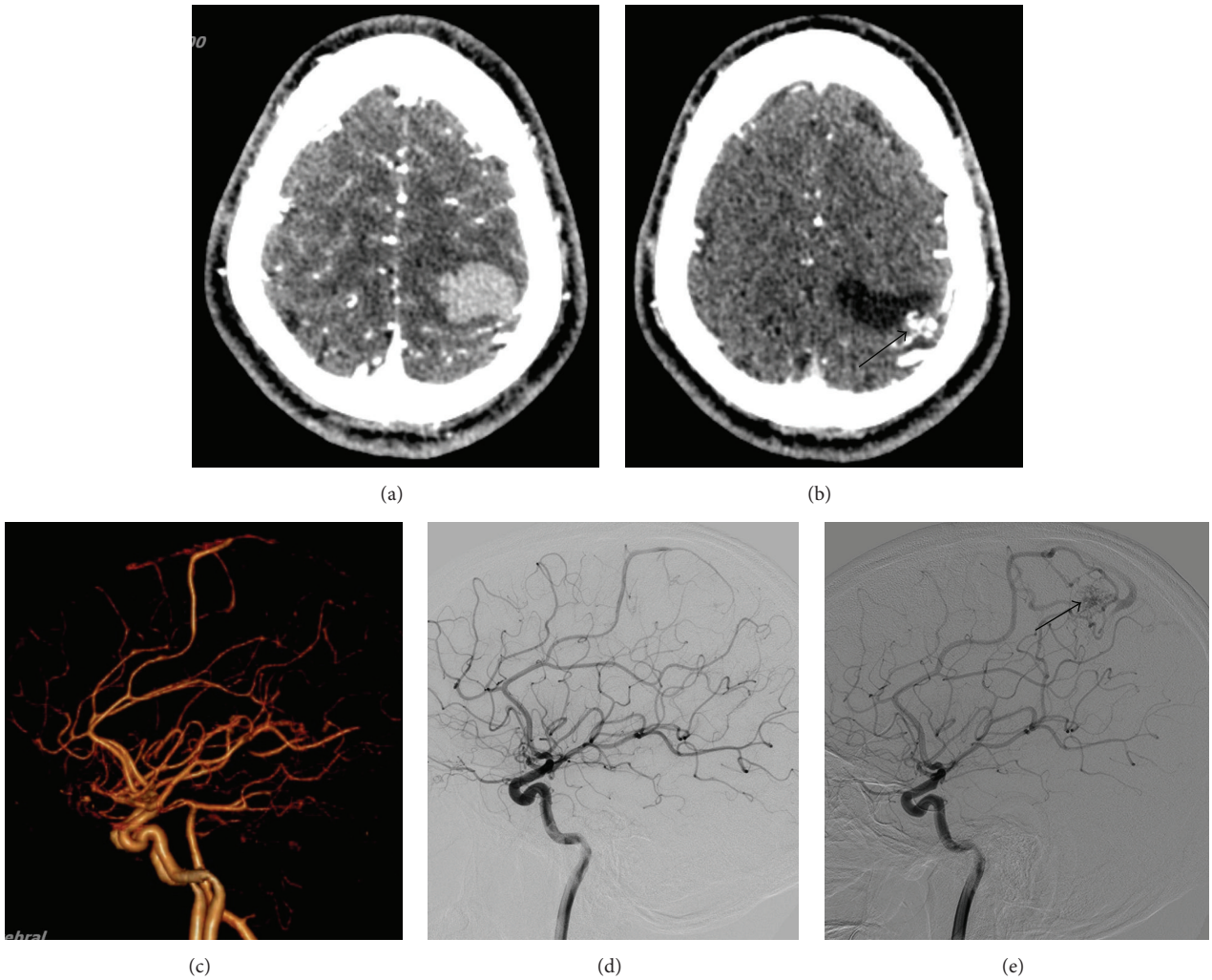

Figure 2: Different imaging findings of a micro-AVMs case before and after the hematoma absorption. (a) Enhanced thin layer CT scanning showed no obvious nidus on the day of the onset. (b) Enhanced thin layer CT scanning showed hematoma absorption and a tiny nidus of dense vessels was found after conservative treatment (arrow indicated). (c) Abnormal feeding artery without any nidus and venous drainage was found during initial CTA on the day of the onset. (d) Abnormal feeding artery without any nidus and venous drainage was found by DSA on the second day since onset. (e) Micro-AVMs, composed of feeding artery, nidus, and venous drainage, were clearly visible by means of DSA 8 months after conservative treatment (arrow indicated).

age for this onset is 32.6 years. Except for a 63-year-old case with history of high blood pressure, no risk factors of cardiovascular diseases were found in these cases, which indicated that there might be a risk of micro-AVMs for young and middle-aged patients presenting with intracerebral hemorrhage without hypertension. The clinical manifestations of these 13 cases were intracranial hemorrhage, and micro-AVMs were reported to have very high risk of hemorrhaging [3–5], which is different from the other larger AVMs. As reported, only 38–70% of AVMs is associated with intracerebral hemorrhage, and it is generally believed that hemorrhaging risk is associated with the angioarchitecture of AVMs [6]. There are two reasons for the hemorrhage bleeding caused by micro-AVMs [4, 5]: the first reason is that the volume of lesion is small and flow volume is low, so that ischemia symptoms due to compressive or steal phenomena are not easy to identify; on the other hand, compared with large AVM with high-flow shunting, feeding pedicles of small AVM with low-flow shunting have higher pressure and a greater tendency of hemorrhaging. Bleeding occurs generally around the small bridging arteries that anchor the draining vein to the surrounding parenchyma, where arteriovenous fistula is easy to form and can cause venous outflow hindrance and hyperpressure [7]. Although micro-AVMs volume is small, the occurrence of bleeding can often lead to severe clinical symptoms [3, 5, 8]. The clinical manifestation depends on the location of hemorrhage and the volume of the hematoma, both of which call for an emergency surgery to remove the hematoma. In this study, the mean volume of hematoma is 33 mL, including 6 cases more than 40 mL, which leads to consciousness disturbance and cerebral hernia. In addition, there are 7 cases of limb paralysis, whose hematomas mostly located in

the temporal and frontal cortex surface, so the appearance of bleeding may cause oppression to eloquent area. But after timely treatment, most patients' prognosis was good.

The diagnosis of micro-AVMs is difficult and challenging. In the case of middle-aged and young patients with large superficial hematoma, who had no medical history of high blood pressure, the suspicion of micro-AVMs was relatively high. Hino et al. [9] had reviewed the data of 137 patients with spontaneous subcortical hematoma, of which 41 cases were caused by specific vascular lesions. There are 4 cases where no lesions were detected on initial angiography but were later angiography visible. DSA is the best method for diagnosis for micro-AVMs, and in young patients whose conventional four-vessel cerebral DSA findings were negative or questionable, superselective angiography should be applied to suspicious vessels to increase the ability to reach a diagnosis of micro-AVMs according to the location of hematoma. Cellerini et al. [5] have conducted superselective angiography in 7 cases of suspected patients and confirmed the diagnosis of micro-AVMs. In their conclusion, for young patients with unexplainable bleeding, irrespective of negative or positive results of DSA, further selective microcatheter angiography was beneficial [5, 10]. Early hematoma compression may be one of the causes of negative DSA result and later DSA examination can be applied after hematoma absorption to improve the detection quality [2]. Also some scholars believed that the dynamic enhanced cranial MRA and the t2-weighted MRI images helped to find DSA negative patients [4]. In some cases, where patients developed the brain hernia caused by bleeding and were unable to conduct DSA or MR examination, CTA is expected to become a fast and convenient alternative option. In our study, all patients admitted to the hospital were examined initially by CTA, and the remaining negative CTA patients were examined by DSA. We assumed that the following three characteristics of CTA can help in diagnosis: (1) CTA after reconstruction is presented as micro-AVMs; (2) enhanced thin layer CT scanning can identify the tiny nidus of dense vessels around hematoma; (3) images after the reconstruction of CTA are presented as the abnormal feeding artery or venous drainage. One of the first two rules can be used as the criteria of diagnosis, whereas the third can be used as indirect evidence of diagnosis. In our study, among 13 cases of CTA examination, 10 cases showed the tiny nidus of dense vessels near hematoma, and after reconstruction of CTA, 7 cases were presented as micro-AVMs, 3 cases were found only with abnormal arterial blood supply, and only 1 case was found with abnormal venous drainage. Reconstruction of CTA images often present abnormal arterial or venous blood drainage, and the possible reasons are summarized as below: (1) small volume of micro-AVMs located in the superficial area which may lead to poor imaging after VR reconstruction; (2) the technician's lack of expertise to interpret the indirect signs such as abnormal arterial or venous blood drainage; (3) the hematoma compression, thrombosis, and vascular spasm, and so forth. Therefore, we believed that the diagnosis should not be too dependent on the reconstruction of CTA images, but more dependent on the reading of the original thin layer CT scanning before reconstruction. Through the reading of thin layer CT scanning, the tiny nidus of dense vessels around the hematoma can be found to indicate the location of nidus. For DSA and CTA negative patients, the possible reasons can be summarized as follows: the blood stream being slow, low-flow rate, pathological changes in thrombosis, arterial spasm and hematoma leading to pressure in vessels, and so forth. In the case of a patient with hematoma in eloquent area, DSA and CTA are found without any clear nidus, but with abnormal feeding artery. Eight months later, the CTA indicated a tiny nidus of dense vessels around the hematoma and DSA examination showed clear micro-AVMs (Figures 2(a)–2(e)). We finally assumed that, for patients in a critical condition, who were unable to conduct DSA, the high-quality CTA can serve as a good alternative and an abnormal arterial or venous blood drainage around the hematoma with tiny nidus of dense vessels can be used as a valuable indication for clinical diagnosis. To those who were diagnosed negative with initial CTA examination, we should conduct the DSA detection as soon as possible. For patients with negative result of initial CTA and DSA, from our own experience, repeated DSA examination 4 weeks later is required because at this time the hematoma will be liquefied or absorbed. For the highly suspected vascular disease cases with negative DSA and CTA, the thorough surgical exploration of the hematoma walls under the microscope is necessary.

Surgical resection, endovascular embolization, and radiotherapy are the three main treatment strategies for micro-AVMs. In our series, 10 patients underwent surgical resection: 1 was treated with embolization and 2 received radiotherapy. For the lesion on nonfunctional region of cortex, surgical resection is still the preferred treatment. Precise localization of the lesion is one of the main difficulties of in the operation. According to the preoperative imaging and the relationship between hematoma and lesions, neurosurgeons can largely determine the location of the lesions. In the case of venous drainage located in the superficial cortex, we can find lesions according to the arterialized venous drainage in a retrograde fashion; excision should follow the principle that feeding arteries was cut off firstly. If there no apparent lesion is found in arterial blood supply and venous drainage after craniotomy, we can gently remove hematoma and then search for the lesions according to the location of the hematoma. Lesions usually located in hematoma wall are not difficult to find. Neuronavigation technology or stereotactic technique can be beneficial to the surgery [4]. In this study, there was a case of micro-AVMs located in basal ganglia region and, for surgical operation of this deep micro-AVMs, we adopted neuronavigation with preoperative MRI to locate lesions which could help to minimize the postoperative neurologic damage. Endovascular embolization is highly recommended for treatment of lesions that are difficult to be accessed through surgical approach and with an obvious feeding arterial supply. In this study, we performed Onyx for a case of periventricular micro-AVMs, and the results were quite promising. Even though endovascular embolization of micro-AVMs is reported with good success rates, some studies largely relate it with potential bleeding risk [11]. Comparatively, Onyx's controllability is superior to other liquid embolic agents as it can avoid embolic agents entering normal blood vessels or venous

drainage. We certainly believed that the treatment with Onyx may be safer, but there is no reported curative effect compared to NBCA. For cases that are not suitable for surgery and endovascular embolization, radiotherapy may be considered as a good alternative therapy, because the lesion is small and radiation is usually conducted after hematoma absorption. In this study, we performed X-knife treatment strategy with accuracy and effectiveness through enhanced CT positioning, and moreover, the patients had no complaints of rebleeding during the follow-up period.

5. Conclusions

Although micro-AVMs incidence is rare, significant clinical symptoms with hematoma and bleeding are very common. CTA can be used as a good method of emergency inspection because of its convenience and sensitivity. It is helpful to read carefully enhanced thin layer CT scanning, and abnormal feeding artery or venous drainage can be used as an indication for indirect diagnosis. In addition, surgical resection is still the preferred method of treatment for micro-AVMs, while radiation therapy and endovascular treatment can be used in case of deep lesions.

Conflict of Interests

The authors had no conflict of interests to declare in relation to this paper.

Authors' Contribution

Jing-Fang Hong and Ying-Fang Song contributed equally to this work.

Acknowledgment

This work was supported by Science and Technology Project of Fujian Province (Grant no. 2014Y0036).

References

[1] M. G. Yasargil, *Microneurosurgery: AVM of the Brain—History, Embryology, Pathological Considerations, Hemodynamics, Diagnostic Studies, Microsurgical Anatomy*, Georg Thieme, Stuttgart, Germany, 1987.

[2] R. Willinsky, P. Lasjaunias, J. Comoy, and P. Pruvost, "Cerebral micro arteriovenous malformations (mAVMs). Review of 13 cases," *Acta Neurochirurgica*, vol. 91, no. 1-2, pp. 37–41, 1988.

[3] S. I. Stiver and C. S. Ogilvy, "Micro-arteriovenous malformations: significant hemorrhage from small arteriovenous shunts," *Neurosurgery*, vol. 46, no. 4, pp. 811–819, 2000.

[4] J. F. Alén, A. Lagares, I. Paredes et al., "Cerebral microarteriovenous malformations: a series of 28 cases," *Journal of Neurosurgery*, vol. 119, no. 3, pp. 594–602, 2013.

[5] M. Cellerini, S. Mangiafico, G. Villa et al., "Cerebral microarteriovenous malformations: diagnostic and therpeutic features in a series of patients," *American Journal of Neuroradiology*, vol. 23, no. 6, pp. 945–952, 2002.

[6] R. Kubalek, A. Moghtaderi, J. Klisch, A. Berlis, A. Quiske, and M. Schumacher, "Cerebral arteriovenous malformations: influence of angioarchitecture on bleeding risk," *Acta Neurochirurgica*, vol. 145, no. 12, pp. 1045–1052, 2003.

[7] A. Kader, W. L. Young, J. Pile-Spellman et al., "The influence of hemodynamic and anatomic factors on hemorrhage from cerebral arteriovenous malformations," *Neurosurgery*, vol. 34, no. 5, pp. 801–808, 1994.

[8] A. Andreou, I. Ioannidis, S. Lalloo, N. Nickolaos, and J. V. Byrne, "Endovascular treatment of intracranial microarteriovenous malformations," *Journal of Neurosurgery*, vol. 109, no. 6, pp. 1091–1097, 2008.

[9] A. Hino, M. Fujimoto, T. Yamaki, Y. Iwamoto, and T. Katsumori, "Value of repeat angiography in patients with spontaneous subcortical hemorrhage," *Stroke*, vol. 29, no. 12, pp. 2517–2521, 1998.

[10] P. Perrini, M. Cellerini, S. Mangiafico, and N. Di Lorenzo, "Superselective angiography increases the diagnostic yield in the investigation of intracranial haematomas caused by micro-arteriovenous malformations," *Neurological Sciences*, vol. 25, no. 4, pp. 241–242, 2004.

[11] P. Perrini, A. Scollato, M. Cellerini et al., "Results of surgical and endovascular treatment of intracranial micro-arteriovenous malformations with emphasis on superselective angiography," *Acta Neurochirurgica*, vol. 146, no. 8, pp. 755–766, 2004.

Hindawi Publishing Corporation
BioMed Research International
Volume 2015, Article ID 613247, 12 pages
http://dx.doi.org/10.1155/2015/613247

Research Article

Electrical Bioimpedance Spectroscopy on Acute Unilateral Stroke Patients: Initial Observations regarding Differences between Sides

Fernando Seoane,[1,2] Seyed Reza Atefi,[1] Jens Tomner,[3] Konstantinos Kostulas,[3,4] and Kaj Lindecrantz[1,5]

[1] *School of Technology and Health, KTH-Royal Institute of Technology, Alfred Nobels Allé 8, 14152 Huddinge, Sweden*
[2] *School of Engineering, University of Borås, Allégatan 1, 50190 Borås, Sweden*
[3] *Department of Neurology, R54, Karolinska University Hospital, Huddinge Unit, 141 86 Stockholm, Sweden*
[4] *Department of Clinical Neuroscience, Neuro-Angiological Research Center, Karolinska Institute, Karolinska University Hospital, Huddinge, Sweden*
[5] *Department of Clinical Science, Intervention and Technology, Karolinska Institute, 46 141 86 Stockholm, Sweden*

Correspondence should be addressed to Fernando Seoane; fsm@kth.se

Received 11 March 2015; Accepted 18 May 2015

Academic Editor: Nohra Chalouhi

Purpose. Electrical Bioimpedance Cerebral Monitoring is assessment in real time of health of brain tissue through study of passive dielectric properties of brain. During the last two decades theory and technology have been developed in parallel with animal experiments aiming to confirm feasibility of using bioimpedance-based technology for prompt detection of brain damage. Here, for the first time, we show that electrical bioimpedance measurements for left and right hemispheres are significantly different in acute cases of unilateral stroke within 24 hours from onset. *Methods*. Electrical BIS measurements have been taken in healthy volunteers and patients suffering from acute stroke within 24 hours of onset. BIS measurements have been obtained using SFB7 bioimpedance spectrometer manufactured by Impedimed ltd. and 4-electrode method. Measurement electrodes, current, and voltage have been placed according to 10–20 EEG system obtaining mutual BIS measurements from 4 different channels situated in pairs symmetrically from the midsagittal line. Obtained BIS data has been analyzed, assessing for symmetries and differences regarding healthy control data. *Results*. 7 out of 10 patients for Side-2-Side comparisons and 8 out 10 for central/lateral comparison presented values outside the range defined by healthy control group. When combined only 1 of 10 patients exhibited values within the healthy range. *Conclusions*. If these initial observations are confirmed with more patients, we can foresee emerging of noninvasive monitoring technology for brain damage with the potential to lead to paradigm shift in treatment of brain stroke and traumatic brain damage.

1. Introduction

Stroke is the third cause of death worldwide [1], killing more than five million people annually. However, the devastating consequences of stroke are not limited to these deaths. The consequences also include neurological dysfunction for another approximately five million people, thousands of millions of € in cost for emergency care, rehabilitation, and loss of productivity from those patients with permanent disabilities [2, 3].

There are US Food and Drug Administration (FDA) approved rescue therapies, such as recombinant tissue plasminogen activator rt-PA, for the 80–85% of the strokes that are ischemic, but the effectiveness of this treatment is significantly dependent on the time from onset to treatment [4].

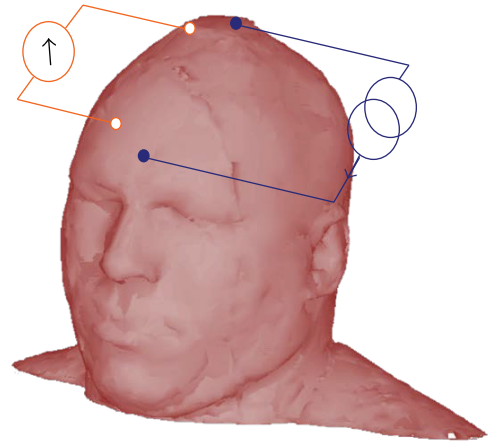

Figure 1: Tetrapolar method for noninvasive EBI measurements. One pair of electrodes is used to stimulate the head with the measurement current and another pair of electrodes senses the resulting voltage difference between the sensing electrodes.

Given the contraindication of rt-PA to patient with hemorrhagic stroke, 15–20% of the cases, proper identification of type of stroke is paramount prior to the initiation of therapy. Therefore successful treatment of stroke requires prior differentiation between ischemic and hemorrhagic damage. Unfortunately a correct differential diagnosis requires access to medical imaging modalities like CT and MRI involving processes that significantly increase the time door-to-needle, consequently delaying the initiation of treatment [5].

Electrical bioimpedance (EBI) technology has been used clinically and experimentally since the 1930s for assessment of several different physiological and pathophysiological mechanisms at cell, tissue, organ, and whole body level [6, 7]. Both applications of continuous single frequency measurements [8–21] and bioimpedance spectroscopy analysis (BIS) are well established in clinical practice [22–27] and their development for new application continues.

The use of EBI for the assessment of brain damage has been investigated from the 1950s [28] and during the last decade several authors have been proposing BIS as a potential useful noninvasive diagnostic tool for assessment of brain damage [29–36].

Recently Atefi et al. [37, 38] showed that it is possible to find differences in BIS measurements on patients having had a stroke. This paper presents clinical observations that suggest that stroke yields changes in cerebral BIS already in the early phases of stroke onset.

2. Methods

2.1. Bioimpedance Measurements. Bioimpedance spectroscopy (BIS) measurements were collected using the four-electrode technique [39] where a pair of silver EEG electrodes is used to inject alternating electrical current into the head and a separate pair of electrodes is used to measure the corresponding voltage difference on the surface of the head; see Figure 1.

The transfer function between the current injecting pair and voltage sensing pair will provide the transfer impedance [40]. In this study current injecting and voltage sensing positions are labeled according to the international 10–20-electrode placement system. BIS from the left hemisphere had current injecting pair placed on frontal and occipital lobes of the left hemisphere (Fp1-O1) forcing the current to propagate into the left hemisphere and the voltage difference was measured in lateral and central areas. Lateral voltage difference was measured between the left frontal and temporal lobes (T6-F8) and the central voltage difference was recorded between left parietal and frontal lobes (P4-F4). Identical measurements on the right hemisphere had Fp2-O2 for current pair, T5-F7 for lateral voltage difference, and P3-F3 for central voltage difference; see Figure 2.

For each patient, the skin on the electrode positions was prepared scrubbing with abrasive paste (EleFix) and then the silver EEG electrodes dipped in electroconductive paste (Elefix) were placed by an EEG expert to ensure accurate electrodes positioning for each subject.

2.2. BIS Instrument and Transfer Impedance Estimation. BIS was recorded by a commercial bioimpedance spectrometer SFB7 manufactured by Impedimed Ltd. The SFB7 records BIS at 256 logarithmically spaced frequency points in the range 3.096–1000 kHz by applying a sinusoidal current with constant RMS amplitude of 200 μA at each frequency point and calculating the transfer impedance at that frequency as the ratio between the current pair and voltage sensing pair. This way SFB7 calculates 256 complex impedance values known as impedance spectra. Impedance spectra from central left volume are labeled as $Z_{\mathrm{CL}}(\omega)$ and the one from right volumes is labeled as $Z_{\mathrm{CR}}(\omega)$. Similarly $Z_{\mathrm{LL}}(\omega)$ and $Z_{\mathrm{LR}}(\omega)$ indicate lateral left and lateral right impedance spectra. This way the resistance spectrum, the *real part of the impedance, will be* denoted as $R_{\mathrm{CL}}(\omega)$, $R_{\mathrm{CR}}(\omega)$ for left and right central

Table 1: Patient details.

Patient	Gender	Age	Lesion	Location	NIH Day 1
A	M	82	Ischemic stroke	Right MCA	19
B	W	44	Ischemic stroke	Left PCA	1
C	W	70	Ischemic stroke	Left PCA	6
D	W	81	Ischemic stroke*	Right PCA	4
E	W	93	Ischemic stroke	Right MCA	8
F	M	82	Hemorrhagic stroke	Lobar Left	1
G	M	66	Hemorrhagic stroke	Deep Right	12
H	W	84	Ischemic stroke	Left PCA	5
I	M	56	Ischemic stroke	Deep Left	1
J	M	71	Hemorrhagic stroke	Lobar Right	2

*See Appendix.

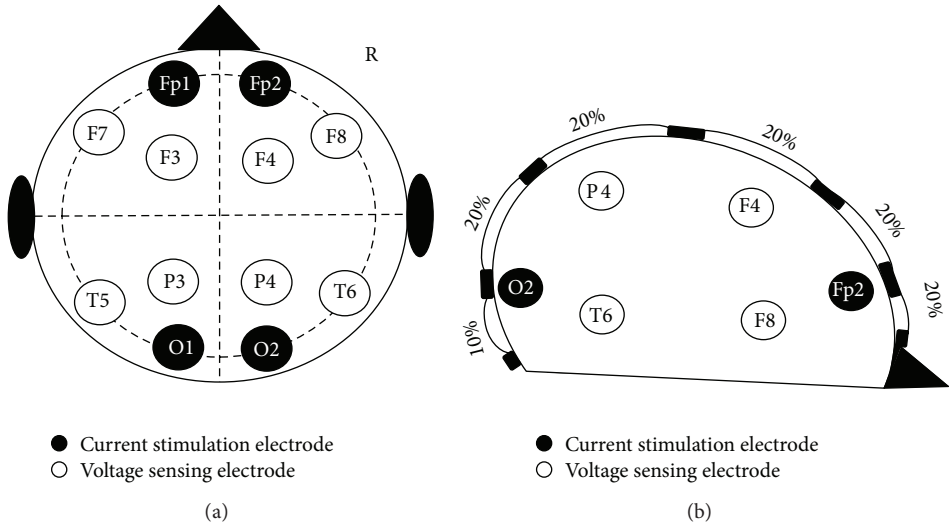

Figure 2: 10–20 international EEG landmarks. Indicates where the stimulating electrodes, filled circles, and the sensing electrodes, hollow circles, were placed for performing the BIS measurement for each of the four measurement channels lateral and central for right and left side.

measurements, respectively, and $R_{LL}(\omega)$ and $R_{LR}(\omega)$ for left and right lateral measurements.

2.3. BIS Measurements on Controls and Patients

Healthy Population. Three male subjects between 29 and 59 years of age and without any previous neurological complication were enrolled to Salhgrenska University Hospital. The Ethics Regional Committee of Gothenburg approved clinical protocols for these measurements.

Stroke Population. Ten patients, five female and five male (mean age 73 ± SD 14), were enrolled from the Stroke Ward at Karolinska University Hospital in Huddinge. The measurements were obtained within the first approximated 24 hours from onset. The precise onset time was not known in several patients, due to onset during sleep. The NIH score was 1–19 (mean 5,9 ± SD 5,5). Four patients had hemorrhagic stroke, one of which bled after administration of rt-PA. The bleedings were located centrally in two patients (one in the right putamen and one in the right medial occipital lobe) and laterally in the other two (one in the left operculum and one in the lateral part of the right occipital lobe). The six ischemic strokes were of various sizes and location. Three were large lesions in the territory supplied by the left posterior artery. Two were infarctions in the region supplied by the right media artery. One patient (patient I) had small infarctions in the left nuclei caudati and putamen not visible on the initial CT scan. Patient details are summarized in Table 1. The Ethics Regional Committee of Stockholm approved all of the clinical protocols.

BIS Measurements. Twenty (20) consecutive Z_{LL}, Z_{LR}, Z_{CL}, and Z_{CR} spectroscopy measurements were recorded from each healthy/patient and the mean resistance of each set was calculated at each measured frequency, for example, *mean of 20 resistance spectra for each set* was calculated and labeled as $R_{LL}(\omega)$, $R_{LR}(\omega)$, $R_{CL}(\omega)$, and $R_{CR}(\omega)$, respectively.

2.4. Symmetry Analysis and Visualization of BIS Data.

Patients admitted with acute stroke, that is, *less than 24 hours*, underwent either CT or MR scans as part of routine clinical

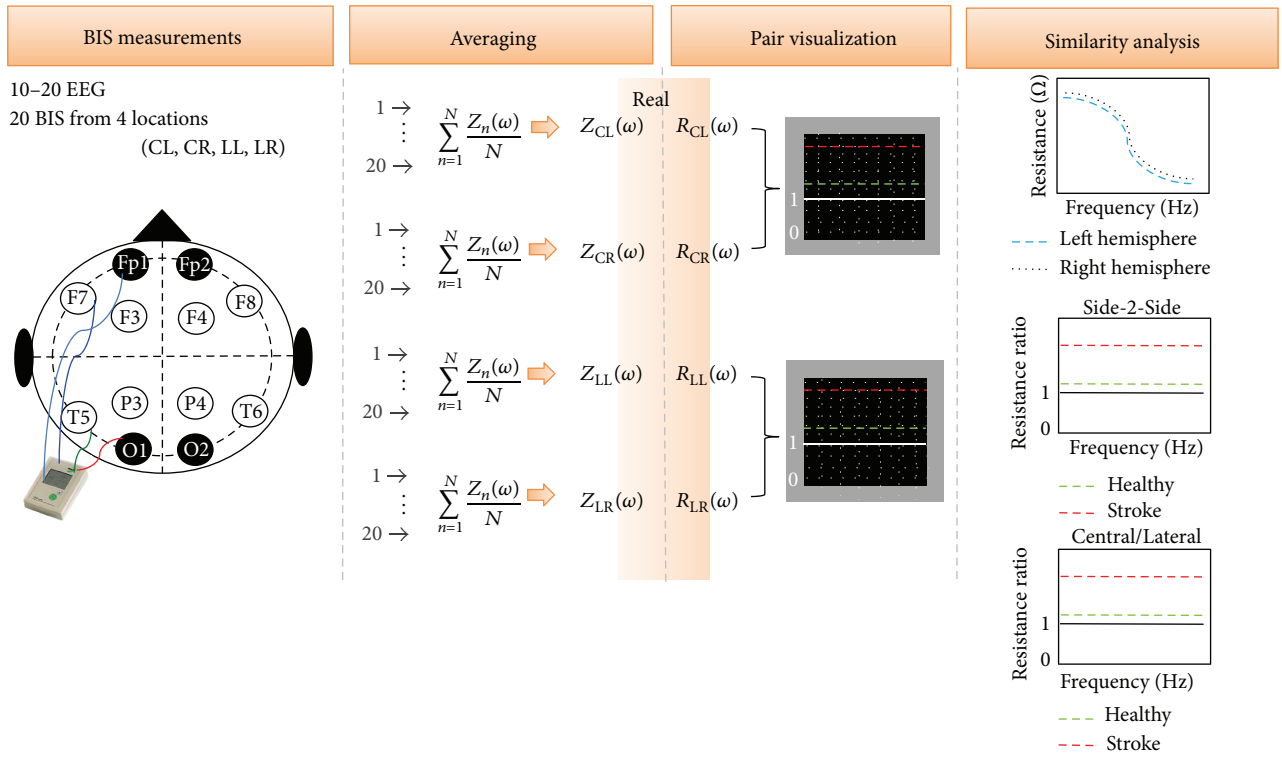

FIGURE 3: BIS recording analysis diagram. 20 consecutive complex BIS measurements are recorded from 4 different volumes of each healthy/stroke ($Z_{CR/ZCL}(\omega)$ and $Z_{LR/LL}(\omega)$), and the real parts ($R_{CR/CL}(\omega)$ and $R_{LR/LL}(\omega)$) are analyzed by pair evaluating symmetry and similarities.

procedures. Following the scan, after obtaining the written consent, BIS recordings were collected from each patient and transferred to MATLAB for data analysis; see Figure 3 for a descriptive diagram.

The core hypothesis for comparison of healthy and damaged brain is that identical volumes from the two hemispheres of healthy subjects should have minimal differences in the impedance spectra between hemispheres, while in cases with unilateral brain injury this should not be the case as the electrical properties of one hemisphere, that is, *in the damaged area* is changed compared to its undamaged counterpart.

In order to observe any differences between healthy and damaged brains, two straightforward approaches have been used:

1st is Side-2-Side ratio: the ratio between symmetrically located BIS measurements has been calculated for the resistance spectrum, that is, *one ratio has been obtained for the left and right lateral measurements and one for the left and right central measurements*.

2nd is central/lateral ratio: the ratio between central and lateral BIS measurements has been obtained for the resistance spectrum; therefore again 2 ratios, one for left and one for right, are obtained from each subject.

In both cases, the ratio function obtained from the stroke patient measurements has been plotted together with the ratio obtained from the healthy control measurements.

3. Results

All the BIS measurements obtained for the healthy control and the stroke patient group are plotted in the Appendix. In this section for improving the readability, only results obtained from the specific comparison required to support the symmetric analysis are presented (Table 2 shows overall comparison for all patients and ratios).

3.1. Healthy Control Cases. The spectral plots included in Figure 4 reproduce the BIS measurements obtained for the 3 control healthy subjects. Observe that the spectra for right with continuous trace (–) and left with dashed trace (- -) are basically paired according to location. In the same plots it is possible observe that the central measurements, with dark trace, present a larger impedance magnitude than the measurements obtained from the lateral locations with light trace.

In Figure 5 it is possible to observe that the Side-2-Side ratio obtained from the symmetrically located BIS measurements on healthy measurements is close to 1. The ratio obtained for central measurements, continuous trace (–),

Table 2: Overall comparison for all patients and ratios.

	Patient									
	A	B	C	D	E	F	G	H	I	J
Ratio comparison										
Side-2-Side central	✗		✗	✗	✗				✗	
Side-2-Side lateral		✗				✗				
Central/Lateral left	✗	✗	✗	✗	✗	✗				
Central/Lateral right		✗				✗	✗	✗		

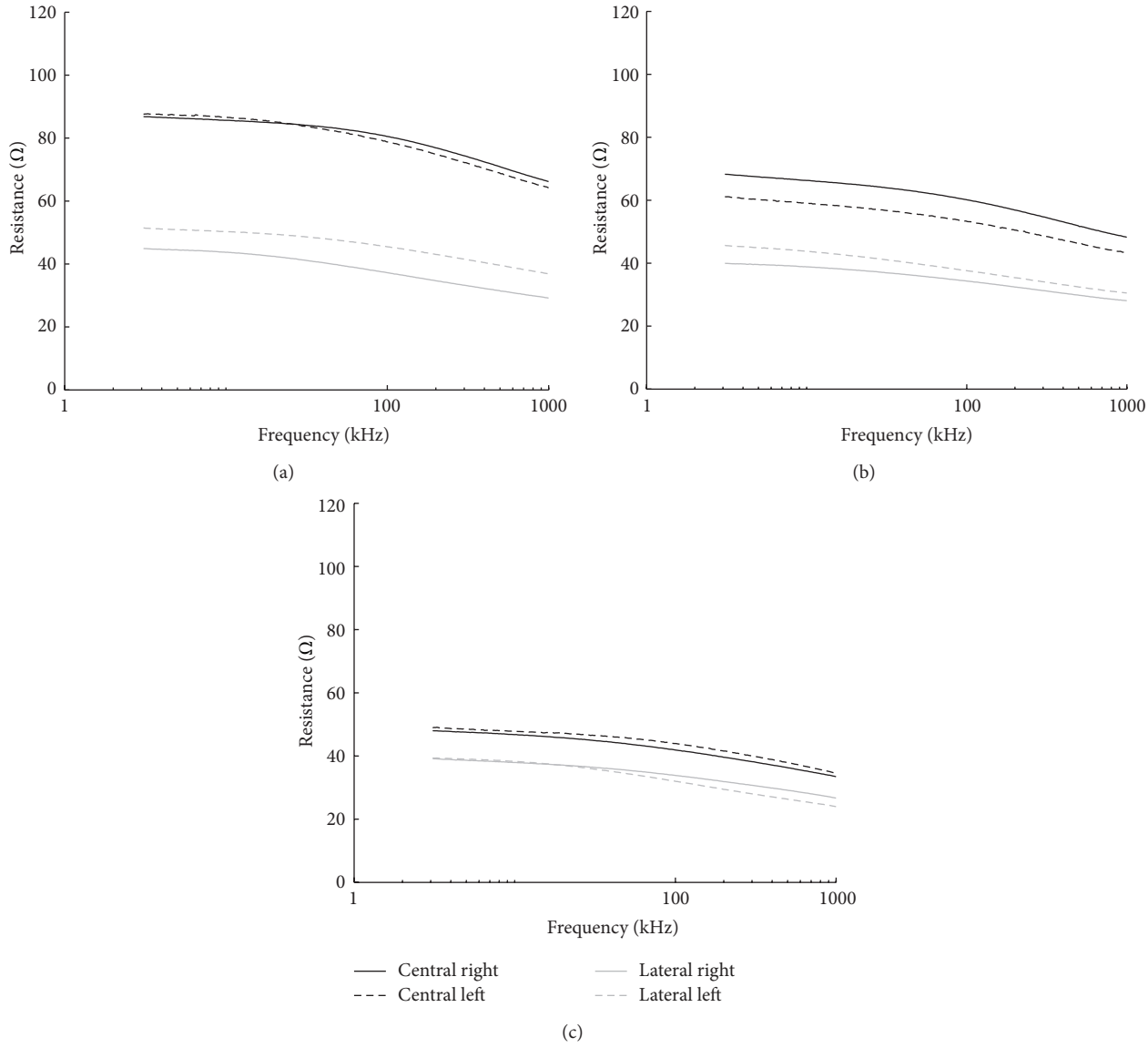

Figure 4: Healthy EBI Spectra. Lateral and central bioimpedance spectrum obtained for each of the 3 healthy volunteers in plots (a), (b), and (c), respectively. Central and lateral bioimpedance spectra are plotted in pairs.

exhibit a smaller dispersion than the ratio exhibit by the lateral measurements with dotted trace (•). Observe that while the deviation from the unity at low frequency is very small, it increases with frequency in some cases.

3.2. Side-2-Side Symmetrical Comparison. In Figure 6(a), when comparing the Side-to-Side ratio obtained for the central BIS measurements performed on all the patients, it is shown that the ratio in at least 5 of the patients, dashed thick

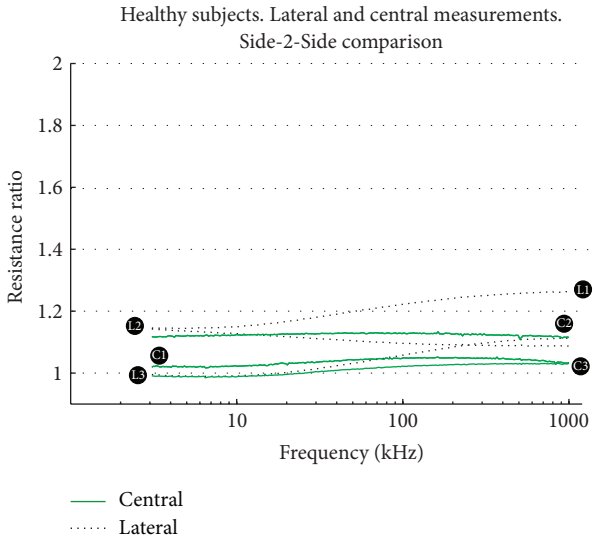

Figure 5: Side-2-Side ratio comparison in healthy EBI spectra. Resistance ratio obtained for lateral and central BIS measurements for the control cases.

trace (- -), exhibits a ratio noticeable larger than the unity and the ratio values for the control measurements denoted by the shadowed area. There are another 5 patients reporting ratio values, continuous thin dark trace (–), within the range exhibited by the control healthy group.

When looking at the Side-to-Side comparison for the lateral measurements, the plot in Figure 6(b) shows that only in 2 cases, dashed trace (- -), the ratio values are outside the shadowed area. For the other cases, plotted with continuous thin dark trace (–), the ratio values fall inside the limits exhibited by the control group, blue shadowed area.

3.3. Central over Lateral Comparison. In Figure 7 the spectral plots representing the ratio are obtained from comparing central and lateral measurements in each subject. The ratio plots obtained for the left side, Figure 7(a), indicate that the ratio values obtained from healthy measurements, range between 1.2 and 1.8 approximately. In the plot it is possible to see that the ratio values from 6 patients (A–F), dashed thick trace (- -), produce ratio values clearly below or above the control range. Patients (G–J) present ratio values within the healthy range, continuous thin dark trace (–). For the right side, in Figure 7(b), we can observe that there are 4 patients (B, F, G, and H) with ratio values, dashed trace (- -), above or below the values 1.25–2.20 defining the healthy range.

4. Discussion

4.1. Side-2-Side Symmetries. The main working hypothesis is that ideally, identical symmetric cerebral hemispheres will exhibit similar impedance spectra, given that the measurements are taken with electrode arrangements using anatomical landmarks from the midsagittal plane.

In reality the cerebral hemispheres are not identical, and the brain is not located within the cranium in perfect symmetry with reference to the 10–20 landmarks. Moreover, it is likely that the electrophysiology technician has certain variability in the placement of electrodes. Such source of error will likely influence in such kind of comparison but, in any case, despite the potential sources of error that might influence the different spectral BIS measurements, it is possible to see that the measurements on healthy volunteers are remarkably similar when paired by symmetry with respect to the midsagittal line as shown in Figures 4 and 5.

The obtained results show that the majority of the patients, 7 out of 10, exhibit a ratio larger than the ratios obtained from the healthy.

In general it is reasonably expected that a lesion in any of the cerebral hemispheres should contribute significantly to modify the current density distribution across the brain and produce noticeably different BIS measurements between channels that would otherwise produce similar, quasi-identical, BIS measurements. A potential exception would be centrally located lesions that could potentially preserve the symmetry, but in this study all lesions were laterally located.

4.2. Other Expected Relationships between BIS Measurements. Another observation that can be done from the BIS measurements performed on healthy volunteers plotted in Figure 4 is that the magnitude of the resistance spectra from the central measurements is larger than lateral measurements. It is naturally expected with the measurement setup use in the study that in healthy brain the BIS measurements recorded from the central locations should be larger than the measurements obtained from the laterally located channels, but in addition it is also naturally expected that the central to lateral relations should have a given maximum value as well, delimiting a healthy range.

When comparing the BIS measurements regarding the central and lateral channels included in the Appendix and the ratios plotted in Figure 7, it is possible to see that in 8 out of 10 patients the values of the obtained ratios are below or above the values obtained for the corresponding healthy control cases.

4.3. Summary of Observations. When analyzing the results from all the comparisons, it is possible to see that up to 9 patients present at least one or more resistance ratios different from those calculated from the healthy control. The majority of the patients, 6 out 10, exhibit 2 or more ratios out from the healthy range. Taking a closer look at those other 4 patients, G–J, we realized that in each of them the location of the brain lesion was at the same level or below the third ventricle or the putamen. Lesions at such depth might require electrodes to be located in specific positions to force the current measurement to flow through deeper structures.

4.4. Injury Depth, Electrode Location, and Impedance Sensitivity. In a BIS measurement, the measurement current is distributed through the volume according to the conductivity

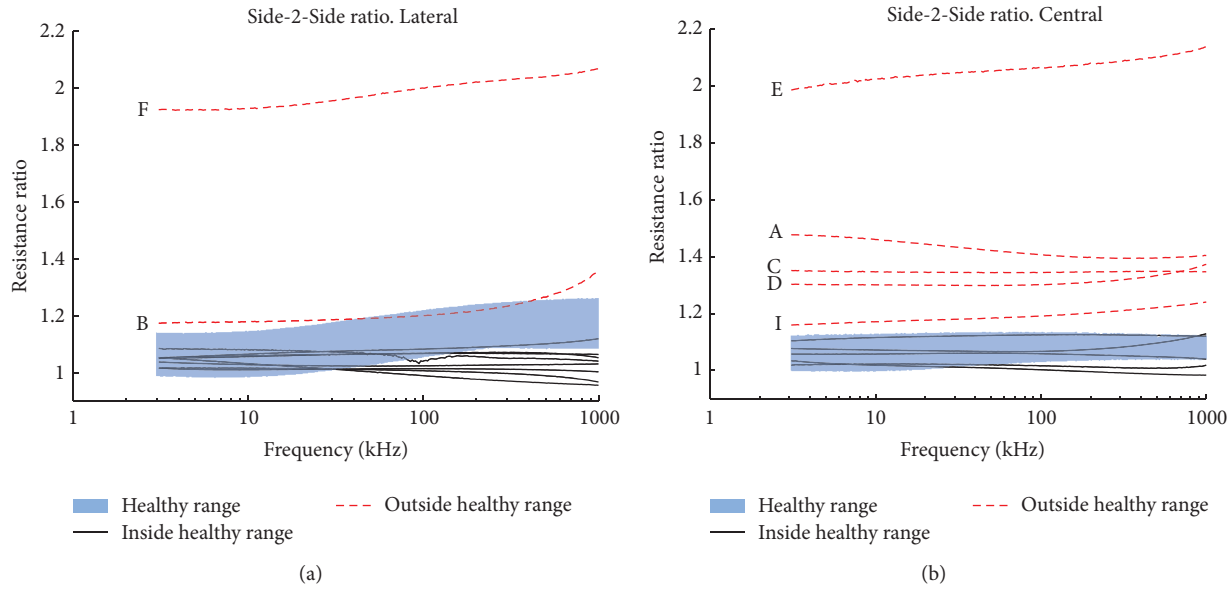

Figure 6: Side-2-Side ratio resistance comparison. Resistance ratio obtained for lateral BIS measurements in (a) and central in (b). The range observed in the control cases for the Side-to-Side ratio is denoted by the shadowed region near the value 1. Notice that the central ratio from patients A, C, D, E, and I in (b) and the lateral ratios from B and F in (a) are outside the healthy range.

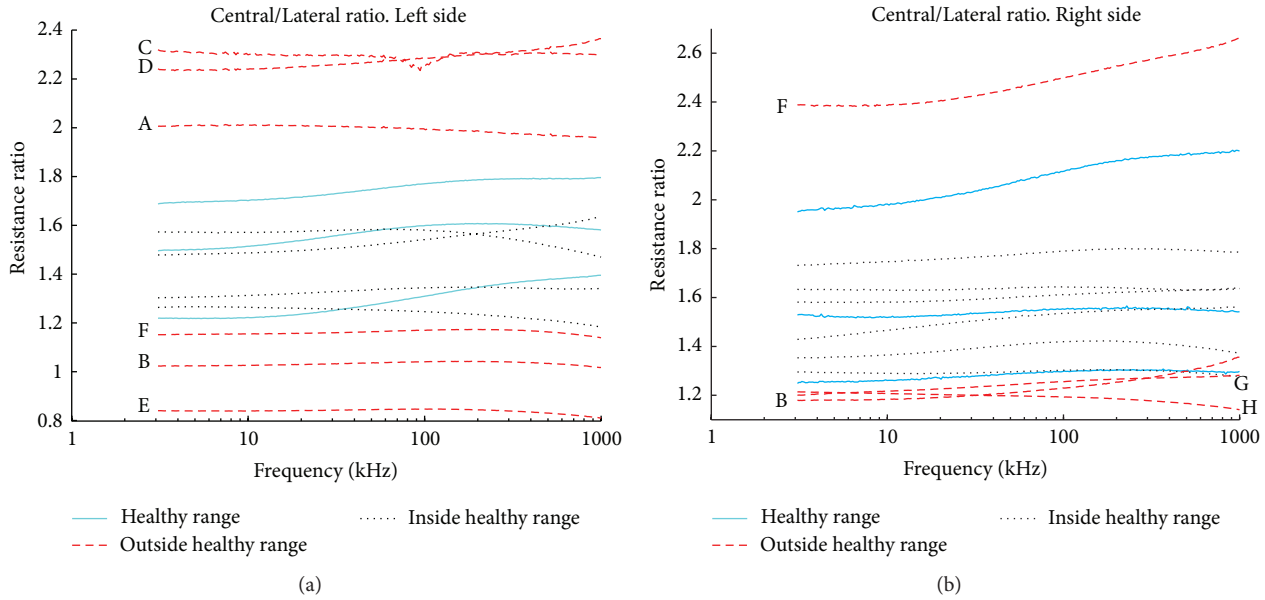

Figure 7: Central over lateral ratio comparison. Resistance ratios obtained from central divided lateral BIS measurements for left in (a) and right in (b) are shown. The range observed in the control cases for the Side-to-Side ratio is denoted by the shadowed region. Notice that the resistance ratio from patients A to F in (a) and B, F, G, and H, in (b) are outside the healthy range.

of the constituting tissue but it will also depend on the location of the different tissue structures in relation to the position of electrodes. With the position of both voltage and sensing electrode used in this study, it is known that the current density and the lead fields through deeper tissue structures are significantly smaller [41] and therefore it will have less contribution to the total measured impedance. Therefore the altered conductivity of the brain injury might not need to produce a noticeable difference in the BIS measurement.

4.5. Relation to Related Work. The value of these initial observations is that they show for the first time that stroke, already in its early phases, modifies the electrical properties of the brain and differences can be observed through

electrical bioimpedance spectroscopy measurements of the head in acute unilateral stroke patients. This way validates the theories and hypothesis presented in [30, 42–45] and complementing simulation results reported recently in [46]. Where in an analogous manner of comparing hemispheric left and right sides over using conductivity images obtained with Electrical Impedance Tomography at a single frequency for each hemisphere should not present any differences in healthy subjects but in patients with unilateral stroke the conductivity images showed observable differences, according to the simulations.

4.6. Brain Damage Identification and Potential Usage of EBCM. The ultimate goal of any novel diagnostic support system for early detection of stroke would be not only to detect the damage but also to differentiate between ischemic and hemorrhagic damage. From that perspective, the preliminary analysis performed in this study indicates that no differentiation between stroke patients with ischemia or hemorrhage could be done on the basis of the recorded BIS measurements. Given the limited number of subjects and considering the many differences among the stroke lesions regarding location and type, clear distinctive differences in the BIS data to allow any kind of type differentiation were not expected in this first attempt of studying BIS data obtained from stroke acute patients.

Differentiation of type of stroke damage based on BIS technology, if possible, would provide bioimpedance with a paramount importance in the stroke triage protocol, that is, not the only way that BIS could be useful when caring for stroke patients. A diagnostic tool available to the Emergency Medicine Services personal onboard of the ambulance that could perform quick and direct assessments about the existence of brain damage would provide significant support to paramedics when deciding to prioritize primary stroke centers against closer nonprimary stroke centers like in stroke triage protocols like in [47].

5. Conclusion and Future

It was known that patients with chronic stroke lesions exhibited differences in BIS measurements [37, 38]; now these initial observations confirm that changes can be noticed from the initial phases, making bioimpedance spectroscopy a potential candidate to base the development of a novel diagnosis support tool for prompt detection of stroke attack. To remove the word potential requires an additional validation that measurements of bioimpedance can indeed detect brain damage within the first hour from onset. In this regard, efforts led by the Royal Institute of Technology, a project proposal has been submitted to the EU H2020 funding program, in which, among other things, the detection performance with time will be evaluated.

As it is known in stroke care *Time is Brain* because early treatment produces better outcome [48]. Therefore to reduce the door-to-needle time when caring for brain damage patient is very important and for that detection of ongoing brain damage is a significant feature but, to eliminate the door-to-needle time when treating acute stroke, it is necessary not only to detect the on-going stroke but also to differentiate the type in the very first stages of the care process, for example, *in the ambulance during acute transport*.

While the replacement of CT technology by BIS technology in the stroke triage protocol seems far away in time and slightly unrealistic at this point, to envision a tool for assessment of brain damage for supporting first responders at the earliest stage of a stroke triage protocol should guide any development in the field of Electrical Bioimpedance Cerebral Monitoring in the near future.

A priori EBI technology fulfills all the requirements to allow the development of such BIS-based tool that is, *portable, noninvasive, affordable, and compact in size*. Although these initial observations on clinical data are very encouraging and validate years of theoretical, simulation, and animal studies yet extensive clinical, biomedical engineering and more theoretical research must be executed towards the development of such diagnostic tool for prompt detection of brain damage. Among them, we can identify targeting the acquisition of reference values for controls and BIS characterization of healthy brain, the study of the several factors influencing the bioimpedance of different types of lesions specifically including size and location of the lesion. Moreover future investigations should include the use of different arrangements of electrodes, to target deeper structures; for such purpose 3D-simulations with realistic anatomic models would be especially helpful.

Appendix

BIS Measurement Plots for Stroke Patients

See Figure 8.

Conflict of Interests

The authors declare that there is no conflict of interests regarding the publication of this paper.

Authors' Contribution

Fernando Seoane, Konstantinos Kostulas, and Kaj Lindecrantz conceived and supervised the study. Fernando Seoane implemented the experimental setup and collected the measurements on healthy subjects and Jens Tomner collected the measurements from stroke patients. Jens Tomner and Konstantinos Kostulas retrieved and processed the imaging and other medically relevant data from the patients. Fernando Seoane and S. Reza Atefi analyzed the data and produced the outline of paper and the figures. All authors were involved in extensive discussions and wrote the paper.

Acknowledgments

Funding for this project was provided by the Innovationkontor Väst (Innovation Office West) verification Project no.

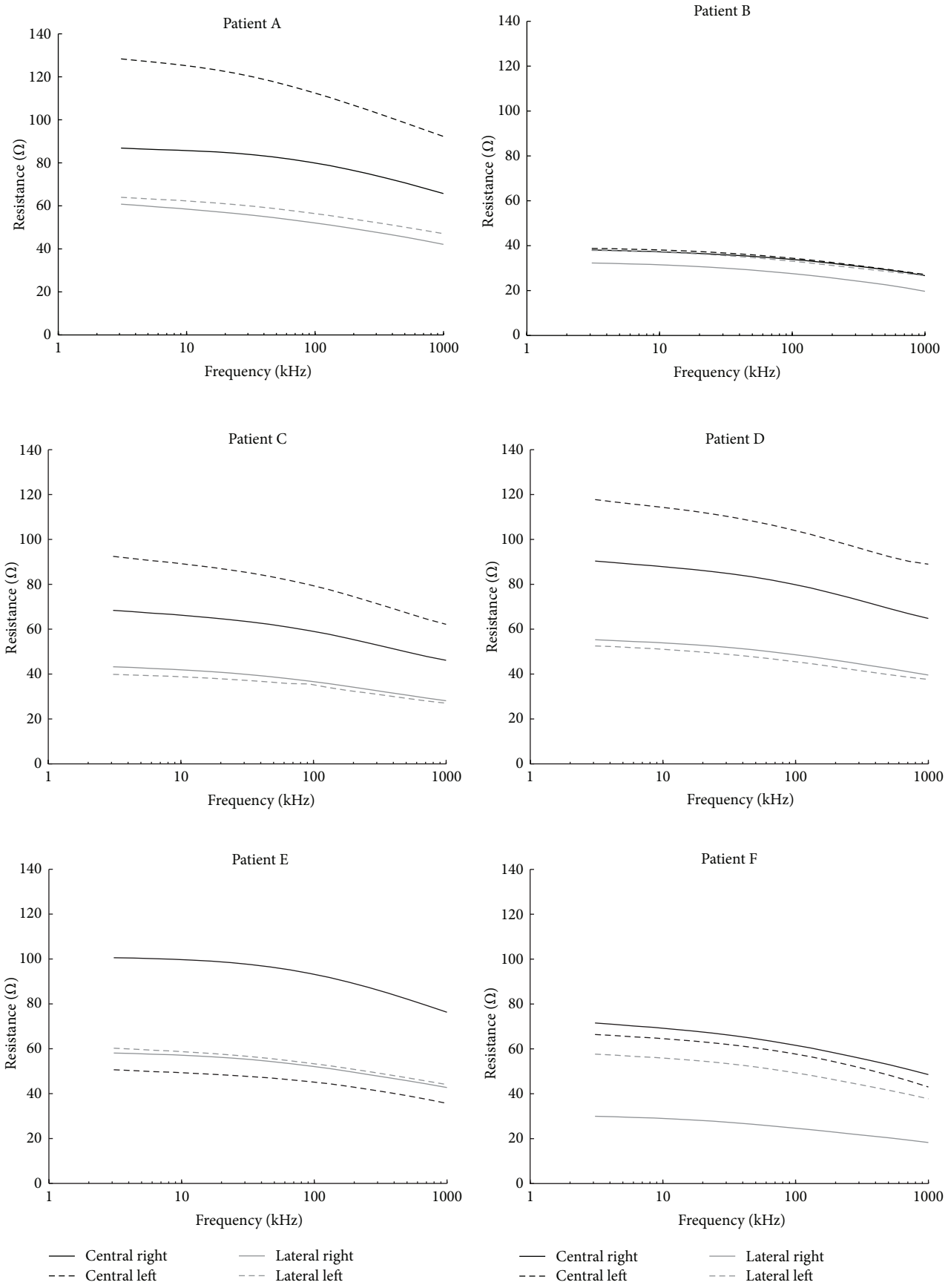

Figure 8: Continued.

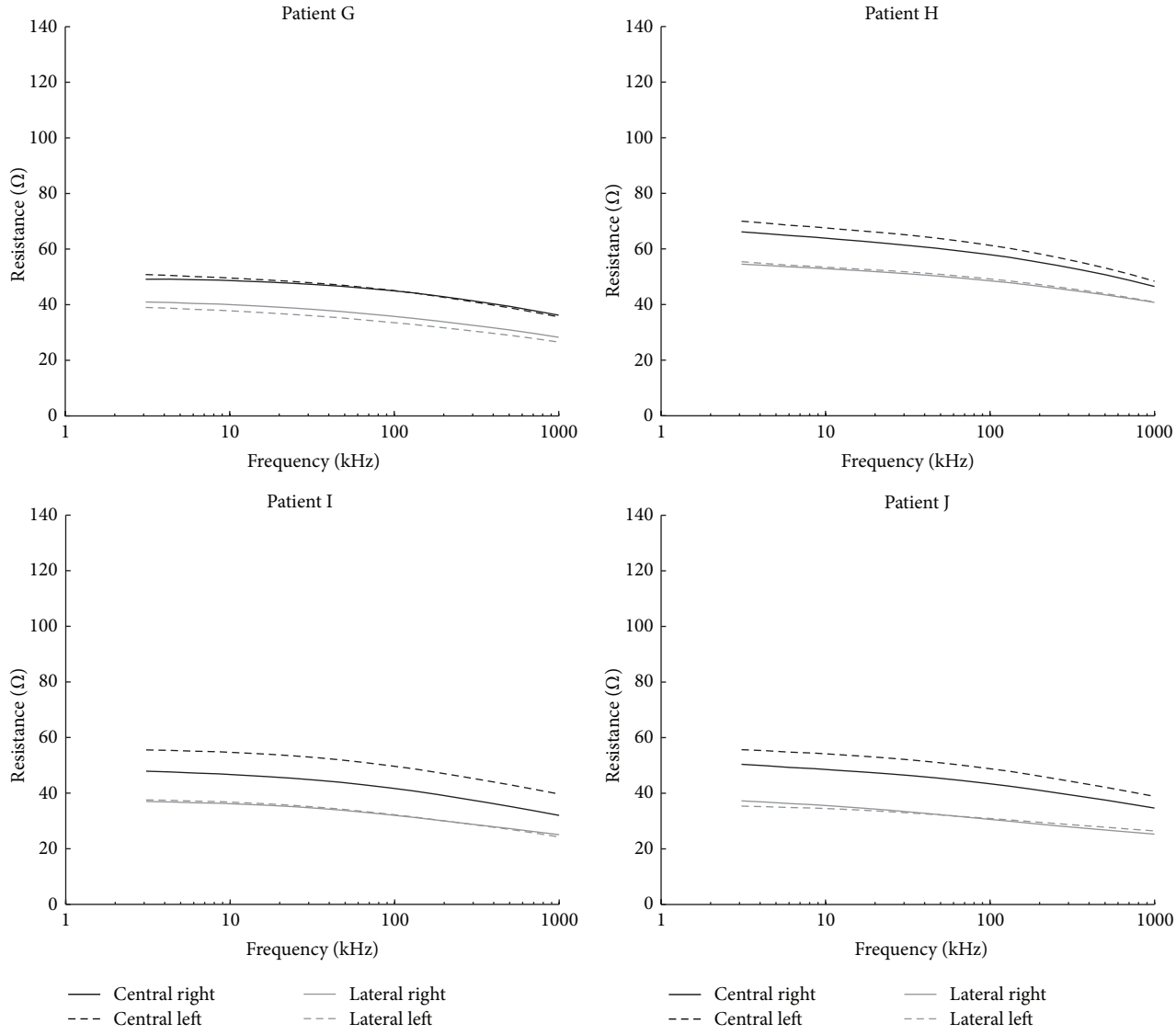

Figure 8: Patient group.

V119. The authors would like to thank Göran Pegenius at Sahlgrenska University Hospital for the support during the collection of BIS measurements on healthy volunteers and the support of Farhad Abtahi during the collection of BIS measurements on stroke patients at Karolinska Hospital.

References

[1] G. A. Donnan, M. Fisher, M. Macleod, and S. M. Davis, "Stroke," *The Lancet*, vol. 371, no. 9624, pp. 1612–1623, 2008.

[2] J. Mackay and G. A. Mensah, *The Atlas of Heart Disease and Stroke*, Myriad, WHO, Geneva, Switzerland, 2004.

[3] W. Rosamond, K. Flegal, K. Furie et al., "Heart disease and stroke statistics—2008 update: a report from the American Heart Association Statistics Committee and Stroke Statistics Subcommittee," *Circulation*, vol. 117, no. 4, pp. e25–e146, 2008.

[4] J. L. Saver, G. C. Fonarow, E. E. Smith et al., "Time to treatment with intravenous tissue plasminogen activator and outcome from acute ischemic stroke," *The Journal of the American Medical Association*, vol. 309, no. 23, pp. 2480–2488, 2013.

[5] A. Meretoja, D. Strbian, S. Mustanoja, T. Tatlisumak, P. J. Lindsberg, and M. Kaste, "Reducing in-hospital delay to 20 minutes in stroke thrombolysis," *Neurology*, vol. 79, no. 4, pp. 306–313, 2012.

[6] J. Nyboer, S. Bango, A. Barnett, and R. H. Halsey, "Radiocardiograms: electrical impedance changes of the heart in relation to electrocardiograms and heart sounds," *Journal of Clinical Investigation*, vol. 19, p. 773, 1940.

[7] E. Atzler and G. Lehmann, "Über ein neues verfahren zur darstellung der herztätigkeit (Dielektrographie)," *Arbeitsphysiologie*, vol. 6, p. 44, 1931.

[8] L. A. Geddes, H. E. Hoff, D. M. Hikman, and A. G. Moore, "The impedance pneumography," *Aerospace Medicine*, vol. 33, pp. 28–33, 1962.

[9] A. F. Heck, W. Reichl, and V. R. Hall, "Impedance pneumography," *The Lancet*, vol. 2, no. 7780, p. 758, 1972.

[10] J. J. Freundlich and J. C. Erickson, "Electrical impedance pneumography for simple nonrestrictive continuous monitoring of respiratory rate, rhythm and tidal volume for surgical patients," *Chest*, vol. 65, no. 2, pp. 181–184, 1974.

[11] M. H. Sim, M. Y. Kim, I. C. Jeong et al., "Development and evaluation of an improved technique for pulmonary function testing using electrical impedance pneumography intended for the diagnosis of chronic obstructive pulmonary disease patients," *Sensors*, vol. 13, no. 11, pp. 15846–15860, 2013.

[12] T. E. Terndrup and J. Rhee, "Available ventilation monitoring methods during pre-hospital cardiopulmonary resuscitation," *Resuscitation*, vol. 71, no. 1, pp. 10–18, 2006.

[13] K. Miyasaka, Y. Kondo, T. Suzuki, H. Sakai, and M. Takata, "Toward better home respiratory monitoring: a comparison of impedance and inductance pneumography," *Acta Paediatrica Japonica*, vol. 36, no. 3, pp. 307–310, 1994.

[14] M. Patino, D. T. Redford, T. W. Quigley, M. Mahmoud, C. D. Kurth, and P. Szmuk, "Accuracy of acoustic respiration rate monitoring in pediatric patients," *Paediatric Anaesthesia*, vol. 23, no. 12, pp. 1166–1173, 2013.

[15] N. Nassi, R. Piumelli, E. Lombardi, L. Landini, G. Donzelli, and M. De Martino, "Comparison between pulse oximetry and transthoracic impedance alarm traces during home monitoring," *Archives of Disease in Childhood*, vol. 93, no. 2, pp. 126–132, 2008.

[16] A. R. Tonelli, L. Alkukhun, V. Arelli et al., "Value of impedance cardiography during 6-minute walk test in pulmonary hypertension," *Clinical and Translational Science*, vol. 6, no. 6, pp. 474–480, 2013.

[17] R. Morris, I. Sunesara, L. Rush et al., "Maternal hemodynamics by thoracic impedance cardiography for normal pregnancy and the postpartum period," *Obstetrics and Gynecology*, vol. 123, no. 2, pp. 318–324, 2014.

[18] R. N. McCarthy and D. Dosh, "Assessment of pulmonary edema in acute congestive heart failure with impedance cardiography," *Journal of the American Osteopathic Association*, vol. 74, no. 9, p. 879, 1975.

[19] J. P. Rasmussen, B. Sorensen, and T. Kann, "Evaluation of impedance cardiography as a non-invasive means of measuring systolic time intervals and cardiac output," *Acta Anaesthesiologica Scandinavica*, vol. 19, no. 3, pp. 210–218, 1975.

[20] W. G. Kubicek, A. H. From, R. P. Patterson, and et al, "Impedance cardiography as a noninvasive means to monitor cardiac function," *Journal of the Association for the Advancement of Medical Instrumentation*, vol. 4, no. 2, pp. 79–84, 1970.

[21] B. G. Krohn, E. Dunne, O. Magidson et al., "The electrical impedance cardiogram in health and disease," *The American Heart Journal*, vol. 76, no. 3, pp. 377–387, 1968.

[22] U. M. Moissl, P. Wabel, P. W. Chamney et al., "Body fluid volume determination via body composition spectroscopy in health and disease," *Physiological Measurement*, vol. 27, no. 9, pp. 921–933, 2006.

[23] M. Y. Jaffrin and H. Morel, "Body fluid volumes measurements by impedance: a review of bioimpedance spectroscopy (BIS) and bioimpedance analysis (BIA) methods," *Medical Engineering and Physics*, vol. 30, no. 10, pp. 1257–1269, 2008.

[24] H. P. Schwan, "The practical success of impedance techniques from an historical perspective," *Annals of the New York Academy of Sciences*, vol. 873, pp. 1–12, 1999.

[25] P. Åberg, U. Birgersson, P. Elsner, P. Mohr, and S. Ollmar, "Electrical impedance spectroscopy and the diagnostic accuracy for malignant melanoma," *Experimental Dermatology*, vol. 20, no. 8, pp. 648–652, 2011.

[26] U. G. Kyle, I. Bosaeus, A. D. de Lorenzo et al., "Bioelectrical impedance analysis—part II: utilization in clinical practice," *Clinical Nutrition*, vol. 23, no. 6, pp. 1430–1453, 2004.

[27] A. De Lorenzo, A. Andreoli, J. Matthie, and P. Withers, "Predicting body cell mass with bioimpedance by using theoretical methods: a technological review," *Journal of Applied Physiology*, vol. 82, no. 5, pp. 1542–1558, 1997.

[28] S. Ochs and A. van Harreveld, "Cerebral impedance changes after circulatory arrest," *The American Journal of Physiology*, vol. 187, no. 1, pp. 180–192, 1956.

[29] B. E. Lingwood, K. R. Dunster, G. N. Healy, L. C. Ward, and P. B. Colditz, "Cerebral impedance and neurological outcome following a mild or severe hypoxic/ischemic episode in neonatal piglets," *Brain Research*, vol. 969, no. 1-2, pp. 160–167, 2003.

[30] F. Seoane and K. Lindecrantz, "Electrical bioimpedance cerebral monitoring," in *Encyclopedia of Healthcare Information Systems*, pp. 480–486, IGI Global, Hershey, Pa, USA, 2008.

[31] F. Seoane, K. Lindecrantz, T. Olsson, I. Kjellmer, A. Flisberg, and R. Bågenholm, "Spectroscopy study of the dynamics of the transencephalic electrical impedance in the perinatal brain during hypoxia," *Physiological Measurement*, vol. 26, no. 5, pp. 849–863, 2005.

[32] F. S. Martínez, *Electrical Bioimpedance Cerebral Monitoring*, Chalmers Tekniska Högskola, Göteborg, Sweden, 2007.

[33] D. S. Holder, "Feasibility of developing a method of imaging neuronal activity in the human brain: a theoretical review," *Medical and Biological Engineering and Computing*, vol. 25, no. 1, pp. 2–11, 1987.

[34] D. S. Holder, "Detection of cerebral ischaemia in the anaesthetised rat by impedance measurement with scalp electrodes: implications for non-invasive imaging of stroke by electrical impedance tomography," *Clinical Physics and Physiological Measurement*, vol. 13, no. 1, pp. 63–75, 1992.

[35] D. S. Holder, "Impedance changes during the compound nerve action potential: Implications for impedance imaging of neuronal depolarisation in the brain," *Medical and Biological Engineering and Computing*, vol. 30, no. 2, pp. 140–146, 1992.

[36] D. S. Holder and A. R. Gardner-Medwin, "Some possible neurological applications of applied potential tomography," *Clinical Physics and Physiological Measurement*, vol. 9, no. 4, pp. 111–119, 1988.

[37] S. R. Atefi, F. Seoane, T. Thorlin, and K. Lindecrantz, "Stroke damage detection using classification trees on electrical bioimpedance cerebral spectroscopy measurements," *Sensors*, vol. 13, no. 8, pp. 10074–10086, 2013.

[38] S. R. Atefi, F. Seoane, and K. Lindecrantz, "Electrical bioimpedance cerebral monitoring. Preliminary results from measurements on stroke patients," in *Proceedings of the 34th Annual International Conference of the IEEE Engineering in Medicine and Biology Society (EMBS '12)*, pp. 126–129, September 2012.

[39] H. P. Schwan and C. D. Ferris, "Four-electrode null techniques for impedance measurement with high resolution," *Review of Scientific Instruments*, vol. 39, no. 4, pp. 481–485, 1968.

[40] O. H. Schmitt, "Lead vectors and transfer impedance," *Annals of the New York Academy of Sciences*, vol. 65, no. 6, pp. 1092–1109, 1957.

[41] F. Seoane, M. Lu, M. Persson, and K. Lindecrantz, "Electrical bioimpedance cerebral monitoring. A study of the current density distribution and impedance sensitivity maps on a 3D

realistic head model," in *Proceedings of the 3rd International IEEE EMBS Conference on Neural Engineering*, pp. 256–260, IEEE, Kohala Coast, Hawaii, USA, May 2007.

[42] F. Seoane, "Electrical bioimpedance cerebral monitoring: fundamental steps towards clinical application," in *Signal & Systems*, p. 154, Chalmers University of Technology, Gothenburg, Sweden, 2007.

[43] L. Horesh, O. Gilad, A. Romsauerova, S. R. Arridge, and D. S. Holder, "Stroke type detection by multi-frequency electrical impedance tomography MFEIT. A feasibility study," in *Proceedings of the 6th Conference on Biomedical Applications of Electrical Impedance Tomography*, University College London, London, UK, 2005.

[44] A. McEwan, A. Romsauerova, L. Horesh, and D. S. Holder, "Performance improvements in a MF-EIT system for acute stroke: the UCL Mk2.5," in *Proceedings of the World Congress on Medical Physics and Biomedical Engineering 2006*, R. Magjarevic and J. H. Nagel, Eds., pp. 3886–3889, Springer, Berlin, Germany, 2007.

[45] G. Bonmassar and S. Iwaki, "The shape of electrical impedance spectroscopy (EIS) is altered in stroke patients," in *Proceedings of the 26th Annual International Conference of the IEEE Engineering in Medicine and Biology Society*, pp. 3443–3446, IEEE, San Francisco, Calif, USA, September 2004.

[46] J. Ma, C. Xu, M. Dai et al., "Exploratory study on the methodology of fast imaging of unilateral stroke lesions by electrical impedance asymmetry in human heads," *The Scientific World Journal*, vol. 2014, Article ID 534012, 18 pages, 2014.

[47] S. Prabhakaran, K. O'Neill, L. Stein-Spencer, J. Walter, and M. J. Alberts, "Prehospital triage to primary stroke centers and rate of stroke thrombolysis," *JAMA Neurology*, vol. 70, no. 9, pp. 1126–1132, 2013.

[48] J. R. Marler, B. C. Tilley, M. Lu et al., "Early stroke treatment associated with better outcome: the NINDS rt-PA stroke Study," *Neurology*, vol. 55, no. 11, pp. 1649–1655, 2000.

Hindawi Publishing Corporation
BioMed Research International
Volume 2015, Article ID 258279, 4 pages
http://dx.doi.org/10.1155/2015/258279

Research Article

The Level of Circulating Endothelial Progenitor Cell Is Associated with Cerebral Vasoreactivity: A Pilot Study

Chih-Ping Chung,[1,2] Po-Hsun Huang,[2,3] Jia-Shiong Chen,[2,3] Jaw-Wen Chen,[2,3] and Kuang-Yao Yang[2,4]

[1]*Department of Neurology, Taipei Veterans General Hospital, Taipei, Taiwan*
[2]*National Yang Ming University, Taipei, Taiwan*
[3]*Division of Cardiology, Department of Internal Medicine, Taipei Veterans General Hospital, Taipei, Taiwan*
[4]*Department of Chest Medicine, Taipei Veterans General Hospital, Taipei 11217, Taiwan*

Correspondence should be addressed to Kuang-Yao Yang; kyyang@vghtpe.gov.tw

Received 6 July 2015; Revised 30 September 2015; Accepted 1 October 2015

Academic Editor: Vida Demarin

Endothelial progenitor cell is known to be able to repair injured vessels. We assessed the hypothesis that endothelial progenitor cell also modulates cerebral endothelial function in healthy status. We used transcranial color-coded sonography to measure middle cerebral arterial vasoreactivity to CO_2 (breath-holding index) in healthy subjects and observed its relationship with the number of circulating CD34CD133+ cells. To detect significant correlations between each characteristic and breath-holding index of middle cerebral artery, we used univariate and multivariate regression analyses. 22 young healthy subjects were included in the present study (6 men, 16 women; mean age: 28.45 ± 3.98 years, range: 22–34 years). The mean breath-holding index and $CD45^{low}CD34+CD133+$ cells number were 0.95 ± 0.48% and 0.52 ± 0.26, respectively. The level of CD34CD133+ cells was independently associated with middle cerebral artery's vasoreactivity ($r = 0.439, P = 0.04$). Our results suggest that endothelial progenitor cell also modulates healthy cerebral vessels' endothelial function. This ability of endothelial progenitor cell could be potentially applied therapeutically and for prevention in conditions with cerebral endothelial dysfunction and cerebral ischemia.

1. Introduction

Circulating endothelial progenitor cell (CPC), mainly derived from the bone marrow, is identified by the surface expression of CD34 and CD133 epitopes (CD34+CD133+ cells) [1]. In response to ischemic stimuli, endothelial progenitor cell (EPC) will be mobilized from bone marrow to the ischemic sites with increased number of CPCs [2]. Increasing evidences have shown that EPC could contribute to, though to variant extents, reendothelialization and vasculogenesis after vascular damage [3–6]. Clinical studies have also proved the association of CPC with injured cerebral vessels [7–10]. Patients with a lower CPC number after acute ischemic stroke had a greater stroke severity and a poorer outcome [7–10]. Furthermore, numbers of CPCs have an inverse correlation with numbers of cerebral infarcts and a positive correlation with regional cerebral blood flow in patients with previous ischemic strokes [8].

Cerebral vascular endothelial function could be evaluated by cerebral vasoreactivity (CVR), which keeps cerebral blood flow (CBF) constant in response to physiological or pathological conditions. Although several vascular risk factors are associated with a decreased number of CPCs, in a study using flow-mediated brachial vasoreactivity measurement in healthy individuals, the numbers of CPCs were an independent and better predictor of vascular reactivity than the conventional vascular risk factors [11]. These results suggest that, under the status of endothelial injury by certain vascular risk factors, CPC might play a pivotal role in the vascular endothelial function repair. However, little is known about the role of CPC in cerebral endothelial function of healthy individuals without any vascular risk

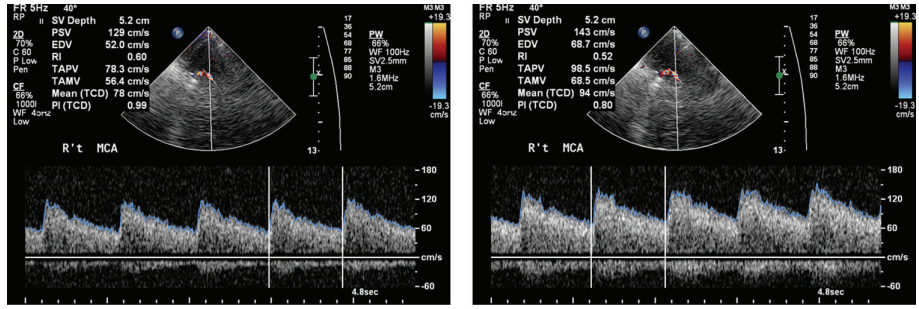

$V_{\text{baseline}} = 56.4\,\text{cm/s}$ $V_{\text{CO}_2} = 68.5\,\text{cm/s}$

$$\text{BHI} = (V_{\text{CO}_2} - V_{\text{baseline}})/V_{\text{baseline}} * 100/20 = 1.07$$

Figure 1: The breath-holing index (BHI) after 20 seconds of breath-holding calculated as percent increase in middle cerebral artery (MCA) mean blood velocity recorded by breath-holding divided by seconds of breath-holding ($[V_{\text{CO}_2} - V_{\text{baseline}}/V_{\text{baseline}}] * 100/20$).

factors. We hypothesized that CPC is associated with cerebral endothelial function maintenance in healthy status without any evidence of vascular injury. CVR to CO_2 is a surrogate of cerebral endothelial function [12]. In the present study, we used breath-holding test to measure CVR in healthy young subjects and to observe its relationship with the number of CPCs.

2. Materials and Methods

2.1. Subjects. Young healthy volunteers were recruited. People with hypertension, diabetes mellitus, heart diseases, dyslipidemia, and smoking history would be excluded. The Institutional Review Board of Taiwan Veterans General Hospital approved the study protocol and written informed consent was obtained from all the participants before recruiting into this study.

2.2. The Level of CPC. 10 mL of peripheral blood samples was collected between 10.00 and 11.00 h, at least one hour after breakfast. Total mononuclear cells (MNCs) were isolated by density gradient centrifugation with Histopaque-1077 (density 1.077 g/mL, Sigma-Aldrich, St. Louis, MO). Isolated MNCs were then incubated with 10 μL of FITC-conjugated anti-human CD34 mAb (Biolegend, San Diego, USA), 3 μL of PE-conjugated anti-human mAb CD133 (Miltenyi Biotec Ltd., Surrey, UK), 10 μL of PerCP-conjugated anti-human CD45 mAb (Becton Dickinson), and 10 μL of APC-conjugated anti-human KDR mAb (R&D Systems Inc., Minneapolis, Minnesota, USA) at 4°C for 30 min prior to four-color flow cytometry analysis (FACScan, Becton Dickinson, Sunnyvale, California, USA). Control isotype immunoglobulin (Ig) G1 and IgG2a antibodies were obtained from Becton Dickinson. The CPCs were represented as $CD45^{low}$CD34+CD133+ cells. The level of CPC was expressed as the percentage of $CD45^{low}$CD34+CD133+ cell number/MNCs number (%). To assess the reproducibility of CPC measurements, CPCs were measured from 2 separate blood samples in 10 subjects, and there was a strong correlation between the 2 measurements ($r = 0.90$, $P < 0.001$).

2.3. Transcranial Color-Coded Sonography. To minimize the angle-corrected bias, we used transcranial color-coded sonography (TCCS) (iU22; Philips, New York, NY, USA), instead of transcranial Doppler (TCD), to evaluate the blood flow velocity in middle cerebral artery (MCA). TCCS was conducted by the same examiner using the Philips ultrasound system (iU22; Philips, New York, NY, USA). We used a center transmit frequency of 2 MHz in color mode, and Doppler gate at 5 to 10 mm. Angle-corrected velocity was determined whenever angle correction was less than 60 degrees in a straight arterial segment of at least 2 mm in length in all other cases. The waveform of the M1 segment of the MCA was determined through temporal skull window from depths of 45 to 65 mm as unidirectional signals toward the probe at the mesencephalic plane (Figure 1).

2.4. Breath-Holding Index (BHI). All individuals performed the TCCS immediately after blood drawing and were lying for rest for at least 5 minutes before the TCCS examination. Firstly, the time-averaged-mean-velocity (TAMV) at baseline (V_{baseline}) was obtained from the average of the mean blood flow velocity of three randomized cardiac cycles on Doppler spectrum. Individuals were then instructed to hold their breath after a normal expiration for 20 seconds. The TAMV of the last cardiac cycle at the end of breath-holding was recorded as the increased MCA blood flow in response to CO_2 (V_{CO_2}). TAMV acquisition was continuous from baseline to the end of breath-holding to make sure Doppler cursor was at the same position. TAMV measurements were made using built-in software (iU22; Philips, New York, NY, USA). The BHI was calculated from these data as percent increase in MCA mean blood velocity after breath-holding divided by seconds of breath-holding ($[V_{\text{CO}_2} - V_{\text{baseline}}/V_{\text{baseline}}] * 100/20$) (Figure 1) [13, 14]. In all individuals, we measured the BHI of MCA on the right side. Compared with transcranial Doppler, TCCS detects MCA flow velocity more reliably with visual support (color signals and anatomic associations with the other vasculatures and brain structures) and angle correction. In 10 subjects, the coefficient of variation of the measured BHI of MCA (an interval of 1 h) was 5%.

Table 1: Clinical characteristics of subjects and the correlations between each variable and middle cerebral artery breath-holding index.

	Subjects ($n = 22$)	R	P value
Age, years	28.45 ± 3.98	−0.081	0.719
Gender, M/F	6/16	−0.047	0.835
Physiological values			
Systolic BP, mmHg	111.32 ± 11.15	−0.019	0.933
Diastolic BP, mmHg	69.36 ± 7.13	−0.036	0.874
Heart rate, beats/min	75.86 ± 9.44	−0.075	0.741
Body mass index, kg/m^2	21.34 ± 2.94	0.171	0.448
Metabolic values			
Total cholesterol, mg/dL	176.09 ± 15.63	−0.091	0.688
LDL-cholesterol, mg/dL	88.50 ± 15.96	−0.014	0.535
HDL-cholesterol, mg/dL	45.59 ± 15.56	−0.037	0.871
Fasting glucose, mg/dL	79.27 ± 11.25	0.189	0.400
C-reactive protein, mg/dL	0.05 ± 0.03	0.137	0.545

2.5. Statistical Analysis. Data were reported as the mean ± SD for numeric variables and as the number (percent) for categorical variables. Continuous variables were tested for normal distribution by the Kolmogorov-Smirnov test, and all variables passed it ($P < 0.05$). To detect significant correlations between each characteristic and BHI of MCA, we used univariate and multivariate regression analyses. The result of a correlation was represented by the correlation coefficient (r). It ranges from −1.0 to +1.0. The closer r is to +1 or −1, the more closely the two variables are related. If r is close to 0, it means that there is no relationship between the variables. For all tests, $P < 0.05$ was considered statistically significant. All analyses were performed with SAS software, version 9.1 (SAS Institute Inc., Cary, NC).

3. Results

Twenty-two healthy volunteers (6 men, 16 women; mean age: 28.45 ± 3.98 years, range: 22–34 years) were recruited. None had history of hypertension, diabetes mellitus, heart diseases, dyslipidemia, obesity, and smoking habits.

The clinical characteristics of the volunteers are demonstrated in Table 1. There are also results of univariate and multivariate regression analyses for detecting any possible correlation between the BHI of MCA and each characteristic. The results showed that age, gender, and physiological (BP, HR, and BMI) and metabolic (total cholesterol, HDL, LDL, fasting sugar, and CRP) values were not associated with BHI, respectively.

Table 2 demonstrates the results of white blood cell profiles and sonographic data. Only the level of CPC had a significant effect on MCA's vasoreactivity response to CO_2 in the multivariate analysis ($r = 0.439$, $P = 0.04$) (Figure 2).

4. Discussion

Current interest in EPCs centers predominantly on their role in angiogenesis and repairing of injured endothelium. We are the first to show that CPC is associated with cerebral endothelial function maintenance in healthy subjects. In our study, the level of CPC is the only predictor of CVR in healthy young individuals without any evidence of vascular injury.

The previous study has shown that the endothelial function assessed by flow-mediated dilatation of brachial artery was significantly associated with the number of EPC colonies in healthy middle-aged men [11]. The present study reveals that the number of CPCs is also associated with the cerebral vasoreactivity in the brain circulation. A lower level of CPCs has been found in (1) subjects with more severe age-related white matter changes [15], one kind of cerebral small vessel disease, and (2) ischemic stroke patients with unfavorable outcomes [7, 9, 10]. We postulate that a dysfunctional cerebral vasoreactivity may be involved in the pathophysiology.

The mechanism linking a lower level of CPCs and decreased cerebral vasoreactivity might be the paracrine

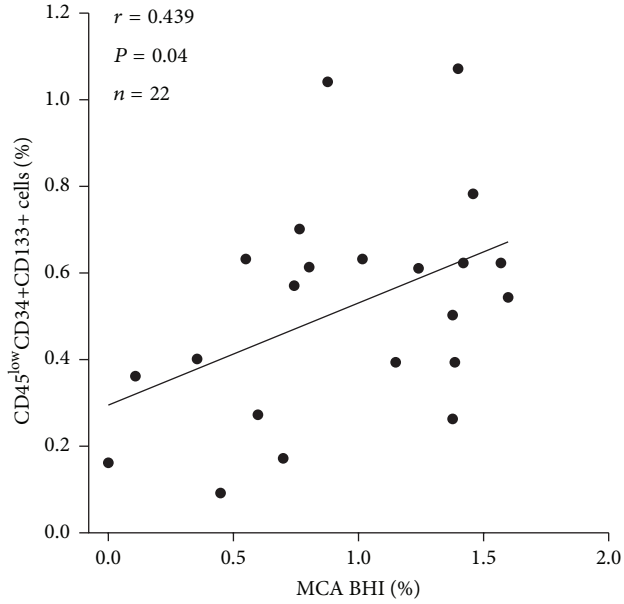

Figure 2: Relationship between breath-holding index (BHI) of middle cerebral artery (MCA) and the level of circulating endothelial progenitor cell (CPC).

Table 2: White blood cell profile and sonographic parameters of subjects and the correlations between each variable and middle cerebral artery breath-holding index.

	Subjects ($n = 22$)	R	P value
Blood cell levels			
White blood cells, /μL	6591 ± 957.63	0.017	0.940
Mononuclear cells, /μL	525.45 ± 228.76	−0.177	0.432
CD45^{low}CD34+CD133+ cells, %	0.52 ± 0.26	0.439	0.041*
Middle cerebral artery			
$V_{baseline}$, cm/s	80.40 ± 14.49	−0.383	0.078
V_{CO_2}, cm/s	92.23 ± 20.59	−0.061	0.786
Breath-holding index, %	0.95 ± 0.48	—	—

*Significant after multivariate analysis.

effect of CPCs. Study has found that one of the CPC's functions is to promote cerebral endothelial function by increasing prostacyclin (PGI_2) production and intracellular concentration of cAMP found in animals [16]. Otherwise, low levels of CPCs have been shown to be associated with higher levels of homocysteine [17]. Since homocysteine causes endothelial dysfunction [18], elevated levels of homocysteine may mediate the relationship between a lower level of CPCs and decreased cerebral vasoreactivity.

Our results suggest that CPC not only plays a critical role of vascular repair and promotes new vessels formation in ischemic tissues, but also modulates vasoreactivity in healthy vessels. This ability of CPC could be applied therapeutically to improve CBF through cerebral autoregulation enhancement in cerebral ischemia but not yet infarcted lesions (penumbra) or cerebral hypoperfusion status with poor cerebral autoregulation (e.g., leukoaraiosis; severe internal carotid artery stenosis).

There are limitations of the present study. It should be noted that this pilot study had a relatively small sample size and that future larger studies are needed to elucidate the relationship between CPC and cerebral autoregulation. In addition, another limitation of the study is related to its cross-sectional nature, and further longitudinal studies are needed to determine the temporal relationships. Besides, studies using another index of cerebral autoregulation other than BHI should be conducted to test our present results.

5. Conclusion

The results of this pilot study suggest that EPC modulates healthy cerebral vessels' endothelial function. This ability of EPC could be potentially applied therapeutically and for prevention in conditions with cerebral endothelial dysfunction and cerebral ischemia. Further studies on a larger population of healthy individuals and cerebrovascular diseases patients are needed.

Conflict of Interests

The authors declare that there is no conflict of interests regarding the publication of this paper.

Acknowledgment

This work was supported by Yen Tjing Ling Medical Foundation (CI-104-2).

References

[1] A. M. Leone, M. Valgimigli, M. B. Giannico et al., "From bone marrow to the arterial wall: the ongoing tale of endothelial progenitor cells," *European Heart Journal*, vol. 30, no. 8, pp. 890–899, 2009.

[2] S. Rafii and D. Lyden, "Therapeutic stem and progenitor cell transplantation for organ vascularization and regeneration," *Nature Medicine*, vol. 9, no. 6, pp. 702–712, 2003.

[3] T. Asahara, T. Murohara, A. Sullivan et al., "Isolation of putative progenitor endothelial cells for angiogenesis," *Science*, vol. 275, no. 5302, pp. 964–967, 1997.

[4] K. Hamano, M. Nishida, K. Hirata et al., "Local implantation of autologous bone marrow cells for therapeutic angiogenesis in patients with ischemic heart disease—clinical trial and preliminary results," *Japanese Circulation Journal*, vol. 65, no. 9, pp. 845–847, 2001.

[5] A. Taguchi, M. Ohtani, T. Soma, M. Watanabe, and N. Kinosita, "Therapeutic angiogenesis by autologous bone-marrow transplantation in a general hospital setting," *European Journal of Vascular and Endovascular Surgery*, vol. 25, no. 3, pp. 276–278, 2003.

[6] E. Tateishi-Yuyama, H. Matsubara, T. Murohara et al., "Therapeutic angiogenesis for patients with limb ischaemia by autologous transplantation of bone-marrow cells: a pilot study and a randomised controlled trial," *The Lancet*, vol. 360, no. 9331, pp. 427–435, 2002.

[7] T. Sobrino, O. Hurtado, M. Á. Moro et al., "The increase of circulating endothelial progenitor cells after acute ischemic stroke is associated with good outcome," *Stroke*, vol. 38, no. 10, pp. 2759–2764, 2007.

[8] A. Taguchi, T. Matsuyama, H. Moriwaki et al., "Circulating CD34-positive cells provide an index of cerebrovascular function," *Circulation*, vol. 109, no. 24, pp. 2972–2975, 2004.

[9] A. Taguchi, N. Nakagomi, T. Matsuyama et al., "Circulating CD34-positive cells have prognostic value for neurologic function in patients with past cerebral infarction," *Journal of Cerebral Blood Flow and Metabolism*, vol. 29, no. 1, pp. 34–38, 2009.

[10] H.-K. Yip, L.-T. Chang, W.-N. Chang et al., "Level and value of circulating endothelial progenitor cells in patients after acute ischemic stroke," *Stroke*, vol. 39, no. 1, pp. 69–74, 2008.

[11] J. M. Hill, G. Zalos, J. P. J. Halcox et al., "Circulating endothelial progenitor cells, vascular function, and cardiovascular risk," *The New England Journal of Medicine*, vol. 348, no. 7, pp. 593–600, 2003.

[12] S. Lavi, D. Gaitini, V. Milloul, and G. Jacob, "Impaired cerebral CO_2 vasoreactivity: association with endothelial dysfunction," *The American Journal of Physiology—Heart and Circulatory Physiology*, vol. 291, no. 4, pp. H1856–H1861, 2006.

[13] H. S. Markus and M. J. G. Harrison, "Estimation of cerebrovascular reactivity using transcranial Doppler, including the use of breath-holding as the vasodilatory stimulus," *Stroke*, vol. 23, no. 5, pp. 668–673, 1992.

[14] M. Müller, M. Voges, U. Piepgras, and K. Schimrigk, "Assessment of cerebral vasomotor reactivity by transcranial Doppler ultrasound and breath-holding. A comparison with acetazolamide as vasodilatory stimulus," *Stroke*, vol. 26, no. 1, pp. 96–100, 1995.

[15] G. Jickling, A. Salam, A. Mohammad et al., "Circulating endothelial progenitor cells and age-related white matter changes," *Stroke*, vol. 40, no. 10, pp. 3191–3196, 2009.

[16] A. V. R. Santhanam, L. A. Smith, T. He, K. A. Nath, and Z. S. Katusic, "Endothelial progenitor cells stimulate cerebrovascular production of prostacyclin by paracrine activation of cyclooxygenase-2," *Circulation Research*, vol. 100, no. 9, pp. 1379–1388, 2007.

[17] M. M. Alam, A. A. Mohammad, U. Shuaib et al., "Homocysteine reduces endothelial progenitor cells in stroke patients through apoptosis," *Journal of Cerebral Blood Flow and Metabolism*, vol. 29, no. 1, pp. 157–165, 2009.

[18] A. Hassan, B. J. Hunt, M. O'Sullivan et al., "Homocysteine is a risk factor for cerebral small vessel disease, acting via endothelial dysfunction," *Brain*, vol. 127, no. 1, pp. 212–219, 2004.

Hindawi Publishing Corporation
BioMed Research International
Volume 2015, Article ID 839820, 5 pages
http://dx.doi.org/10.1155/2015/839820

Clinical Study

Acute Cardioembolic and Thrombotic Middle Cerebral Artery Occlusions Have Different Morphological Susceptibility Signs on T2*-Weighted Magnetic Resonance Images

Mei Zheng and Dong-sheng Fan

Department of Neurology, Peking University Third Hospital, Beijing 100191, China

Correspondence should be addressed to Dong-sheng Fan; dsfan2010@aliyun.com

Received 31 July 2015; Revised 9 September 2015; Accepted 20 September 2015

Academic Editor: Sung-Chun Tang

Presence of susceptibility sign on middle cerebral artery (MCA) in T2*-weighted magnetic resonance (MR) images has been reported to detect acute MCA thromboembolic occlusion. However, the pathophysiologic course of thrombotic MCA occlusion differs from embolic occlusion, which might induce different imaging characters. Our study found that the occurrence rate of the MCA susceptibility sign in cardioembolism (CE) patients was significantly higher than in large artery atherosclerosis (LAA) patients, and the diameter of the MCA susceptibility sign for CE was greater than for LAA. Moreover, the patients with hemorrhagic transformation had MCA susceptibility signs with a significant larger mean diameter than patients without hemorrhagic transformation. Therefore, we hypothesized that the morphology of susceptibility signs could be used to differentiate acute cardioembolic and thrombotic MCA occlusions, which helped to select appropriate treatment strategies for different patients.

1. Introduction

Previous studies have reported that the middle cerebral artery (MCA) susceptibility sign in T2*-weighted magnetic resonance (MR) images can be indicative of an acute thromboembolic occlusion [1–5]. Acute thrombi and emboli contain large amounts of deoxygenated hemoglobin, which can severely shorten T2-weighted signals. This magnetic susceptibility effect produces a nonuniform magnetic field and a rapid dephasing of proton spins, which result in signal loss that is best observed on T2* susceptibility-weighted images [6]. The MCA susceptibility sign presents as a significantly decreased signal within an MCA trunk that exceeds the normal vessel diameter [6]. The hyperdense MCA sign (HMCAS) is a well-established marker of early ischemia on noncontrast computed tomography (CT). Recent studies show that the MCA susceptibility sign is more sensitive in predicting acute thromboembolism than HMCAS in CT [7] and can be used to predict the immediate effectiveness of intra-arterial thrombolysis [3].

Cardioembolic (CE) stroke is usually associated with high mortality as it has larger infarct size and higher rate of hemorrhage transformation compared to thrombotic occlusion. The etiology of ischemic stroke affects prognosis, outcome, and management. Traditionally, we distinguish CE from large artery atherosclerosis (LAA) through information provided by the speed of onset, history of atrial fibrillation, and infarct size in imaging data. However, whether there are direct signs to differentiate CE from LAA has not been well studied. The objective of this study is to explore the differences in MCA susceptibility sign between emboli and thrombi.

2. Methods

2.1. Subjects. From August 2010 to November 2012, 115 patients with acute MCA occlusion were admitted to our institution. The inclusion criteria for acute MCA occlusion patients were as follows: (1) all of the patients met the 2010 Chinese guidelines for the diagnosis and management of acute ischemic stroke [8]; (2) acute MCA occlusion was the

first attack; (3) the diffusion-weighted image (DWI), T2*-weighted MR image, and head and neck MR angiogram (MRA) were completed within 24 hours of symptom onset; and (4) DWI confirmed that the infarct was distributed in the unilateral MCA area. The exclusion criteria were as follows: (1) there are recurrent cerebral infarction and past cerebral hemorrhage; (2) MCA occlusion is caused by Moyamoya disease, arterial dissection, vasculitis, tumor, and blood hypercoagulability, among other causes; (3) thrombolytic or anticoagulant therapies were performed prior to the imaging examination; (4) MRA confirmed that the internal carotid artery contained moderate stenosis or occlusion; and (5) metal dentures affected T2*-weighted MR image quality. Eight-four patients met these criteria eventually (Figure 1). Among these 84 patients, there were 63 men (age range, 41–89 years; mean age, 63.6 years) and 21 women (age range, 47–86 years; mean age, 64.4 years). Our institutional review board approved this study, but patient informed consent was not required because this study was retrospective.

The patients were divided into two groups according to the Trial of Org 10172 Acute Stroke Treatment (TOAST) criteria [9]: CE and LAA. CE patients had classic clinical manifestations, including a previous TIA or stroke in more than one vascular territory or systemic embolism, together with high-risk and medium-risk cardiac source for the embolus. LAA patients had history of intermittent claudication, TIA in the same vascular territory, and evidence of large artery arthrosclerosis other than responsible vessel. There were 18 (21%) patients in CE and 66 (79%) patients in LAA.

Stroke severity was assessed by using the National Institutes of Health Stroke Scale (NIHSS). All stroke severity examinations were performed at admission and 1 week after onset by a stroke neurologist. The mean NIHSS score at admission was 11.3 (range, 4–25) and 1 week later 9.1 (range, 0–25).

2.2. MRI/MRA Protocol. All patients were examined on a 1.5-T MRI unit (Sonata, SIEMENS, Erlangen, Germany). For T2*-weighted MRI, the slice thickness was 5 mm, and the intersection gap was 2 mm. For DWI using an echo-planar sequence, the slice thickness was 5 mm, and the b values were 0 and 2,000 s/mm^2. Additional parameters for the acute stroke MR protocol were as follows: axial fast spin-echo T2-weighted MRI (repetition time (TR), 3700 ms; echo time (TE), 95 ms; excitations, 1; slice thickness, 5 mm; slice gap, 1 mm; matrix size, 256 × 256; field of view, 240 mm) and 3-dimensional time-of-flight MR angiographic images (TR, 39 ms; TE, 6.5 ms; excitations, 1; slab thickness, 60 mm; partitions, 60; matrix size, 160 × 512; field of view, 200 mm).

2.3. Image Analysis. The imaging data of all selected patients met consensus reading by two experienced neuroradiologists Sun A-P. and Sun Q.-L. who were blinded to the patients' clinical information. MRI criteria for MCA susceptibility sign were defined as low-signal images along the blood vessel and exceeding vessel diameter of the MCA [7], especially compared to the contralateral artery (Figures 2 and 3). The signs were judged to be present on the basis of only unanimous decision. If a disagreement had occurred, the sign would have been judged as absent. The diameter, length, occurrence, and location (M1 or M2) of the low-signal images were analyzed. The measurement method used ImageJ software (Version 1.46, NIH, Bethesda, MD, USA, http://rsb.info.nih.gov/ij/index.html). Infarct size was expressed as a percentage of the high-signal area in DWI and the area of ipsilateral hemisphere.

2.4. Statistical Analysis. The Statistical Package for Social Sciences (SPSS version 16.0, SPSS Inc., USA) was used for statistical analysis. Numeric values were expressed as the means ± standard deviations (SD), and categorical variables were expressed as percentages. The independent-samples t-test was used to compare the numeric values between CE and LAA. The Pearson Chi-Square test was used to evaluate the categorical data between the two groups. A value of $P < 0.05$ was considered statistically significant.

3. Results

3.1. Clinical Characteristics of CE and LAA Patients with Acute MCA Occlusions. Among the 84 patients studied, there were 18 patients in CE and 66 in LAA. The differences between the two patient groups in terms of patient sex (male/female, 14/4 versus 69/17), history of hypertension (61.1 versus 68.2%), diabetes (33.3% versus 28.8), hyperlipidemia (66.7% versus 54.6%), or smoking (27.8% versus 36.4%) were not statistically significant ($P > 0.05$). On average, CE patients were significantly older than LAA patients (70.5 ± 5.9 years versus 62.3 ± 11.2 years, $P < 0.01$) and had a higher proportion of history of coronary heart disease (50.0% versus 22.7%, $P < 0.05$). CE patients had a significantly higher NIHSS score than LAA patients at admission (14.8±5.3 versus 10.3±4.6, $P < 0.01$) and after 1 week (12.2±6.3 versus 8.3±5.7, $P < 0.05$) (Table 1).

3.2. Different Morphologies of MCA Susceptibility Signs in CE and LAA Patients. Among the 84 acute MCA occlusion patients, 63 (75%) presented an MCA susceptibility sign. A greater number of CE patients were positive for the MCA susceptibility sign compared to LAA patients (100% versus 68.2%, $P < 0.01$). Compared with LAA patients, CE patients had larger-diameter low-signal images at the occluded artery (5.4 ± 0.9 mm versus 3.9 ± 1.0 mm, $P < 0.01$), but the lengths were shorter (11.2 ± 2.2 mm versus 16.6 ± 4.2 mm, $P < 0.01$) (Figures 2(b) and 3(b)). The cut-off value were 4.385 mm and 14.89 mm, respectively. M1 was the most common site of positive MCA susceptibility sign without difference between two groups (M1/M2, 14/4 versus 36/9, $P > 0.05$). Compared with LAA patients, CE patients had significantly larger infarct areas (32.6 ± 21.5% versus 18.4 ± 12.7%, $P < 0.01$) and a higher rate of hemorrhagic transformation (27.8% versus 7.6%, $P < 0.05$) (Table 2).

In 63 cases with a positive MCA susceptibility sign, the diameters of the low-signal images in patients with hemorrhagic transformation were significantly larger than in those without hemorrhagic transformation (5.4 ± 0.9 mm versus 4.1 ± 1.2 mm, $P < 0.01$), although their lengths did not differ (14.4 ± 3.4 mm versus 15.2 ± 4.7 mm, $P > 0.05$).

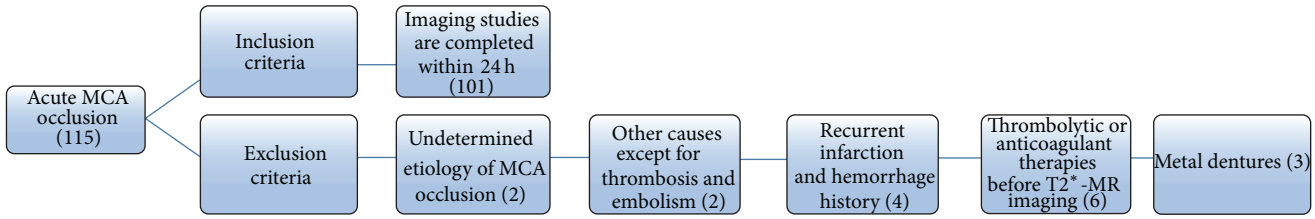

Figure 1: Patients selection flowchart.

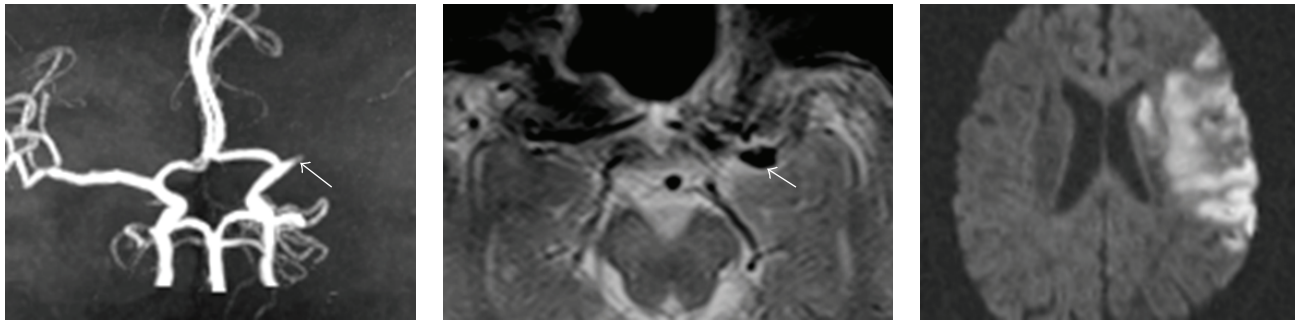

(a) (b) (c)

Figure 2: The MCA susceptibility sign in CE patients. (a) MRA reveals an MCA occlusion. (b) T2*-weighted MR imaging indicates a large diameter and a short, low-signal image along the MCA. (c) DWI shows a large-acreage cerebral infarction.

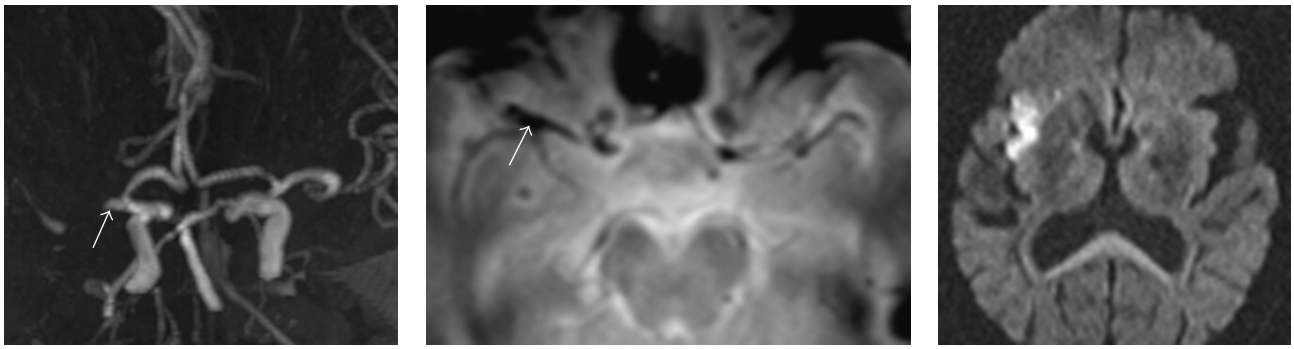

(a) (b) (c)

Figure 3: The MCA susceptibility sign in LAA patients. (a) MRA reveals an MCA occlusion. (b) T2*-weighted MR imaging indicates a low-signal image with a relatively small diameter and long length along the MCA. (c) DWI shows that the infarct size was relatively small compared to CE patients.

Table 1: Clinical manifestations and risk factors of CE and LAA patients with acute MCA occlusions.

Types	Total (n = 84)	CE (n = 18)	LAA (n = 66)	t/χ^2 values	P values
Sex (male/female)	63/21	14/4	49/17	$\chi^2 = 0.094$	0.762
Mean age (years, mean ± SD)	64.1 ± 10.8	70.5 ± 5.9	62.3 ± 11.2	$t = 2.975$	0.004
Hypertension history (n, %)	56 (66.7)	11 (61.1)	45 (68.2)	$\chi^2 = 0.318$	0.578
Diabetes history (n, %)	25 (29.8)	6 (33.3)	19 (28.8)	$\chi^2 = 0.140$	0.713
Coronary heart disease history (n, %)	24 (28.6)	9 (50.0)	15 (22.7)	$\chi^2 = 5.155$	0.023
Hyperlipidemia history (n, %)	48 (57.1)	12 (66.7)	36 (54.6)	$\chi^2 = 0.848$	0.363
Smoking history (n, %)	29 (34.5)	5 (27.8)	24 (36.4)	$\chi^2 = 0.461$	0.503
NIHSS score at admission (mean ± SD)	11.3 ± 5.0	14.8 ± 5.3	10.3 ± 4.6	$t = 3.585$	0.001
NIHSS score at 1 week later (mean ± SD)	9.1 ± 6.0	12.2 ± 6.3	8.3 ± 5.7	$t = 2.513$	0.014

Table 2: The characteristics of MCA susceptibility signs in CE and LAA patients.

Types	Total ($n = 84$)	CE ($n = 18$)	LAA ($n = 66$)	t/χ^2 values	P values
MSS positives* (%)	63 (75.0)	18 (100)	45 (68.2)	$\chi^2 = 7.636$	0.005
Diameter of MSS (mm)	4.1 ± 1.0	5.4 ± 0.9	3.9 ± 1.0	$t = 5.567$	0.000
Length of MSS (%)	15.1 ± 4.5	11.2 ± 2.2	16.6 ± 4.2	$t = -5.135$	0.000
Location of MSS (M1/M2)	50/13	14/4	36/9	$\chi^2 = 0.039$	0.847
Infarct area (%)	21.5 ± 16.0	32.6 ± 21.5	18.4 ± 12.7	$t = 3.577$	0.001
Hemorrhage transformation (%)	10 (11.9)	5 (27.8)	5 (7.6)	$\chi^2 = 5.504$	0.019

*MSS: MCA susceptibility sign.

4. Discussion

In this study, we find that emboli and thrombi in acute occlude MCA have different shape of susceptibility sign in T2*-MRI. The susceptibility sign of emboli has a larger diameter and relatively shorter length than thrombi, and large diameter of susceptibility sign is related to hemorrhage transformation.

In this study, T2*-weighted MRI can sensitively detect acute thromboembolic MCA occlusion. 75% patients among 84 acute MCA occlusions have a positive susceptibility sign. HMCAS on CT was thought to be the important early changes in acute ischemic stroke of MCA territory previously [10, 11]. However, a recent study indicates that 3D susceptibility-based perfusion MRI allows the identification of acute MCA thromboembolism with a sensitivity higher than that of CT [7]. Compare with LAA, CE patients have a higher occurrence rate of positive MCA susceptibility signs in our study (18 of 18, 100%, versus 45 of 66, 68.2%). Kim et al. [3] drew the same conclusion, as 13 of 16 patients with a positive MCA susceptibility sign had a history of atrial fibrillation and no evidence of LAA stenosis by digital subtraction angiography. Cho et al. [12] also concluded that MCA susceptibility is an independent predictor of CE stroke. In their data, MCA susceptibility was more commonly associated with CE stroke patients (31 of 40, 77.5%) than with other stroke subtypes (14 of 55, 25.5%). However, the rate of susceptibility sign in LAA might be underestimated in these studies, as MCA stenosis sometimes were exaggerated as occlusion in MRA which would induce false-negative results of MCA susceptibility sign more easily in LAA patients.

Different composition of thromboemboli in CE and LAA may create different shape of susceptibility sign although deoxygenated hemoglobin in the thromboemboli is the main material producing susceptibility sign. Cardiogenic emboli are primarily composed of red thrombi, which contain numerous erythrocytes and some fibrin. Intra-arterial primary clots, however, are mainly composed of white thrombi that consist of varying amounts of cellular debris, fibrin, and platelets, but only a small number of red blood cells [13–15].

An important finding of this study is that the MCA susceptibility sign in CE patients is larger in diameter than that found in LAA patients. There is strong evidence in our study that the large diameters of MCA susceptibility signs are associated with hemorrhagic transformation. The destruction of the extracellular matrix integrity is considered to be the cause of hemorrhagic transformation, especially parenchymal hemorrhage after acute infarction [16, 17]. However, arterial wall destruction is hard to observe by current imaging technology. A recent study reported that increased permeability is present in the basal ganglia region in patients with parenchymal hemorrhage after acute stroke [18]. As the bleeding site is close to the MCA trunk, the destruction of the focal arterial wall might be the anatomic basis of the parenchymal hemorrhage.

For acute thromboembolic MCA occlusions, the optimal treatment option is thrombolysis [19]. However, the symptoms deteriorate once hemorrhagic transformation occurs after intravenous thrombolysis. The selection of appropriate candidate patients for thrombolysis is vitally important for a favorable prognosis. Atrial fibrillation has been testified as the independent risk factors for symptomatic intracranial hemorrhage and no early recanalization after thrombolysis [20, 21]. Our study indicates that larger diameters of MCA susceptibility sign often present in CE patients and accompany more hemorrhage transformation. Thus, the shape of thromboemboli in T2*-MR imaging can help us to manage patients with acute MCA occlusion. Recent study reported that HMCAS length >10 mm or persistence of HMCAS on follow-up CT scan was associated with poor outcome after intravenous thrombolysis and needed ancillary therapy [22, 23]. Susceptibility vessel sign has been used to predict artery recanalization [24] and metabolic state of infarcted brain tissue [25].

The limitation of our study is that the cases did not have a unified treatment plan. Thus we cannot come to a conclusion about the effect of MCA susceptibility to the prognosis of stroke treatment. Our next work will aim at the predictive role of the shape of MCA susceptibility sign on outcomes of intravenous thrombolysis in CE and LAA patients.

5. Conclusion

The morphology of susceptibility signs on T2*-weighted MR images can be used to differentiate acute cardioembolic and thrombotic MCA occlusions. The larger diameters of MCA susceptibility signs in CE patients indicate a greater probability of hemorrhagic transformation after acute cerebral infarction.

Conflict of Interests

The authors declare that they have no conflict of interests.

Authors' Contribution

Mei Zheng contributed to conception and design, carrying out data analysis, and drafting the paper. Dong-sheng Fan contributed to conception and design and revising the paper as the principal investigator for the overall program. All authors read and approved the final paper.

Acknowledgments

This work was supported by Grants from the Natural Science Foundation of China (81200969), a Grant from Beijing Municipal Science and Technology Commission (2010001-1), and a Grant from the Clinical Key Projects of Chinese Ministry of Health. The authors thank Dr. Sun A-Ping and Dr. Sun Qing-Li for medical imaging reading.

References

[1] N. Morita, M. Harada, M. Uno et al., "Ischemic findings of T2*-weighted 3-tesla MRI in acute stroke patients," *Cerebrovascular Diseases*, vol. 26, no. 4, pp. 367–375, 2008.

[2] E. Assouline, K. Benziane, D. Reizine et al., "Intra-arterial thrombus visualized on T2* gradient echo imaging in acute ischemic stroke," *Cerebrovascular Diseases*, vol. 20, no. 1, pp. 6–11, 2005.

[3] H. S. Kim, D. H. Lee, C. G. Choi, S. J. Kim, and D. C. Suh, "Progression of middle cerebral artery susceptibility sign on T2*-weighted images: its effect on recanalization and clinical outcome after thrombolysis," *American Journal of Roentgenology*, vol. 187, no. 6, pp. W650–W657, 2006.

[4] D. Lingegowda, B. Thomas, V. Vaghela, D. R. Hingwala, C. Kesavadas, and P. N. Sylaja, "'Susceptibility sign' on susceptibility-weighted imaging in acute ischemic stroke," *Neurology India*, vol. 60, no. 2, pp. 160–164, 2012.

[5] Y. Sakamoto, K. Kimura, and K. Sakai, "M1 susceptibility vessel sign and hyperdense middle cerebral artery sign in hyperacute stroke patients," *European Neurology*, vol. 68, no. 2, pp. 93–97, 2012.

[6] R. A. Clark, A. T. Watanabe, W. G. Bradley Jr., and J. D. Roberts, "Acute hematomas: effects of deoxygenation, hematocrit, and fibrin-clot formation and retraction on T2 shortening," *Radiology*, vol. 175, no. 1, pp. 201–206, 1990.

[7] S. Flacke, H. Urbach, E. Keller et al., "Middle cerebral artery (MCA) susceptibility sign at susceptibility-based perfusion MR imaging: clinical importance and comparison with hyperdense MCA sign at CT," *Radiology*, vol. 215, no. 2, pp. 476–482, 2000.

[8] Chinese Medical Association, "The 2010 Chinese guidelines for the diagnosis and management of acute ischemic stroke," *Chinese Journal of Neurology*, vol. 43, no. 2, pp. 146–153, 2010.

[9] H. P. Adams Jr., B. H. Bendixen, L. J. Kappelle et al., "Classification of subtype of acute ischemic stroke. Definitions for use in a multicenter clinical trial. TOAST. Trial of Org 10172 in Acute Stroke Treatment," *Stroke*, vol. 24, no. 1, pp. 35–41, 1993.

[10] D. Leys, J. P. Pruvo, O. Godefroy, P. Rondepierre, and X. Leclerc, "Prevalence and significance of hyperdense middle cerebral artery in acute stroke," *Stroke*, vol. 23, no. 3, pp. 317–324, 1992.

[11] V. K. Sharma, N. Venketasubramanian, H. L. Teoh, and B. P. L. Chan, "Hyperdense middle cerebral artery sign and stroke outcomes after intravenous thrombolysis," *Cerebrovascular Diseases*, vol. 31, no. 2, pp. 207–208, 2011.

[12] K.-H. Cho, J. S. Kim, S. U. Kwon, A.-H. Cho, and D.-W. Kang, "Significance of susceptibility vessel sign on T2*-weighted gradient echo imaging for identification of stroke subtypes," *Stroke*, vol. 36, no. 11, pp. 2379–2383, 2005.

[13] J. Ogata, C. Yutani, R. Otsubo et al., "Heart and vessel pathology underlying brain infarction in 142 stroke patients," *Annals of Neurology*, vol. 63, no. 6, pp. 770–781, 2008.

[14] J. M. Niesten, I. C. van der Schaaf, L. van Dam et al., "Histopathologic composition of cerebral thrombi of acute stroke patients is correlated with stroke subtype and thrombus attenuation," *PLoS ONE*, vol. 9, no. 2, Article ID e88882, 2014.

[15] S. K. Kim, W. Yoon, T. S. Kim, H. S. Kim, T. W. Heo, and M. S. Park, "Histologic analysis of retrieved clots in acute ischemic stroke: correlation with stroke etiology and gradient-echo MRI," *American Journal of Neuroradiology*, 2015.

[16] A. Rosell, C. Foerch, Y. Murata, and E. H. Lo, "Mechanisms and markers for hemorrhagic transformation after stroke," in *Cerebral Hemorrhage*, vol. 105 of *Acta Neurochirurgica Supplementum*, pp. 173–178, Springer, Berlin, Germany, 2008.

[17] J. Hom, J. W. Dankbaar, B. P. Soares et al., "Blood-brain barrier permeability assessed by perfusion CT predicts symptomatic hemorrhagic transformation and malignant edema in acute ischemic stroke," *American Journal of Neuroradiology*, vol. 32, no. 1, pp. 41–48, 2011.

[18] O. Y. Bang, J. L. Saver, J. R. Alger et al., "Patterns and predictors of blood-brain barrier permeability derangements in acute ischemic stroke," *Stroke*, vol. 40, no. 2, pp. 454–461, 2009.

[19] J. M. Wardlaw, G. Zoppo, T. Yamaguchi, and E. Berge, "Thrombolysis for acute ischaemic stroke," *Cochrane Database of Systematic Reviews*, no. 3, Article ID CD000213, 2003.

[20] P. A. Dharmasaroja, S. Muengtaweepongsa, J. Pattaraarchachai, and P. Dharmasaroja, "Intracerebral hemorrhage following intravenous thrombolysis in Thai patients with acute ischemic stroke," *Journal of Clinical Neuroscience*, vol. 19, no. 6, pp. 799–803, 2012.

[21] K. Kimura, Y. Iguchi, S. Yamashita, K. Shibazaki, K. Kobayashi, and T. Inoue, "Atrial fibrillation as an independent predictor for no early recanalization after IV-t-PA in acute ischemic stroke," *Journal of the Neurological Sciences*, vol. 267, no. 1-2, pp. 57–61, 2008.

[22] N. Shobha, S. Bal, M. Boyko et al., "Measurement of length of hyperdense MCA sign in acute ischemic stroke predicts disappearance after IV tPA," *Journal of Neuroimaging*, vol. 24, no. 1, pp. 7–10, 2014.

[23] P. R. Paliwal, A. Ahmad, L. Shen et al., "Persistence of hyperdense middle cerebral artery sign on follow-up CT scan after intravenous thrombolysis is associated with poor outcome," *Cerebrovascular Diseases*, vol. 33, no. 5, pp. 446–452, 2012.

[24] K. Kimura, Y. Iguchi, K. Shibazaki, M. Watanabe, T. Iwanaga, and J. Aoki, "M1 susceptibility vessel sign on T2* as a strong predictor for no early recanalization after IV-t-PA in acute ischemic stroke," *Stroke*, vol. 40, no. 9, pp. 3130–3132, 2009.

[25] S. K. Baik, W. Choi, S. J. Oh et al., "Change in cortical vessel signs on susceptibility-weighted images after full recanalization in hyperacute ischemic stroke," *Cerebrovascular Diseases*, vol. 34, no. 3, pp. 206–212, 2012.

Hindawi Publishing Corporation
BioMed Research International
Volume 2015, Article ID 939387, 9 pages
http://dx.doi.org/10.1155/2015/939387

Research Article

Implantation of 3D-Printed Patient-Specific Aneurysm Models into Cadaveric Specimens: A New Training Paradigm to Allow for Improvements in Cerebrovascular Surgery and Research

Arnau Benet,[1] Julio Plata-Bello,[1,2] Adib A. Abla,[1] Gabriel Acevedo-Bolton,[3] David Saloner,[4] and Michael T. Lawton[1]

[1] *Skull Base and Cerebrovascular Laboratory, Department of Neurosurgery, University of California San Francisco, San Francisco, CA 94143, USA*
[2] *Department of Neurosurgery, Hospital Universitario de Canarias, 38320 Tenerife, Spain*
[3] *Department of Neurosurgery, University of California San Francisco, San Francisco, CA 94143, USA*
[4] *Center for Cerebrovascular Research, University of California San Francisco, San Francisco, CA 94143, USA*

Correspondence should be addressed to Arnau Benet; beneta@neurosurg.ucsf.edu

Received 16 April 2015; Accepted 21 June 2015

Academic Editor: Xianli Lv

Aim. To evaluate the feasibility of implanting 3D-printed brain aneurysm model in human cadavers and to assess their utility in neurosurgical research, complex case management/planning, and operative training. *Methods*. Two 3D-printed aneurysm models, basilar apex and middle cerebral artery, were generated and implanted in four cadaveric specimens. The aneurysms were implanted at the same anatomical region as the modeled patient. Pterional and orbitozygomatic approaches were done on each specimen. The aneurysm implant, manipulation capabilities, and surgical clipping were evaluated. *Results*. The 3D aneurysm models were successfully implanted to the cadaveric specimens' arterial circulation in all cases. The features of the neck in terms of flexibility and its relationship with other arterial branches allowed for the practice of surgical maneuvering characteristic to aneurysm clipping. Furthermore, the relationship of the aneurysm dome with the surrounding structures allowed for better understanding of the aneurysmal local mass effect. Noticeably, all of these observations were done in a realistic environment provided by our customized embalming model for neurosurgical simulation. *Conclusion*. 3D aneurysms models implanted in cadaveric specimens may represent an untapped training method for replicating clip technique; for practicing certain approaches to aneurysms specific to a particular patient; and for improving neurosurgical research.

1. Introduction

Cerebrovascular surgery is challenging and requires refined technical skills and thorough knowledge of both brain vasculature and skull base approaches. Progressive technical advances and good outcomes in patients with aneurysms treated with endovascular techniques have modified surgical indications for aneurysm clipping [1, 2]. At present, very complex and challenging cases are presented more often to cerebrovascular surgeons practicing at tertiary centers.

Research and training are essential for safe surgical treatment of challenging cerebrovascular lesions. Surgical research is critical for designing better approaches for the treatment of difficult-to-reach aneurysms (e.g., basilar apex aneurysms) and arteriovascular malformations (AVMs). Also, educational models for cerebrovascular surgery are very important to prepare neurosurgeons in managing challenging lesions early in their careers.

At present, there are two main models for surgical training that complement surgical experience: augmented-reality computer models and cadaveric surgical simulation. Although very promising, the augmented-reality computerized models do not provide a realistic surgical environment due to many technological limitations (e.g., lack of brain

manipulation or realistic surgical feedback). Cadaveric surgical simulation is one of the best complements to surgical experience as it allows very realistic surgical scenarios to be simulated. Our group has recently published a customized embalming formula for neurosurgical research that preserved the natural physical features of the brain, most importantly retraction qualities, therefore providing a very realistic surgical environment [3]. There are several reports on neurosurgical educational models using human cadavers in the literature [4–8]. Aboud et al. designed a model to simulate human blood flow in disease-free human cadavers for neurosurgical training [7]. However, none of the models described in the literature include the simulation of cerebrovascular surgical scenarios in cadavers, using aneurysm models of lesions from actual patients.

We propose a model of cerebrovascular surgical simulation that includes, for the first time, the implantation of 3D-printed replicas from real cerebrovascular lesions in human cadavers. Using 3D-printed aneurysm models obtained from patient's radiological studies, we recreated several surgical scenarios to investigate the potential use of this model for neurosurgical research and training. In this report, we describe our method and provide initial results on the application of this model to basilar apex and middle cerebral artery aneurysms.

2. Materials and Methods

In this model, we generated 3D-printed aneurysms from preoperative radiological studies of previously selected patients and implanted them into 2 human cadavers (4 specimens) prepared for surgical simulation. We also performed different approaches on each side of the specimens to evaluate the manipulation capabilities, visualization, and surgical exposure of the models and discuss their potential role in cerebrovascular research and education.

2.1. Preparation of Cadaveric Heads. The human heads were sectioned in the neck at the level of C7. The carotid and vertebral arteries as well as the jugular veins were dissected 1 cm cranially from the section level to allow cannulation. Tubing of different size was introduced into each vessel and ligated using 2-0 suture. Then, the vessels were profusely irrigated with saline solution until all blood and blood clots were cleared out from the vasculature. Next, a customized embalming solution [3] was manually injected through all cannulated vessels repeatedly and the specimen was stored for one week at room temperature. At this point, the specimens were divided into two groups: (a) cerebrovascular training or (b) surgical research. The criteria for selection were designed to assign those specimens with best quality to the surgical research group and included donors younger than 75 years old and minimal degeneration of the spinal cord at the edge of the neck section (which was used to infer the quality of the encephalon before dissection). For training purposes, and to simulate surgical bleeding, the specimens were connected to two liquid reservoirs inside pressure bags [7]. The tubing previously introduced in the arteries was connected to one reservoir containing red colored saline solution at variable arterial pressure (approximately 120–140 mmHg). Tubing from the jugular veins was connected to a reservoir containing dark blue saline solution at low pressure (40–60 mmHg). After several training sessions, the specimens in this group, already embalmed, were transferred to the research group for bypass investigation.

The specimens selected for research were prepared for latex injection to ease vessel identification during dissection and maintain the vasculature in optimal conditions for all research time. Red latex was injected to the common carotids and vertebral arteries bilaterally until the arterial system was completely filled. Then, dark blue latex was injected to both jugular veins. Next, all tubing was clamped and the specimens were stored immersed in embalming solution for 72 hours to allow the latex to cure.

2.2. Aneurysm Model Production. The patient database of the senior author (M. T. Lawton) was searched for patient selection. For research purposes, our selection criteria include the following: (1) an aneurysm is considered suitable for surgical treatment (broad neck, complex anatomy, and perforators arising from the neck/dome), but surgical access is deemed complex or no proximal control could be guaranteed; (2) surgical treatment was suboptimal (incomplete closure, perforator entrapment); (3) poor patient outcome is related to the surgical approach; (4) intraoperative aneurysm rupture is present. For training purposes, we use the following inclusion criteria: (1) aneurysm shape is best suited for surgical treatment; (2) aneurysm is accessible from one approach; (3) proximal control of the aneurysm is feasible. After patient selection, the radiological studies were anonymized and transferred to the center for cerebrovascular research for aneurysm model reconstruction.

Part of our preoperative radiological protocol for patients with cerebral aneurysms includes contrast-enhanced magnetic resonance angiography (CE-MRA) (TR = 5.5 ms, TE = 1.8 ms, 0.5 × 0.5 × 1.2 mm) and a balanced fast field echo sequence (TR = 5.2 ms, TE = 1.8 ms, 0.5 × 0.5 × 1.2 mm), which were acquired on an *Intera* 1.5T scanner (Phillips Healthcare, Best, Netherlands). These studies are always set in the same volume and orientation to visualize the vessel lumen and surrounding thrombus. The CE-MRA dataset was loaded into a dedicated software package [9] (*ITK-SNAP*, http://www.itksnap.org/) for segmentation (Figure 1). The software generated an accurate real-sized surface of the lumen, which was then saved. The balanced fast field echo dataset was then loaded into a new window along with the CE-MRA surface. The intraluminal thrombus dimension was labeled manually while the CE-MRA surface served as a marker for the lumen position (Figure 1(a)). The combined surfaces were saved and exported to a 3D volume file (Figures 1(b) and 1(c)), which was printed in 3D (Fathom, Oakland, CA) using rubber-like material (tangoBlackPlus) with shore hardness $A = 25$.

2.3. Aneurysm Implantation. The 3D aneurysm model was implanted in the specimens at the same anatomical region

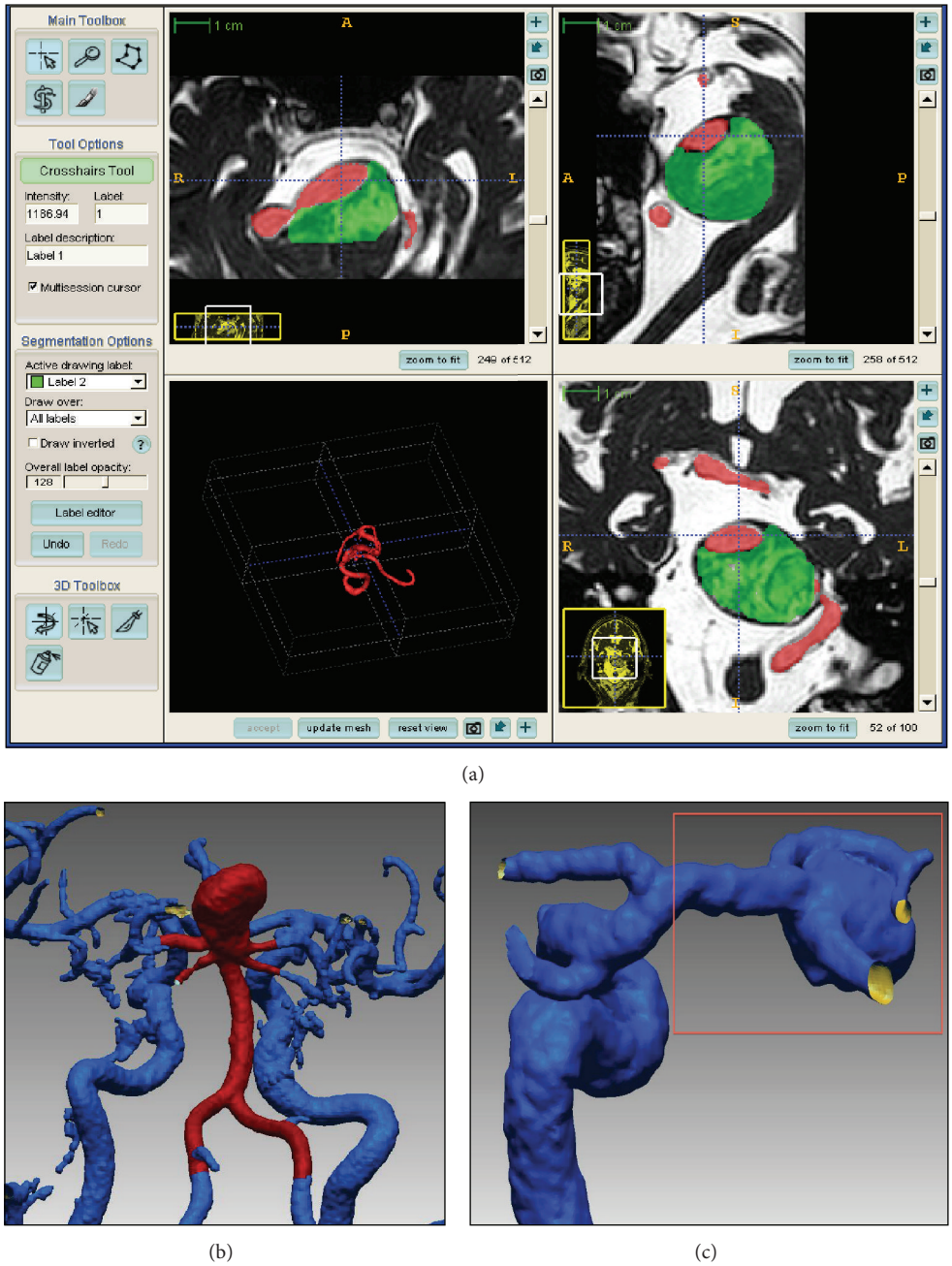

(a)

(b)

(c)

Figure 1: Radiological reconstruction of the 3D aneurysm model from a selected patient. Using dedicated software, the aneurysm thrombus (green) and lumen (red) were identified and labeled in each slice of the magnetic resonance of the selected patient (a). The software-generated vascular model was obtained for a patient with a basilar apex (b) and middle cerebral artery (c) aneurysm and the zone of interest was selected and cropped for printing (brown square).

where it was originally located in the patient. An open craniotomy was performed in the specimen, and the implantation zone was exposed using standard surgical techniques: dural opening, arachnoid dissection, cerebrospinal fluid suction, and brain retraction. A surgical microscope (Carl Zeiss Pentero) was used for intradural dissection. The implantation zone was carefully exposed with minimal dissection of the arachnoid cisterns. The aneurysm model was implanted to the vasculature using cyanoacrylate (Loctite) with anastomosis of the surrounding vessels to create a vascular model similar to that of the actual patient. In the research group, the branches of the 3D model were glued to the latex in the lumen of the cadaver vasculature. In contrast, the branches of the 3D models implanted in the training group were anastomosed to the cadaver vessels using 8-0 sutures. This was possible because the lumen of the vessels in the training group was

Table 1: Surgical simulation experiments for aneurysm clipping in cadaver.

3D model	Approach for implantation	Side of implantation	Approach for clipping
Basilar tip	Orbitozygomatic	Left	Right orbitozygomatic
	Orbitozygomatic	Right	Left orbitozygomatic
	Orbitozygomatic	Left	Right orbitopterional
	Orbitozygomatic	Right	Left orbitopterional
Middle cerebral artery	Pterional	Left	Left pterional
	Minipterional	Right	Right minipterional
	Pterional	Left	Left pterional
	Pterional	Right	Right minipterional

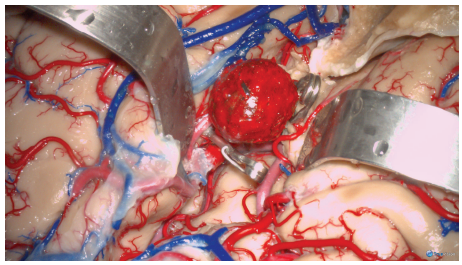

Figure 2: Surgical simulation photograph of a 3D-printed aneurysm model implanted in a left-side opercular artery. The sylvian fissure was completely split and the opercular arteries (M2) were exposed. The aneurysm was implanted into the proximal segment of one opercular artery. Both temporal clips and permanent clipping of the aneurysm neck were trained during the surgical simulation.

hollow, and the 8-0 needle could be passed through the 3D model's branches without deforming. To implant giant aneurysms that generate mass effect to the surrounding tissue, a Foley catheter was inserted first by us and inflated progressively at the implantation side to create anatomical deformity related to mass effect and obtain the room required to implant the aneurysm model.

3. Results

Basilar apex and middle cerebral artery aneurysm models were created for evaluation. We selected these aneurysms from the senior surgeon's database because they represent two frequent lesions. We also selected the basilar apex model to illustrate a lesion that requires further surgical research [10, 11]. A pterional approach was performed. The sylvian fissure was carefully dissected as previously described [12] and the deep sylvian cistern was exposed. A Foley catheter was inserted into the anterior half of the deep sylvian cistern and inflated 5 mL to create mass effect. The procedure was resumed the next day to allow full expansion of the sylvian fissure. Following this, the aneurysm replica was glued to the target middle cerebral artery, proximal M2 (Figure 2). After clipping techniques and possible bypass anastomoses were tried, the aneurysm was detached from the specimen.

Next, the orbitozygomatic (OZ) piece was taken [13]. The frontal and temporal opercula were retracted and the carotid cistern was dissected. The temporal pole was untethered by dividing the vein to the sphenoparietal sinus and cutting arachnoid adhesions to the middle fossa. Next, the temporal lobe was retracted posteriorly and laterally to expose the interpeduncular cistern through the carotid-oculomotor triangle. The precommunicating segment of the posterior cerebral artery (P1) was followed proximally to the basilar apex with extreme care to preserve the thalamoperforators. At this point, the Foley catheter was inserted and inflated 3 mL to create room for implantation and left under pressure overnight. Finally, the basilar apex aneurysm model was implanted (Figures 3(a), 3(c), and 3(e)). A contralateral OZ was performed to simulate the surgical clipping of the basilar apex model (Figures 3(b), 3(d), and 3(f)). One permanent clip was used during the clipping simulation experiment to obliterate the aneurysm in the basilar apex model.

The 3D aneurysm models were successfully implanted to the specimen arterial circulation in all cases. The flexibility of the neck and branches of the aneurysm model allowed successful clipping and manipulation similar to those of a partially thrombosed aneurysm. The dome was also stiff enough to produce mass effect to the surrounding structures and preserve the original size and shape.

Four surgical approaches were successfully performed in each specimen (Table 1). The implanted aneurysm model maintained the original position consistently in all simulations. A navigation probe was successfully passed through the recreated surgical exposure, proving that morphometric comparative studies applied to neurosurgical simulation are possible using a real aneurysm model.

3.1. Model Applications in Cerebrovascular Surgical Simulation. This method provided three main advantages for cerebrovascular surgical training. (1) The aneurysm implantation technique required meticulous dissection of disease-free anatomy, which provided the prospect of learning the surgical anatomy of the implant zone before being distorted by the aneurysm model. (2) The mass effect created by the Foley catheter and the introduction of the aneurysm model into the normal vasculature offered a unique opportunity to understand the patients' neurological disease state caused by tissue compression and identify the critical structures beyond the aneurysm dome that must be preserved during aneurysm dissection including vital arterial perforators. (3) An aneurysm replica implanted into a human cadaver prepared for bleeding simulation provided an optimal surgical

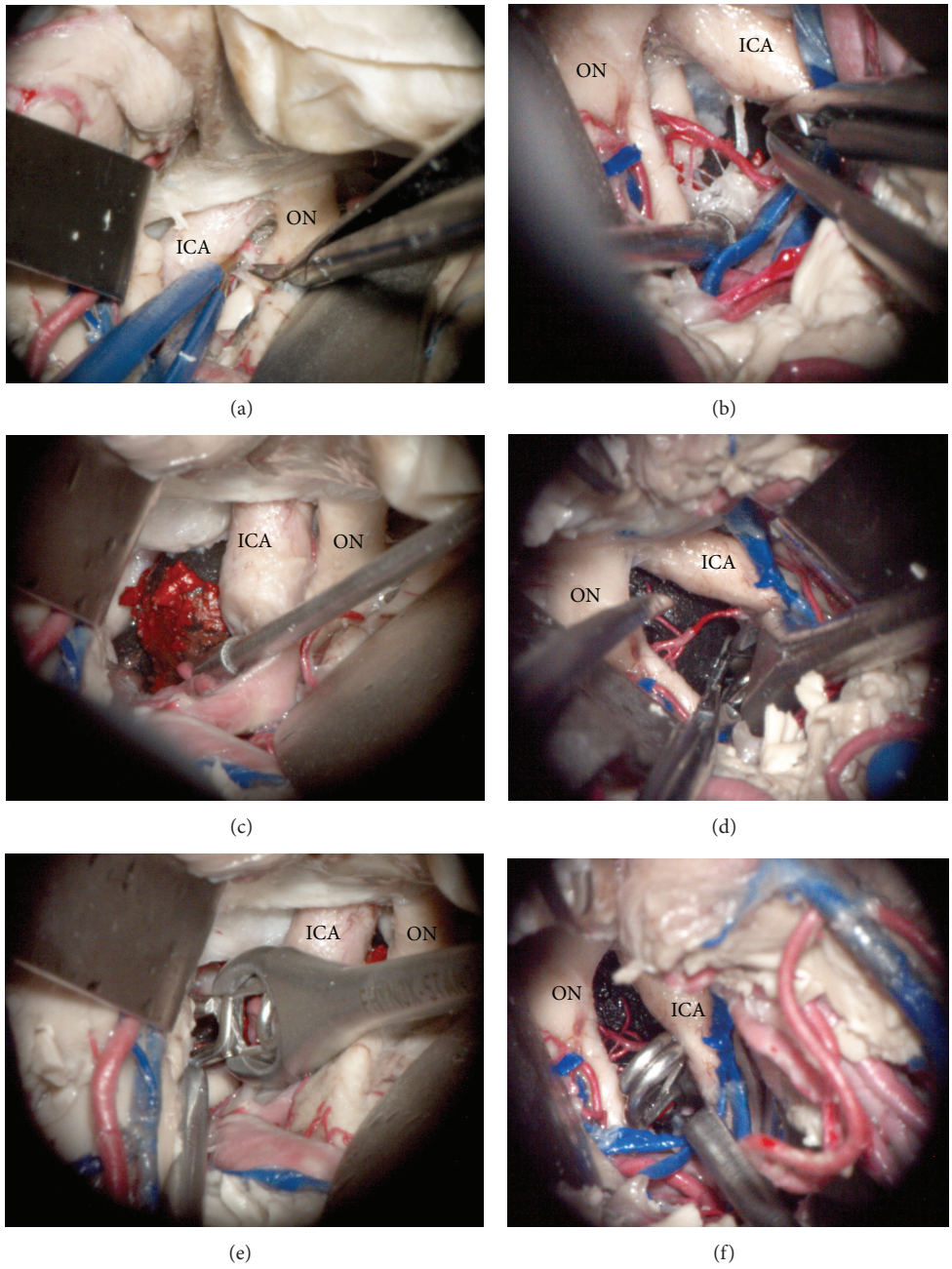

Figure 3: Microscopic photography of left (a, c, and e) and right (b, d, and f) surgical simulation experiments for implanting and clipping a basilar tip aneurysm. After a wide sylvian fissure split, the left carotid cistern was dissected to access the interpeduncular fossa (a). The 3D aneurysm model was successfully implanted through the oculomotor triangle and positioned to match the target anatomy, basilar apex (c). Next, an angled aneurysm clip was introduced and positioned across the aneurysm neck in the basilar apex (e). Then, the right transsylvian approach was performed with the aneurysm model already implanted. The arachnoid dissection and perforator arteries manipulation were affected by the aneurysm mass effect (b). The dome of the previously implanted aneurysm was mobilized to identify the aneurysm neck (d) and an angled clip was applied to the basilar apex aneurysm neck (f). ICA: internal carotid artery, ON: optic nerve.

simulation scenario to learn and train dissection techniques and maneuvers to safely clip and bypass real aneurysms.

The permanent implantation of an exact replica of a patient aneurysm provided unlimited time to conduct research; cadaver features remained constant throughout the experiments. Four surgical approaches were successfully performed in each specimen. The implanted aneurysm model maintained the original position consistently in all simulations. A navigation probe was successfully passed through the recreated surgical exposure and to the implanted aneurysm, demonstrating that future morphometric comparative studies could be carried out using a real aneurysm model.

4. Discussion

The development of the neuroendovascular field has brought new perspectives to vascular neurosurgery. On one hand, endovascular procedures are becoming safer and more applicable to many types of aneurysms [14], increasing the rate of aneurysms treated with this method [1]. On the other hand, in many centers, the cases that are considered for surgery are the most complex ones, whose endovascular treatments have failed or are unsuitable [1, 15]. Because the number of aneurysms considered for surgery is decreasing and becoming limited to the most complex ones, the degree of expertise required for its treatment is becoming harder to achieve. In fact, the current caseload has been reportedly limited even for simple cerebral aneurysms [16]. This volume-outcome effect has been reinforced by larger regional and national databases [17]. Due to this, new methods have to be considered for effective microsurgical training and simulation to prepare future generations for surgical aneurysm clipping [18].

This work presents a novel and promising anatomical model for the study and training of brain aneurysm surgery. In this model, the neck and branches of the aneurysms showed flexibility similar to that of the living human. The rigidity of the aneurysm dome was optimal to simulate compression to the surrounding brain structures. Although tested in only four specimens, the 3D aneurysm model presented here proves feasible for implantation in the embalmed cadaver and optimally emulates the features of an aneurysm.

Other 3D aneurysm models have been previously reported. D'Urso et al. (1999) created biomodels of cerebrovascular lesions and stressed their use for complex case preparation or when radiological data is unsatisfactory [19]. Similarly, Wurm et al. (2004) reported the utility of solid plastic 3D models to better understand the anatomy of aneurysms, further illustrating the superiority of 3D models to other imaging methods [20]. In 2009, Kimura et al. used a 3D aneurysm model effectively for preoperative simulation and surgical training [18]. The model by Kimura et al. successfully allowed the practice of clipping due to its softness and elastic features, exceeding other previous 3D models in that it allowed for surgical training. In some cases, they also developed a hard 3D model for representing the skull base and the rest of the vasculature [18]. Similar results were subsequently reported with a 3D model proposed by Mashiko et al. (2011) [21]. Like the previous models, the ability to estimate the clip(s) position, size, and shape preoperatively when using our model allows one to avoid the occlusion of parent vessels and to predict the best combination of clips to obliterate the aneurysm. However, when the 3D model is implanted in a cadaveric head, there are more anatomic-related aspects that can be identified and analyzed (e.g., angle of attack, clip fenestration, and limited exposure). Thus, we have gone a step further in the recreation of an aneurysm operative environment in that the previous aneurysm models were not implanted in a naturalistic environment.

Although 3D radiological reconstructions have notably improved the display of brain aneurysms and have provided an important tool for neurosurgeons, there are certain cases where this information might be insufficient to properly conceive certain features of an aneurysm such as intraluminal thrombus. Furthermore, the 3D reconstruction does not identify the relationships between the surrounding brain structures and the aneurysm, which are essential in vascular surgery. In the most complex cases, the creation of a 3D 1:1 replica of the patient's aneurysm and its subsequent implantation in a cadaveric specimen may assist the surgeon in determining how to attack the aneurysm by selecting the best positioning and approach. Bearing this in mind, standard craniotomies may be modified to achieve better visualization and control of the lesion and to avoid potential damages to other brain structures secondary to manipulation. As previously stated, using this sort of 3D model allows one to predict the type and number of clips as well as the way they should be applied for best results [18]. In fact, the neurosurgeon can recreate the surgical procedure in the laboratory and modify his/her previous strategy (originally based on radiological reconstructions) as he/she realizes that certain modifications can improve the feasibility of the surgical procedure and, eventually, the final outcome of the patient. Therefore, the model proposed in this report allows for a thorough study and optimal design of a particular case, which could be considered a form of personalized surgical therapy. Although the most important limitation of this procedure is that the bony anatomy in the cadaver would not be specific to the patient who needs treatment, this model provides the most realistic method to test the different surgical options and weigh their differential benefits and risks for a particular type of aneurysm. In other words, the 3D aneurysm model implanted in a cadaveric specimen would prepare the neurosurgeon to the "surgical battle," choosing the best strategy to defeat a specific and carefully assessed enemy with the least collateral damages.

The impact that this cadaveric simulation model may have in the training of resident neurosurgeons and inexperienced neurosurgeons should also be taken into consideration. As previously stated, endovascular success is leading to limited exposure to aneurysm surgery during residency training [22]. In centers with large experience and comprehensive cerebrovascular teams, this situation exposes residents to challenging cases early in their training, without adequate experience in the simplest cases. However, in centers without a strong cerebrovascular caseload, residents may not be confronted with enough cases to achieve self-confidence and skills in the management of aneurysms to safely transit them to unsupervised practice. Several studies have demonstrated a negative correlation between operative outcomes and the experience of a surgeon [23–25]. Therefore, there is a greater need for developing measures that ensure training is tailored to maintain proficiency in cerebral aneurysm surgery [22].

3D virtual reality environments have been created as a tool for neurosurgical trainees to learn surgical approaches to vascular lesions [26]. Although the advances in virtual reality computerized models and neuronavigation have been presented as potential contributors to training surgical skills [27], it is widely agreed that human cadaveric models are anatomically the most realistic ones [28].

With this in mind, the application of the 3D aneurysm implantation model presented here may help overcome

decreased clinical exposure to simple aneurysm cases by including hands-on training in the most frequently surgically treated aneurysms. All the previous 3D aneurysm models reported have emphasized the potential utility of this biomodels for trainees [18–20, 29]. This educational feature has also been considered in the present work; as explained above, a 3D model for training purposes was created (see Section 2) and suitably implanted in a cadaveric specimen. Advanced residents and novel neurosurgeons could take advantage of this model and revise the approaches to the most frequent aneurysms stepwise in a more realistic environment. The repeated exposure and participation in operative procedures are considered essential in a surgical training program [30]. Training with cadaveric-implanted 3D models could lead to increased competence required to provide safe and efficient treatment to the most urgent and complex cases. In addition, this model might also be useful in objectively evaluating the acquisition of core competence and skills in cerebrovascular surgery.

Although the utility of 3D models may be accepted as useful tool for surgical planning and training, it should not be considered as a substitute of the active participation in real neurovascular surgeries. These models should be considered as tools for developing microsurgical abilities that can be later applied to real patients under supervision of an experienced surgeon. The use of these new educational tools, one day, may not only compensate for decreased microsurgical experience, but also improve neurovascular surgery clinical outcomes.

The models used in the present study were rigid and compact to represent both partially thrombosed aneurysms and the mass effect against the surrounding anatomy. However, the current printing technology allows for hollow-type vessel printing, which our team had successfully printed in the past. One of the benefits of 3D-printed aneurysms for teaching and training institutions is that they can be used multiple times and implanted in different locations with similar target vessel diameter, posterior inferior cerebellar artery and anterior inferior cerebellar artery.

Another potential application of the presented model is surgical research. 3D radiological models were developed to simulate the intra-aneurismal hemodynamic, which is associated with aneurysmal growth and whose appropriate evaluation is critical for endovascular procedures [31–34]. However, when surgery is the selected treatment, it is common to confront cases where the surgical approach is controversial (e.g., basilar tip aneurysms) or is not as standardized as others. Assessing the different approaches for controversial microsurgical management of complex aneurysms (aneurysms without a sole optimal approach) can provide scientific solutions to surgical dilemma. We are currently using this model to assess the available surgical approaches to several complex and controversial aneurysm cases by means of morphometric analysis (surgical freedom, surgical corridor, surgical exposure, and angles of attack) and comparative anatomical evaluation. This method represents an improvement in the field of neurosurgical research as it allows measurements and exposures to be made on an actual aneurysm (surgical target) in an aneurysm-related spatial distortion rather than in a random anatomical point.

Considering that this method adds to the cost of the conventional cadaveric training, it is essential to select appropriate cases for performing such 3D model implantations and eventually recreating the surgical conditions. Most simple 3D aneurysm models may be useful for residents training, and standard models can be generated to this purpose, which could lead to industrial production and lowering costs. Nevertheless, complex cases that typically have specific aneurysm features must be carefully selected. In this regard, large/giant size aneurysms are proven to be largely associated with the outcome and surgical difficulty [1]. Moreover, the location (being posterior circulation aneurysms of high complexity), previous coiling, and complex patterns of perforators might be other features that increase the complexity when surgically clipping an aneurysm. In all cases that present one or more of these complexities, the model presented in this report may be helpful for getting the best surgical result.

4.1. Study Limitations. At present, 3D printers are limited to models larger than 1 mm if plastic compounds are chosen. Therefore, patients with very small aneurysms cannot be reproduced using our model. The reproduction of the exact features of an aneurysm from a particular patient can be challenging and limited by the current resolution of the radiological studies. Perforator branches taking off from the aneurysm dome and/or its vicinity are not typically identifiable in an MRI. Thus, inability to reconstruct real aneurysm perforators is of technological nature and therefore an absolute limitation of the present. However, the constant resolution optimization in medical technology could potentially make perforators visible in routine patient neuroimaging and overcome this limitation. Therefore, legitimate reconstruction of aneurysm perforators is a future possibility. In the meantime, an approximation to realistic aneurysm perforator reconstruction could be based on postoperative photographic review and deliberate generation and rendering of the perforators in the model creation process.

Using postmortem models has inherent limitations. In this model, evaluation of both successful aneurysm clipping and preservation of surrounding perforators is limited to visual inspection. One of the obvious limitations of the present model is the lack of clinical deficits from perforator entrapment or sustained retraction. However, we see this limitation as one of the benefits of our model, which can serve as a harmless battleground for cerebrovascular innovation through practice. In the same way, cerebral "relaxation" with the use of intravenous mannitol and other strategies used in anesthesia to ease surgical maneuverability are not possible to recreate. However, we see this limitation as another benefit of our model as it forces new surgical strategies to be tested in a surgical scenario much more limited than the real procedure in patients. The reader should note that a customized embalming formula for neurosurgical simulation was used [3]. The specimens embalmed with our method provided significantly better retraction profiles than those treated with classic embalming solutions. Successful aneurysm implantation, especially of giant aneurysms, is highly dependent on brain manipulation. We routinely use the customized

embalming solution for neurosurgical simulation and have not tried our 3D aneurysm implantation model in specimens embalmed with other solutions.

5. Conclusion

Cerebrovascular surgery is a demanding specialty that requires the acquisition of certain microsurgical skills for successfully clipping aneurysms. Shifting surgical trends brings to cerebrovascular surgery increasingly complex cases, which may require treatment by less experienced neurosurgeons. Our 3D aneurysm model represents a good surgical model for studying relative cerebrovascular anatomy, for confirming the aneurysm's relationship with other brain structures, and for identifying which surgical approaches are the most suitable for confronting certain aneurysm.

This model provides a substantial improvement in cerebrovascular surgical simulation. The application of this model in cerebrovascular research could provide an unparalleled opportunity to design better surgical options for patient-specific aneurysms in cadavers. This method allows surgical exposure similar to that in the real surgical procedure, replicating the constraints of particular surgical corridors in the setting of clip application and the relative surgical freedom to apply aneurysm clips between specific surgical corridors (on a cadaver) to certain patient-specific aneurysms.

It may serve as an indispensable tool for selecting the most suitable surgical approach in complex cases. The contribution of these models in operative training and neurosurgical research are now as important now as ever, given the continuous decline in case volume in complex cerebrovascular surgical cases available for resident training.

Conflict of Interests

The authors have no conflict of interests related to the methods or devices used in the present study.

Acknowledgments

The authors wish to thank Mr. Karl McElroy for his dedicated work in optimizing the cadaveric preparation for this study. Also, they want to express their gratitude to those who will their bodies to the advance of research.

References

[1] N. Sanai, N. Caldwell, D. J. Englot, and M. T. Lawton, "Advanced technical skills are required for microsurgical clipping of posterior communicating artery aneurysms in the endovascular era," *Neurosurgery*, vol. 71, no. 2, pp. 285–294, 2012.

[2] M. T. Lawton and R. Du, "Effect of the neurosurgeon's surgical experience on outcomes from intraoperative aneurysmal rupture," *Neurosurgery*, vol. 57, no. 1, pp. 9–15, 2005.

[3] A. Benet, J. Rincon-Torroella, M. T. Lawton, and J. J. G. Sánchez, "Novel embalming solution for neurosurgical simulation in cadavers: laboratory investigation," *Journal of Neurosurgery*, vol. 120, no. 5, pp. 1229–1237, 2014.

[4] M. G. Abdelwahab, D. D. Cavalcanti, and M. C. Preul, "Role of computer technology in neurosurgery," *Minerva Chirurgica*, vol. 65, no. 4, pp. 409–428, 2010.

[5] J. C. Fernandez-Miranda, J. Barges-Coll, D. M. Prevedello et al., "Animal model for endoscopic neurosurgical training: technical note," *Minimally Invasive Neurosurgery*, vol. 53, no. 5-6, pp. 286–289, 2010.

[6] J. Olabe, J. Olabe, and V. Sancho, "Human cadaver brain infusion model for neurosurgical training," *Surgical Neurology*, vol. 72, no. 6, pp. 700–702, 2009.

[7] E. Aboud, O. Al-Mefty, and M. G. Yaşargil, "New laboratory model for neurosurgical training that simulates live surgery," *Journal of Neurosurgery*, vol. 97, no. 6, pp. 1367–1372, 2002.

[8] T. Menovsky, "A human skull cast model for training of intracranial microneurosurgical skills," *Microsurgery*, vol. 20, no. 7, pp. 311–313, 2000.

[9] P. A. Yushkevich, J. Piven, H. C. Hazlett et al., "User-guided 3D active contour segmentation of anatomical structures: significantly improved efficiency and reliability," *NeuroImage*, vol. 31, no. 3, pp. 1116–1128, 2006.

[10] M. T. Lawton, "Basilar apex aneurysms: surgical results and perspectives from an initial experience," *Neurosurgery*, vol. 50, no. 1, pp. 1–8, 2002.

[11] N. Sanai, P. Tarapore, A. C. Lee, and M. T. Lawton, "The current role of microsurgery for posterior circulation aneurysms: a selective approach in the endovascular era," *Neurosurgery*, vol. 62, no. 6, pp. 1236–1249, 2008.

[12] M. B. Potts, E. F. Chang, W. L. Young, and M. T. Lawton, "Transsylvian-transinsular approaches to the insula and basal ganglia: operative techniques and results with vascular lesions," *Neurosurgery*, vol. 70, no. 4, pp. 824–834, 2012.

[13] F. P. K. Hsu, R. E. Clatterbuck, and R. F. Spetzler, "Orbitozygomatic approach to basilar apex aneurysms," *Neurosurgery*, vol. 56, no. 1, pp. 172–176, 2005.

[14] R. B. Scott, F. Eccles, A. J. Molyneux, R. S. C. Kerr, P. M. Rothwell, and K. Carpenter, "Improved cognitive outcomes with endovascular coiling of ruptured intracranial aneurysms: neuropsychological outcomes from the International Subarachnoid Aneurysm Trial (ISAT)," *Stroke*, vol. 41, no. 8, pp. 1743–1747, 2010.

[15] K. A. Choudhari, M. S. Ramachandran, M. O. McCarron, and C. Kaliaperumal, "Aneurysms unsuitable for endovascular intervention: surgical outcome and management challenges over a 5-year period following International Subarachnoid Haemorrhage Trial (ISAT)," *Clinical Neurology and Neurosurgery*, vol. 109, no. 10, pp. 868–875, 2007.

[16] M. K. Morgan, N. N. Assaad, and A. S. Davidson, "How does the participation of a resident surgeon in procedures for small intracranial aneurysms impact patient outcome?" *Journal of Neurosurgery*, vol. 106, no. 6, pp. 961–964, 2007.

[17] J. A. Cowan Jr., J. B. Dimick, R. M. Wainess, G. R. Upchurch Jr., and B. G. Thompson, "Outcomes after cerebral aneurysm clip occlusion in the United States: the need for evidence-based hospital referral," *Journal of Neurosurgery*, vol. 99, no. 6, pp. 947–952, 2003.

[18] T. Kimura, A. Morita, K. Nishimura et al., "Simulation of and training for cerebral aneurysm clipping with 3-dimensional models," *Neurosurgery*, vol. 65, no. 4, pp. 719–725, 2009.

[19] P. S. D'Urso, R. G. Thompson, R. L. Atkinson et al., "Cerebrovascular biomodelling: a technical note," *Surgical Neurology*, vol. 52, no. 5, pp. 490–500, 1999.

[20] G. Wurm, B. Tomancok, P. Pogady, K. Holl, and J. Trenkler, "Cerebrovascular stereolithographic biomodeling for aneurysm

surgery: technical note," *Journal of Neurosurgery*, vol. 100, no. 1, pp. 139–145, 2004.

[21] T. Mashiko, K. Otani, R. Kawano et al., "Development of three-dimensional hollow elastic model for cerebral aneurysm clipping simulation enabling rapid and low cost prototyping," *World Neurosurgery*, vol. 83, no. 3, pp. 351–361, 2015.

[22] R. R. Vindlacheruvu, J. E. Dervin, and P. J. Kane, "The impact of interventional neuroradiology on neurosurgical training," *Annals of the Royal College of Surgeons of England*, vol. 85, no. 1, pp. 3–9, 2003.

[23] D. D. Cochrane and J. R. W. Kestle, "The influence of surgical operative experience on the duration of first ventriculoperitoneal shunt function and infection," *Pediatric Neurosurgery*, vol. 38, no. 6, pp. 295–301, 2003.

[24] A. Dardik, G. P. Burleyson, H. Bowman et al., "Surgical repair of ruptured abdominal aortic aneurysms in the state of Maryland: factors influencing outcome among 527 recent cases," *Journal of Vascular Surgery*, vol. 28, no. 3, pp. 413–421, 1998.

[25] J. W. Hammond, W. S. Queale, T. K. Kim, and E. G. McFarland, "Surgeon experience and clinical and economic outcomes for shoulder arthroplasty," *The Journal of Bone & Joint Surgery—American Volume*, vol. 85, no. 12, pp. 2318–2324, 2003.

[26] N. Agarwal, P. J. Schmitt, V. Sukul, and C. J. Prestigiacomo, "Surgical approaches to complex vascular lesions: the use of virtual reality and stereoscopic analysis as a tool for resident and student education," *BMJ Case Reports*, vol. 2012, 2012.

[27] P. Marinho, L. Thines, L. Verscheure, S. Mordon, J.-P. Lejeune, and M. Vermandel, "Recent advances in cerebrovascular simulation and neuronavigation for the optimization of intracranial aneurysm clipping," *Computer Aided Surgery*, vol. 17, no. 2, pp. 47–55, 2012.

[28] J. Olabe, J. Olabe, J. M. Roda, and V. Sancho, "Human cadaver brain infusion skull model for neurosurgical training," *Surgical Neurology International*, vol. 2, article 54, 2011.

[29] G. Wurm, M. Lehner, B. Tomancok, R. Kleiser, and K. Nussbaumer, "Cerebrovascular biomodeling for aneurysm surgery: simulation-based training by means of rapid prototyping technologies," *Surgical Innovation*, vol. 18, no. 3, pp. 294–306, 2011.

[30] S. I. Woodrow, M. Bernstein, and M. C. Wallace, "Safety of intracranial aneurysm surgery performed in a postgraduate training program: implications for training," *Journal of Neurosurgery*, vol. 102, no. 4, pp. 616–621, 2005.

[31] J. Mikhal, D. J. Kroon, C. H. Slump, and B. J. Geurts, "Flow prediction in cerebral aneurysms based on geometry reconstruction from 3D rotational angiography," *International Journal for Numerical Methods in Biomedical Engineering*, vol. 29, no. 7, pp. 777–805, 2013.

[32] J. J. Schneiders, H. A. Marquering, L. Antiga, R. van den Berg, E. VanBavel, and C. B. Majoie, "Intracranial aneurysm neck size overestimation with 3D rotational angiography: the impact on intra-aneurysmal hemodynamics simulated with computational fluid dynamics," *The American Journal of Neuroradiology*, vol. 34, no. 1, pp. 121–128, 2013.

[33] P. van Ooij, J. J. Schneiders, H. A. Marquering, C. B. Majoie, E. van Bavel, and A. J. Nederveen, "3D cine phase-contrast MRI at 3T in intracranial aneurysms compared with patient-specific computational fluid dynamics," *The American Journal of Neuroradiology*, vol. 34, no. 9, pp. 1785–1791, 2013.

[34] S.-I. Sugiyama, H. Meng, K. Funamoto et al., "Hemodynamic analysis of growing intracranial aneurysms arising from a posterior inferior cerebellar artery," *World Neurosurgery*, vol. 78, no. 5, pp. 462–468, 2012.

Hindawi Publishing Corporation
BioMed Research International
Volume 2015, Article ID 490209, 10 pages
http://dx.doi.org/10.1155/2015/490209

Research Article

Arctigenin, a Potent Ingredient of *Arctium lappa* L., Induces Endothelial Nitric Oxide Synthase and Attenuates Subarachnoid Hemorrhage-Induced Vasospasm through PI3K/Akt Pathway in a Rat Model

Chih-Zen Chang,[1,2,3] Shu-Chuan Wu,[2] Chia-Mao Chang,[2,4] Chih-Lung Lin,[1,2] and Aij-Lie Kwan[1,2]

[1]*Department of Surgery, Faculty of Medicine, School of Medicine, Kaohsiung Medical University, Kaohsiung 807, Taiwan*
[2]*Division of Neurosurgery, Department of Surgery, Kaohsiung Medical University Hospital, Kaohsiung 807, Taiwan*
[3]*Department of Surgery, Kaohsiung Municipal Ta Tung Hospital, Kaohsiung, Taiwan*
[4]*Department of Surgery, Kaohsiung Municipal Hsiao Kang Hospital, Kaohsiung, Taiwan*

Correspondence should be addressed to Chih-Zen Chang; changchihzen2002@yahoo.com.tw

Received 1 May 2015; Accepted 27 May 2015

Academic Editor: Aaron S. Dumont

Upregulation of protein kinase B (PKB, also known as Akt) is observed within the cerebral arteries of subarachnoid hemorrhage (SAH) animals. This study is of interest to examine Arctigenin, a potent antioxidant, on endothelial nitric oxide synthase (eNOS) and Akt pathways in a SAH in vitro study. Basilar arteries (BAs) were obtained to examine phosphatidylinositol-3-kinase (PI3K), phospho-PI3K, Akt, phospho-Akt (Western blot) and morphological examination. Endothelins (ETs) and eNOS evaluation (Western blot and immunostaining) were also determined. Arctigenin treatment significantly alleviates disrupted endothelial cells and tortured internal elastic layer observed in the SAH groups ($p < 0.01$). The reduced eNOS protein and phospho-Akt expression in the SAH groups were relieved by the treatment of Arctigenin ($p < 0.01$). This result confirmed that Arctigenin might exert dural effects in preventing SAH-induced vasospasm through upregulating eNOS expression via the PI3K/Akt signaling pathway and attenuate endothelins after SAH. Arctigenin shows therapeutic promise in the treatment of cerebral vasospasm following SAH.

1. Introduction

Delayed ischemic neurological deficit and acute cerebral ischemia subordinate to subarachnoid hemorrhage (SAH) have become a serious and fatal subcategory of stroke in patients following a ruptured aneurysm [1–4]. Connolly et al. stated the mortality rate in SAH patients ranged from 27% to 44%, and almost half of SAH patients survive with serious sequel of cognitive and functional impairment [5, 6]. Despite more than a half century of studies trying to correct and prevent vasospasm, so far there is no definitive treatment to reverse this devastating condition [7–10].

A mounting body of both direct and indirect evidence shows that spasmogens or ligands are critical in the development and maintenance of cerebral vasospasm [11–15]. Basic and cellular studies also imply two major hypotheses on cerebral vasospasm: one focuses on the synergic roles of nitric oxide (NO), nitric oxide synthase (NOs) [16–21], and endothelin-1 (ET-1) [11, 20, 22–25] and the other on intracellular signal transduction [26–30]. The putative importance of NO/ET and mitogen-activation protein kinase has not been fully emphasized; even its role in the genesis of cerebral vasospasm has been unclear. Owing to lack of effective therapies to halt this condition in SAH patients, continuous studies have focused on the pathogenesis of SAH.

Nitric oxide (NO), an effective endogenous vasodilator, is essential to vascular homeostasis and angiogenesis [31, 32]. Endothelial NO synthase is phosphorylated by various stimulations including activation of phosphatidylinositol 3-kinase (PI3K)/protein kinase B (Akt) pathway in endothelial cells [16]. Likewise, endothelin-1 (ET-1), known as a potent vasoconstrictor and promitogen, is implicated in the pathogenesis of various cardiovascular, renal, pulmonary, and central nervous system disorders [33–37]. Through coupling with ETA, a G protein receptor, ET-1, mediates vasoconstriction, whereas with ETB, it exerts a vasodilatation effect through the release of nitric oxide (NO) and prostacyclin [38]. Recent studies suggest that ET-1 stimulates the proliferation of vascular smooth muscle cells and adjudicates the interactions between leukocytes and cerebrovascular endothelium [10]. Through binding to distinct receptors, ET-1 is believed to play a critic role on mediating a variety of vascular diseases.

Arctigenin, an extract from *Arctium lappa* L., has been reported to have a variety of pharmacological activities including antioxidant, anti-inflammatory, antiproliferative, and antiviral activity [34, 39–42]. It has been shown potent in vitro anti-influenza A virus and neuroprotective against Japanese encephalitis in a mouse model [43]. In a rodent study of transient middle cerebral artery occlusion, Arctigenin was demonstrated to be neuroprotective by suppressing microglia activation and decreasing IL-1β and TNF-α expression as well as ameliorating memory impairment in Alzheimer's disease in vitro study [44, 45].

Taking these findings together, it is reasonable to hypothesize that Arctigenin is able to reverse basilar artery spasm through activating phospho-Akt and subsequent increased eNOS expression. We used two-hemorrhage SAH model, measured the diameter of basilar artery, and examined the expression of ET-1, eNOS, and phospho-Akt in the basilar artery following SAH.

2. Methods

2.1. Materials. Arctigenin, $C_{21}H_{24}O_6$, an extract from *A. lappa* plant, was bought from Excel Biomedical Inc., Neihu Dist, Taipei 114, Taiwan, authorized by Cayman Chemical. Polyclonal anti-rat Anti-PI3K antibody (PI3K (P85) antibody), anti-phospho-PI3K antibody (phospho-PI3K (P85) (Tyr458)/(p55) (Tyr199) antibody), anti-Akt antibody (Akt antibody), and anti-phospho-Akt antibody (phospho-Akt (Ser473)) were obtained from Cell Signaling Technology (Beverly, MA 01915, USA). Horseradish peroxidase-conjugated (HRP) goat anti-rabbit IgG was purchased from R&D Systems, Inc. (Minneapolis, MN 55413, USA). CNM protein extraction kits were from Biochain (Hayward, CA 94545, USA). Arctigenin in a minipump was prepared by Ms. Wu SC (Kaohsiung Medical University Hospital, Kaohsiung 807, Taiwan, ROC), and 0.9% saline was used as a vehicle.

2.2. Induction of Experimental SAH. Fifty-four male Sprague-Dawley rats, weighing between 340 and 440 g (NLAC, Education Research Resource, National Laboratory Animal Center, Taiwan), were used in this study. All the experimental protocols were authorized and superintended by the University of Kaohsiung Medicine Animal Research Committee and were compliant with the Declaration of Helsinki (1964). A modified double hemorrhage SAH model was employed [46]. The rats received anesthesia by an intraperitoneal injection of 7 mg/kg Zoletil 50 (VIRBAC, L.I.D., Carros 06516, France). 0.1 mL/100 gm fresh arterial blood was withdrawn from tail artery and injected into the cisterna magna using a stereotactic apparatus (Stoelting, Wood Dale, IL 60191, USA). After the induction, animals were placed in ventral recumbent position for 30 min. to let ventral blood clot formation. After monitoring for respiratory distress and giving mechanical ventilation if necessary, the animals were returned to the vivarium until becoming fully awake. A habitat with a 12 h light-dark cycle and access to food and water ad lib was offered. To perform the induction of 2nd SAH, the animals received repeated injection of SAH at 48 h after 1st SAH to maintain the tendency of delayed vasoconstriction. Thereafter, the animals received perfusion-fixation 72 h after 2nd SAH.

2.3. General Design of Experiments and Treatment Groups. The animals were randomly assigned into the following subgroups (9 rats/group): (1) sham operated (no SAH), (2) SAH only, (3) SAH-plus vehicle, SAH rats receiving Arctigenin treatment (4) 50 μM/kg/day, (5) 150 μM/kg/day, and (6) 450 μM/kg/day. The dosage was adjusted according to the study of a rabbit arterial ring test. The first injection was given at 1 hr after induction of SAH by using an osmotic minpump (Alzet corp, Palo Alto, CA 94301, USA) intraperitoneally. The animals were sacrificed by perfusion-fixation 72 h after SAH. Cortical tissue samples were obtained by means of placing a 20-gauge needle inserted 5 mm in depth into the skull bone through a burr hole craniectomy at a 24 h interval.

2.4. Perfusion-Fixation. By the end of the study, the animals were reanesthetized by administration of Zoletil 50 (7 mg/kg). The femoral artery was catheterized to monitor blood pressure and obtain blood to determine arterial blood gas, Na^+, K^+, GOT, and GPT levels. Perfusion-fixation was performed as opening the thorax, and the left ventricle was canalled with a NO18 catheter by clamping the descending aorta and opening the right atrium simultaneously. 100 mL 0.01 M phosphate buffer (pH 7.4) was perfused followed by fixation with 100 mL 2% paraformaldehyde in the PBS solution at 36°C under a pressure of 80 mm Hg. The harvested brain was immersed in a fixative at 4°C overnight. Visual inspection made sure that formed clots overlay the basilar artery (BA) in all SAH animals.

2.5. Measurement of Basilar Artery (BA) Cross-Sectional Area. Five selected cross-sections from the BA of each animal were randomly analyzed by an examiner blinded to the treatment groups. The tissues were frozen instantly and cut into 25 μm-thick sections (Reichert-Jung Ultracut E ultramicrotome). They were then stained with hematoxylin and eosin for video-assisted microscopy and the analysis of BA cross-sectional area.

Table 1: Physiological parameters among the experimental groups.

Group	Parameter					
	Body weight (gm)	Systolic Blood pressure	GOT/GPT (IU/L)	BUN/Cr (mg/dL)	pH	Temperature (°C)
Sham	374 ± 24	104 ± 12	9.2 ± 3.1/7.1 ± 2.8	4.0 ± 2.3/0.23 ± 0.14	7.36 ± 0.04	36.5 ± 0.33
SAH	360 ± 31	111 ± 8	10.2 ± 4.0/11.2 ± 3.0	9.4 ± 1.3/0.55 ± 0.14	7.37 ± 0.10	36.1 ± 0.41
SAH + Vehicle	359 ± 46	102 ± 12	12.4 ± 4.0/10.6 ± 3.8	10.2 ± 3.5/0.48 ± 0.16	7.38 ± 0.15	36.6 ± 0.42
SAH + Arctigenin						
50 μM/kg/day	366 ± 49	108 ± 13	10.8 ± 4.2/13.4 ± 4.8	10.4 ± 4.3/0.88 ± 0.35	7.36 ± 0.14	36.8 ± 0.32
150 μM/kg/day	368 ± 36	100 ± 12	12.6 ± 3.8/7.8 ± 4.2	11.6 ± 4.1/1.3 ± 0.38	7.36 ± 0.41	36.6 ± 0.51
450 μM/kg/day	370 ± 42	94 ± 34	13.5 ± 2.6/7.8 ± 3.8	12.4 ± 2.6/0.86 ± 0.43	7.38 ± 0.13	36.7 ± 0.13

Results are expressed as the mean ± SEM, $n = 9$; $p < 0.01$ versus SAH condition by one-way analysis of variance (ANOVA) analyses followed by Mann-Whitney U-test.

2.6. Hemodynamic Measurements. Heart rate, blood pressure, and rectal temperature were monitored in the animals before and after Arctigenin administration at intervals of 12 h after the induction of SAH by using a tail-cuff method (SC1000 Single Channel System, Hatteras Instruments, NC 27518, USA) and a rectal thermometer (BIO-BRET-2-ISO. FL 33780, USA).

2.7. Immunostaining of Basilar Artery (BA) with NOS Antibody. Video-assisted microscope (×400) was used to identify NOS within endothelial cells. Concisely, isolated rat basilar arteries were perfused and fixed with 4% paraformaldehyde. Coronal sections of the basilar arteries were stored overnight on slides at −80°C in accordance with the supplier's instructions. Rabbit polyclonal anti-rat NOS antibody (Alpha Diagnostic Intl. Inc., San Antonio, TX 78244, USA) was used at a dilation of 1 : 40, and immunostaining was performed for 40 min at 25°C followed by drying overnight as described in the supplier's instruction. Five successive sections of each specimen were photographed, and the lumen cross-sectional area was measured for morphometric analysis.

2.8. Determination of ET-1. On the three days subsequent to first induction of hemorrhage, the ET-1 levels in CSF were determined by a commercially available ELISA kit (Immuno-Biological Lab. Co., Ltd., Gunma 375-0005, Japan). The upper limit of quantification was 2000 pg/mL for ET-1 as indicated in the supplier's instruction.

2.9. Determination of Nitric Oxide Synthase (NOS). The NOS bioactivity of isolated basilar arteries was detected by quantifying the alteration of L-arginine to L-citrulline. A commercially available kit (Bioxytech NOS Assay Kit, Oxis International, CA 90210, USA) was obtained to examine NOS. Briefly, protein extracted from vessels was incubated with radiolabeled L-arginine in the presence or in the absence of 1 mmol/L NOS inhibitor NG-nitro-L-arginine methyl ester. The response was ended by adding of 50 mmol/L HEPES buffer containing 5 mmol/L EDTA. Radiolabeled L-citrulline was counted after the removal of excess L-arginine with equilibrated resin and centrifugation at 10,000 rpm.

2.10. Immunoblotting for PI3K, Phospho-PI3K (P85), Akt, and Phospho-Akt. Basilar artery samples (six animals/each group) were homogenized in M-PER Mammalian Protein Extraction Reagent (Pierce, Rockford, IL 61101, USA) mixed with protease inhibitor (Complete Mini; Roche, Mannheim 14080, Germany) and then centrifuged at 15,000 rpm for 20 min. The homogenate contained 30 μg of protein stirred with LDS sample buffer (containing 40% glycerol, 4% lithium dodecyl sulfate (LDS), 0.8 M triethanolamine-Cl pH 7.6, 4% Ficoll-400, 0.025% phenol red, 0.025% Coomassie G250, 2 mM EDTA disodium, NuPAGE LDS Sample Buffer (4x) NP0007; Invitrogen, Carlsbad, CA 92008, USA). Samples were loaded for 8% sodium-dodecyl sulfate-polyacrylamide gel electrophoresis (SDS-PAGE) and then separated after centrifuging at 15,000 rpm for 10 min. The sample was mounted onto a polyvinylidene difluoride membrane and then incubated in blocking buffer (5% nonfat dry milk in Tris-buffered saline with 0.2% Tween 20) at room temperature. Rabbit polyclonal anti-rat PI3K, phospho-PI3K (P85), Akt and phospho-Akt antibody (1 : 200; Cell Signaling Technology, Beverly, MA 01915, USA) was used according to the manufacturer's instructions, while β-Actin (monoclonal anti-β-actin, dilution 1 : 40,000; Sigma-Aldrich, Taipei 100, Taiwan) was used as a control. A secondary antibody was conjugated with horseradish peroxidase (HRP) in TBS-t at room temperature for 1 hr. Optical densities were measured by an enhanced Pierce chemiluminescent image analyzer (a GS-700 digital densitometer, GMI, Ramsey, MN 55303, USA).

2.11. Statistical Analysis. Data are expressed as the means ± standard deviation. For group comparisons, all statistical analyses were determined with one-way analysis of variance, with the Bonferroni post hoc test and Mann-Whitney U test. Difference, at a probability value less than 0.01, was considered significant.

3. Results

3.1. General Observation. Throughout this study, all animals showed no significant differences in the physiological parameters recorded, including glutamate oxaloacetate transaminase (GOT), glutamate pyruvate transaminase (GPT), blood urea nitrogen (BUN), creatinine, pH, and arterial blood gas analysis among all groups (Table 1). Slight lower systemic blood pressure was observed in the 450 μM/Kg/day Arctigenin treatment SAH group. It proved that continued

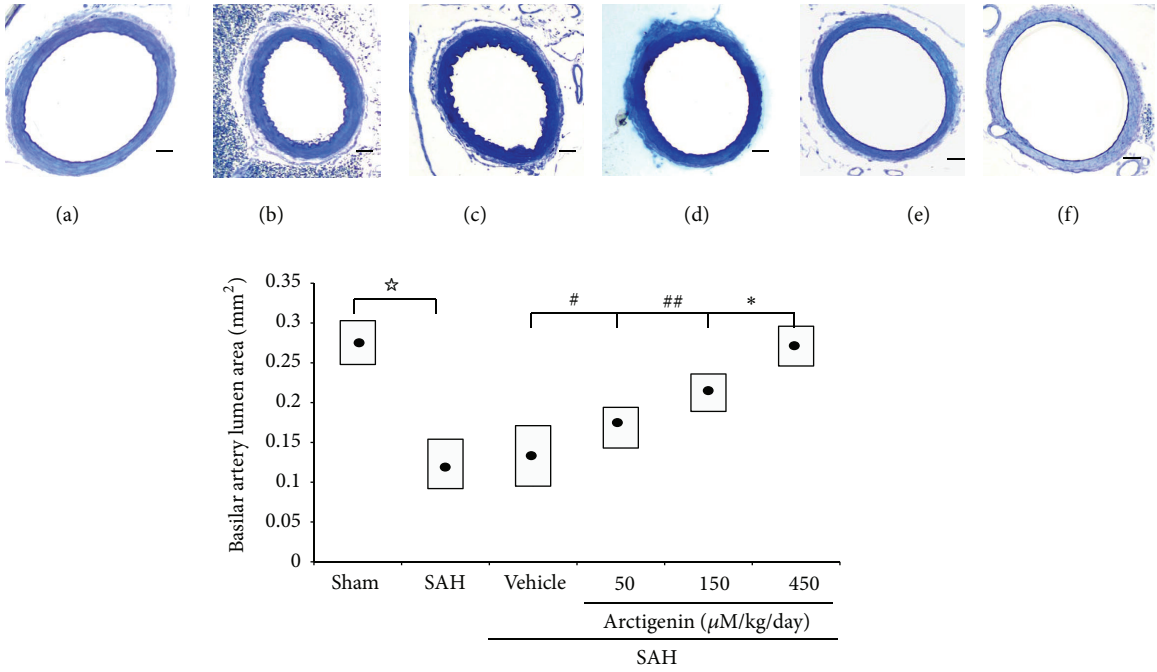

FIGURE 1: Bar graphs demonstrating mean cross-sectional areas of BAs. The mean cross-sectional areas of BAs in the SAH-only and SAH-plus vehicle groups are reduced by 56 and 53%, respectively, when compared with the control (no SAH) group. The protective effect of Arctigenin achieves statistical significance when compared with the SAH-plus vehicle group. Upper panel: BA cross-section area, (a) Sham-operated; (b) SAH-only; (c) SAH + Vehicle; SAH rats receiving Arctigenin treatment of (d) 75 μM/Kg; (e) 150 μM/Kg; (f) 450 μM/Kg. $^{\star}p < 0.01$, comparison between the Sham-operated and the SAH group; $^{*}p < 0.01$; $^{\#,\#\#}p > 0.01$. Standard bar = 200 μm.

Arctigenin pumping in the selected dosage has a number of pleiotropic effects but is devoid of hepatic and renal toxicity.

3.2. Morphometric Analysis. The lumen area was significantly increased while the radial wall thickness, which has been considered an index of chronic inflammation, was decreased in both of the Arctigenin groups when compared with those of the SAH groups. Lumen cross-sectional areas in the sham-operated, SAH-only vehicle, and 50/150/450 μM/kg Arctigenin treatment SAH groups were 0.28 ± 0.014, 0.14 ± 0.018, 0.15 ± 0.023, 0.17 ± 0.022, 0.24 ± 0.032, and 0.25 ± 0.025 (mean ± SD) mm^2, respectively (Figure 1, bottom panel).

3.3. ELISA for ET-1. The concentration of ET-1 in the CSF reached the peak at 48 hr after the induction of SAH; 408 ± 35 pg/mL was found as the baseline value in the sham-operated animals. The levels of ET-1 were significantly decreased by 22%, 51%, and 46% in 50 μM/kg/day, 150 μM/kg/day, and 450 μM/kg/day Arctigenin administration respectively, as compared with 2414 ± 85 pg/mL of the SAH + vehicle group (Figure 2).

3.4. Activated eNOS. Radiolabeled L-citrulline analysis showed higher eNOS protein in the healthy controls. Treatment with 50/150 uM/Kg Arctigenin did cause a significant increase in the bioactivity of the eNOS protein compared with rats of the SAH groups (Figure 3). Treatment of 450 μM Arctigenin increased the eNOS expression 1.4-fold when compared with SAH + vehicle rats, which corresponds to the observation in the BA eNOS immunostaining (Figure 3, upper panel).

3.5. Levels of PI3k, Phosphor-PI3K (P85), Akt, and Phosphor-Akt. Even with trends for downregulation of PI3K/Akt signaling pathway following induction of SAH, there were no significant differences among the five experimental groups (Figure 4). Levels of phospho-PI3K and phospho-Akt were increased significantly in animals subjected to SAH (SAH-only, and SAH-plus vehicle treatment groups) when compared to that in healthy controls ($p < 0.01$, and $p < 0.01$ resp.; Figure 4). Treatment with Arctigenin had less effect on the levels of PI3K/Akt after SAH, while treatment with Arctigenin significantly induced the levels of the phosphor-PI3K/Akt after SAH ($p < 0.01$ and $p < 0.01$. resp., Figure 5) when compared with that of SAH-plus vehicle group.

4. Discussion

In this study, we have shown that Arctigenin, a potent antioxidant, is able to increase Akt activation and attenuate vascular constriction in rats subjected to SAH. It is plausible that antivasospasm effects of Arctigenin account partly for simultaneous modulation of eNOS accompanying with muscarinic and β-adrenergic receptors activation. ET-1 is proven to be among the most potent causative factors of cerebral vasospasm after SAH. The biosynthesis of ET-1 is composed of conversing the natively precursor big ET-1 to

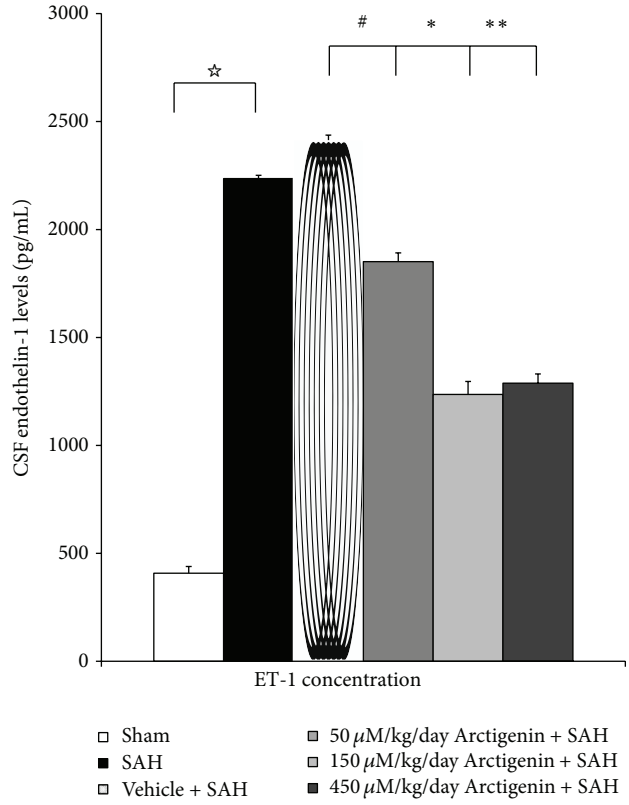

Figure 2: The effect of Arctigenin on the change ET-1in CSF after the induction of SAH (ELISA). Arctigenin dose-dependently attenuates ET-1 in the SAH rats, when compared with the SAH group. Data in the figure are presented as mean ± SD ($n = 9$). $^{\star}p < 0.01$, compared between the Sham-operated and the SAH group; $^{*,**}p < 0.01$, and $^{\#}p > 0.01$ when compared with the SAH + vehicle group.

the mature peptide ET-1 to -5 by a nonpeptide proteinase, endothelin converting enzyme (ECE) [14, 23]. Extracellular ET-1, produced in endothelial cells and glia cells, can adjust cerebrovascular tone via interactions with specific ET-A and -B receptors on the membranes of smooth muscle and endothelial cells [7, 31]. Owing to the crucial role of active ET-1, it is conceivable that inhibition of activated ETs could be amenable to the treatment of SAH-induced vasospasm. This study offers first evidence that Arctigenin exerts antivasospastic effect by means of inhibiting the production of ET-1.

NO, a potent endothelium-derived relaxant, has been well characterized in SAH-induced vasospasm. Three subtypes are included in the NOS family: neuronal (nNOS), inducible (iNOS), and endothelial (eNOS). eNOS mainly exists in the endothelium. The iNOS phenotype is detected only at low levels in humans [20]. NO plays a decisive role in modulating vascular tension and is also an important pathophysiological mediator in cardiovascular disorders and activates soluble guanylyl cyclase, which leads to the production of cGMP [39]. In Neuschmelting et al.'s study, NO donors effectively reduced the production of ET-1 from porcine-cultured aortic endothelial cells [20]. In this study, expression of eNOS is induced by Arctigenin in animals subject to SAH, which may contribute to its vascular dilatation effects. In light of previous findings showing that NO modulates the production of ET-1, the result of the study disclosing Arctigenin exerts the vasodilation effect through both the suppression of ET-1 and enhancement of NOS merits further evaluation.

Dimmeler et al. demonstrated that Akt phosphorylated the Serine 1177 site of eNOS protein and enhanced eNOS activity. Through inhibiting the PI3K/Akt pathway, it led to the prevention of eNOS activation [16]. Akt plays a crucial role in eNOS activity and is important in endothelial cell migration and angiogenesis, protection in ventilator-associated pulmonary injury [36]. It also protected intestinal tissue in the situation of intestinal ischemia [37]. The onset of Akt cascade is activated by tyrosine kinases, integrins, B and T cell receptors, cytokine receptors, G-protein coupled receptors, and other stimuli that promote the production of phosphatidylinositol 3,4,5 triphosphates (PIP3) by phosphoinositide 3-kinase (PI3K). There are three related isoforms of Akt: Akt1, Akt2, and Akt3. Akt1 is a key signaling protein in the cellular survival pathway. Akt2 serves as a critical signaling molecule in the insulin signaling pathway, but the role of Akt3 remains unclear [47]. Akt is a major mediator of cell survival by direct inhibition of proapoptotic signals such as the proapoptotic regulator Bad and the Fox01 and Myc family of transcription factors [16, 33]. The trafficking of T lymphocyte to lymphoid tissues is controlled by the expression of adhesion molecules related downstream of Akt [32]. In Endo et al.'s study, Akt has been shown to downregulate superoxide dismutase-associated neuron apoptosis in SAH [17].

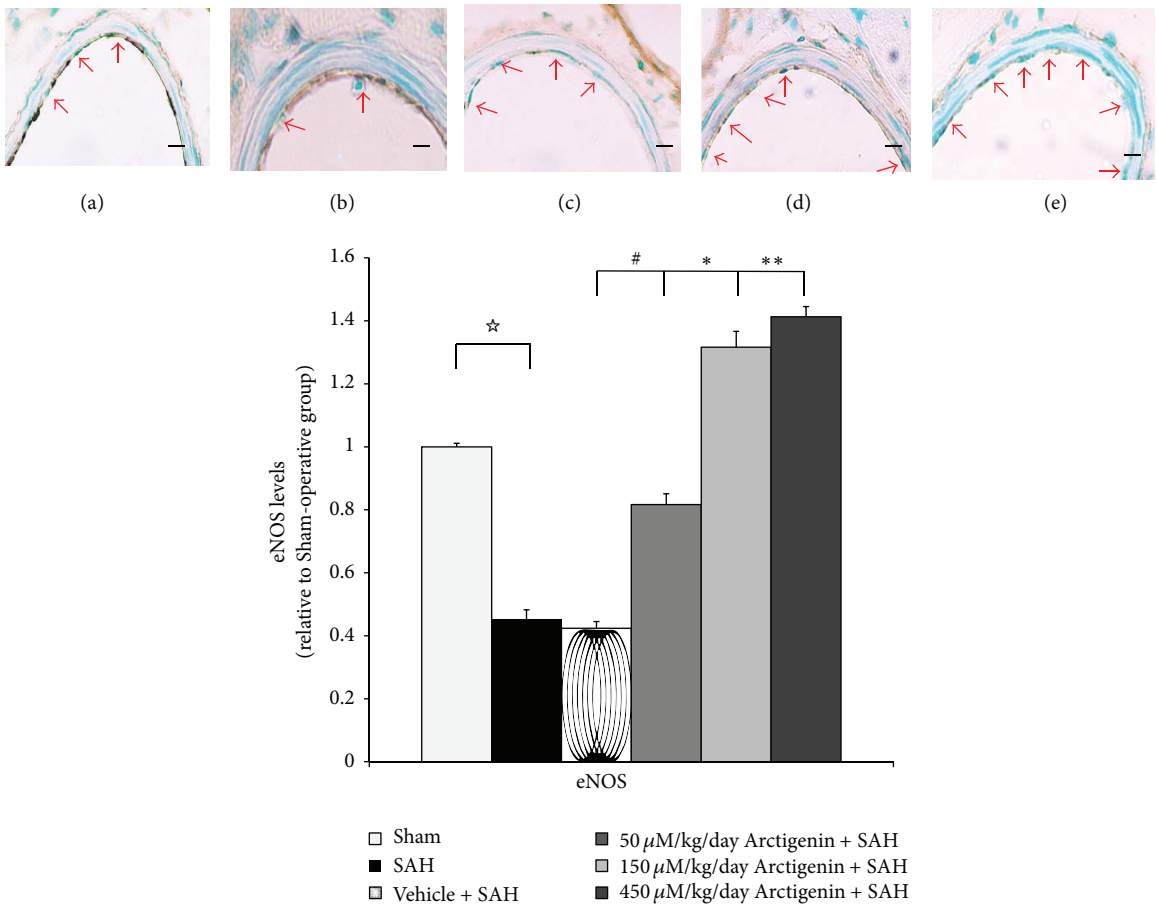

FIGURE 3: Bar graph depicting Arctigenin on the change eNOS after induction of SAH. Upper panel: NOS immunostaining (arrowhead), the groups are depicted as (a) healthy control, (b) SAH-only and SAH rats receiving, (c) 75 μM/Kg, (d) 150 μM/Kg, and (e) 450 μM/Kg Arctigenin treatment. The effect of Arctigenin is relevant to eNOs dose-dependently. Data in the figure are presented as mean ± SD ($n = 9$). $^{\star}p < 0.01$, compared the Sham-operated to the SAH group; $^{*,**}p < 0.01$, and $^{\#}p > 0.01$ when compared with the SAH + vehicle group.

Ishrat et al. also stated progesterone exerts neuroprotective effect through the Akt signaling pathway [15]. In this study, expression of phospho-PI3K and phosphor-Akt was dose-dependently induced by Arctigenin in animals subject to SAH, which may contribute to its vascular dilatation effects and correspond to its effect on the eNOS.

Arctigenin, as an active ingredient extracted from *A lappa* (L.), has been used to exert many pharmacological functions such as antidiabetes, antitumor, antioxidant, and neuroprotective effect [39, 40, 44]. In this study, Arctigenin was found able to inhibit ET-1 production and enhance eNOS by the activation of the PI3k/Akt signaling pathways.

Currently, treatments for cerebral aneurysms and associated vasospasm are complicated and disappointing. Besides, patients with vasospasm have more inpatient cost and longer hospital stay, and definite effective medical treatment against vasospasm is still lacking [5]. Clinically, oral nimodipine treatment for SAH patients might improve functional outcome but not contribute to the improvement of vasospasm [6]. A phase 3 randomized trial of MASH-2 published results that magnesium sulfate did not improve clinical outcome in 1,203 patients with aneurysmal SAH [13]. Herein, we found that Arctigenin effectively inhibited PI3k/Akt pathways and increased eNOS activation. This result thus highly strengthened the potential of this natural product in its antivasospasm in the SAH study.

In summary, the results of this study show that continued administration of Arctigenin, at a selected therapeutic dosage, is safe and efficacious in the prevention of vasospasm in this experimental model and is meritorious of further investigation. Decreased levels of ET-1 as well as activated eNOS, phospho-PI3k and Akt may contribute to the anti-apoptotic and antivasoconstrictive effect of this compound. Besides, 150 uM/kg of Arctigenin is similarly effective as that of 450 uM/kg and exerts a dual effect on the Akt-related NOS pathway and ET-1 related inflammatory cascade.

5. Conclusions

The outcome of SAH patients is persistently devastating, and has changed little after decades of research and treatment focusing on cerebral vasospasm. These accumulated results arouse interest to consider the pathogenesis of SAH-induced

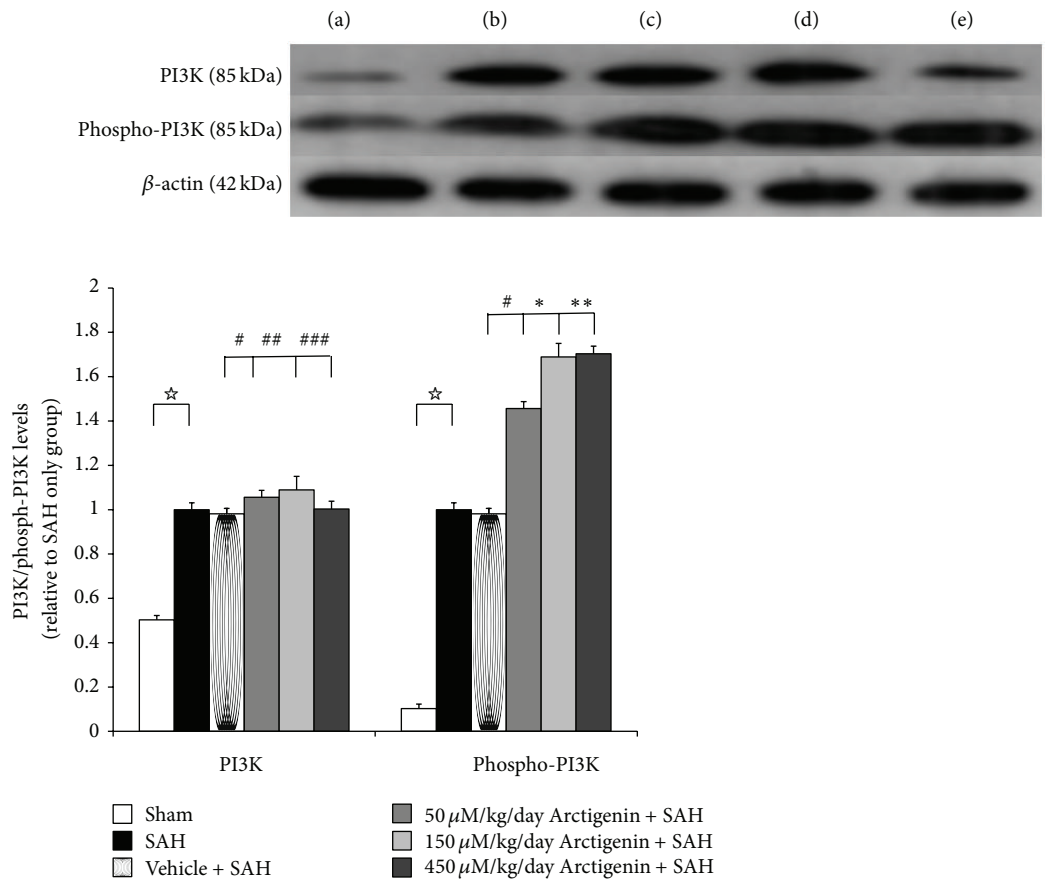

Figure 4: The immunohistochemical study of PI3K/phospho-PI3K expression (western blot). Upper panel: the groups are stated similar to that of Figure 3. The assay showed the reduced phosphorylation of PI3K in the SAH groups when compared with the control group. Arctigenin dose-dependently induced the expression of activated PI3D signaling when compared with the SAH groups. Data in the figure are presented as mean ± SD. ($^{\star}p < 0.01$, compared with the SAH group; $^{*,**}p < 0.01$, $^{\#,\#\#,\#\#\#}p > 0.01$, indicates comparison among the 75/150/450 μM/kg Arctigenin and SAH + vehicle groups, resp.).

EBI and its effects dictating the patient's outcome. The ultrashort activated ET-1 and NOS following SAH lead to transient vasoconstriction and a cascade of followed neuroinflammatory reactions maintains the intensity of vasoconstriction. The spasms accompanying SAH may be another complicated pathway underlying the development and maintenance of delayed vasospasm. This study shows that administration of Arctigenin, a natural ingredient, induces eNOS, and diminishes SAH-induced ET-1 related vasospasm in a rodent model of SAH. Our result also suggests that Arctigenin could prove clinically useful in treating SAH-associated morbidity.

Abbreviations

BA: Basilar artery
Caspases: Cysteine requiring aspartate proteases
CSF: Cerebrospinal fluid
ET-1: Endothelin-1
ETs: Endothelins
eNOS: Endothelial nitric oxide synthase
HRP: Horseradish peroxidase
IEL: Internal elastic lamina
IL-1 & -6: Interleukins 1 and 6
PBS: Phosphate-buffered saline
PGs: Prostaglandins
PI3K: Phosphatidylinositol 3-kinase
PKB, Akt: Protein kinase B
SAH: Subarachnoid hemorrhage
TNF-α: Tumor necrotic factor-α.

Conflict of Interests

There is no conflict of interests related to this paper.

Acknowledgments

Chih-Zen Chang assisted in the planning and composing the paper; Shu-Chuan Wu, Master, helped the data collection and carried out the study. Chia-Mao Chang assisted in the data collection and analysis. Chih-Lung Lin helped the grand

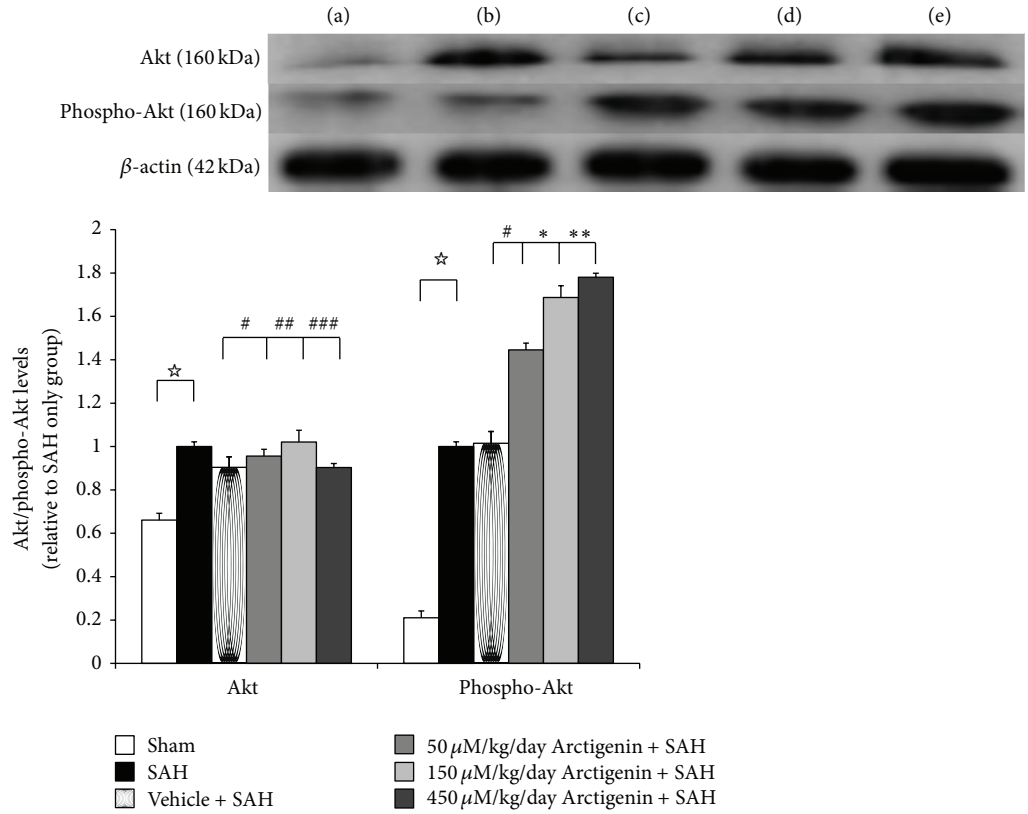

FIGURE 5: The effect of Arctigenin on the immunohistochemical study of Akt/phospho-Akt expression (western blot). Upper panel: the groups are as depicted in Figure 3. The assay showed Arctigenin induced Akt/phospho-Akt immunoreactivity in the SAH rats when compared with the SAH groups. All values are mean ± SD. $^{\star}\,p < 0.01$, comparison with the SAH group; $^{*,**}\,p < 0.01$, and $^{\#,\#\#,\#\#\#}\,p > 0.01$, compared with the SAH + vehicle group.

gathering and Aij-Lie Kwan assisted in the experimental planning and support.

References

[1] J. P. Dreier, S. Major, A. Manning et al., "Cortical spreading ischaemia is a novel process involved in ischaemic damage in patients with aneurysmal subarachnoid haemorrhage," *Brain*, vol. 132, no. 7, pp. 1866–1881, 2009.

[2] G. Grasso, "An overview of new pharmacological treatments for cerebrovascular dysfunction after experimental subarachnoid hemorrhage," *Brain Research Reviews*, vol. 44, no. 1, pp. 49–63, 2004.

[3] A. G. Kolias, J. Sen, and A. Belli, "Pathogenesis of cerebral vasospasm following aneurysmal subarachnoid hemorrhage: putative mechanisms and novel approaches," *Journal of Neuroscience Research*, vol. 87, no. 1, pp. 1–11, 2009.

[4] M. N. Stienen, R. Weisshaupt, J. Fandino et al., "Current practice in neuropsychological outcome reporting after aneurysmal subarachnoid haemorrhage," *Acta Neurochirurgica*, vol. 155, no. 11, pp. 2045–2051, 2013.

[5] C.-H. Chou, S. D. Reed, J. S. Allsbrook, J. L. Steele, K. A. Schulman, and M. J. Alexander, "Costs of vasospasm in patients with aneurysmal subarachnoid hemorrhage," *Neurosurgery*, vol. 67, no. 2, pp. 345–351, 2010.

[6] E. S. Connolly, A. A. Rabinstein, J. R. Carhuapoma et al., "Guidelines for the management of aneurysmal subarachnoid hemorrhage: a guideline for healthcare professionals from the american heart association/american stroke association," *Stroke*, vol. 43, no. 6, pp. 1711–1737, 2012.

[7] K. P. Budohoski, M. Czosnyka, P. Smielewski et al., "Impairment of cerebral autoregulation predicts delayed cerebral ischemia after subarachnoid hemorrhage: a prospective observational study," *Stroke*, vol. 43, no. 12, pp. 3230–3237, 2012.

[8] R. P. Ostrowski, A. R. Colohan, and J. H. Zhang, "Molecular mechanisms of early brain injury after subarachnoid hemorrhage," *Neurological Research*, vol. 28, no. 4, pp. 399–414, 2006.

[9] M. Sabri, A. Kawashima, J. Ai, and R. L. Macdonald, "Neuronal and astrocytic apoptosis after subarachnoid hemorrhage: a possible cause for poor prognosis," *Brain Research*, vol. 1238, pp. 163–171, 2008.

[10] H. Vatter, J. Konczalla, S. Weidauer et al., "Effect of delayed cerebral vasospasm on cerebrovascular endothelin A receptor expression and function," *Journal of Neurosurgery*, vol. 107, no. 1, pp. 121–127, 2007.

[11] S. Ansar, P. Vikman, M. Nielsen, and L. Edvinsson, "Cerebrovascular ETB, 5-HT1B, and AT1 receptor upregulation correlates with reduction in regional CBF after subarachnoid hemorrhage," *The American Journal of Physiology—Heart and Circulatory Physiology*, vol. 293, no. 6, pp. H3750–H3758, 2007.

[12] J. Cahill, J. W. Calvert, I. Solaroglu, and J. H. Zhang, "Vasospasm and p53-induced apoptosis in an experimental model of subarachnoid hemorrhage," *Stroke*, vol. 37, no. 7, pp. 1868–1874, 2006.

[13] S. M. D. Mees, A. Algra, W. P. Vandertop et al., "Magnesium for aneurysmal subarachnoid haemorrhage (MASH-2): a randomised placebo-controlled trial," *The Lancet*, vol. 380, no. 9836, pp. 44–49, 2012.

[14] K. Fabender, B. Hodapp, S. Rossol et al., "Endothelin-1 in subarachnoid hemorrhage: an acute-phase reactant produced by cerebrospinal fluid leukocytes," *Stroke*, vol. 31, no. 12, pp. 2971–2975, 2000.

[15] T. Ishrat, I. Sayeed, F. Atif, F. Hua, and D. G. Stein, "Progesterone is neuroprotective against ischemic brain injury through its effects on the phosphoinositide 3-kinase/protein kinase B signaling pathway," *Neuroscience*, vol. 210, pp. 442–450, 2012.

[16] S. Dimmeler, I. Fleming, B. Fisslthaler, C. Hermann, R. Busse, and A. M. Zeiher, "Activation of nitric oxide synthase in endothelial cells by Akt-dependent phosphorylation," *Nature*, vol. 399, no. 6736, pp. 601–605, 1999.

[17] H. Endo, C. Nito, H. Kamada, F. Yu, and P. H. Chan, "Reduction in oxidative stress by superoxide dismutase overexpression attenuates acute brain injury after subarachnoid hemorrhage via activation of Akt/glycogen synthase kinase-3β survival signaling," *Journal of Cerebral Blood Flow and Metabolism*, vol. 27, no. 5, pp. 975–982, 2007.

[18] E. N. Momin, K. E. Schwab, K. L. Chaichana, R. Miller-Lotan, A. P. Levy, and R. J. Tamargo, "Controlled delivery of nitric oxide inhibits leukocyte migration and prevents vasospasm in haptoglobin 2-2 mice after subarachnoid hemorrhage," *Neurosurgery*, vol. 65, no. 5, pp. 937–945, 2009.

[19] M. A. Moro, A. Cárdenas, O. Hurtado, J. C. Leza, and I. Lizasoain, "Role of nitric oxide after brain ischaemia," *Cell Calcium*, vol. 36, no. 3-4, pp. 265–275, 2004.

[20] V. Neuschmelting, S. Marbacher, A.-R. Fathi, S. M. Jakob, and J. Fandino, "Elevated level of endothelin-1 in cerebrospinal fluid and lack of nitric oxide in basilar arterial plasma associated with cerebral vasospasm after subarachnoid haemorrhage in rabbits," *Acta Neurochirurgica*, vol. 151, no. 7, pp. 795–801, 2009.

[21] K. Yamashiro, A. B. Milsom, J. Duchene et al., "Alterations in nitric oxide and endothelin-1 bioactivity underlie cerebrovascular dysfunction in ApoE-deficient mice," *Journal of Cerebral Blood Flow and Metabolism*, vol. 30, no. 8, pp. 1494–1503, 2010.

[22] D. M. Arrick and W. G. Mayhan, "Inhibition of endothelin-1 receptors improves impaired nitric oxide synthase-dependent dilation of cerebral arterioles in type-1 diabetic rats," *Microcirculation*, vol. 17, no. 6, pp. 439–446, 2010.

[23] C.-Z. Chang, S.-C. Wu, and A.-L. Kwan, "Magnesium lithospermate B, an active extract of salvia miltiorrhiza, mediates SGC/CGMP/PKG translocation in experimental vasospasm," *BioMed Research International*, vol. 2014, Article ID 272101, 9 pages, 2014.

[24] S. Kästner, M. F. Oertel, W. Scharbrodt, M. Krause, D.-K. Böker, and W. Deinsberger, "Endothelin-1 in plasma, cisternal CSF and microdialysate following aneurysmal SAH," *Acta Neurochirurgica*, vol. 147, no. 12, pp. 1271–1279, 2005.

[25] A. Xie, Y. Aihara, V. A. Bouryi et al., "Novel mechanism of endothelin-1-induced vasospasm after subarachnoid hemorrhage," *Journal of Cerebral Blood Flow and Metabolism*, vol. 27, no. 10, pp. 1692–1701, 2007.

[26] K. Mori, T. Yamamoto, M. Miyazaki et al., "Optimal cerebrospinal fluid magnesium ion concentration for vasodilatory effect and duration after intracisternal injection of magnesium sulfate solution in a canine subarachnoid hemorrhage model: laboratory investigation," *Journal of Neurosurgery*, vol. 114, no. 4, pp. 1168–1175, 2011.

[27] T. Sasaki, H. Kasuya, H. Onda et al., "Role of p38 mitogen-activated protein kinase on cerebral vasospasm after subarachnoid hemorrhage," *Stroke*, vol. 35, no. 6, pp. 1466–1470, 2004.

[28] P. Vikman, S. Beg, T. Khurana, J. Hansen-Schwartz, and L. Edvinsson, "Gene expression and molecular changes in cerebral arteries following subarachnoid hemorrhage in the rat," *Journal of Neurosurgery*, vol. 105, no. 3, pp. 438–444, 2006.

[29] Z. Wang, G. Chen, W.-W. Zhu, and D. Zhou, "Activation of nuclear factor-erythroid 2-related factor 2 (Nrf2) in the basilar artery after subarachnoid hemorrhage in rats," *Annals of Clinical and Laboratory Science*, vol. 40, no. 3, pp. 233–239, 2010.

[30] C. Zhou, M. Yamaguchi, G. Kusaka, C. Schonholz, A. Nanda, and J. H. Zhang, "Caspase inhibitors prevent endothelial apoptosis and cerebral vasospasm in dog model of experimental subarachnoid hemorrhage," *Journal of Cerebral Blood Flow and Metabolism*, vol. 24, no. 4, pp. 419–431, 2004.

[31] M. Herrera, N. J. Hong, P. A. Ortiz, and J. L. Garvin, "Endothelin-1 Lnhibits thick ascending limb transport via Akt-stimulated nitric oxide production," *The Journal of Biological Chemistry*, vol. 284, no. 3, pp. 1454–1460, 2009.

[32] K. Kawasaki, R. S. Smith Jr., C.-M. Hsieh, J. Sun, J. Chao, and J. K. Liao, "Activation of the phosphatidylinositol 3-kinase/protein kinase Akt pathway mediates nitric oxide-induced endothelial cell migration and angiogenesis," *Molecular and Cellular Biology*, vol. 23, no. 16, pp. 5726–5737, 2003.

[33] S. R. Datta, A. Brunet, and M. E. Greenberg, "Cellular survival: a play in three akts," *Genes and Development*, vol. 13, no. 22, pp. 2905–2927, 1999.

[34] A. Li, J. Wang, M. Wu, X. Zhang, and H. Zhang, "The inhibition of activated hepatic stellate cells proliferation by arctigenin through G_0/G_1 phase cell cycle arrest: persistent $p27^{Kip1}$ induction by interfering with PI3K/Akt/FOXO3a signaling pathway," *European Journal of Pharmacology*, vol. 747, pp. 71–87, 2015.

[35] C. Liu, T. Su, F. Li et al., "PI3K/Akt signaling transduction pathway is involved in rat vascular smooth muscle cell proliferation induced by apelin-13," *Acta Biochimica et Biophysica Sinica*, vol. 42, no. 6, pp. 396–402, 2010.

[36] X.-Q. Peng, M. Damarla, J. Skirball et al., "Protective role of PI3-kinase/Akt/eNOS signaling in mechanical stress through inhibition of p38 mitogen-activated protein kinase in mouse lung," *Acta Pharmacologica Sinica*, vol. 31, no. 2, pp. 175–183, 2010.

[37] F. Roviezzo, S. Cuzzocrea, A. Di Lorenzo et al., "Protective role of PI3-kinase-Akt-eNOS signalling pathway in intestinal injury associated with splanchnic artery occlusion shock," *British Journal of Pharmacology*, vol. 151, no. 3, pp. 377–383, 2007.

[38] J.-P. Gratton, G. Cournoyer, and P. D'Orléans-Juste, "Endothelin-B receptor-dependent modulation of the pressor and prostacyclin-releasing properties of dynamically converted big endothelin-1 in the anesthetized rabbit," *Journal of Cardiovascular Pharmacology*, vol. 31, no. 1, pp. S161–S163, 1998.

[39] M. K. Cho, J. W. Park, Y. P. Jang, Y. C. Kim, and S. G. Kim, "Potent inhibition of lipopolysaccharide-inducible nitric oxide synthase expression by dibenzylbutyrolactone lignans through inhibition of I-kappaBalpha phosphorylation and of p65 nuclear translocation in macrophages," *International Immunopharmacology*, vol. 2, no. 1, pp. 105–116, 2002.

[40] Y. P. Jang, S. R. Kim, Y. H. Choi et al., "Arctigenin protects cultured cortical neurons from glutamate-induced neurodegeneration by binding to kainate receptor," *Journal of Neuroscience Research*, vol. 68, no. 2, pp. 233–240, 2002.

[41] Y. Jeong, J. Park, D. Kim, and H. Kim, "Arctigenin increases hemeoxygenase-1 gene expression by modulating PI3K/AKT signaling pathway in rat primary astrocytes," *Biomolecules and Therapeutics*, vol. 22, no. 6, pp. 497–502, 2014.

[42] H. Liu, Y. Yang, X. Cai, Y. Gao, J. Du, and S. Chen, "The effects of arctigenin on human rheumatoid arthritis fibroblast-like synoviocytes," *Pharmaceutical Biology*, vol. 5, pp. 1–6, 2015.

[43] V. Swarup, J. Ghosh, M. K. Mishra, and A. Basu, "Novel strategy for treatment of Japanese encephalitis using arctigenin, a plant lignan," *Journal of Antimicrobial Chemotherapy*, vol. 61, no. 3, pp. 679–688, 2008.

[44] T. Fan, W. L. Jiang, J. Zhu, and Y. F. Zhang, "Arctigenin protects focal cerebral ischemia-reperfusion rats through inhibiting neuroinflammation," *Biological and Pharmaceutical Bulletin*, vol. 35, no. 11, pp. 2004–2009, 2012.

[45] Z. Zhu, J. Yan, W. Jiang et al., "Arctigenin effectively ameliorates memory impairment in Alzheimer's disease model mice targeting both β-amyloid production and clearance," *Journal of Neuroscience*, vol. 33, no. 32, pp. 13138–13149, 2013.

[46] F. Raslan, C. Albert-Weißenberger, T. Westermaier, S. Saker, C. Kleinschnitz, and J.-Y. Lee, "A modified double injection model of cisterna magna for the study of delayed cerebral vasospasm following subarachnoid hemorrhage in rats," *Experimental and Translational Stroke Medicine*, vol. 4, no. 1, article 23, 2012.

[47] B. D. Manning and L. C. Cantley, "AKT/PKB signaling: navigating downstream," *Cell*, vol. 129, no. 7, pp. 1261–1274, 2007.

Hindawi Publishing Corporation
BioMed Research International
Volume 2015, Article ID 540217, 7 pages
http://dx.doi.org/10.1155/2015/540217

Research Article

Middle Cerebral Artery Atherosclerotic Plaques in Recent Small Subcortical Infarction: A Three-Dimensional High-resolution MR Study

Xiao-Dong Zou,[1] Yiu-Cho Chung,[2] Lei Zhang,[2] Ying Han,[1,3,4] Qi Yang,[5] and Jianping Jia[1,3,4]

[1]*Department of Neurology, Xuan Wu Hospital, Capital Medical University, Beijing 100053, China*
[2]*Paul C. Lauterbur Research Center for Biomedical Imaging, Shenzhen Institutes of Advanced Technology, Chinese Academy of Sciences, Shenzhen 518055, China*
[3]*Beijing Key Laboratory of Geriatric Cognitive Disorders, Beijing 100053, China*
[4]*Neurodegenerative Laboratory of Ministry of Education of the People's Republic of China, Beijing 100053, China*
[5]*Department of Radiology, Xuan Wu Hospital, Capital Medical University, Beijing 100053, China*

Correspondence should be addressed to Jianping Jia; jiajp@vip.126.com

Received 21 June 2015; Accepted 16 August 2015

Academic Editor: Robert M. Starke

Purpose. Conventional two-dimensional vessel wall imaging has been used to depict the middle cerebral artery (MCA) wall in patients with recent small subcortical infarctions (RSSIs). However, its clinical use has been limited by restricted spatial coverage, low signal-to-noise ratio (SNR), and long scan time. We used a novel three-dimensional high-resolution MR imaging (3D HR-MRI) technique to investigate the presence, locations, and contrast-enhanced patterns of MCA plaques and their relationship with RSSI. *Methods*. Nineteen consecutive patients with RSSI but no luminal stenosis on MR angiography were prospectively enrolled. 3D HR-MRI was performed using a T1w-SPACE sequence at 3.0 T. The presence, locations, and contrast-enhanced patterns of the MCA plaques on the ipsilateral and contralateral sides to the RSSI were analyzed. *Results*. Eighteen patients successfully completed the study. MCA atherosclerotic plaques occurred more frequently on the ipsilateral than the contralateral side to the RSSI (72.2% versus 33.3%, $P = 0.044$). The occurrence of superiorly located plaques was significantly higher on the ipsilateral than the contralateral side of the MCA (66.7% versus 27.8%; $P = 0.044$). *Conclusions*. Superiorly located plaques are closely associated with RSSI. 3D high-resolution vessel wall imaging may be a potential tool for etiologic assessment of ischemic stroke.

1. Introduction

Small subcortical infarction (SSI) is a unique entity with a distinct pathogenesis [1]. Traditionally, SSI is believed to be caused by intrinsic diseases of the perforating arterioles [2, 3]. However, the study by Adachi et al. revealed that large artery disease may also lead to SSIs [4]. Distinguishing between the two vasculopathies may help guide optimal therapy. Many conventional modalities exist for imaging luminal stenosis, including CT angiography and MR angiography (MRA). However, they cannot identify atherosclerotic plaques undergoing expansive remodeling on the intracranial vessel wall which do not lead to luminal stenosis. Thus, direct imaging of the intracranial vessel wall itself offers the potential to discriminate such pathologies.

Using two-dimensional high-resolution MR imaging (2D HR-MRI), several studies have demonstrated that atherosclerotic plaques can be detected in patients with single subcortical infarctions (42–60%) [5–8]. Xu et al. compared the characteristics of plaques on the ipsilateral side with those on the contralateral side and reported that superiorly located plaques of middle cerebral artery (MCA) are associated with acute deep brain infarctions [6]. However, 2D technique with relatively low spatial resolution and limited coverage has difficulty identifying small plaques on the vessel walls, especially at the distal tortuous intracranial arteries [9]. Furthermore, there has been limited study of contrast-enhanced high-resolution atherosclerotic plaque imaging in patients with recent SSI (RSSI) but no significant luminal stenosis at the MCA.

In this study, we aimed to compare the presence, locations, and contrast-enhanced patterns of plaques on the ipsilateral and contralateral side of the RSSI using contrast-enhanced three-dimensional HR-MRI (3D HR-MRI).

2. Materials and Methods

2.1. Study Population. From September 2013 to March 2014, 19 consecutive patients were prospectively recruited into the current study. Patients were enrolled in this study if the following criteria were met: (1) a recent single infarction (maximal infarction diameter $\leq$ 2 cm) that is believed to be responsible for the clinical symptoms reported within the past 4 weeks: this infarct should have been identified in the territory of the lenticulostriate arteries as confirmed by diffusion-weighted imaging (DWI); (2) no ipsilateral MCA stenosis based on the MRA; (3) one or more risk factors for atherosclerosis (hypertension, diabetes, hyperlipidemia, and smoking). All eligible patients first underwent comprehensive examinations including MRI of the brain (T1- and T2-weighted images, DWI), MRA of the MCA, transcranial Doppler, carotid duplex, electrocardiography, and echocardiography. We excluded patients with the following: (1) one or more stenoses at the ipsilateral intracranial internal carotid artery or relevant extracranial arteries; (2) a definite cardioembolic source; (3) other nonatherosclerotic vasculopathies. Among these patients, those who were unable to undergo a second MRI scan for any reason were also excluded. In this study, the term "recent small subcortical infarction" followed the definition described by Wardlaw et al. [10]. The study protocol was approved by the institutional review board of our hospital. All patients gave written informed consent before undergoing the second MR examination.

2.2. Imaging Protocol. The examination was performed on a 3.0 T MRI system (Siemens Magnetom Verio, Erlangen, Germany) using a 32-channel head coil. The examination protocol included 3D time-of-flight MRA, DWI, and pre- and postcontrast 3D T1-weighted HR-MRI.

The 3D HR-MRI was performed using a variant of a 3D turbo spin echo technique known as T1w-SPACE [11]. The technique has good blood suppression properties and high sampling efficiency [12]. The imaging parameters optimized for T1 contrast that were used included the following [13]: TR/TE = 938 ms/24 ms; turbo factor = 29; echo spacing = 4.54 ms; iPAT = 2; average = 1.4 (partial averaging); isotropic voxel resolution varied between $(0.5\,\text{mm})^3$ and $(0.7\,\text{mm})^3$, and the average scan time was 8 min (6–10 min, depending on the spatial resolution). For contrast-enhanced T1w-SPACE, 0.1 mmol/kg body weight of gadopentetate dimeglumine (BeiLu Pharmaceutical Co., Ltd, Beijing, China) was manually injected. All subjects included in this study underwent MRI examination within 4 weeks of symptom onset.

2.3. Image Analysis. All images were analyzed by two experienced readers. One reader (Qi Yang) is a neuroradiologist with 10-year clinical experience; another reader (Yiu-Cho Chung) is an MR scientist working on plaque imaging for more than 10 years. Both were independently blinded to the patients' clinical information and other images before they reviewed the T1w-SPACE images. The discrepancies between the readers were resolved by consensus reading.

Image analysis was performed on a workstation (Leonardo, Siemens). The infarction at the penetrator territory of the MCA was assessed based on a previously published template [14]. The presence of MCA plaques was identified using both pre- and postcontrast T1w-SPACE images. The two 3D image sets were first coregistered using commercial software (Syngo Fusion, Siemens). In the images, plaques were identified using the criteria by Klein et al. [5]. A plaque has focal wall thickening when it is evident on both the short axis and long axis of the vessel compared with the nearby vessel wall. Care was taken to ensure that the short-axis views of the vessels were perpendicular to the M1 segment of MCA. The end of the M1 segment was defined as the portion at the Sylvian fissure and included the bifurcation [15]. MCAs on both the ipsilateral and contralateral sides of the infarction lesion were reviewed for the presence of plaque.

As most lenticulostriate arteries arise from the superior wall of the MCA trunk [16], the locations of the plaques were analyzed. Based on the position of maximal wall thickening, the cross-sectional locations of the plaques were classified as superior or inferior [8]. A plaque was considered a superiorly located plaque when its maximal thickness was at the superior side of the MCA (Figure 1(d)). Otherwise, it was classified as an inferiorly located plaque (Figure 1(e)). If the plaque thickness was similar on both the superior and inferior sides of the vessel, the plaque was considered to be involved from both sides of the MCA (Figure 1(f)).

Two-dimensional short-axis images of the plaques that were generated from the registered pre- and postcontrast T1w-SPACE images were used to find the plaque enhancement ratio as follows. Region of interest (ROI) of the thickened MCA vessel walls was first defined. The mean signal intensities (SI) of the MCA vessel wall at the ROI on the registered pre- and postcontrast T1w-SPACE were measured. They were then normalized by the SI of the nearby gray matter regions in the pre- and postcontrast images using the method described by Lou et al. [17]. Following [17], a plaque was enhanced when its SI increased by more than 20%.

2.4. Statistical Analysis. Continuous data were expressed as mean $\pm$ standard deviation. Categorical data were expressed as counts and percentages. The interobserver agreement for the identification of the plaques was assessed by calculating kappa (κ). A value of $\kappa > 0.8$ would indicate almost perfect agreement. Student's t-test was used for quantitative data comparison, while Fisher exact test was used for qualitative data comparison. Statistical significance was defined as a P value of <0.05. All statistical analyses were performed using SPSS software (SPSS Inc., version 19, Chicago, IL, USA).

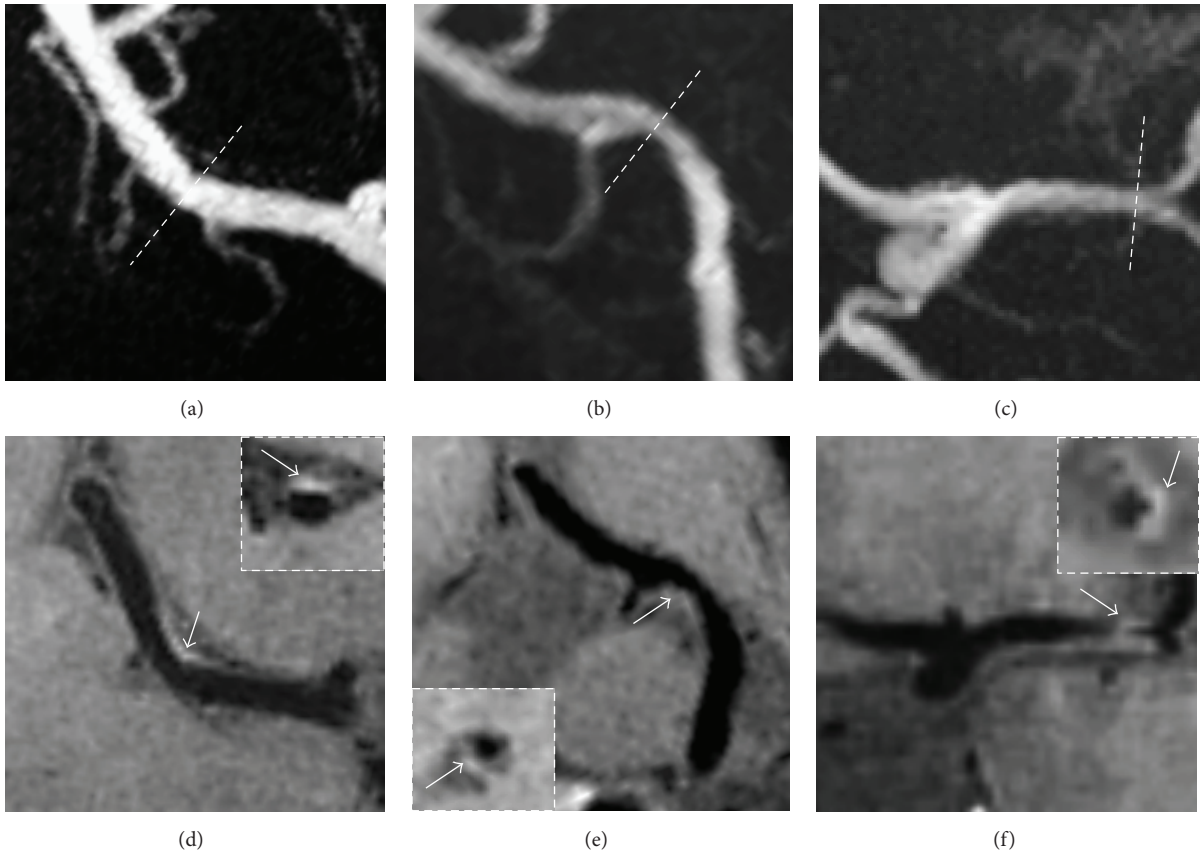

Figure 1: Contrast-enhanced 3D HR-MRI images from three patients. (a)–(c): MRA images show no stenosis on the relevant MCAs in these patients (*short dash line*). (d)–(f): Contrast-enhanced 3D HR-MRI images of the corresponding patients show the plaques and their positions along the MCAs (see arrow): (d) superiorly located superior; (e) inferiorly located plaque; (f) plaque involving both superior and inferior wall.

3. Results

3.1. Patients Baseline Characteristics. Eighteen patients successfully completed 3D contrast-enhanced high-resolution vessel wall imaging. One patient was excluded because of suboptimal image quality from the examination. The details of the patients' demographics and main clinical characteristics are shown in Table 1.

3.2. Presence and Locations of MCA Plaques. Of the 18 patients (totally 36 MCAs), 3D HR-MRI detected 21 plaques that appeared to cause no stenosis on MRA. On precontrast images, 14 plaques were detected and 12 of them were enhanced in postcontrast images. On postcontrast images, MCA atherosclerotic plaques were found in 19 vessels. Superiorly located plaques were found in 17 (89.5%) of the 19 MCAs with plaques. The percentage of atherosclerotic plaques in all the 36 MCAs detected on postcontrast T1w-SPACE images was higher than that on precontrast T1w-SPACE images (52.8% versus 38.9%) (Table 2). Figure 1 showed three typical cases in which plaques were found at different positions of the MCA arterial wall. The distribution of the plaques found on the ipsilateral and contralateral sides of the lesions was shown in Table 3. Three of the 14 plaques found at the ipsilateral MCAs were located near the bifurcation of the M1 segment. Figure 2 showed one such case where eccentric vessel wall thickening was located near the bifurcation. MCA plaques occurred more often in the ipsilateral than the contralateral MCA (72.2% versus 33.3%; $P = 0.044$). In addition, the prevalence of superiorly located plaques was

Table 1: Demographic and baseline characteristics of the patients.

	RSSI ($n = 18$)
Age, median (range)	54.6 (40–70)
Male gender, %	16 (88.9)
Hypertension, %	12 (66.7%)
Diabetes, %	4 (22.2%)
Hyperlipidemia, %	10 (55.6%)
Current smoker, %	13 (72.2%)
NIHSS, median (range)	2.78 (0–12)
Maximum infarction diameter, mm, median (range)	14.7 (8.8–20)
Time from stroke onset to the second MRI, days, median (range)	12 (3–28)

Except for ranges, values are counts (percentages).

Table 2: Presence and positions of atherosclerotic plaques around the ipsilateral and contralateral MCAs.

Patient number	Infarction site	Ipsilateral				Contralateral			
		Precontrast		Postcontrast		Precontrast		Postcontrast	
		Presence	Position	Presence	Position	Presence	Position	Presence	Position
1	Left	Yes	Down	Yes	Up + down	No		No	
2	Left	Yes	Up	Yes	Up	Yes	Up	Yes	Up
3	Left	No		No		No		No	
4	Left	Yes	Up	Yes	Up	Yes	Up	Yes	Up
5	Left	Yes	Up + down	Yes	Up	No		No	
6	Left	Yes	Down	Yes	Down	No		No	
7	Left	Yes	Up	Yes	Up	Yes	Up	Yes	Down
8	Left	Yes	Up	Yes	Up + down	No		No	
9	Left	No		No		No		No	
10	Left	Yes	Up + down	Yes	Up	No		No	
11	Left	Yes	Up	Yes	Up + down	No		No	
12	Right	No		No		No		No	
13	Right	No		No		No		No	
14	Right	Yes	Up + down	Yes	Up + down	Yes	Up + down	Yes	Up + down
15	Right	No		Yes	Up	No		Yes	Up + down
16	Right	No		Yes	Up	No		Yes	Up + down
17	Right	No		No		No		No	
18	Right	No		Yes	Up	No		No	

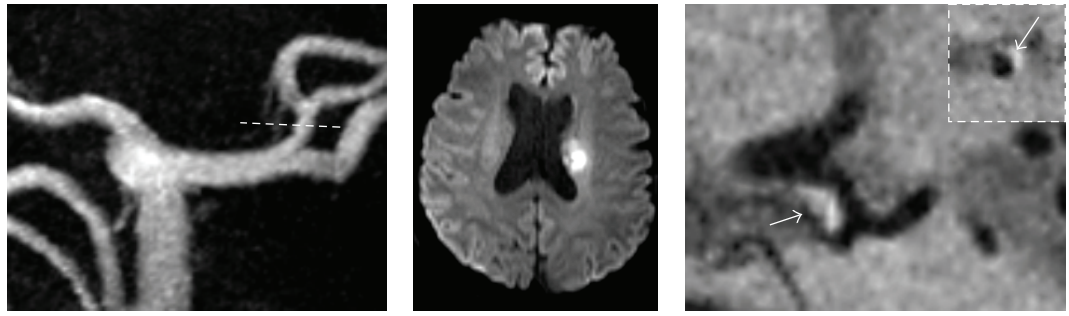

(a) (b) (c)

Figure 2: A 56-year-old man with right-side weakness and dysarthria. (a) MRA shows no stenosis on the left MCA; (b) the diffusion-weighted image shows a hypertensive lesion in the left lenticular nucleus with rostral extension to the coronal radiate; (c) the T1-weighted SPACE postcontrast images show apparent eccentric wall thickening (arrow) in close proximity to bifurcation ipsilateral to the infarction on both the long axis and the short axis of the vessel.

Table 3: Ipsilateral and contralateral MCA wall findings.

Wall findings	Ipsilateral MCA ($n = 18$)	Contralateral MCA ($n = 18$)	P value
Presence of plaque	13 (72.2%)	6 (33.3%)	**0.044**
Superior wall	12 (66.7%)*	5 (27.8%)**	**0.044**
Inferior wall	5 (27.8%)	4 (22.2%)	1.000

Values are counts (percentages). Statistically significant values are shown in bold font.
MCA: middle cerebral artery.
*Of the 12 superiorly located plaques, 4 are also inferiorly involved.
**Of the 5 superiorly located plaques, 3 are also inferiorly involved.

significantly higher in the ipsilateral than the contralateral MCA (66.7% versus 27.8%; $P = 0.044$). Weighted κ value of the interobserver agreement for the identification of the plaques was 0.828 (95% confidence interval [CI], 0.62–1.00).

3.3. Plaque Enhancement. The percentages of superiorly located plaques with increased SI at both the ipsilateral and contralateral MCA were 58.8% ± 34.9% and 72.2% ± 43.5%, respectively ($P = 0.512$ using Student's t-test). Table 4 showed the signal enhancement of the plaques that were centered on the superior side of the MCAs (superiorly located plaques) on both the ipsilateral and contralateral sides of the RSSIs.

4. Discussion

In this study, we investigated the MCA atherosclerotic lesions in patients with RSSI using contrast-enhanced 3D HR-MRI. We found that atherosclerotic plaques were observed frequently at the MCA ipsilateral to the infarction lesions and were often located at the superior side of the vessel wall.

Table 4: Enhancement of superiorly located plaques between ipsilateral and contralateral MCA.

Enhancement	Ipsilateral MCA ($n = 12$)	Contralateral MCA ($n = 5$)
Absence (<20%)	1 (8.3%)	1 (20.0%)
Presence (≥20%)	11 (91.7%)	4 (80.0%)

Values are counts (percentages).

Assessment of lumen integrity is of limited value for the etiology of stroke because lumens are usually preserved by positive remodeling at the early stages of atherosclerosis. MRI of the vessel wall allows visualization of plaque morphology and characterization of plaque composition. Previous studies reported that positive arterial remodeling is more often associated with morphological predictors of plaque instability and plaque rupture [18, 19]. In our study, all 18 patients showed no obvious stenosis on time-of-flight MRA. However, with our 3D HR-MRI vessel wall imaging technique, we found 21 plaques in the patients, suggesting the presence of remodeling in the MCAs.

In patients with RSSI, plaques were present in 72.2% of the ipsilateral MCAs. This percentage of plaque is higher than that reported in previous studies (45.6–50%) [6, 7]. Such a high prevalence may be due to the use of novel 3D isotropic high-resolution vessel wall imaging. The 3D image sets allow multiplanar projection reconstruction (MPR) of images in arbitrary plane with no gap or image blurring. Compared with conventional 2D techniques [9], the ability to visualize vessel walls in various orientations improves the detection of plaques. Another advantage of 3D vessel wall imaging is that it further improves spatial coverage from the ostium of the MCA to the far end of the distal part [20]. In this regard, we found three cases in which plaques were located at the bifurcation of the M1 segment of the MCA, ipsilateral to the RSSI, which would have been missed by conventional 2D techniques. These findings are meaningful since lateral lenticulostriate arteries can originate at the bifurcation of the MCA or the nearby regions [21]. Our results therefore suggest that large artery disease may be an important cause of RSSI. The RSSI with relevant plaques in our study would be regarded as small artery diseases using other classification methods such as TOAST (Trial of ORG 10172 in Acute Stroke Treatment) [22] and SSS-TOAST (Stop Stroke Study-TOAST) [23] using conventional imaging techniques. However, these cases would have been classified as large artery disease according to the Chinese ischemic stroke subclassification [24]. Thus, 3D high-resolution vessel wall imaging would be a useful tool for etiologic assessment of ischemic stroke.

3D HR-MR can cover the entire range of bilateral MCAs in less than ten minutes and is more time-efficient compared with conventional 2D techniques. It allows the comparison between the ipsilateral MCAs of symptomatic RSSI with the contralateral MCAs. We found that plaques on both sides of RSSI were mostly superiorly located (92.3% on the ipsilateral side versus 83.3% on the contralateral side). As plaques occurred more often on the ipsilateral (72.2%) than on the contralateral sides (33.3%), the percentage of superiorly located plaques on the MCA ipsilateral to the RSSI was higher than that contralateral to the RSSI (66.7% versus 27.8%; $P = 0.044$). The superiorly located plaques commonly involve the orifices of penetrating arteries and may play an important role in the development of RSSIs [25]. A previous study reported that SSIs may be caused by perforator occlusion due to an atheroma at the MCA [26]. In light of these findings, our results support the association between superiorly located plaques and the RSSI.

Contrast enhancement of the plaque has been recognized as an important marker of vulnerability in extracranial carotid and coronary arteries [27, 28]. A previous study showed that coronary wall enhancement in patients with acute myocardial infarction was associated with elevated systemic inflammatory markers [28]. The use of contrast agent in our study for intracranial vessel wall imaging helps the detection of the probable culprit plaques in stroke patients. We found that the enhancement patterns were consistent and largely confined to the vessels supplying the area of acute infarction (Figure 3). Unexpectedly, the mean percentage increases in SI of superiorly located plaques on the ipsilateral and contralateral sides of RSSI were very similar (58.8% versus 72.2%). Several recent small sample size studies found that enhancement of plaques was strongly associated with ischemic events [29–31]. However, Klein et al. had reservations about such associations [32]. Compared to the plaques in previous contrast enhancement studies where patients have atherosclerotic plaques leading to stenosis of intracranial arteries, the plaques in our study were small and nonstenotic. Note that the percentage of enhanced plaques also depended on the assessment methods, which may be done qualitatively (comparison with pituitary [29]) or quantitatively [30]. Here, the quantitative method used to assess plaque enhancement together with the small number of contralateral MCA plaques might lead to bias on the results relating plaque enhancement and RSSI. Whether the enhancement of MCA plaques is a good prognostic tool for ischemic stroke needs to be confirmed in a larger patient cohort and follow-up studies. Nevertheless, contrast-enhanced 3D HR-MRI has the potential to help subclassify stroke more accurately and unravel the pathogenic mechanism of SSI. Such new information may have a significant impact on the treatment strategy for patients. For instance, aggressive treatment to optimize plaque stabilization, including intensive lipid-lowering and anti-inflammatory medications, may be more appropriate for patients with superiorly located enhanced plaques.

There were several limitations in our study. First, the sample size was relatively small and data from age-matched healthy control subjects were unavailable for comparison. Second, the plaques that were detected cannot be verified by histopathology. Also, the culprit plaques could not be identified as the branch artery ostia cannot be clearly visualized in the images. Third, the spatial resolution of the images varied among different patients (isotropic voxel size varied from 0.125 to 0.343 mm^3). Despite the varying voxel size used in different patients, the lowest spatial resolution in terms of

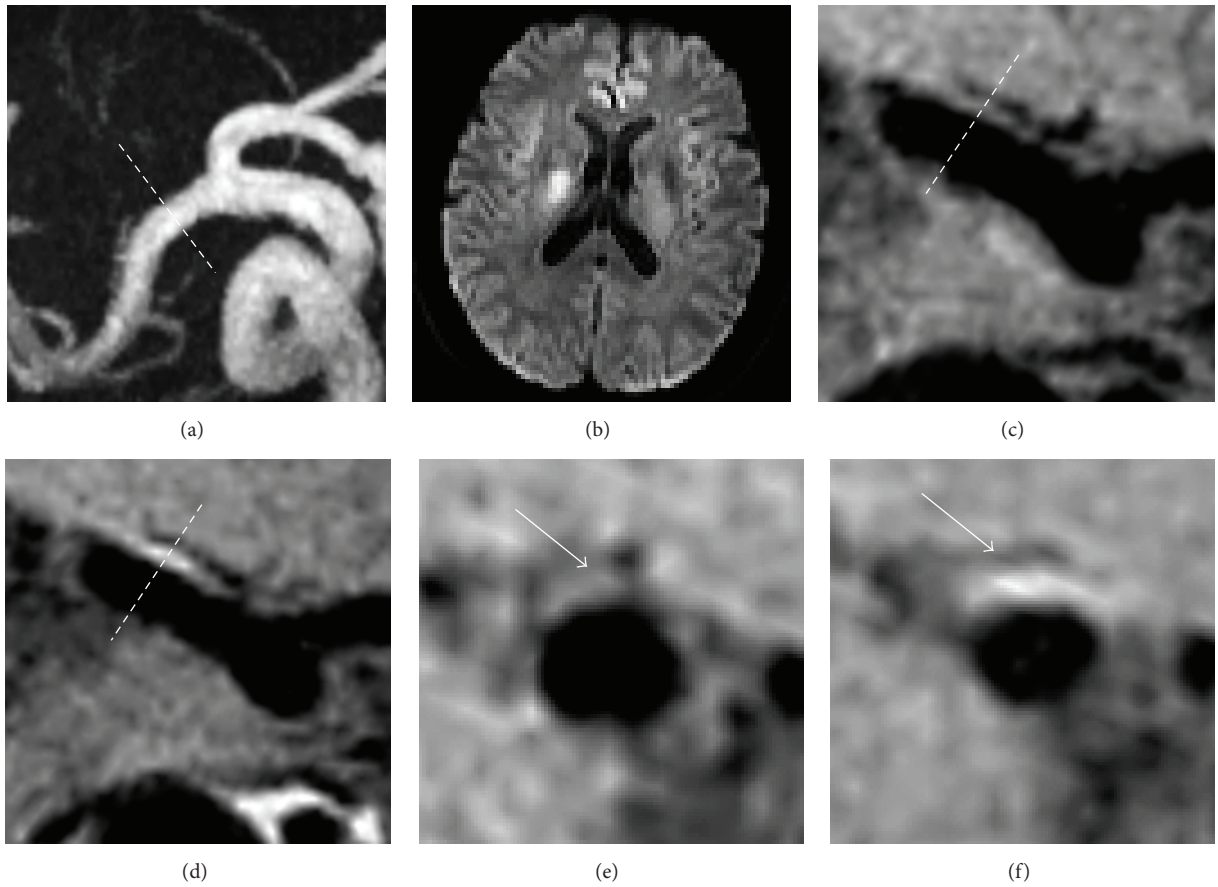

Figure 3: A 59-year-old man with left-side weakness. (a) MRA shows no stenosis on right MCA; (b) the diffusion-weighted image shows a hypertensive lesion in the right lenticular nucleus which extends to the coronal radiate; precontrast T1-weighted SPACE images did not show eccentric wall thickening clearly on both the long axis (c) and short axis ((e), arrow) of the MCA; postcontrast T1-weighted SPACE images show wall thickening ipsilateral to the infarct on both the long axis (d) and short axis ((f), arrow) of the MCA.

voxel size in this study is still comparable to other studies using 2D techniques where the voxel sizes were in the range of 0.33 mm^3 to 0.36 mm^3. Additionally, our study population included only symptomatic patients with a normal lumen, and the results may not be directly applicable to patients with MCA stenosis caused by atherosclerotic plaques.

5. Conclusions

The current findings indicate that 3D high-resolution vessel wall imaging improves the visualization of MCA plaques and holds promise as a valuable alternative to current 2D MRI techniques. Our results suggest that atherosclerosis may be more prevalent among patients with RSSI than commonly believed. Superiorly located MCA plaques are associated with ipsilateral infarctions and may have an important role in the pathogenesis of RSSI. Plaques found in these patients with RSSI are mostly enhanced. Further studies are required to explore the relevance of these findings to the subclassification of stroke.

Conflict of Interests

The authors declare that they have no conflict of interests.

Authors' Contribution

Xiao-Dong Zou and Yiu-Cho Chung contributed equally to this paper.

Acknowledgments

The authors would like to thank Dr. Xin Liu for the valuable discussions. This study was supported by Key Medical Professional Development Plan of Beijing Municipal Administration of Hospitals (ZY201301), the Major Project of the Science and Technology Plan of the Beijing Municipal Science & Technology Commission (D111107003111009), and the Key Project of the National Natural Science Foundation of China (30830045), and Kallikrein Medical Research Program (201206006) This study was also

supported by 2013CB733800/2013CB733803, 81470077, JCYJ20140417113430589, and JSGG20141020103440414.

References

[1] J. Boiten, J. Lodder, and F. Kessels, "Two clinically distinct lacunar infarct entities? A hypothesis," *Stroke*, vol. 24, no. 5, pp. 652–656, 1993.

[2] C. M. Fisher, "Lacunes: small, deep cerebral infarcts," *Neurology*, vol. 15, pp. 774–784, 1965.

[3] C. M. Fisher, "The arterial lesions underlying lacunes," *Acta Neuropathologica*, vol. 12, no. 1, pp. 1–15, 1969.

[4] T. Adachi, S. Kobayashi, S. Yamaguchi, and K. Okada, "MRI findings of small subcortical 'lacunar-like' infarction resulting from large vessel disease," *Journal of Neurology*, vol. 247, no. 4, pp. 280–285, 2000.

[5] I. F. Klein, P. C. Lavallée, M. Mazighi, E. Schouman-Claeys, J. Labreuche, and P. Amarenco, "Basilar artery atherosclerotic plaques in paramedian and lacunar pontine infarctions: a high-resolution MRI study," *Stroke*, vol. 41, no. 7, pp. 1405–1409, 2010.

[6] W.-H. Xu, M.-L. Li, J.-W. Niu, F. Feng, Z.-Y. Jin, and S. Gao, "Intracranial artery atherosclerosis and lumen dilation in cerebral small-vessel diseases: a high-resolution MRI Study," *CNS Neuroscience & Therapeutics*, vol. 20, no. 4, pp. 364–367, 2014.

[7] J. Chung, B. J. Kim, C. H. Sohn, B. Yoon, and S. Lee, "Branch atheromatous plaque: a major cause of lacunar infarction (high-resolution MRI study)," *Cerebrovascular Diseases Extra*, vol. 2, no. 1, pp. 36–44, 2012.

[8] Y. Yoon, D. H. Lee, D.-W. Kang, S. U. Kwon, and J. S. Kim, "Single subcortical infarction and atherosclerotic plaques in the middle cerebral artery: high-resolution magnetic resonance imaging findings," *Stroke*, vol. 44, no. 9, pp. 2462–2467, 2013.

[9] Y. Qiao, D. A. Steinman, Q. Qin et al., "Intracranial arterial wall imaging using three-dimensional high isotropic resolution black blood MRI at 3.0 Tesla," *Journal of Magnetic Resonance Imaging*, vol. 34, no. 1, pp. 22–30, 2011.

[10] J. M. Wardlaw, E. E. Smith, G. J. Biessels et al., "Neuroimaging standards for research into small vessel disease and its contribution to ageing and neurodegeneration," *The Lancet Neurology*, vol. 12, no. 8, pp. 822–838, 2013.

[11] J. Park, J. P. Mugler III, W. Horger, and B. Kiefer, "Optimized T1-weighted contrast for single-slab 3D turbo spin-echo imaging with long echo trains: application to whole-brain imaging," *Magnetic Resonance in Medicine*, vol. 58, no. 5, pp. 982–992, 2007.

[12] G. Mihai, Y.-C. Chung, A. Merchant, O. P. Simonetti, and S. Rajagopalan, "T1-weighted-space dark blood whole body magnetic resonance angiography (DB-WBMRA): initial experience," *Journal of Magnetic Resonance Imaging*, vol. 31, no. 2, pp. 502–509, 2010.

[13] L. Zhang, N. Zhang, J. Wu et al., "High resolution three dimensional intracranial arterial wall imaging at 3T using T1 weighted SPACE," *Magnetic Resonance Imaging*, 2015.

[14] L. Tatu, T. Moulin, J. Bogousslavsky, and H. Duvernoy, "Arterial territories of the human brain: cerebral hemispheres," *Neurology*, vol. 50, no. 6, pp. 1699–1708, 1998.

[15] H. Gibo, C. C. Carver, A. L. Rhoton Jr., C. Lenkey, and R. J. Mitchell, "Microsurgical anatomy of the middle cerebral artery," *Journal of Neurosurgery*, vol. 54, no. 2, pp. 151–169, 1981.

[16] F. Umansky, F. B. Gomes, M. Dujovny et al., "The perforating branches of the middle cerebral artery. A microanatomical study," *Journal of Neurosurgery*, vol. 62, no. 2, pp. 261–268, 1985.

[17] X. Lou, N. Ma, H. Shen, K. Shi, W. Jiang, and L. Ma, "Noninvasive visualization of the basilar artery wall and branch ostia with high-resolution three-dimensional black-blood sequence at 3 tesla," *Journal of Magnetic Resonance Imaging*, vol. 39, no. 4, pp. 911–916, 2014.

[18] A. M. Varnava, P. G. Mills, and M. J. Davies, "Relationship between coronary artery remodeling and plaque vulnerability," *Circulation*, vol. 105, no. 8, pp. 939–943, 2002.

[19] W.-H. Xu, M.-L. Li, S. Gao et al., "In vivo high-resolution MR imaging of symptomatic and asymptomatic middle cerebral artery atherosclerotic stenosis," *Atherosclerosis*, vol. 212, no. 2, pp. 507–511, 2010.

[20] L. Antiga, B. A. Wasserman, and D. A. Steinman, "On the overestimation of early wall thickening at the carotid bulb by black blood MRI, with implications for coronary and vulnerable plaque imaging," *Magnetic Resonance in Medicine*, vol. 60, no. 5, pp. 1020–1028, 2008.

[21] S. V. Marinkovic, M. S. Kovacevic, and J. M. Marinkovic, "Perforating branches of the middle cerebral artery. Microsurgical anatomy of their extracerebral segments," *Journal of Neurosurgery*, vol. 63, no. 2, pp. 266–271, 1985.

[22] H. P. Adams Jr., B. H. Bendixen, L. J. Kappelle et al., "Classification of subtype of acute ischemic stroke: definitions for use in a multicenter clinical trial," *Stroke*, vol. 24, no. 1, pp. 35–41, 1993.

[23] H. Ay, K. L. Furie, A. Singhal, W. S. Smith, A. G. Sorensen, and W. J. Koroshetz, "An evidence-based causative classification system for acute ischemic stroke," *Annals of Neurology*, vol. 58, no. 5, pp. 688–697, 2005.

[24] S. Gao, Y. J. Wang, A. D. Xu, Y. S. Li, and D. Z. Wang, "Chinese ischemic stroke subclassification," *Frontiers in Neurology*, vol. 2, article 6, 2011.

[25] W.-H. Xu, M.-L. Li, S. Gao et al., "Plaque distribution of stenotic middle cerebral artery and its clinical relevance," *Stroke*, vol. 42, no. 10, pp. 2957–2959, 2011.

[26] C. M. Fisher, "Capsular infarcts. The underlying vascular lesions," *Archives of Neurology*, vol. 36, no. 2, pp. 65–73, 1979.

[27] A. Millon, L. Boussel, M. Brevet et al., "Clinical and histological significance of gadolinium enhancement in carotid atherosclerotic plaque," *Stroke*, vol. 43, no. 11, pp. 3023–3028, 2012.

[28] T. Ibrahim, M. R. Makowski, A. Jankauskas et al., "Serial contrast-enhanced cardiac magnetic resonance imaging demonstrates regression of hyperenhancement within the coronary artery wall in patients after acute myocardial infarction," *JACC: Cardiovascular Imaging*, vol. 2, no. 5, pp. 580–588, 2009.

[29] M. Skarpathiotakis, D. M. Mandell, R. H. Swartz, G. Tomlinson, and D. J. Mikulis, "Intracranial atherosclerotic plaque enhancement in patients with ischemic stroke," *American Journal of Neuroradiology*, vol. 34, no. 2, pp. 299–304, 2013.

[30] P. Vakil, J. Vranic, M. C. Hurley et al., "T1 gadolinium enhancement of intracranial atherosclerotic plaques associated with symptomatic ischemic presentations," *American Journal of Neuroradiology*, vol. 34, no. 12, pp. 2252–2258, 2013.

[31] Y. Qiao, S. R. Zeiler, S. Mirbagheri et al., "Intracranial plaque enhancement in patients with cerebrovascular events on high-spatial-resolution MR images," *Radiology*, vol. 271, no. 2, pp. 534–542, 2014.

[32] I. F. Klein, P. C. Lavallée, P. J. Touboul, E. Schouman-Claeys, and P. Amarenco, "In vivo middle cerebral artery plaque imaging by high-resolution MRI," *Neurology*, vol. 67, no. 2, pp. 327–329, 2006.

Hindawi Publishing Corporation
BioMed Research International
Volume 2015, Article ID 739586, 8 pages
http://dx.doi.org/10.1155/2015/739586

Research Article

SAMHD1 Gene Mutations Are Associated with Cerebral Large-Artery Atherosclerosis

Wei Li,[1,2] Baozhong Xin,[3] Junpeng Yan,[4] Ying Wu,[5] Bo Hu,[6] Liping Liu,[1,2] Yilong Wang,[1,2] Jinwoo Ahn,[5] Jacek Skowronski,[4] Zaiqiang Zhang,[1,2] Yongjun Wang,[1,2] and Heng Wang[3,7,8,9]

[1]*Department of Neurology, Beijing Tiantan Hospital, Capital Medical University, Beijing 100050, China*
[2]*China National Clinical Research Centre for Neurological Diseases, Centre of Stroke, Beijing Institute for Brain Disorders, Beijing Key Laboratory of Translational Medicine for Cerebrovascular Disease, Beijing 100050, China*
[3]*DDC Clinic-Center for Special Needs Children, Middlefield, OH 44062, USA*
[4]*Department of Molecular Biology and Microbiology, Case Western Reserve University School of Medicine, Cleveland, OH 44193, USA*
[5]*Department of Structural Biology, University of Pittsburgh School of Medicine, Pittsburgh, PA 45358, USA*
[6]*Department of Quantitative Health Sciences, Cleveland Clinic, Cleveland, OH 44193, USA*
[7]*Department of Pediatrics, Case Western Reserve University Medical School, Cleveland, OH 44193, USA*
[8]*Rainbow Babies & Children's Hospital, Cleveland, OH 44193, USA*
[9]*Department of Molecular Cardiology, Cleveland Clinic, Cleveland, OH 44195, USA*

Correspondence should be addressed to Yongjun Wang; yongjunwang1962@gmail.com and Heng Wang; wang@ddcclinic.org

Received 26 July 2015; Revised 11 September 2015; Accepted 15 September 2015

Academic Editor: Vida Demarin

Background. To investigate whether one or more *SAMHD1* gene mutations are associated with cerebrovascular disease in the general population using a Chinese stroke cohort. *Methods*. Patients with a Chinese Han background ($N = 300$) diagnosed with either cerebral large-artery atherosclerosis (LAA, $n = 100$), cerebral small vessel disease (SVD, $n = 100$), or other stroke-free neurological disorders (control, $n = 100$) were recruited. Genomic DNA from the whole blood of each patient was isolated, and direct sequencing of the *SAMHD1* gene was performed. Both wild type and mutant SAMHD1 proteins identified from the patients were expressed in *E. coli* and purified; then their dNTPase activities and ability to form stable tetramers were analysed *in vitro*. *Results*. Three heterozygous mutations, including two missense mutations c.64C>T (P22S) and c.841G>A (p.E281K) and one splice site mutation c.696+2T>A, were identified in the LAA group with a prevalence of 3%. No mutations were found in the patients with SVD or the controls ($p = 0.05$). The mutant SAMHD1 proteins were functionally impaired in terms of their catalytic activity as a dNTPase and ability to assemble stable tetramers. *Conclusions*. Heterozygous *SAMHD1* gene mutations might cause genetic predispositions that interact with other risk factors, resulting in increased vulnerability to stroke.

1. Introduction

Increasing evidence suggests that there is a significant genetic predisposition to cerebrovascular disorders, and these genetic risk factors may account for some portion of the unexplained risk of stroke [1–4]. Identifying these genetic risk factors will not only allow better risk prediction but also provide valuable insights into the mechanism of disease development. The discovery of novel genes associated with stroke may reveal novel pathways involved in stroke pathogenesis, thereby resulting in new targeted treatments and effective prevention [5].

We have recently described a cohort of patients from the Old Order Amish, an inbred population who present a functional loss of the *SAMHD1* (sterile alpha motif and histidine-aspartate (HD) domain-containing protein-1) gene resulting from a homozygous c.1411-2A>G mutation [6]. Although this autosomal recessive condition is heterogeneous, involving multiple systems, the presence of cerebral vasculopathy appears to be a major hallmark of the condition [6, 7]. Similar

cerebrovascular findings have also been reported in patients with other *SAMHD1* mutations [8, 9].

The *SAMHD1* gene was originally identified from a human dendritic cell cDNA library as an ortholog of the mouse IFN-γ-induced gene *Mg11* [10] and was recently linked to a rare genetic condition, Aicardi-Goutières syndrome [11]. Recent studies have revealed that SAMHD1 is a dGTP-regulated deoxyribonucleoside triphosphate triphosphohydrolase (dNTPase) [12–15], and its tetramerisation is required for biological activity [16, 17]. Due to this structural feature, it has been tempting to speculate that a single mutation in one allele of the *SAMHD1* gene may act in a dominant negative manner with the potential to become pathogenic in humans [18].

Considering the roles of the *SAMHD1* gene in human innate immunity [10], the clinical findings of monogenic linkage studies [11], and its unique structural requirement for catalytic and biological activity [12–18], we hypothesised that the *SAMHD1* gene may be associated with stroke in the general population. In this study, we investigated this hypothesis in a stroke cohort with a completely different ethnic background from that of the original studies linking *SAMHD1* mutations to cerebral vasculopathy.

2. Methods

2.1. Patients. Patients with a Chinese Han background were recruited from Tiantan Hospital in Beijing, China, from June 2009 to September 2012, either as consecutive outpatients or as inpatients admitted to the Neurology department. Comprehensive clinical evaluations, consisting of a stroke risk assessment and routine hematologic and metabolic assays, including C-reactive protein, erythrocyte sedimentation rate (ESR), and a fasting lipid profile, were performed for each subject. All subjects underwent brain MR imaging with angiography or a CT scan, carotid artery ultrasound, and transcranial Doppler screening. The study was approved by the Ethics Committees/Institutional Review Board of Beijing Tiantan Hospital, Capital Medical University, and written informed consent was obtained from each participant or his/her legal guardian.

Among the 1765 patients with cerebral large-artery atherosclerosis (LAA) and the 428 patients with cerebral small vessel disease (SVD) recruited throughout this investigation, 100 patients from each group were randomly selected to participate in the study. In addition, 100 stroke-free patients were selected as a control group. All 300 subjects were of Chinese Han genetic background. Detailed patient information is summarized in Table 1.

Large-artery atherosclerosis was defined as a stroke caused by atherosclerosis and was categorised as carotid, vertebral, or basilar artery stenosis of more than 50% according to carotid artery ultrasound or MR angiography. A patient with SVD was defined as having one of four imaging features (lacunar infarcts, leukoaraiosis, microbleeds, and dilatation of the perivascular spaces), whereas patients with subcortical lesions of more than 1.5 cm in diameter, a cortical infarct of any size, a potential cardioembolic source, parent artery stenosis, and other large-vessel diseases were excluded. The control group was recruited from stroke-free patients who had another type of neurological disorder, such as epilepsy or Parkinson's disease, but were free of any symptomatic cerebrovascular disease, such as transient ischemic attack. Asymptomatic cerebrovascular diseases were also ruled out in control individuals according to MR imaging or CT scans.

Table 1: Age and gender distributions among the patients.

	LAA ($n = 100$)	SVD ($n = 100$)	Control ($n = 100$)
Age (years)	59.3 ± 9.5	59.8 ± 9.1	62.9 ± 6.3
Gender (M/F)	76/24	55/45	50/50

LAA = cerebral large-artery atherosclerosis; SVD = cerebral small vessel disease.
Control = stroke-free control.
The ages are expressed as the means ± SD, with N in parentheses indicating the total number of patients in each group.

2.2. DNA Sequencing and Mutation Identification. Genomic DNA from whole blood collected from each patient was isolated as previously described [19]. PCR primers were designed to amplify each of the 16 protein-coding exons of the *SAMHD1* gene and their flanking intronic sequences. Direct sequencing of the PCR products was performed using an ABI 3130XL sequencer, and sequencing files were analysed using PolyPhred software. Sample sequences were compared with the reference sequences from GenBank to identify sequence variants. GenBank accession numbers NM_015474.3 and NP_056289.2 were used as the *SAMHD1* cDNA and protein sequence references.

2.3. Recombinant SAMHD1 Proteins and Activity Assays. Wild type and mutant SAMHD1 proteins bearing missense mutations identified in patients from this cohort were expressed in *E. coli* and purified to near homogeneity as described previously [16, 20]. The effect of mutations on SAMHD1 function was assessed using two assays: (i) dNTPase activity *in vitro* and (ii) the ability to assemble stable tetramers, the functional form of the enzyme [16, 17]. The dNTPase assays were performed in 10 mM Tris-HCl, pH 7.5, 50 mM NaCl, 5 mM $MgCl_2$, and 100 nM recombinant SAMHD1 in the presence of the indicated concentrations of dGTP at 25°C. The dG nucleoside products in reaction aliquots were collected at various time points and then quantified by HPLC as described previously [16]. To assess the tetramerisation ability of SAMHD1, 100 μL aliquots of SAMHD1 (250 nM) were mixed with dGTP at the indicated concentrations (0 to 200 μM), injected into the analytical Superdex200 column (24 mL), equilibrated with Tris-HCl, pH 7.8, 50 mM NaCl, 5% glycerol, and 0.02% sodium azide, and separated at a flow rate of 0.8 mL/min [16]. The elution profiles were recorded by monitoring fluorescence traces with an excitation wavelength of 282 nm and an emission wavelength of 313 nm. The areas of the peaks corresponding to the SAMHD1 tetramer (ordinate) were plotted as a function of dGTP concentrations (abscissa).

Table 2: Additional clinical features in patients with *SAMHD1* mutations.

	Gender	Age (years)	Stroke risk factors	Mutations identified
Case 1	M	58	Hypertension Hyperlipidaemia Hyperhomocysteinaemia Smoking Drinking	Exon 1 c.64C>T (p.Pro22Ser)
Case 2	M	39	Hyperlipidaemia Smoking Drinking	Intron 6 c.696+2T>A (putative aberrant splicing)
Case 3	M	56	Hypertension Hyperlipidaemia Smoking Drinking	Exon 7 c.841G>A (p.Glu281Lys)

2.4. Statistical Analysis. Age was summarised using means and standard deviations, and gender was summarised using frequencies for patient groups. The Fisher exact test was used to compare the *SAMHD1* mutation frequencies between the groups. A two-sided p value less than 0.05 was considered statistically significant. All analyses were conducted using SAS 9.2 (Cary, NC).

3. Results

Genomic DNA sequencing of the *SAMHD1* gene in all study subjects revealed numerous sequence variants in all three groups (see Supplemental Table e-1 available online at http://dx.doi.org/10.1155/2015/739586). However, of all detected variants, only three variants identified in the LAA group were predicted to affect the protein (Table 2, Figure 1). In contrast, none of the other variants identified in the SVD and control groups caused a change in the SAMHD1 amino acid sequence. The three mutations identified in the LAA group included two missense mutations, c.64C>T (P22S) and c.841G>A (p.E281K), and one splice site mutation c.696+2T>A in intron 6, leading to a putative aberrant splicing event. As shown in Figure 2, the two missense mutations, P22S and E281K, caused amino acid substitutions located proximally to the conserved SAM domain and in the catalytic core of the enzyme, respectively.

The calculated prevalence of *SAMHD1* mutations in the patients of the LAA group was 3%, compared to none in the primary SVD and control groups ($p = 0.05$). The three patients identified with *SAMHD1* mutations in the LAA group were all males. Stroke risk factors, such as hypertension, hyperlipidaemia, hyperhomocysteinaemia, and tobacco and alcohol use, were also identified in all three patients (Table 2).

None of the three variants has been reported previously or is present in the 1000 Genomes Project database (http://www.1000genomes.org/). In the ExAC database (http://exac.broadinstitute.org/), the P22S and E281K missense mutations have only been observed in a frequency of 0.0008% and 0.002%, respectively. *In silico* prediction programs predicted the P22S variant to be deleterious (SIFT) or probably damaging (PolyPhen-2), whereas the E281K was predicted as benign variant by both programs.

The association of two missense mutations (P22S and E281K) with stroke suggested that they may have a deleterious effect on SAMHD1-folding and/or function. As a first step to assess this possibility, we examined the recently solved crystal structure of the dGTP-bound SAMHD1 catalytic core (residues 113–626) [17]. The E281 residue is located in the SAMHD1 catalytic core in a loop that appears to be disordered in the structure (Figure 3(a)). The P22 residue resides in the N-terminus, proximal to the SAM domain, and is not present in the structure. Hence, while revealing that both stroke-associated SAMHD1 variant mutations were likely located in unstructured regions, which are known to be frequently involved in interactions with ligands, this information unfortunately failed to provide any direct clues regarding the possible impact of mutations on SAMHD1 structure and function.

We next investigated the biochemical activities of the two substitution variants in the context of full-length SAMHD1 proteins. Biochemical and structural characterisation of SAMHD1 established that the biologically active form is a tetramer induced by dGTP binding at allosteric regulatory sites of the enzyme [16, 17]. Therefore, to assess the possible adverse effects of these mutations on SAMHD1 function, the propensity of SAMHD1 to undergo dGTP-ligand-induced tetramerisation was determined over a wide range of dGTP concentrations. As shown in Figures 3(b) and 3(c), wild type SAMHD1 and both mutants showed increased tetramer content with increasing dGTP concentrations. However, both the P22S and E281K substitutions led to a dramatic reduction in ligand-dependent tetramerisation compared to wild type SAMHD1, even in the presence of the highest dGTP concentration, which indicates that these variants are functionally defective. Thus, we determined the dNTPase activities of both mutants and wild type SAMHD1 as a control (Figure 3(d)). The catalytic activity of the E281K mutant was severely diminished, as predicted by the results of tetramerisation assays (Figures 3(b) and 3(c)). The P22S mutant also showed

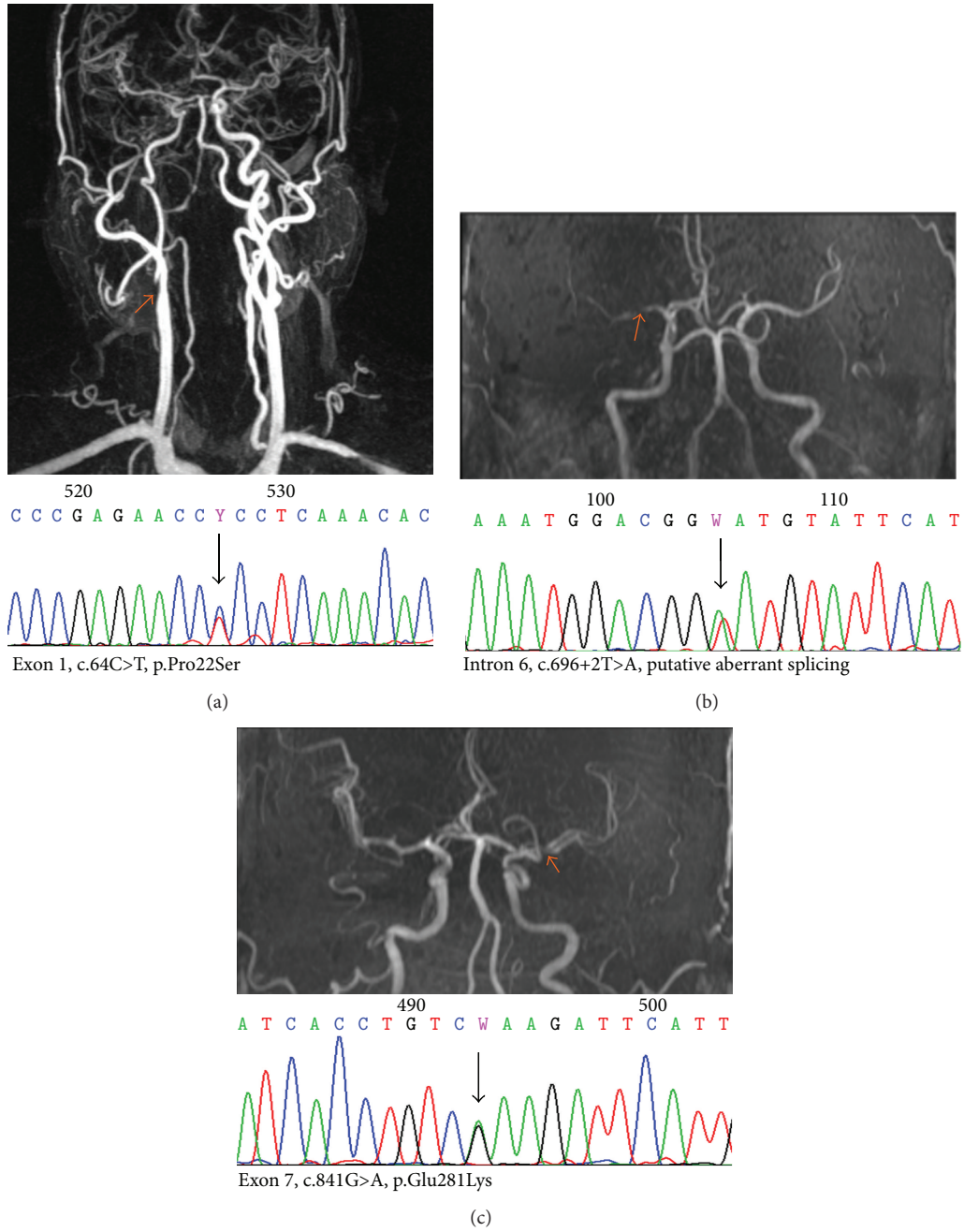

Figure 1: Radiologic findings of the cerebral large arteries in 3 patients with *SAMHD1* gene mutations. In each panel (a–c) the abnormal neuroimaging findings (upper) and sequence electropherogram with the identified *SAMHD1* mutation (lower) are shown. The imaging examination was performed with either contrast-enhanced magnetic resonance angiography (a) or magnetic resonance angiography (b and c). Orange-coloured arrows indicate stenoses of the large arteries and black arrows show the mutations of the *SAMHD1* gene.

greatly reduced catalytic activity. Taken together, the results of these functional analyses indicate that both mutations exert a negative effect on the biological functions of SAMHD1.

4. Discussion

SAMHD1 was originally identified in a human dendritic cell cDNA library as an ortholog of the mouse IFN-γ-induced gene Mg11 and was previously called dendritic cell derived IFN-γ-induced protein (DCIP) [10]. High expression levels of the protein in human macrophage and dendritic cells suggested a role in the innate immune response [10, 21, 22]. A previous linkage study of *SAMHD1* with Aicardi-Goutières syndrome associated the gene with a human disease for the first time [11]. Recent studies of *SAMHD1* during HIV infection have significantly increased our understanding of its important role in restricting viral infections [12, 13, 23], as well as its biochemical functions [14–18]. The present study

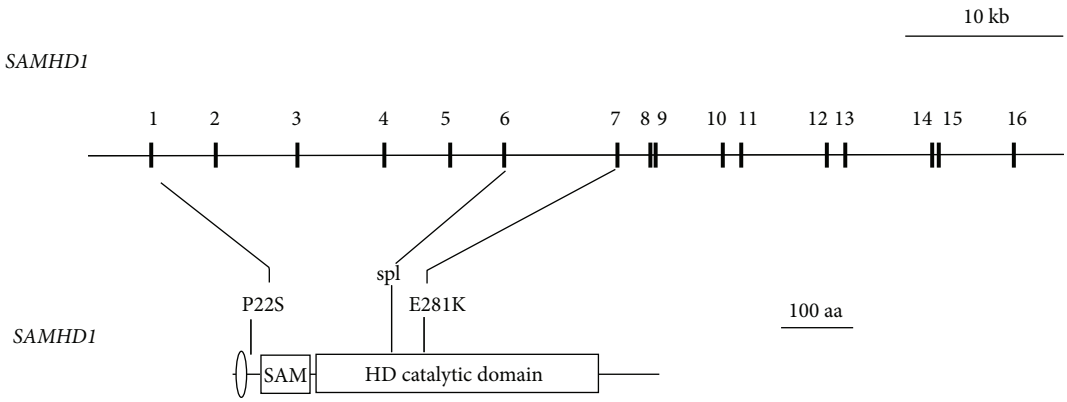

Figure 2: *SAMHD1* mutations in LAA patients. Schematic representation of the 16-exon *SAMHD1* gene (upper panel) and its 626-amino-acid gene product (lower panel). Sixteen exons encode a 626-amino-acid protein that comprises two structural domains. The SAM (sterile alpha motif) and HD (histidine-aspartate) domains are connected by a flexible linker. An oval indicates the location of a nuclear localisation signal. Locations of the missense (P22S, Q281K) and exon 6 splice donor (spl) mutations found in LAA patients are indicated.

revealed that *SAMHD1* gene mutations are associated with LAA in a Chinese stroke cohort.

In this study, heterozygous mutations have been identified in three patients with LAA, representing 3% of the patients in the group, whereas no mutations were found among 200 patients with SVD or stroke-free controls. We have previously described an autosomal recessive condition in the Old Order Amish population in which a functional loss of *SAMHD1* occurs due to a homozygous c.1411-2A>G mutation [6], with cerebral vasculopathy and an early onset of stroke being major hallmarks. Hence, we have proposed "SAMS (an acronym of cerebrovascular stenosis, aneurysm, moyamoya, and stroke) association" as the name of the disease [7]. The SAMS association seems to affect both large and small cerebral vessels, although cerebral vasculopathy is more predominant in large vessels [6]. In this study, we found that the heterozygous mutations in *SAMHD1* were only associated with LAA.

The phenotype of the patients with heterozygous *SAMHD1* gene mutations appeared less severe than that of SAMS-associated patients. The three individuals with *SAMHD1* mutations from the LAA group showed no signs of other system involvements, unlike the patients with SAMS association [6]. Therefore, based on the course and severity of the disease, one might speculate that the patients with heterozygous mutations manifest a mild type of SAMS association.

However, it should be noted that, along with *SAMHD1* mutations, multiple stroke risk factors, such as hypertension, hyperlipidaemia, hyperhomocysteinaemia, and alcohol and tobacco use, were also identified in all three patients. Thus, we suggest that *SAMHD1* mutations might create a genetic predisposition for stroke that leads to an increased vulnerability to stroke in those patients by interacting with other risk factors.

The exact mechanism of how the *SAMHD1* mutations serve as a genetic predisposition for stroke remains unclear. However, our functional studies indicate that the missense mutations c.64C>T (P22S) and c.841G>A (E281K) identified in the stroke patients impair the function of the SAMHD1 protein (Figures 3(b)–3(d)). It is interesting to note that residue 281 was not resolved in the SAMHD1 dimer structure, an inactive conformer of the enzyme, nor the tetramer, the catalytically active form [16, 17]. In both crystal structures, the loop containing residue 281 resides at the surface of the protein, away from both the ligand-binding allosteric site and the catalytic site. However, the E281K mutant failed to form a stable ligand-bound tetramer and showed a concomitant reduction in its catalytic activity. Thus, it is tempting to speculate that the unresolved region, including residue 281, may interact with a region of SAMHD1 other than the catalytic core to stabilise the tetramer. Consistent with this notion, the P22S mutant located at the N-terminus exerted a similar effect, although the difference was less significant. The other mutation, c.696+2T>A, was predicted to produce a SAMHD1 protein with severely truncated catalytic domains, precluding it from being an active dNTPase. Increasing evidence indicates that SAMHD1 may act as an immunomodulator that plays a protective role by preventing the self-activation of innate immunity [24, 25]. Our reported findings here suggest that impaired functions of this protein might result in an unremittingly proinflammatory status in the affected individuals, thus directly or indirectly initiating progression of the pathological process of LAA. Several lines of evidence implicate SAMHD1 in immune function, as it is upregulated in response to viral infections and is thought to play a role in mediating TNF-α proinflammatory responses [22, 26, 27]. However, TNF-α is significantly associated with large-artery atherosclerosis [28], suggesting that SAMHD1 may initiate the progression of LAA via the TNF-α pathway. Indeed, abnormal laboratory findings, including elevated ESR, immunoglobulin G, neopterin, and TNF-α, have been found in patients with the homozygous mutation [6], whereas moderately increased levels of cytokines have been observed in heterozygous carriers of the c.1411-2A>G mutation (unpublished data).

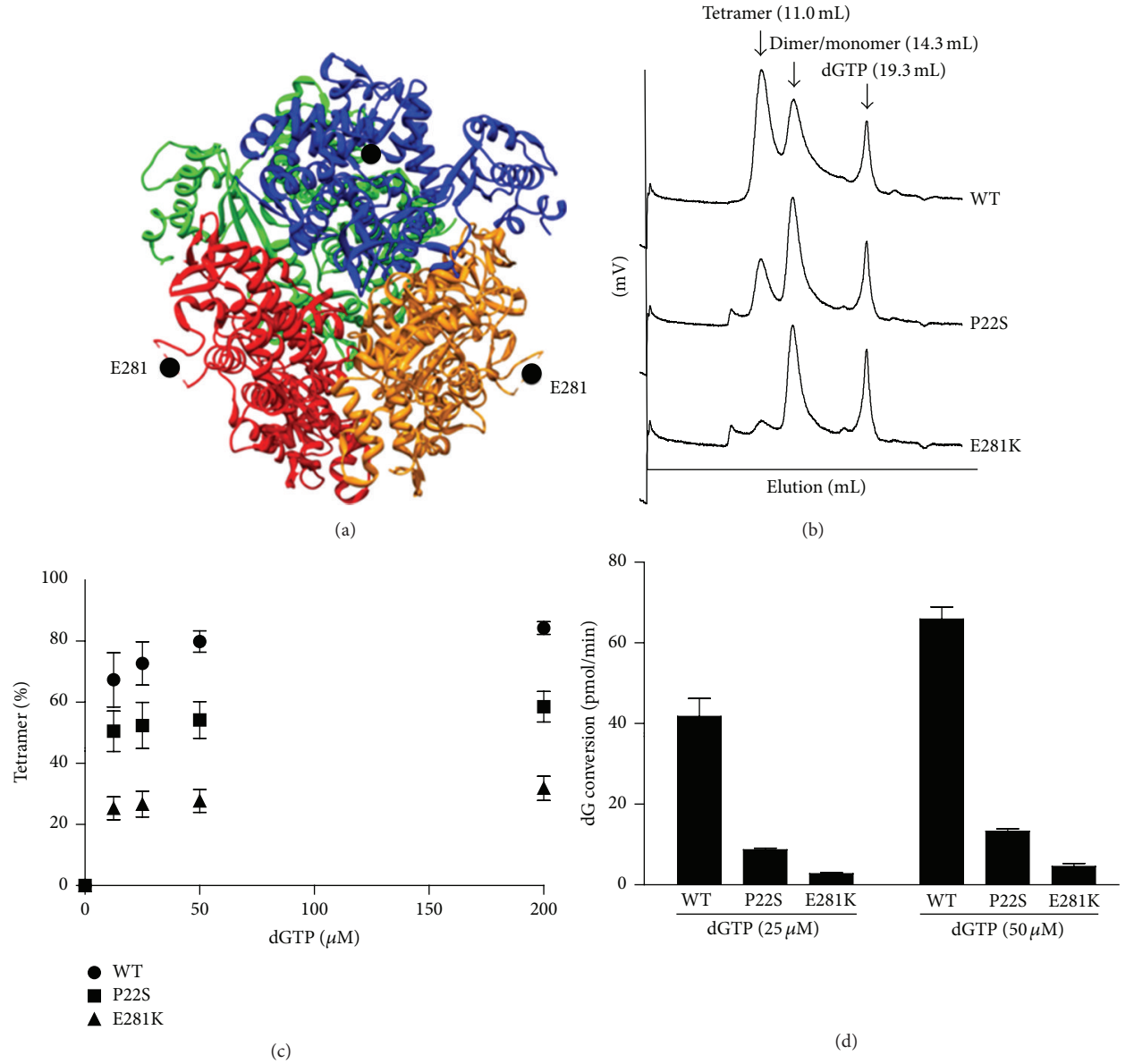

Figure 3: *SAMHD1* mutations from individuals with stroke diminish SAMHD1 tetramerisation and dNTP hydrolase activity. (a) The crystal structure of the tetrameric SAMHD1 catalytic core (residues 113–626; PDB ID, 4BZB) is shown with the position of residue E281 (•) indicated. Residues 278–283 (SPVEDS) were not resolved [17]. Each subunit is rendered with a different colour. (b) SAMHD1 stroke patient mutations interfere with SAMHD1 tetramerisation. Wild type and mutant recombinant SAMHD1 proteins (250 nM) were preincubated with dGTP (25 μM), and the mixtures were separated on an analytical gel filtration column. The peaks corresponding to SAMHD1 tetramers, dimers/monomers, and dGTP are indicated. (c) The extent of SAMHD1 tetramerisation was determined with various concentrations of dGTP (0 to 200 μM) as described in (b). (d) dGTP-dependent dGTPase activity of recombinant SAMHD1. The standard error from triplicate samples is shown.

The vast majority of strokes are increasingly recognized as polygenic events. Although monogenic causes of stroke are rare, identification of these genes and mutations is important to provide critical information for the diagnosis, treatment, and prognosis of affected individuals. Furthermore, identifying novel gene variants associated with stroke may reveal novel pathways involved in stroke pathogenesis and thus result in new targeted treatments and more effective prevention of stroke. In this study, although the incidence of *SAMHD1* mutations in LAA patients was only 3%, this prevalence is noteworthy in light of the complexity of the multiple genetic and environmental risk factors that influence the disease. Because the study was intentionally performed in a completely different population from that of the original studies linking *SAMHD1* mutations and cerebral vasculopathy, the implication may be more prominent. Further studies involving additional patient populations and exploring the mechanism underlying the effect of *SAMHD1* mutations on

the development of LAA in the general population will be valuable, not only for patients who are directly affected but also for stroke patients in general.

Conflict of Interests

The authors have no conflict of interests.

Acknowledgments

The authors appreciate the support from all the study participants. They thank all of the physicians at the Beijing Tiantan Hospital who provided help with patient recruitment and clinical evaluations. They are grateful to Shanghai Genesky Bio-Tech Co., Ltd., for the technical support and data analysis of DNA sequencing and to Maria DeLucia, Jennifer Mehrens, and Caili Hao for their excellent technical assistance. This work was supported by the Clinical Database and Biological Samples Establishment for Cerebrovascular Diseases in Beijing (D09050703560904), Beijing Biobank of Cerebral Vascular Disease (D131100005313003), National Key Technology Research and Development Program of the Ministry of Science and Technology of China (2013BAI09B03), BIBD-PXM2013_014226_07_000084, Key Project of the Beijing Board of Education Science and Technology (KM201410025028), Basic-Clinical Research Cooperation Fund of Capital Medical University (14JL54), Elisabeth Severance Prentiss Foundation, Reinberger Foundation, Leonard Krieger Fund of the Cleveland Foundation (L2009-0078), and William Bingham Foundation, as well as by NIH Grants (AI100673 and P50GM082251).

References

[1] R. L. Sacco, J. H. Ellenberg, J. P. Mohr et al., "Infarcts of undetermined cause: the NINCDS stroke data bank," *Annals of Neurology*, vol. 25, no. 4, pp. 382–390, 1989.

[2] J. Francis, S. Raghunathan, and P. Khanna, "The role of genetics in stroke," *Postgraduate Medical Journal*, vol. 83, no. 983, pp. 590–595, 2007.

[3] H. S. Markus, "Stroke genetics," *Human Molecular Genetics*, vol. 20, no. 2, pp. R124–R131, 2011.

[4] P. Munot, Y. J. Crow, and V. Ganesan, "Paediatric stroke: genetic insights into disease mechanisms and treatment targets," *The Lancet Neurology*, vol. 10, no. 3, pp. 264–274, 2011.

[5] H. S. Markus, "Stroke genetics: prospects for personalized medicine," *BMC Medicine*, vol. 10, article 113, 2012.

[6] B. Xin, S. Jones, E. G. Puffenberger et al., "Homozygous mutation in SAMHD1 gene causes cerebral vasculopathy and early onset stroke," *Proceedings of the National Academy of Sciences of the United States of America*, vol. 108, no. 13, pp. 5372–5377, 2011.

[7] B. Xin, W. Li, A. Bright, C. Hinze, and H. Wang, "Cerebral vasculopathy is a common hallmark in individuals with *SAMHD1* mutations," *Proceedings of the National Academy of Sciences of the United States of America*, vol. 108, no. 26, article E233, 2011.

[8] H. Thiele, M. du Moulin, K. Barczyk et al., "Cerebral arterial stenoses and stroke: novel features of Aicardi-Goutières syndrome caused by the Arg164X mutation in SAMHD1 are associated with altered cytokine expression," *Human Mutation*, vol. 31, no. 11, pp. E1836–E1850, 2010.

[9] V. Ramesh, B. Bernardi, A. Stafa et al., "Intracerebral large artery disease in Aicardi-Goutières syndrome implicates SAMHD1 in vascular homeostasis," *Developmental Medicine and Child Neurology*, vol. 52, no. 8, pp. 725–732, 2010.

[10] N. Li, W. Zhang, and X. Cao, "Identification of human homologue of mouse IFN-γ induced protein from human dendritic cells," *Immunology Letters*, vol. 74, no. 3, pp. 221–224, 2000.

[11] G. I. Rice, J. Bond, A. Asipu et al., "Mutations involved in Aicardi-Goutières syndrome implicate SAMHD1 as regulator of the innate immune response," *Nature Genetics*, vol. 41, no. 7, pp. 829–832, 2009.

[12] N. Laguette, B. Sobhian, N. Casartelli et al., "SAMHD1 is the dendritic- and myeloid-cell-specific HIV-1 restriction factor counteracted by Vpx," *Nature*, vol. 474, no. 7353, pp. 654–657, 2011.

[13] K. Hrecka, C. Hao, M. Gierszewska et al., "Vpx relieves inhibition of HIV-1 infection of macrophages mediated by the SAMHD1 protein," *Nature*, vol. 474, no. 7353, pp. 658–661, 2011.

[14] R. D. Powell, P. J. Holland, T. Hollis, and F. W. Perrino, "Aicardi-Goutières syndrome gene and HIV-1 restriction factor SAMHD1 is a dGTP-regulated deoxynucleotide triphosphohydrolase," *Journal of Biological Chemistry*, vol. 286, no. 51, pp. 43596–43600, 2011.

[15] D. C. Goldstone, V. Ennis-Adeniran, J. J. Hedden et al., "HIV-1 restriction factor SAMHD1 is a deoxynucleoside triphosphate triphosphohydrolase," *Nature*, vol. 480, no. 7377, pp. 379–382, 2011.

[16] J. Yan, S. Kaur, M. DeLucia et al., "Tetramerization of SAMHD1 is required for biological activity and inhibition of HIV infection," *Journal of Biological Chemistry*, vol. 288, no. 15, pp. 10406–10417, 2013.

[17] X. Ji, Y. Wu, J. Yan et al., "Mechanism of allosteric activation of SAMHD1 by dGTP," *Nature Structural and Molecular Biology*, vol. 20, no. 11, pp. 1304–1309, 2013.

[18] C. Chahwan and R. Chahwan, "Aicardi-Goutieres syndrome: from patients to genes and beyond," *Clinical Genetics*, vol. 81, no. 5, pp. 413–420, 2012.

[19] W. Li, B. Hu, G.-L. Li et al., "Heterozygote genotypes at rs2222823 and rs2811712 SNP loci are associated with cerebral small vessel disease in Han Chinese population," *CNS Neuroscience and Therapeutics*, vol. 18, no. 7, pp. 558–565, 2012.

[20] J. Ahn, C. Hao, J. Yan et al., "HIV/simian immunodeficiency virus (SIV) accessory virulence factor Vpx loads the host cell restriction factor SAMHD1 onto the E3 ubiquitin ligase complex CRL4DCAF1," *Journal of Biological Chemistry*, vol. 287, no. 15, pp. 12550–12558, 2012.

[21] D. Zhao, D. Peng, L. Li, Q. Zhang, and C. Zhang, "Inhibition of G1P3 expression found in the differential display study on respiratory syncytial virus infection," *Virology Journal*, vol. 5, article 114, 2008.

[22] W. Liao, Z. Bao, C. Cheng, Y.-K. Mok, and W. S. F. Wong, "Dendritic cell-derived interferon-γ-induced protein mediates tumor necrosis factor-α stimulation of human lung fibroblasts," *Proteomics*, vol. 8, no. 13, pp. 2640–2650, 2008.

[23] A. Berger, A. F. R. Sommer, J. Zwarg et al., "SAMHD1-deficient CD14+ cells from individuals with Aicardi-Goutières syndrome are highly susceptible to HIV-1 infection," *PLoS Pathogens*, vol. 7, no. 12, Article ID e1002425, 2011.

[24] Y. J. Crow, A. Vanderver, S. Orcesi, T. W. Kuijpers, and G. I. Rice, "Therapies in Aicardi-Goutières syndrome," *Clinical & Experimental Immunology*, vol. 175, no. 1, pp. 1–8, 2014.

[25] M. A. Lee-Kirsch, C. Wolf, and C. Günther, "Aicardi–Goutières syndrome: a model disease for systemic autoimmunity," *Clinical and Experimental Immunology*, vol. 175, no. 1, pp. 17–24, 2014.

[26] Z. C. Hartman, A. Kiang, R. S. Everett et al., "Adenovirus infection triggers a rapid, MyD88-regulated transcriptome response critical to acute-phase and adaptive immune responses in vivo," *Journal of Virology*, vol. 81, no. 4, pp. 1796–1812, 2007.

[27] C. Préhaud, F. Mégret, M. Lafage, and M. Lafon, "Virus infection switches TLR-3-positive human neurons to become strong producers of beta interferon," *Journal of Virology*, vol. 79, no. 20, pp. 12893–12904, 2005.

[28] A. Munshi, K. Rajeshwar, S. Kaul et al., "Association of tumor necrosis factor-α and matrix metalloproteinase-3 gene variants with stroke," *European Journal of Neurology*, vol. 18, no. 8, pp. 1053–1059, 2011.